TO JEN.

AND TO MY PARENTS.

STUDIES OF NEGATIVE IONS FORMED BY LOW ENERGY ELECTRON IMPACT

by

Peter W. Harland

Thesis presented for the Degree of Doctor of Philosophy of the University of Edinburgh in the Faculty of Science

September, 1971.

INDEX

Page No.

ACKNOWLEDGEMENTS

I wish to express my thanks to Dr. J. Thynne whose continued interest and suggestions have been a source of inspiration throughout the course of this work.

I would also like to thank Professor C. Kemball for the provision of library and laboratory facilities, Dr.'s Rankine and Cradock for preparing most of the inorganic samples investigated and Mr. A. King for his unrelenting patience and expertise in tracking down and correcting unpredictable electronic faults.

Acknowledgement is also due to Dr. K. MacNeil who wrote and tested the computer program used extensively throughout this work for the analysis of ionisation data and to Miss J. Logan who wrote the computer program used for the calculation of electron affinities (Chapter 4).

I am also grateful to the S.R.C. for the award of a studentship for three years.

ABSTRACT

In this thesis the processes responsible for the formation of negative ions by the interaction of low energy electrons (0 to 15eV) with molecules in the gas phase have been investigated. Particular attention has been paid to the processes known as associative resonance capture and dissociative resonance capture. For a molecule AB, associative resonance capture is described by the equation $AB + e \longrightarrow AB^-$, where the metastable molecular negative ion AB^- is formed by the capture of slow electrons. Dissociative resonance capture, described by the equation $AB^- \longrightarrow A^- + B$, results in the formation of a stable negative ion and can occur throughout the energy range studied.

A historical review of the theoretical approach to electron-attachment is followed by detailed accounts of the most recent theoretical treatments of associative and dissociative resonance capture. The time-of-flight mass spectrometer used for this study has been described in some detail as have the experimental procedures developed. The various devices used to overcome the problems created by the broad electron energy distribution, which is due to the use of thermionically emitted electron beams, have been critically reviewed and the analytical deconvolution procedure adopted in this study has been described in detail.

Autodetachment lifetimes and capture cross-sections for the associative attachment of electrons by several groups of organic and inorganic molecules have been measured

and comparisons made with the predictions of the statistical theory for associative electron capture. Attempts to calculate electron affinities from this theory, using the lifetimes and cross-sections measured, met with some success for simple molecules and enabled conclusions to be made concerning the adequacy and limitations of the theoretical treatment.

From studies of the electron energy dependence of negative ion formation for several groups of inorganic and organic molecules, various ionisation processes have been identified. Deconvolution of the ionisation curves has enabled accurate appearance potential data to be determined and, in many cases, allowed bond dissociation energies, electron affinities and heats of formation of various species to be evaluated.

CHAPTER 1

INTRODUCTION

Although studies of positive and negative ion formation in the gas phase were carried out by J.J. Thomson[1] as early as 1913 until recently the processes involved in negative ion formation have attracted only a small fraction of the attention received by positive ionisation processes. This has been due largely to the experimental difficulties associated with the detection of negative ions, which are formed with a characteristically low probability often some orders of magnitude less than for positive ion formation, e.g. with methane $CH_4^+/C^- \sim 10^4$. Also since such ions are often formed in the energy range below 2eV the influence of contact potentials, space charge effects and stray electric and magnetic fields necessarily affect the ionisation efficiency curves, linearity of the electron energy scale and difficulties may be encountered in the unequivocal interpretation of negative ion data.

Ionisation and dissociative electron capture studies of various molecules may yield basic data regarding electron affinities, bond dissociation energies, electron capture cross-sections, heats of formation of ions and autodetachment lifetimes of temporary molecular negative ion states which are of value in leading to a clearer understanding of ions and molecules.

Electron attachment to certain polyatomic molecules in the gas phase may result in the formation of temporary molecular negative ion states (lifetimes up to 10^{-3} seconds)

which can be directly investigated using time-of-flight techniques[2] thus providing a rare opportunity to observe directly an intermediate state, so often postulated in many branches of chemistry. The electron capture properties of such molecules, particularly sulphur hexafluoride, have already been utilised to great advantage in the control of arc discharges, for plasma quenching and as an insulating medium, many times more effective than air, in Van de Graaff accelerators, high voltage equipment and power transmission lines. In chemistry, electron capture processes and negative ion formation play an important role, both in condensed and gaseous phases, and as such have found many practical applications. Their presence in flames has led to the suggestion that they play an important role in combustion processes.[3] Negative ion mass spectra, which are generally much simpler than positive ion spectra, have been effectively employed in the analysis of organic and inorganic compounds.[5]

The presence of free electrons in the upper atmosphere formed by photoionisation and photodetachment processes plays a dominant role in radio and television communications through the reflection of electromagnetic radiation. Their formation and build up near the nose cone of space vehicles when re-entering the upper reaches of the atmosphere is largely responsible for the characteristic communication blackout. This problem may eventually be partially solved with the development of more effective electron scavengers and suitable supporting media. The negative ions present in the ionosphere and reactions in which they may be involved are still

largely uninvestigated[6] by comparison with the detailed knowledge made available for positive ions by various methods including rocket-borne mass spectrometers.

The objectives of the study were (i) to examine the interaction of slow electrons (0-15eV) with a variety of inorganic and organic molecules, (ii) through a detailed investigation of the associative and dissociative capture reactions obtain a better understanding of such interactions and (iii) where possible, to determine previously unknown molecular and radical parameters.

Measurements of the autodetachment lifetimes and associative capture cross-sections for a large variety of organic and inorganic molecules were undertaken with a view to evaluating the reliability of the theoretical model which has been proposed for associative electron capture through a correlation of the experimental data with the predictions of the model.

Dissociative electron capture processes were examined in several groups of chemically interesting molecules; inorganic fluorides, fluorophosphines, perfluorocarbons, fluoroketones, fluoroaldehydes and the stable free radical bis-trifluoromethyl nitroxide. Many of the reactions responsible for ion formation by a particular molecule were identified and discussed with those of the other members of the group; electron affinities and bond energies were calculated and compared to available literature values. The effects of the energy spread of the ionising electron beam on the experimental data were partially removed by the application of iterative smoothing and unfolding methods.

CHAPTER 2

THE THEORY OF ELECTRON-MOLECULE ATTACHMENT PROCESSES

When a low energy electron (less than 100eV) interacts with a molecule under single collision conditions, depending on the energy of the electron and the nature of the molecule, one of the following attachment processes may occur:

(i) Associative Resonance Capture,

$$AB + e \longrightarrow AB^{-*}$$

(ii) Dissociative Resonance Capture,

$$AB + e \longrightarrow A^{-} + B$$

(iii) Ion Pair Formation,

$$AB + e \longrightarrow A^{-} + B^{+}$$

For ease of presentation AB is shown as a diatomic molecule but A or B may be a group or groups of atoms and processes (ii) and (iii) above may involve the rupture of several bonds.

(a) Qualitative description of attachment processes.

(i) Associative resonance capture.

Interaction between a slow electron (~0eV) and a molecule which has a positive electron affinity may lead to the formation of a molecular negative ion state (AB^{-*}) which has a lifetime amenable to investigation by time-of-flight techniques i.e. $T_a > 10^{-6}$sec.

$$AB + e \xrightarrow{\sigma_a} AB^{-*} \xrightarrow{T_a^{-1}} AB(\text{or } AB^{*}) + e$$

The electron affinity, E, is defined as the difference between the ground electronic, vibrational and rotational level of the neutral atom or molecule and that for the negative

ion. The magnitude of σ_a, the attachment cross-section, is determined by the vibrational overlap integral (the integral over the product of the vibrational eigenfunctions of the two states involved) whilst T_a, the autodetachment lifetime, depends upon the degrees of freedom available in the ion for distribution of the kinetic energy of the incident electron. In the absence of collisional stabilisation, ejection of the electron (autodetachment) will take place when the molecule returns to a suitable configuration. The cross-section for autodetachment, σ_{ad}, is equal to $\sigma_a p_{ad}$, where p_{ad}, the autodetachment probability, depends upon the extent of dissociative attachment which is in competition with it.

At the low pressures (10^{-6} torr) normally employed in the mass spectrometer ion source, collisions with a third body, in which the excess energy may be transferred, are too infrequent for stabilisation to take place. In experiments using higher pressures, swarm beam experiments for example (up to 1000 torr), stabilisation may occur to a significant extent.

A simple two-dimensional representation of the potential energy surfaces involved in associative capture is illustrated in Fig. 2.1(a). In this, AB represents the ground electronic state of the neutral molecule, where a,b, is the amplitude of oscillation for the lowest vibrational state. AB^- represents the ground electronic state of the negative ion. An incident electron with energy close to E_1 excites the neutral molecule to the state represented by a',b', in the figure. The probability of capture to form a vibrationally excited AB^- ion

(a) ASSOCIATIVE RESONANCE CAPTURE

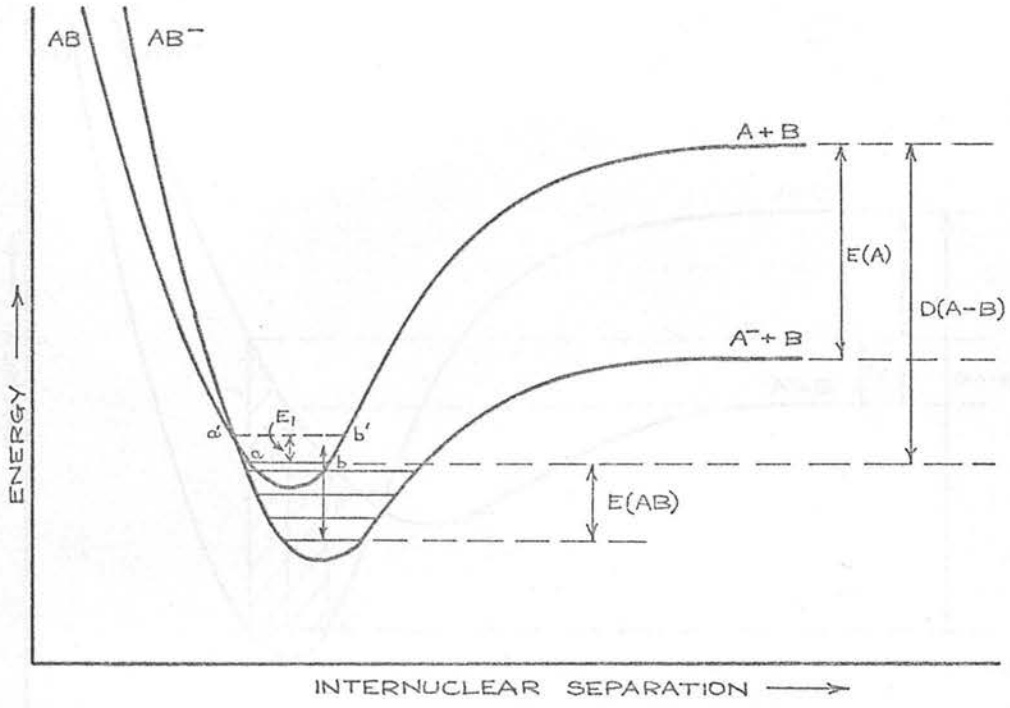

(b) DISSOCIATIVE RESONANCE CAPTURE

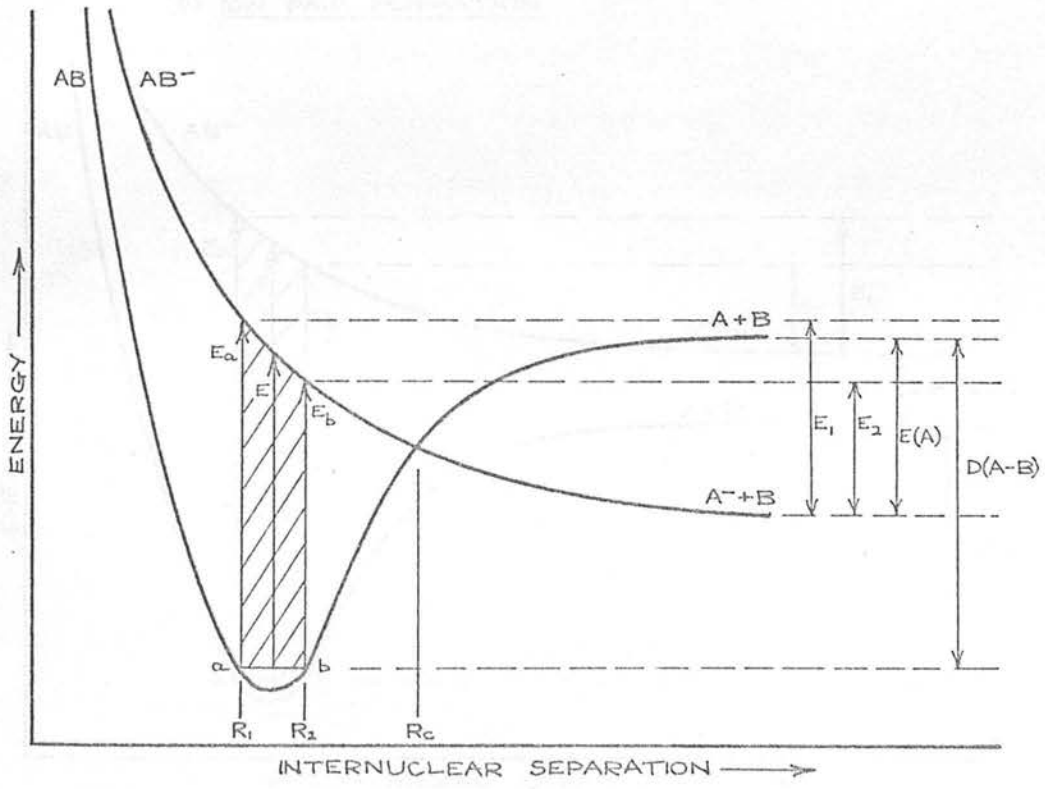

Fig 2.1

(a) DISSOCIATIVE RESONANCE CAPTURE
VERTICAL ONSET

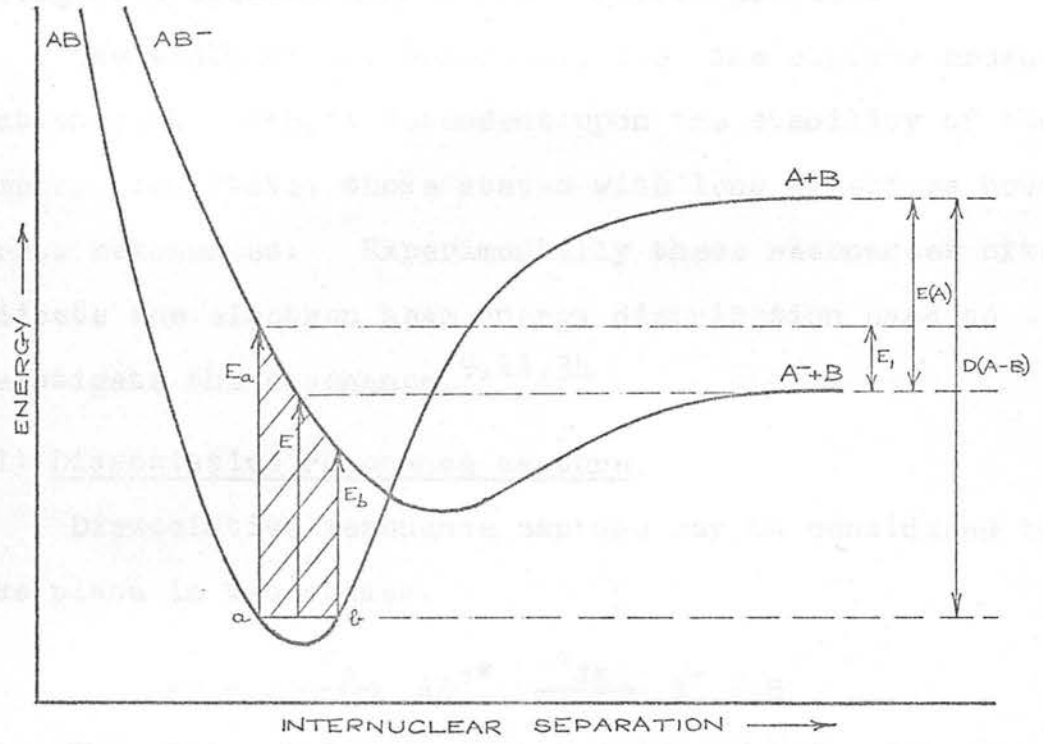

(b) ION PAIR FORMATION

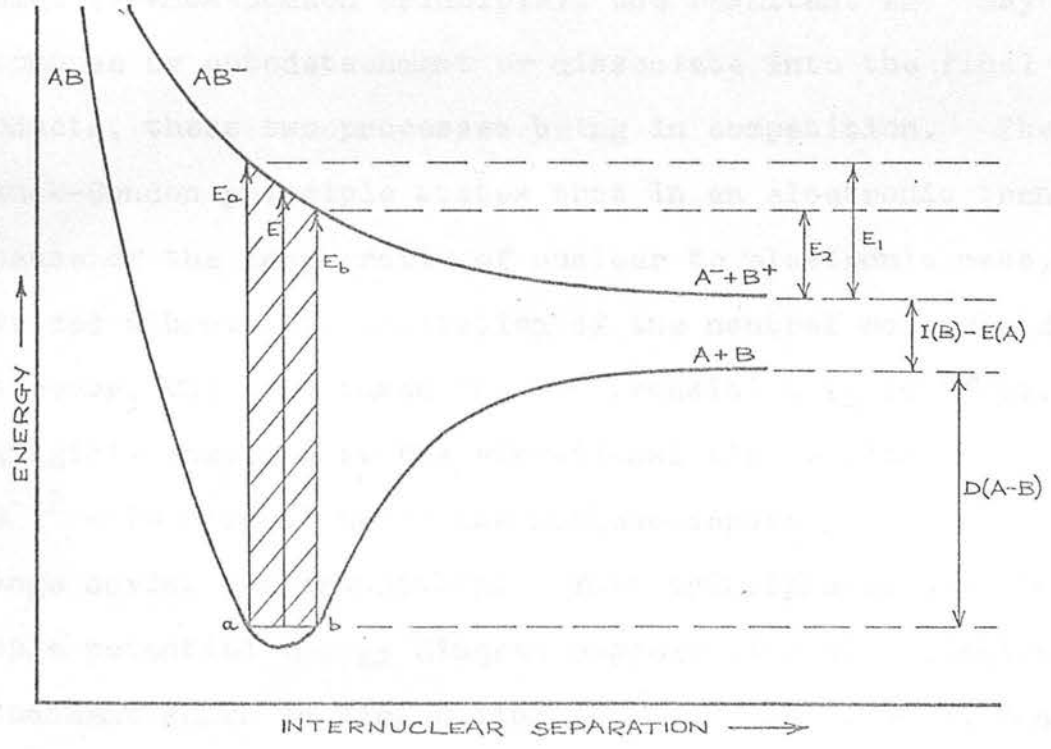

Fig 2.2

is then high and, in the absence of stabilisation, the ion undergoes autodetachment by the reverse process.

The width of the resonance, i.e. the capture cross-section peak width, is dependent upon the stability of the compound ion state, those states with long lifetimes having narrow resonances. Experimentally these resonances often indicate the electron beam energy distribution used to investigate the resonance.[9,11,34]

(ii) Dissociative resonance capture.

Dissociative resonance capture may be considered to take place in two stages.

$$AB + e \xrightarrow{\sigma_a} AB^{-*} \xrightarrow{\sigma_{da}} A^- + B$$

The electron is first captured by the neutral molecule without alteration of the positions and velocities of the nuclei (Franck-Condon principle), the resultant AB^{-*} may then decompose by autodetachment or dissociate into the final products, these two processes being in competition. The Franck-Condon principle states that in an electronic transition, because of the large ratio of nuclear to electronic mass, provided vibrational excitation of the neutral molecule does not occur, the time taken for the transition ($\leq 10^{-15}$ sec.) is negligible compared to the vibrational time period (10^{-12} - 10^{-13} sec.) hence the nuclear separation will not change during the transition. This principle is used in the simple potential energy diagram representing dissociative attachment shown in Fig. 2.1(b). A vertical (Franck-Condon) transition from the ground state of the molecule AB to the

repulsive surface representing an electronically excited AB^- state results from the capture of an electron in the energy range E_a to E_b. The transient parent negative ion state (lifetime $\sim 10^{-13}$sec.) decomposes along the surface shown to form the negative ion A^- and the radical B, provided that it does not undergo autodetachment reverting back to the ground or an excited state of the neutral molecule, AB. The dissociation fragments formed will have distributed between them kinetic energies in the range E_1 to E_2 according to the principle of conservation of momentum:

$$\frac{KE(A^-)}{KE(B)} = \frac{M(B)}{M(A^-)}$$

where KE represents the kinetic energies and $M(A^-)$ and M(B) are the masses of A^- and B respectively.

In the Franck-Condon region, where the potential curve of AB^- lies above that of AB, Fig. 2.1(b), the molecule ion is unstable towards autodetachment. The cross-section for dissociative attachment, σ_{da}, is therefore dependent on σ_a, the cross-section for electron detachment to AB, and the probability (p_{da}) that AB^- will dissociate without autodetachment is therefore given by $\sigma_a p_{da}$, where the probability p_{da} was defined by Holstein[67] as being equal to e^{-T_s/T_a}, where T_a is the autodetachment lifetime and T_s the stabilisation time required for the nuclei to reach the crossing point of the AB and AB^- potential curves, shown as R_C in Fig. 2.1(b).

$$\sigma_{da} = \sigma_a e^{-T_s/T_a} \quad \ldots\ldots\ldots\ldots\ldots (1)$$

Once the neutral and ion have separated to the crossing point R_C the system is stable towards autodetachment. The region between R_1 and R_C in which the negative ion is unstable towards electron ejection and in which competition between the two processes takes place, is called the autodetachment region. The cross-hatched region, between the classical turning points of the molecule in its ground vibrational level, R_1 to R_2, is called the Franck-Condon region.

Dissociative electron capture normally occurs in the 0 - 15eV energy range. The energy at which the fragment ion A^- first appears, the appearance potential $A(A^-)$, is related to the electron affinity of A, E(A), and the bond dissociation energy, D(A-B), by the energy balance equation:

$$D(A\text{-}B) = A(A^-) + E(A) + EE_{A^-,B} + KE_{A^-,B} \quad \ldots\ldots\ldots (2)$$

where EE_{A^-} is the internal excitation of A^- and KE_{A^-} is the kinetic energy imparted to A^- during the process. Since it is difficult to measure the excess energy terms in practice they are usually omitted and equation (2) written as follows:

$$D(A\text{-}B) \leq A(A^-) + E(A) \quad \ldots\ldots\ldots\ldots\ldots\ldots (3)$$

The parameter deduced from measured appearance potentials thus provides either a lower or an upper limit.

The shape of the capture cross-section resulting from a dissociative attachment process is illustrated in Fig. 2.3(b) using the reflection method. In this, Ψ^2, the square of the initial vibrational wave function of AB, which is the probability of the molecule AB having a particular internuclear separation, is reflected from the AB^- curve in the Franck-Condon region onto the energy axis; the shape of the ionisation

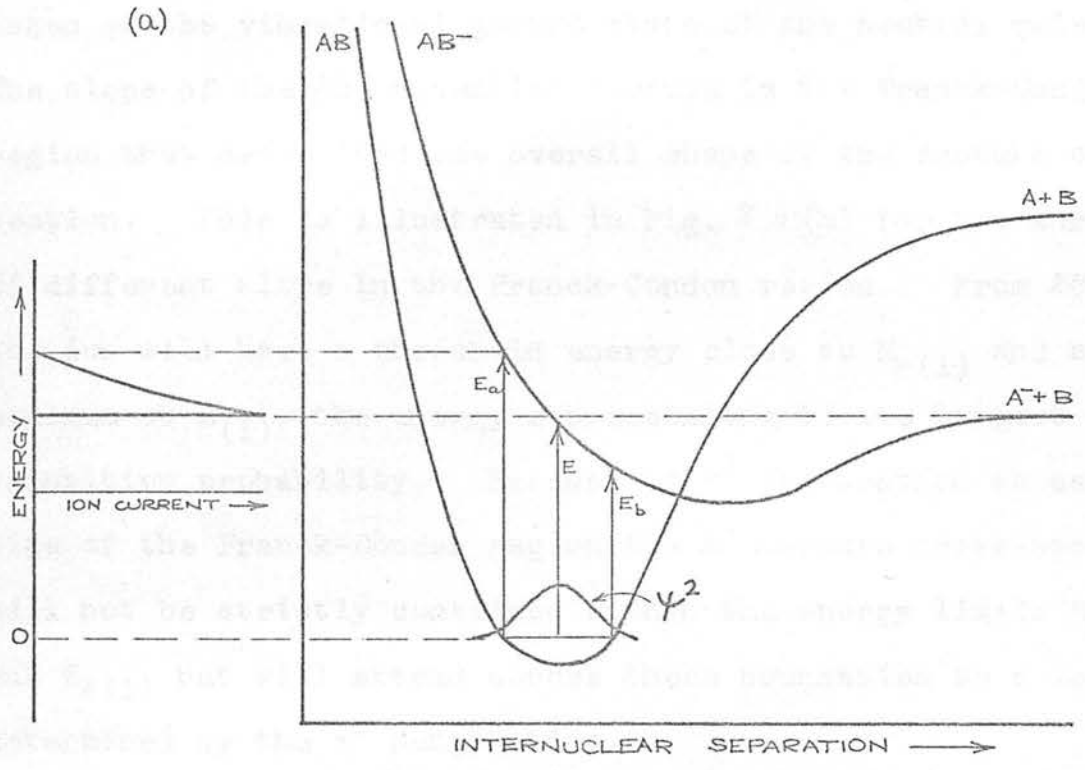
(a)
AB
AB⁻
A+B
A⁻+B
E_a
E
E_b
ψ^2
ENERGY
ION CURRENT
0
INTERNUCLEAR SEPARATION

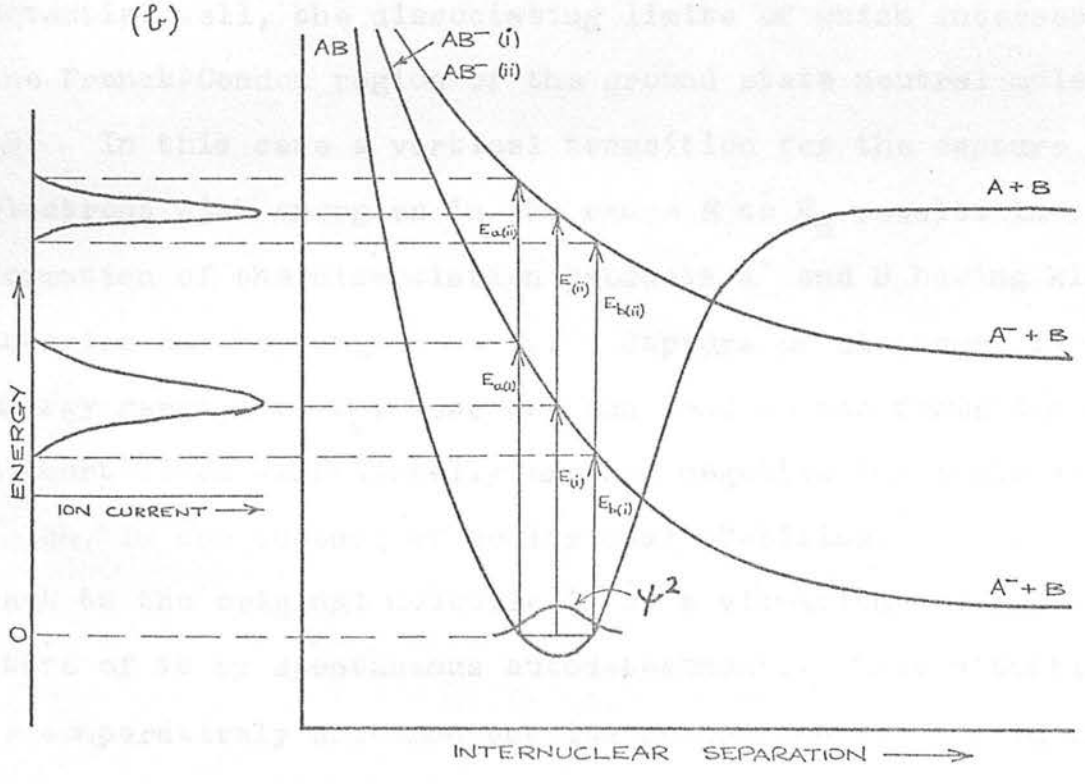
(b)
AB
AB⁻ (i)
AB⁻ (ii)
A+B
A⁻+B
$E_{a(ii)}$
$E_{(ii)}$
$E_{b(ii)}$
$E_{a(i)}$
$E_{(i)}$
$E_{b(i)}$
ψ^2
ENERGY
ION CURRENT
0
INTERNUCLEAR SEPARATION

Fig 2.3

efficiency curve is then produced. The zero of energy is taken as the vibrational ground state of the neutral molecule. The slope of the AB^- potential surface in the Franck-Condon region thus determines the overall shape of the capture cross-section. This is illustrated in Fig. 2.3(b) for two surfaces of different slope in the Franck-Condon region. From AB(i) the ion will have a threshold energy close to $E_{b(i)}$ and a maximum at $E_{(i)}$, the energy corresponding to the largest transition probability. Because of Ψ^2 penetration at each side of the Franck-Condon region the A^- capture cross-section will not be strictly contained within the energy limits $E_{b(i)}$ and $E_{a(i)}$ but will extend across these boundaries to a degree determined by the Ψ^2 penetration.

Fig. 2.2(a) illustrates a further situation leading to dissociative electron capture in which the AB^- ion has a potential well, the dissociating limits of which intersect the Franck-Condon region of the ground state neutral molecule AB. In this case a vertical transition for the capture of electrons with energies in the range E to E_a results in formation of the dissociation products A^- and B having kinetic energies in the range 0 to E_1. Capture of electrons in the energy range E to E_b, however, can lead to the formation of a short-lived vibrationally excited negative ion state AB^- which, in the absence of collisional stabilisation, reverts back to the original molecule AB or a vibrationally excited state of it by spontaneous autodetachment. This situation is comparatively uncommon but its occurrence results in the phenomenon of vertical onset illustrated by the capture cross-

section profile in Fig. 2.3(a). The capture peak attains maximum cross-section at threshold and the ion is formed with zero kinetic energy at the threshold.

(iii) Ion-pair formation

Formation of a negative ion by an ion-pair reaction is not a resonance process as the scattered electron can carry away excess energy and the process can take place over a wide energy range from threshold.

$$AB + e \longrightarrow A^- + B^+ + e(\text{or } e^*)$$

This is illustrated in Fig. 2.2(b) where a vertical transition to the surface AB^- gives rise to ion-pair formation with the fragments sharing translational energies in the range E_1 to E_2. The appearance potential for the positive and negative ion formed is given by the following expression:

$$A(A^-) = A(B^+) = D(A\text{-}B) + I(B) - E(A) + EE + KE \ldots (4)$$

where I(B), the ionisation potential of B, must be greater than the electron affinity of A, E(A), in order for the process to be exothermic. The magnitude of the I(B) term generally restricts the occurrence of ion-pair formation to the energy range above 10eV.

(b) Theoretical review.

Theoretical treatments of unimolecular electron capture have, up to the present time, been restricted to diatomic molecules and particularly the experimental data obtained for H_2 and O_2. The work of Rapp et al.[68] and Schulz[69,70,71] for

electron attachment in H_2 and its isotopes has been the foundation around which much of the theoretical approach has been constructed. This has resulted in a detailed description of the molecular negative ion states of H_2 involved and the isotope effects observed but extrapolation of these findings to polyatomic molecules is prevented by the lack of knowledge of the molecular negative ion states involved.

The complexity of polyatomic molecules and of the parent and fragment ions resulting from electron capture have precluded any substantial quantitative theoretical treatment. However, several qualitative approaches to resonant electron capture have proved useful in understanding the experimental data obtained for such systems.

The first theoretical treatment of unimolecular electron capture was presented in 1935 by Bloch and Bradbury[72] in an attempt to explain the experimental results of Bradbury[73] on electron capture by molecular oxygen to form O_2^-. Their proposed mechanism was the capture of an electron from a free state into a bound state in the molecule through a weak coupling between the electron motion and the nuclear motion of the molecule. The excess energy of formation (the kinetic energy of the incident electron and the electron affinity of O_2) was distributed by excitation of the molecular vibrational and rotational energy levels. Collisional stabilisation by transfer of this energy to third bodies then occurred. Restriction of the approach to diatomic molecules and application of the Born-Oppenheimer approximation using perturbation theory with the nuclear kinetic energy as the

perturbation enabled calculation of the transition probability from a free to a bound electronic state and the lifetime of the resulting vibrationally and rotationally excited negative ion state. The theory also gave a dependence of the phenomenon on the average energy of the incident electrons which agreed with the experimental observations.

Bloch and Bradbury's approach[72] was later modified by Massey (1950)[74] and then Stanton (1960).[75] They also argued that the influence of the kinetic energy of the nuclei on the electronic wave function gave rise to transitions which resulted in electron capture and Massey provided an expression for the effective capture cross-section of the process concerned. Stanton obtained an expression similar to Massey's but also considering the selection rules involved in electron capture by the Bloch-Bradbury mechanism. Chen (1963)[76] used this approach to calculate the cross-section for dissociative attachment to hydrogen and to provide an exact description of dissociative attachment processes by a finite set of coupled equations. This method did not give a clear picture for autodetachment and was reformulated by Bardsley et al.[77](1964) using the Kapur-Peierls formalism in order to account for competitive autodetachment from the molecular negative ion state.

The treatment of electron attachment to molecules using the resonance scattering theories has since proved to be the most lucrative approach. The major contributions by Bardsley et al. (1964),[77] Chen (1966),[78] Chen and Peacher (1967),[79] and O'Malley (1966,1967)[80,81] have been summarised

and discussed in the review article by Bardsley and Mandl (1968).[82]

Taylor et al. (1966)[83] presented a qualitative description for the resonant compound negative ion states in atoms and molecules with a general quasistationary method through which the energies of resonant states could be calculated from intuitively selected trial functions. It was pointed out that all quasistationary methods and scattering theory methods are special forms of Feshbach's general theory of resonant scattering.[90,91] A qualitative classification of Feshbach resonances in polyatomic molecules was presented in the review article by Bardsley and Mandl (1968).[82]

The term resonance, as applied to electron capture, refers to a state in which an electron is temporarily captured by a molecule thereby forming a metastable molecular negative ion state. Most of the resonant scattering treatments are formulated using the Born-Oppenheimer separation and treating electron capture as an electronic transition from a continuum (free state) to a discrete electronic state, when the final state is degenerate with the continuum it is classified as a resonance.

Electron attachment, treated as a nuclear-excited Feshbach resonance, has been put onto a semi-theoretical footing by Compton et al.[37] In this, the attachment cross-section, σ_a, the autodetachment lifetime, T_a, and the molecular electron affinity, E, are related by the principle of detailed balance. A knowledge of σ_a and T_a, determined experimentally, can then be used to estimate E. This approach, discussed

fully below, has been used in conjunction with experimental data determined in this study for the calculation of electron affinities (Chapter 4) for several small polyatomic molecules.

(c) Discussion of resonance phenomena.

Taylor et al.[83] recognised two distinct types of resonant states in electron-atom and electron-molecule scattering which, from the analogy to nuclear physics, they called 'core-excited' and 'single-particle' resonance states.

A core-excited resonance state is formed when the influence of the approaching electron causes promotion of one or more of the target electrons into an excited level so that the nucleus or nuclei are less well screened by the electrons of the atom or molecule. The electron, then confronted with a slight positive charge, binds to form a negative ion for a short period of time. Because the electron in the field of the excited target state can go into a bound state, i.e. the energy of the negative ion resonant state is below the energy of the excited parent target states, or a virtual state i.e. the energy of the negative ion resonant state is above the energy of the excited target states, core-excited resonances are subdivided into Types I and II respectively.

Type I core-excited resonant states, being more effectively bound, have relatively longer lifetimes and much of the energy associated with the incident electron may become distributed about the nuclear framework and possibly result in bond dissociation. Alternatively, the molecule may return to a configuration favourable to electron ejection, the ion decaying back to the target molecule plus the scattered

electron. The long lifetime can give rise to resonances which are narrow in energy whereas the shorter lifetime of the Type II core-excited states results in broad resonances for both elastic and inelastic scattering. This imposes considerable difficulties in their detection and the experimental evidence for this type of resonance is very scarce.

The second type of resonance, the single-particle or potential resonance, occurs when the negative ion is formed by the incoming electron moving in the field of the target ground state. A combination of polarisation, exchange and centrifugal barrier effects lead to the electron being trapped for a short time (less than 10^{-14}sec.). These effects produce a potential which is considerably weaker than that seen by the electron in the case of core-excited resonances and hence the negative ion states exhibit broad resonances.

The qualitative description of resonant states presented by Taylor et al.[83] is primarily aimed at an understanding of elastic scattering in atomic systems, the discussion of electron-molecule interactions is restricted to diatomic systems and particularly to the results of Schulz for H_2.[69,70,71] Extrapolation of Taylor's classification to polyatomic molecules is not as convenient as the use of the qualitative description of Feshbach resonances given in the review article by Bardsley and Mandl[82] which is primarily designed for polyatomic systems. In this, the single-particle resonant states of Taylor et al.[83] are referred to as shape resonances. Feshbach resonances, equivalent to the core-

excited states of Taylor et al.,[83] are divided into two classifications depending on whether the kinetic energy of the electron is absorbed into the electronic or nuclear motion of the target.

The first type, electron-excited Feshbach resonance states, are those in which the incident electron excites single or multiple electronic target states, the energy lost by the electron in exciting the target leaves it with insufficient energy to escape while the target remains in its excited state. Before the electron can be emitted it must re-absorb energy from the target. Most of the resonances which have been observed in atomic systems are of this type and they normally exhibit narrow resonances.

The second type, nuclear-excited Feshbach resonances, are those in which the kinetic energy of the incident electron is absorbed solely into the nuclear motion of the target, the electronic motion being unaffected. This type of resonance is observed for the low energy electron attachment to large polyatomic molecules in which the distribution of the excess energy amongst the vibrationally excited levels of stable electronic states can result in resonances with extremely long lifetimes (up to 10^{-3}sec.). Collisional stabilisation may then lead to molecular negative ions with 'infinite' lifetimes. The long lifetimes of nuclear excited Feshbach resonant states correspond to very narrow resonances. All of the long-lived polyatomic parent negative ions studied during the course of this work correspond to nuclear-excited Feshbach resonant states of the molecule and in all cases,

possibly with the exception of c-C_7F_{14}, the resonance width was found to reflect the electron energy distribution used in the measurements. A statistical model, developed by Compton et al.[37] to explain their electron attachment data for nuclear-excited Feshbach resonant states in some polyatomic molecules, has been used in conjunction with the experimental data obtained in this work (Chapter 4) and a detailed description of this approach is presented in the following section.

(d) Theoretical approach to associative resonance capture.

The existence of a long-lived (> 10^{-6}sec.) molecular negative ion state was first reported by Edelson et al.[2] who showed that the SF_6^- ion was metastable and subject to auto-detachment with an average lifetime of approximately 10 μsec. Asundi and Craggs[84] and Hickam and Fox[9] have suggested that the energy of the captured electron is shared with the many degrees of freedom of the large and generally symmetric molecule for a time amenable to observation in a conventional mass spectrometer. Compton et al.[37,85] extended the range of long-lived molecular negative ions to include $C_6H_5NO_2^-$, $(CHO)_2^-$, and $(CH_3CO)_2^-$ and several perfluorocarbons with auto-detachment lifetimes from 2·5 μsec. for $(CHO)_2^-$ to 800 μsec. for c-$C_7F_{14}^-$.

Compton et al.[37] proposed a simple semi-theoretical model to explain the long lifetimes encountered for the nuclear-excited Feshbach resonant states investigated. The molecule is represented as an assembly of weakly coupled

harmonic oscillators, the captured electron dissipating its kinetic energy amongst the various internal degrees of freedom of the molecule, so allowing the ion to exist for some time before relocation of the energy into a mode favourable to autodetachment. The proposed model relates σ_a, the attachment cross-section, T_a, the mean autodetachment lifetime, and E, the molecular electron affinity, at equilibrium. The metastable negative ion AB^{-*} decays with a mean autodetachment lifetime T_a to the original neutral molecule plus a free electron state according to:

$$AB^{-*}_{vib} \underset{\sigma_a}{\overset{T_a^{-1}}{\rightleftharpoons}} AB + e$$

The lifetime of the temporary negative ion state is related to the attachment cross-section through the principle of detailed balance, i.e.,

$$T_a = \frac{\rho^-}{\rho^o} \frac{1}{v\sigma_a} \quad \ldots\ldots\ldots\ldots\ldots\ldots \quad (5)$$

where ρ^- and ρ^o are the respective densities of states for the ion and its fragments of relative velocity v. Measurement of σ_a and T_a and a knowledge of the vibrational frequencies of the molecule can then be used to calculate the electron affinity which is the dominant parameter in ρ^-/ρ^o.

The density of final states, ρ^o, is the product of the densities of states of the dissociated fragments, i.e. $\rho^o = \rho_e . \rho_M$ where $\rho_M = 1$ if it is assumed that the molecule is left in its ground vibrational state. This appears to be a reasonable assumption considering the very low electron energy prior to attachment (~0·05eV). Compton takes ρ_e, the density

of states of the free electron, from the work of Schiff[86], to be:

$$\rho_e = \frac{m^2 v}{\pi^2 \hbar^3} \quad \ldots\ldots\ldots\ldots\ldots\ldots \quad (6)$$

as ρ_M is taken to be unity $\rho_e = \rho^o$ and,

$$\rho^o = \frac{m^2 v}{\pi^2 \hbar^3} \quad \ldots\ldots\ldots\ldots\ldots\ldots \quad (7)$$

The density of states for the negative ion, ρ^-, is calculated from the continuous energy density expression of Rabinovitch and Diesen[87] for a molecule (or ion) having N degrees of freedom and vibrational frequencies ν_i:

$$\rho^- = \frac{[\epsilon + (1 - \beta\omega)E_z]^{N-1}}{\Gamma(N) \prod_{i=1}^{N} h\nu_i} \quad \ldots\ldots\ldots \quad (8)$$

where E_z is the zero point energy (one half the sum of all $h\nu_i$), ϵ is the energy of the molecule (or ion) in excess of E_z i.e. the sum of the electron affinity, E, the kinetic energy of the incident electron, e_{ke}, and the average vibrational energy of the original molecular system above E_z, $f(E)dE$, $\Gamma(N)$ is the gamma function of N where N was taken to be $3n - 6$ for non-linear polyatomic molecules of n atoms, and $(1 - \beta\omega)$ is an empirical correction factor.[88]

$f(E)dE$, the thermal ($300{\cdot}16^oK$) vibrational energy distribution for the molecule was calculated in 0·1 Kcal intervals of energy, E, using the expression:[87]

$$f(E) = \frac{e^{-E/RT}(E+(1-\beta\omega)E_z)^{N-1}dE}{\int_o^{\infty} e^{-E/RT}(E+(1-\beta\omega)E_z)^{N-1}dE} \quad \ldots\ldots\ldots (9)$$

the results of this procedure for several systems and its overall significance to the determination of E from ϵ is discussed in Chapter 4.

$(1-\beta\omega)$, called the Whitten-Rabinovitch empirical correction factor, has to be computed for each molecule. Its value is critical at lower energies, $\epsilon < 2E_z$, but above this the spread of values, arising from the difference in vibrational frequency patterns, is very small and $(1-\beta\omega)$ tends to unity. β is a modified frequency dispersion parameter which takes some account of this;[88]

$$\beta = \frac{N-1<\nu^2>}{N<\nu>^2}$$

$$= \frac{N-1}{N} \frac{[\Sigma h\nu^2/N]}{[\Sigma h\nu/N]^2}$$

$$= \frac{N-1\ \Sigma h\nu^2}{(\Sigma h\nu)^2} \quad \ldots\ldots\ldots\ldots\ldots\ldots \quad (10)$$

The parameter ω is a function of $E' = \epsilon/E_z$ and is calculated as follows;[88]

$$\text{for } E' = 0{\cdot}1 - 1{\cdot}0 \quad \omega = [5E' + 2{\cdot}73(E')^{0{\cdot}5} + 3{\cdot}51]^{-1} \ldots \quad (11)$$

$$\text{and for } E' = 1{\cdot}0 - 8{\cdot}0 \quad \ln \omega = -1{\cdot}0506(E')^{0{\cdot}25} \ldots\ldots\ldots \quad (12)$$

Use of these expressions involves an error of less than 1% in ρ^- for $N \leq 30$.

Substituting back into equation (8) and assuming the spin degeneracy of the negative ion to be two leads to the expression relating T_a, σ_a and E;

$$T_a = \frac{2\pi^2\hbar^3}{m^2v} \frac{[\epsilon+(1-\beta\omega)E_z]^{N-1}}{\Gamma(N) \prod_{i=1}^{N} h\nu_i . v\sigma_a} \quad \ldots\ldots\ldots\ldots\ldots\ldots \quad (13)$$

rearranging and solving for ϵ

$$\epsilon + (1-\beta\omega)E_z = [T_a\sigma_a.4\pi m^2v^2\Gamma(N)\prod_{i=1}^{N} h\nu_i.h^{-3}]^{1/N-1} \quad .....(14)$$

ϵ is first computed with $(1-\beta\omega)$ set to unity, the electron affinity is then approached through iterative calculation terminated when the difference between consecutive values is $\leq 0{\cdot}002$eV.

The application of this approach to actual systems is partly limited by a dearth of vibrational frequency data although for those systems examined by this model the electron affinities calculated were in excellent agreement with the values obtained by the Magnetron technique[4] and from the study of the ionisation efficiency curves for the same ions produced from other systems i.e. $E(SF_4)_{calc} = 1{\cdot}2$eV, $E(SF_4)$ from $SF_4^-/SF_6 \simeq 1{\cdot}2$eV. That useful quantitative data could only be obtained for small ($N < 30$) symmetrical molecules is explained by the following general comments on the limitations of this approach made by Compton et al.,[37] Klots[89] and Collins:[66]

(i) Equation (13) is formulated for ion decay to the ground state neutral molecule. If, however, the captured electron was incident with energy in excess of one or more excited vibrational levels of the neutral molecule the system may decay to vibrationally excited neutral molecular states. This becomes more critical with increasing N as the density of states available renders this decay channel more probable. ρ_M is then increased from one, assumed above, to one plus the possible sums

of vibration overtones below ϵ. Some of the molecules may be in excited vibrational states prior to electron attachment as a result of source temperatures for example. This would similarly increase the number of available neutral molecular states to which the ion could decay. If this number is designated as K, and v_i and v_o are the velocities of the incident and outgoing electron, Collins et al.[66] have modified equation (13) to account for this:

$$T_a = \frac{2\pi^2\hbar^3}{Km^2 v_o} \frac{[\epsilon + (1-\beta\omega)E_z]^{N-1}}{\Gamma(N) \prod_{i=1}^{N} h\nu_i v_i \sigma_a} \quad \ldots\ldots\ldots\ldots \quad (15)$$

this predicts a pronounced drop in T_a with increasing temperature when many vibrational overtones of large molecules become accessible.

(ii) Klots[89] has pointed out that as equilibrium conditions are not satisfied for lifetime measurements in beam experiments equation (14) results in lower limits for electron affinities.

(iii) The negative ion vibrational frequencies are assumed to be the same as those of the neutral molecule. The fact that these equations apply for large molecules makes this a not too unreasonable assumption.

(iv) One assumption inherent in the basic concept of this model is that all vibrational modes share the excess energy available from negative ion formation. This may, however, depend on the negative ion geometry (which

in almost all cases is unknown) and may be a contributing factor to the ineffectiveness of the model in handling large unsymmetrical molecules.

(v) Discrepancies and approximations involved in the measurement of σ_a and T_a carry through to the quantitative data deduced from the model. In practice the magnitudes of T_a and σ_a were found to be fairly insensitive, within their respective experimental errors, on the value of E calculated from equation (14) i.e. using the vibrational frequencies of Ref. 88 for SF_6 the following values calculated for $E(SF_6)$ may be compared to the magnetron value of 1·43eV:-[4]

T_a(this work)μsec.	$\sigma_a cm^2$(ref.35)	$E(SF_6)_{calc}$(eV)
68·1	$0·95 \times 10^{-14}$(v=0·06eV)	1·40
68·1	$1·17 \times 10^{-14}$(v=0·05eV)	1·44
68·1	$1·50 \times 10^{-14}$(v=0·04eV)	1·48
68·1	$2·07 \times 10^{-14}$(v =0·03eV)	1·54

T_a (Christophorou et al.)[37]	$\sigma_a cm^2$(ref.35)	$E(SF_6)_{calc}$(eV)
25·0	$0·95 \times 10^{-14}$	1·25
25·0	$1·17 \times 10^{-14}$	1·29
25·0	$1·50 \times 10^{-14}$	1·34
25·0	$2·07 \times 10^{-14}$	1·39

In this work the thermal electron energy was taken to be 0·05eV and the value of $\sigma_a = 1·17 \times 10^{-14} cm^2$ used for the capture cross-section for SF_6.

(e) Theoretical approach to dissociative resonance capture.

Holstein[67] (1951) proposed that the cross-section for dissociative electron capture, σ_{da}, be given by the product of the attachment cross-section, σ_a, for capture into a repulsive state of the molecular negative ion AB^{-*}, and the probability, e^{-T_s/T_a}, that AB^{-*} will then dissociate without autodetachment:

$$\sigma_{da} = \sigma_a e^{-T_s/T_a} \quad \ldots\ldots\ldots\ldots \quad (1)$$

where T_a is the autodetachment lifetime and T_s, the survival time, is the time taken for the nuclei to reach the crossing point R_C (Fig. 2.1(b)) of the original molecular state and the dissociating negative ion state.

This concept was used by Rapp et al.[68] for a qualitative explanation of the isotope effects observed in their experimental dissociative capture cross-sections for ion formation in H_2, HD and D_2 in the energy range 7 - 18eV. For all ions, H^- and D^-, the ionisation efficiency curves showed a broad peak maximising at about 10eV and having a shoulder about 12eV followed by a narrow, sharper peak of higher cross-section maximising at $14{\cdot}2 \pm 0{\cdot}1$eV. The capture cross-sections at the 14eV peak maxima were measured to be $2{\cdot}08 \times 10^{-20}$, $1{\cdot}45 \times 10^{-20}$ and $0{\cdot}97 \times 10^{-20}$cm^2 for H^-/H_2, H^-+D^-/HD and D^-/D_2 formation respectively. This was rationalised in terms of the competition between dissociation and autodetachment when the intermediate molecular negative ion states are formed. The H_2^- ion, existing for $\sim 10^{-13}$sec., has a finite probability for electron emission leading to a

corresponding depletion in σ_{da}. It was then suggested that autodetachment per unit time would be independent of mass then, since T_s will be longer for the heavier isotopes, relatively more autodetachment will occur and the yield of atomic ions would be lower for the heavier isotopes. In addition to the isotope effect on σ_{da} a small shift in the 14eV peak to higher energies with increasing isotope mass was considered to be real and explained as follows: the ground state vibrational levels lie at lower energies as the mass is increased, the equilibrium separation therefore decreases with increasing mass, leading to transitions to higher portions of the repulsive H_2^- potential energy curve.

Recent theoretical treatments of dissociative capture based on the resonance scattering theory of Feshbach[90,91] have provided an explicit expression for σ_a in equation (1) and predicted the isotope effects on the magnitude and energy dependence of σ_a as observed by Rapp et al.[68] Although Bardsley et al.,[77,81] using the Kapur-Peierls formalism, reached the same conclusions, O'Malley's treatment[80,81] goes beyond the Kapur-Peierls approach by the inclusion of vibrational and rotational states and in considering the effects of direct transitions on dissociative attachment.

Resonance scattering theory[81] provides equation (16) for the dissociative attachment cross-section from the vibrational and electronic ground state of a diatomic molecule:

$$\sigma_{da} = \frac{4\pi^{3/2}}{k_i^2} \bar{g} \frac{\Gamma_a}{\Gamma_d} \exp\left[\frac{(1/2\ \Gamma_a)^2 - (\bar{E}_o - E)^2}{(1/2\Gamma_d)^2}\right] e^{-\rho(E)} \quad ..(16)$$

i.e. $\sigma_{da} = \sigma_a e^{-\rho(E)}$

where E is the incident electron energy, $k_i^2 = (2m/\hbar^2)E$ (k_i is the incident electrons wave-number), $\bar{g}$ is a statistical factor covering the weight factors for rotational and electronic angular momentum and relative spin multiplicity. $\Gamma_{\bar{a}}$ and Γ_a are the partial and total autodetachment widths respectively (and $\hbar/\Gamma_{\bar{a}}$ and $\hbar/\Gamma_a$ are the associated lifetimes) of the compound state and Γ_d is the experimentally observed dissociative cross-section width. $\bar{E}_o = E_o + 1/2\hbar w$, where E_o is the electron energy associated with a transition from the equilibrium position of the ground state molecule and $1/2\ \hbar w$ is the zero point energy associated with the bond broken in the dissociation. Finally, the factor, $e^{-\rho(E)}$ is the survival probability term (equation (1)) given by O'Malley[81] as

$$\rho(E) = \int_{R_E}^{R_C} \frac{\Gamma_a(R)dR}{\hbar\, v(R)} \quad \ldots\ldots\ldots\ldots\ldots \quad (17)$$

where R_E is the internuclear separation at which incident electrons of energy E are captured, R_C is the internuclear separation at the crossing point R_C (Fig. 2.1(b)) and v(R) is the relative separation velocity of the nuclei as a function of the internuclear separation R. Following Holstein,[67] it is assumed that autodetachment becomes insignificant beyond R_C.

Although the lack of knowledge of the nature of the intermediate molecular negative ion states prevent the calculation of absolute magnitudes and energy dependencies

for σ_{da}, equation (16) predicts a mass dependence for σ_{da} as a result of the mass dependent parameters $\rho(E)$ and Γ_d.

As the relative velocity of separation of the nuclei is proportional to $\mu^{-1/2}$, the survival time, T_s, required for the nuclei to separate to the crossing point, R_C, is proportional to $\mu^{1/2}$, that is,

$$\rho \propto \mu^{1/2} \quad \ldots\ldots\ldots\ldots\ldots\ldots \quad (18)$$

this can lead to large isotope effects, the heavier isotopes having the smaller cross-sections.

Γ_d is given by O'Malley as;[81]

$$\Gamma_d = 2v'\left(\frac{\hbar}{\mu w}\right)^{1/2} \quad \ldots\ldots\ldots\ldots \quad (19)$$

where v' is the force acting to separate A^- and B at R_C, w is the frequency of oscillation of the A-B mode and μ is the reduced mass of the AB^{-*} system. The occurrence of $(\Gamma_d)^2$ in the denominator of the σ_a term in equation (16) results in a $\mu^{-1/4}$ dependence of the exponent on the reduced mass. This has two effects: (i) it leads to an isotope effect for the width of the cross-section peak and (ii) the magnitude of the cross-section. Thus the exponential isotope dependence on σ_a is made up of two parts being totally proportional to $\mu^{1/4}$.

Depending on the relative domination of the σ_a or the $\rho(E)$ term on σ_{da} it is difficult to apportion the isotope effect, observed experimentally, between the two terms. O'Malley[81] pointed out that if ρ is small and $E \simeq E_o$ then the σ_a term will produce the only significant mass dependence on σ_{da}. This type of situation has been observed by Sharp and

McDowell[92] as an 'inverse isotope effect' for the formation of H^- from CH_4 and D^- from CD_4 where Christophorou et al.[93] pointed out that $(\frac{\mu CH_3-H}{\mu CD_3-D})^{1/4} = 0{\cdot}84$, close to the ratio of 0·8 found experimentally. The isotope effect for dissociative attachment in H_2O and D_2O has been studied by Compton and Christophorou,[94] and in the hydrogen halides by Christophorou et al.[93] In both cases isotope effects with $\sigma_{da} \propto \mu^{-1/2}$ were reported which were attributed to non-adiabatic terms by Compton and Christophorou but which are difficult to understand theoretically.

In general the isotope effects from the σ_a term are small but they may become important in the case of vertical onsets. Normally the peak value of σ_{da} is not affected much by the mass dependence of Γ_d in the Gaussian term (σ_a term), but the tail of the Gaussian is very dependent upon Γ_d. In the case of vertical onsets, when dissociation is not possible for all internuclear separations in the Franck-Condon region (Fig. 2.2(a)), the peak value for σ_{da}, lying in the tail of the Gaussian, will be very dependent upon μ, therefore σ_a, at threshold, will be much greater for lighter isotopes. This is probably the explanation for the large isotope effect observed by Schulz and Asundi[71] for the 3·75eV peak for H^-/H_2 (and its isotopes). Dissociation takes place from the tail of the $^2\Sigma_u^+$ state of H_2^- which, having a well in the Franck-Condon region, allows dissociation for only certain internuclear separations. This situation is analagous to that depicted in Fig. 2.2(a) in which E corresponds to 3·75eV and AB^{-*} to the $^2\Sigma_u^+$ state of H_2^-. As predicted by the

theory the isotope effects are large; $\sigma_{da} = 1{\cdot}6 \times 10^{-21}cm^2$ for H^-/H_2, $\sigma_{da} = 2{\cdot}1 \times 10^{-22}cm^2$ for H^-+D^-/HD and $\sigma_{da} = 8 \times 10^{-24}cm^2$ for D^-/D_2 and the resonance is broad ~3eV having a maximum at ~2eV with $\sigma_a(E_{max}) = 1 \times 10^{-15}cm^2$.

Compton and Christophorou[94] measured σ_{da}'s for H^-/H_2O and D^-/D_2O and the isotope effects for H^-/H_2O, D^-/D_2O, O^-/H_2O and O^-/D_2O. Isotope effects on both the magnitude and width of σ_{da} were reported. H^-/H_2O and D^-/D_2O were both found to peak at $6{\cdot}5 \pm 0{\cdot}1$eV with capture cross-sections measured to be $6{\cdot}9 \times 10^{-18}$ and $6{\cdot}2 \times 10^{-18}cm^2$ at their respective capture maxima, the D^- peak being ~0·3eV narrower than the H^- peak. The results were examined in terms of equation (1) proposed by Holstein, $\sigma_{da} = \sigma_a e^{-T_s/T_a}$. From the measured cross-sections and the assumption that T_a remains constant for both molecular negative ions, H_2O^{-*} and D_2O^{-*}, Compton and Christophorou deduced that $T_s/T_a > 1$. Auto-detachment is therefore relatively unimportant and σ_{da} and the isotope effects will be dominated by the survival probability term in equations (1) and (16).

A similar study of the hydrogen and deuterium halides by Christophorou et al.[93] showed an increase in the maximum of σ_{da} on the energy scale in going from HCl to HBr to HI, this being accompanied by a simultaneous increase in the magnitude of σ_{da}. The values of T_s and T_a were found to be comparable and very short ($T_s \simeq T_a \simeq 3{\cdot}5 \times 10^{-15}$sec.). The isotope effects on σ_{da} and the magnitude of σ_{da} are therefore more dependent upon the σ_a term in equations (1) and (16). The results of Schulz and Asundi[71] for the 3·75eV resonance in H_2

were similarly treated and showed that for vertical onsets T_s/T_a is large, being 4·68 for this process. Autodetachment is therefore the determining factor on the magnitude of σ_{da} which is consequently very small. The survival probability term therefore dominates equations (1) and (16) and the isotope effects are expected to be large, as observed.

Christophorou and Stockdale[95] summarised and evaluated these observations, and many more available from the literature, within the framework of the resonance scattering theory. The dissociative capture cross-section at the peak maximum, $\sigma_{da}(E_{max})$, was found to be a strong function of the peak energy, E_{max}, with a break in this dependence at the energy for which electronic excitation of the neutral molecule can occur. From a plot of $\sigma_{da}(E_{max})$ vs. E_{max} for the experimental results for over 30 molecules, both diatomic and polyatomic, molecules were found to fall into three groups; Group I, for which E_{max} is lower than the energy of known excited states of the molecule and the negative ion is purely repulsive in the Franck-Condon region; Group II, for which E_{max} is greater than or equal to known excited electronic states of the molecule and Group III for which the negative ion state is only attractive in part of the Franck-Condon region, allowing dissociation to occur over a limited range of internuclear separations only.

The molecules making up Group I are partly or fully halogenated diatomic and polyatomic compounds yielding halogen negative ions for low energy electron impact. The magnitude of σ_{da} is mainly determined by σ_a, as T_s, which is a strong

function of the steepness of the AB^{-*} potential curve, is short and dissociation is therefore fast. T_s/T_a is in the order of 1 to 2 therefore σ_{da} is large and the isotope effects are small. Thus molecular negative ion states in this group appear to correspond to the single-particle or potential resonant states of Taylor et al.[83] and the shape-resonances of Bardsley and Mandl.[82]

The molecules in Group II are mainly diatomic and triatomic yielding H^-(or D^-) and O^- negative ions. The molecular negative ion states can be identified with the core-excited resonant states of Taylor et al.[83] and the electron-excited Feshbach resonance states of Bardsley and Mandl[82] where, in addition to elastic, inelastic (to vibrationally and rotationally excited neutral molecular states) and dissociative capture channels available to Group I molecules, the overlap of the wavefunctions of the molecular negative ion state and the electronically excited molecular state, makes the additional scattering channel to the electronically excited molecular state much more probable. The magnitude of σ_{da} is therefore determined by both σ_a and the survival probability. The importance of autodetachment, reflected in the value of $T_s/T_a = 4{\cdot}8$ for the H^- ion formed from H_2 at 10eV, results in large isotope effects.

Group III consists of the vertical onset processes i.e. the 3·75eV process in H_2, HD and D_2, the 9·62eV process in CO, the 7·42eV process in NO and possibly the 4·35eV process in CO_2.[95] A substantial attractive potential in the negative ion state results in a greater opportunity for autodetachment

and hence the cross-sections are all small and the isotope effects large.

Besides the isotope and energy dependence effects on σ_{da} successfully predicted by equation (16), O'Malley was able to explain and reproduce the striking temperature effects on the dissociative capture cross-section in O_2 found experimentally by Fite et al.[96] O'Malley[81] employed a semi-empirical approach, assuming a Maxwellian distribution of vibrational and rotational states. Equation (16) was then used and the final-state potential curve of O_2^- was parametrized to fit the experimental data. The observed temperature shift, such that at 2100°K the cross-section peak, $\sigma_{da}(E_{max})$, was shifted to lower energy by 1eV while the apparent onset was reduced by over 2eV, was found to be caused by the effect on excited vibrational states of the rapidly varying survival probability, a measure of the competition between autodetachment and dissociation.

CHAPTER 3

EXPERIMENTAL

The experimental work described in this study was carried out using a Bendix Model 3015 Time-of-Flight Mass Spectrometer. The theory and design of such instruments has been described in detail by Stephens[31] and by Wiley and McLaren,[32,33] and only a brief machine description followed by a more detailed account of the normal operating procedure will be given here.

(a) Basic machine description

Fig. 3.1 is a schematic diagram of the apparatus which basically consists of an electron gun, a collision chamber where ions are formed, a linear field-free drift tube for mass analysis of the ions and a fast response Magnetic-Electron Multiplier with associated electronics for ion detection and measurement.

A pulse of electrons, with a selected kinetic energy, is collimated into the collision chamber where it passes through a low pressure gas (10^{-4} - 10^{-7} torr) and onto a trap anode located at the far side of the chamber. The resulting trap current is measured with a microammeter. After each pulse of electrons has passed (duration 0·25 μsec) the ions produced are drawn out of the source region by a pulse applied to the first ion grid and are accelerated by further grids into the drift tube which is normally maintained at 2·8KV. The pulses and potentials applied to the ion drawout grids and ion optics are of reversible polarity in order to

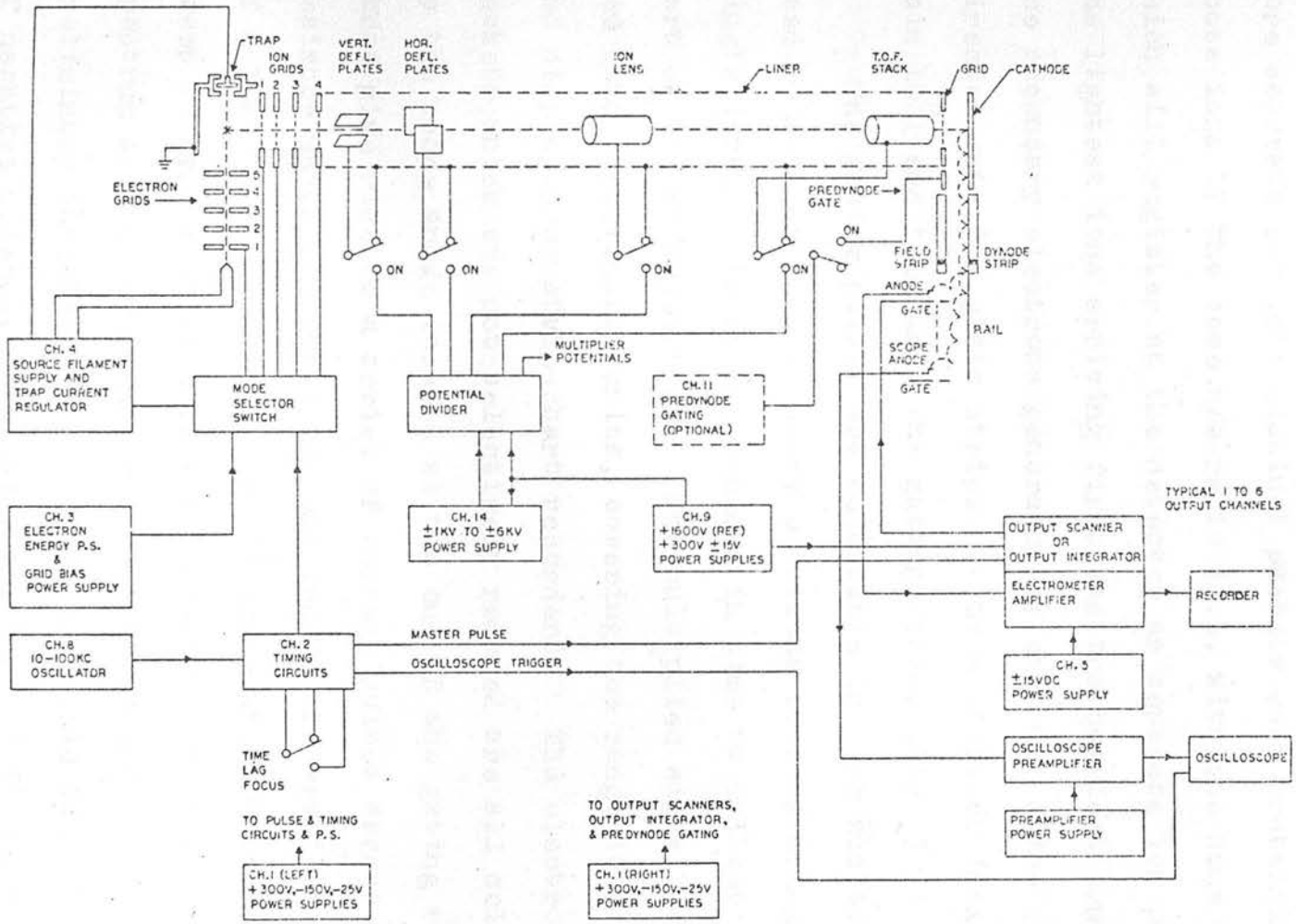

Fig. 3.1 - Model 3015 T.O.F.M.S. Block diagram

accommodate both negative and positive ion studies. The same kinetic energy is thus imparted to all ions of the same charge (i.e. independent of mass). The ion pulse will therefore separate out into distinct packets each containing only those ions of the same m/e ratio (i.e. with the same velocity) which will register at the detector as separate ion pulses, the lightest ions arriving first and the heaviest ions last. The secondary electrons generated by each m/e pulse are directed onto the glass strips of the multiplier (maximum gain 10^8) and then into the gating region (Fig. 3.4).

The gating pulses are adjustable in time and can be used to monitor the secondary electrons corresponding to a single ion mass or can be scanned in time to collect all or part of the mass spectrum. The multiplied signal is then fed into electrometer units, covering the range 10^{-13} - 10^{-7}Amp, and displayed on strip-chart recorders. The electron packets which are not selectively removed are all collected by the scope anode located at the end of the gating region. These give rise to a series of voltage pulses across a resistor which are amplified and fed to the vertical plates of a Tektronix, Type 585A, oscilloscope whose horizontal sweep is synchronised with the ion-drawout pulse. The mass spectrum so displayed on the oscilloscope proved useful in preliminary investigations and for the rapid identification of negative molecule-ions using the time-of-flight adjust to affect neutral and ion separation.

The operating frequency of the spectrometer is variable from 10 to 100 KHz. The repetition cycle at 10 KHz is 100 μsec.

A 2 μsec. delay in ion drawout results from the lag between the electron beam pulse clearing the source and the ion drawout pulse switching on, leaving a useful spectrum time of 98 μsec. Using a 200 cm. drift-tube maintained at 2·8 KV, the useful mass range is 1200 a.m.u. At 100 KHz under the same conditions the useful spectrum time is 8 μsec. and the mass range is reduced to 6 a.m.u.

Variation of the drift-tube potential has a marked effect on the mass range and resolution attainable, the former decreasing and the latter increasing as the drift potential is reduced. The resolution of the time-of-flight Mass Spectrometer is defined as that mass, m, at which, when a peak of mass m + 1 of equal height is introduced, the peak height or amplitude of m will be increased by 1%. The dependence of resolution on the conditions described and on the adjustment of the ion optics gives rise to a variable resolution in the range 150 - 600.

During this work the operating frequency was normally maintained at 17 KHz resulting in an effective mass range of 500 a.m.u. and a resolution suitable for all requirements. The drift tube potential was maintained at 2·8 KV for the dissociative capture work and varied over the range 2 to 4 KV for the autodetachment studies.

(b) Detailed machine operation

The vacuum system was designed to maintain a background pressure in the flight tube sufficiently low as to preclude ion-molecule interactions and to minimise background ion

interference. The vacuum chamber pumping port is located in the flight tube 55 cms. from the source. The flight tube and ionisation chamber were pumped by an Edwards model ED150 mechanical pump backing an Edwards model 6M3A, three-stage, six inch mercury diffusion pump. The mercury partial pressure in the vacuum chamber is lowered by means of a liquid nitrogen trap mounted below the flight tube and supplemented by a refrigerated chevron baffle maintained at $-35^{\circ}C$. A bakeable molecular sieve, located between the forepump and the diffusion pump, serves to trap out harmful vapours before they reach the oil pump and to prevent fore-pump vapours contaminating the vacuum system. The fore-line pressure is measured with a Hastings thermo-couple gauge ($1 - 10^{-3}$ torr) and the drift tube pressure with a Veeco nude-filament ionisation gauge ($10^{-3} - 10^{-10}$ torr). With liquid nitrogen in the trap normal background pressures were in the range $1 - 4 \times 10^{-7}$ torr and in the range $2 - 5 \times 10^{-8}$ torr after overnight baking at $200^{\circ}C$.

Fig. 3.2 is an illustration of the ion source under normal operating conditions for negative ion studies. The electron beam is generated by thermionic emission from a short length (~0·8 cm.) of filament wire, heated by a DC current of 3 to 4 Amps, depending on the resistivity of the wire. Two different filament materials were used during the course of this work, 0·005" diam. tungsten wire being replaced in later work by 0·007" diam. rhenium wire. The rhenium wire was found to be more resistant to chemical attack (particularly by fluorocarbons), less effective for

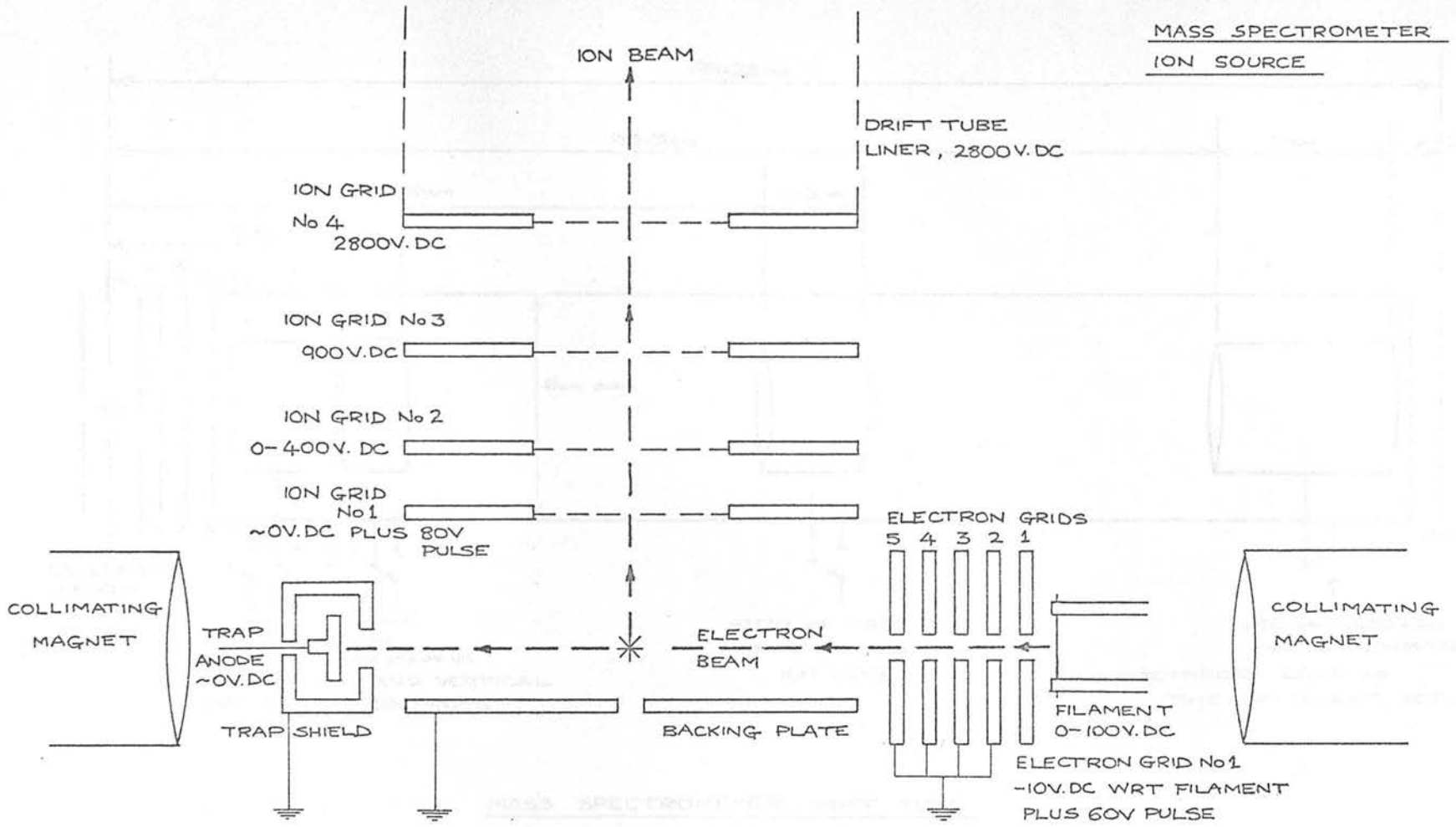
MASS SPECTROMETER
ION SOURCE
ION BEAM
DRIFT TUBE
LINER, 2800V. DC
ION GRID
No 4
2800V. DC
ION GRID No 3
900V. DC
ION GRID No 2
0-400V. DC
ION GRID
No 1
~0V. DC PLUS 80V
PULSE
ELECTRON GRIDS
5 4 3 2 1
COLLIMATING
MAGNET
TRAP
ANODE
~0V. DC
TRAP SHIELD
ELECTRON
BEAM
BACKING PLATE
FILAMENT
0-100V. DC
ELECTRON GRID No 1
-10V. DC WRT FILAMENT
PLUS 60V PULSE
COLLIMATING
MAGNET

Fig 3.2

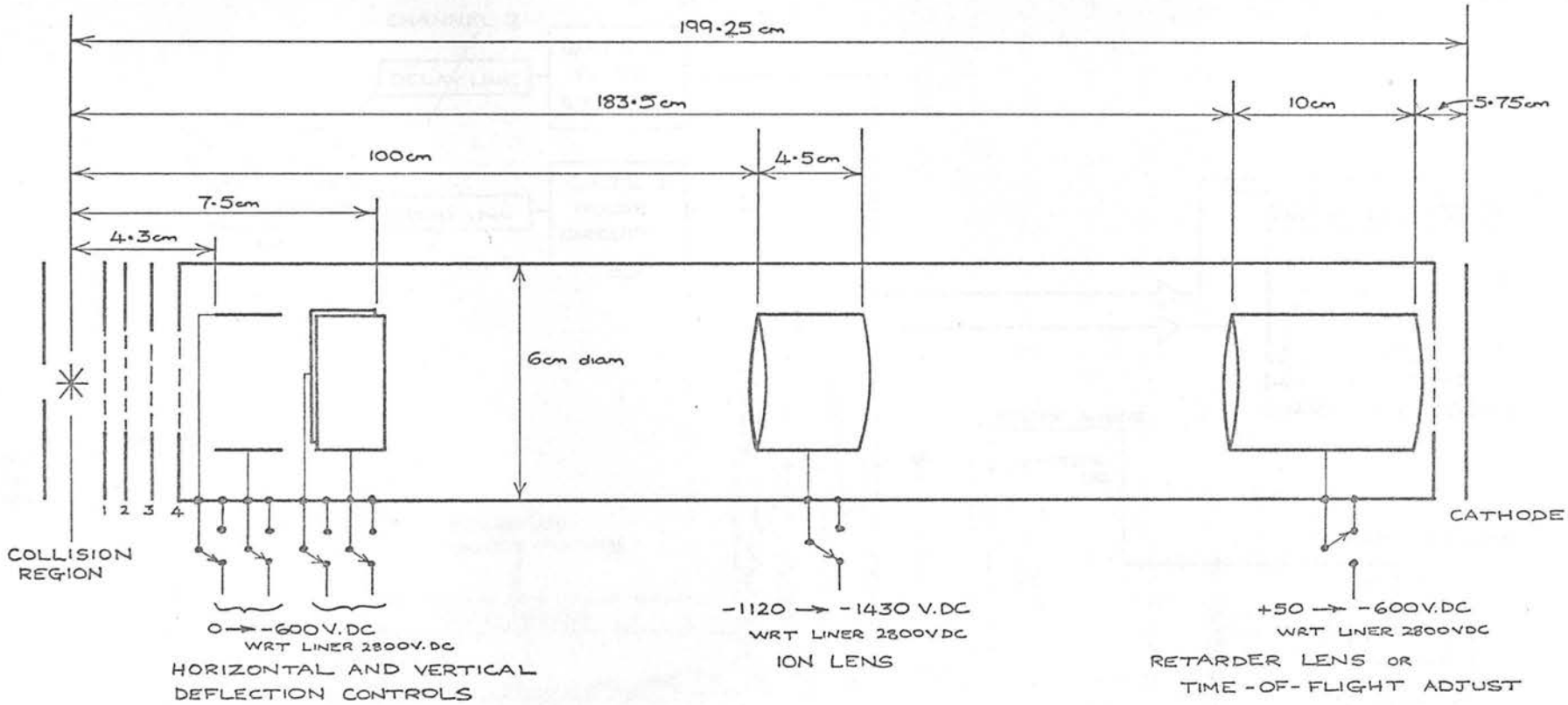

MASS SPECTROMETER DRIFT TUBE

Fig 3.3

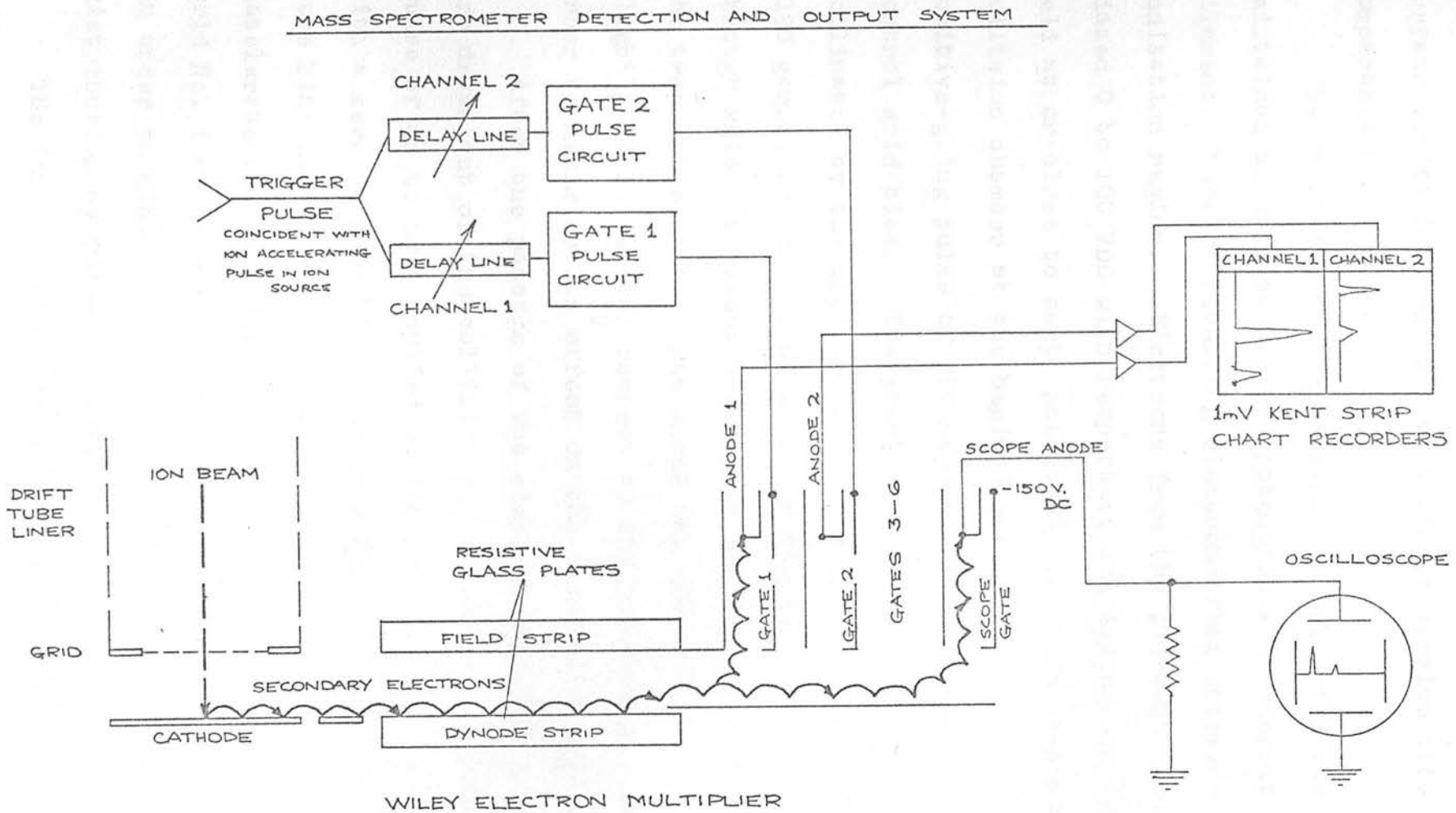
MASS SPECTROMETER DETECTION AND OUTPUT SYSTEM
CHANNEL 2
DELAY LINE
GATE 2 PULSE CIRCUIT
TRIGGER PULSE
COINCIDENT WITH ION ACCELERATING PULSE IN ION SOURCE
DELAY LINE
GATE 1 PULSE CIRCUIT
CHANNEL 1
CHANNEL 1
CHANNEL 2
1mV KENT STRIP CHART RECORDERS
ANODE 1
ANODE 2
SCOPE ANODE
-150V. DC
ION BEAM
DRIFT TUBE LINER
RESISTIVE GLASS PLATES
GATE 1
GATE 2
GATES 3-6
SCOPE GATE
OSCILLOSCOPE
GRID
FIELD STRIP
SECONDARY ELECTRONS
CATHODE
DYNODE STRIP
WILEY ELECTRON MULTIPLIER

Fig 3.4

surface ionisation and to have a longer service life under comparable conditions.

The first electron grid (the control grid) was normally maintained at a negative bias potential with respect to the filament, thereby preventing electrons from entering the ionisation region. Electrons from the filament, which was biased 0 to 100 VDC with respect to the ionisation chamber held at or close to earth potential, can only traverse the collision chamber at the beginning of each cycle when a large positive-going pulse of 250 nanoseconds duration overrides the control grid bias. The short pulse of electrons, collimated by the electron slits and a magnetic field of ~150 gauss, produces ionisation in the low pressure gas sample through which it passes before the electrons are collected at the trap anode. The trap anode was normally biased only slightly positive with respect to the ionisation chamber in order to minimise its effect on the electron energy distribution.

After the passage of the electron beam the ions produced are drawn out of the collision region by a positive-going pulse of up to 80 V applied to ion grid No. 1. Ion grid No. 2 with a zero to 400V bias, ion grid No. 3 with a 30% drift-tube bias and finally ion grid No. 4 with the drift tube bias accelerate the ions into the field-free drift-tube. Ion grid No. 1 was normally maintained at or near to zero bias in order to minimise its effect on the electron energy distribution by field penetration into the ion source.

The ion beam was collimated in the drift-tube by the ion optics and external compensating magnets situated at each end of the tube. The ion optics consist of; (i) horizontal

and vertical deflection plates situated close to the source end of the drift-tube (ii) an ion lens placed at the centre of the tube and (iii) a time-of-flight control positioned close to the detector and normally operated at the drift-tube potential. The time-of-flight control can be biased negative with respect to the drift-tube and serves to separate out the neutral and charged components of a short-lived species which may decay by electron detachment during flight. Fig. 3.3 illustrates the drift-tube and optics and shows the internal dimensions and the bias potentials operating for a +3KV drift potential.

The multiplier was normally operated at maximum gain for negative ion experiments but a much lower gain proved sufficient for positive ion work. The collection gate pulses were of variable height and width but they were normally operated with both at maximum thereby insuring that the electron packets were fully collected. However, this provided insufficient resolution for mass scans and measurements on the separated neutral and ion peaks of a molecule-ion when maximum resolution was required. In these circumstances minimum gate widths (200 n.sec.) were used resulting in a large increase in resolution at the expense of signal intensity. The 5V.DC full-scale output of the electrometer units was stepped down by simple potential dividing circuits to suit the maximum input of the Kent 1 mV potentiometric recorders.

After each filament replacement the electron beam was re-aligned using internal collimating magnets. The filament

bias was set close to maximum and magnet re-orientation achieved by holding large magnets against the source housing and gently tapping the housing with a rubber mallet until maximum trap current was registered on the microammeter. Trap currents in the range 1 to 2 μAmps were obtained, depending on the electron gun alignment, the filament material employed and the filament current.

The presence of stray fields in the source region (which would result in electron beam divergence) was shown to be negligible by insulating the trap anode shield from the source block and connecting it to an electrometer. This indicated that less than 1% of the electron beam failed to reach the trap anode. Switching on the high drift-tube voltage under these conditions had no effect on the electron beam collimation and can be taken to indicate the absence of serious field peak-through into the collision chamber.

When required, the trap current could be maintained constant over the energy range by means of a feedback loop circuit as follows: a small fraction of the trap current is sampled and used to adjust the filament current in order to maintain a set electron emission. At low electron energies, when an unfavourable bias on the filament prevents electrons entering the slit system, the filament current would continue rising to compensate for the declining trap current. Filament disintegration under these conditions is prevented by fixing the maximum level of filament current permissible. Under normal operating conditions, when the trap current was maintained as low as was consistent with reasonable ion

intensities, the upper limit imposed on the filament current was never reached. The selection of trap currents in the range 0·0025 - 0·05 μAmp allowed 'negative electron energies' up to 3 volts (achieved by inserting a mercury dry battery into the filament bias circuit) to be used in negative ion experiments without a serious increase in the rate of filament erosion. High trap currents (greater than 0·1 μAmp) were found to cause a substantial broadening of the electron energy distribution, as a result of space charge effects, and to increase filament erosion and surface ionisation due to the increased filament temperatures. Trap currents in the 0·1 μAmp region were only used for very low cross-section ions when all other methods for signal intensification had failed.

The ion drawout delay time was maintained at minimum for most of the work reported here, although the effect of increased ion residence in the source before drawout was investigated in relation to the autodetachment work. Ion grid No. 1 was permanently maintained at ~0V.DC bias and the pulse amplitude was normally operated at maximum. Slight changes in the pulse amplitude were required to maintain ion resolution for drift-tube potentials less than 3 KV when the beam becomes particularly vulnerable to energy defocussing which results from ion diffusion prior to drawout.

The bias on ion grid No. 2 was empirically adjusted to optimum signal and was usually close to the maximum value. The magnet assembly around the multiplier was adjusted to the position of maximum gain followed by realignment of the

compensating magnets. The source compensating magnets were varied in strength by the addition or removal of iron shims until all the masses in the spectrum peaked with the same potential applied to the ion vertical deflection plates in the flight tube. The multiplier compensating magnets were similarly treated, to produce simultaneous peaking of all masses on adjustment of the horizontal deflection plate potentials. Focussing was completed with the ion lens.

(c) The inlet system

The Bendix Model 1072 Heated Molecular Leak Inlet System used in this study is shown diagrammatically in Fig. 3.5. The complete gas-handling assembly is of stainless steel and is enclosed in a stainless steel oven bakeable to 220°C. Valves 2 to 12 are Hoke bellow valves containing teflon seats in stainless steel seat holders and valve 1 is a Hoke valve with teflon packing.

The gas line is pumped by a Welch rotary-vane mechanical pump (to 0·01 torr) backing a Consolidated Vacuum two stage water cooled oil diffusion pump (maximum 1×10^{-6} torr). The pressure is measured at D and E by Hastings thermocouple gauges and at F by a micromanometer sensor (up to 10 torr) feeding a Baratron type 77 meter reading to an accuracy of greater than $\pm 1 \times 10^{-2}$ torr. The Baratron compares pressures to 0·05% accuracy and is unaffected by ionisation, cooling characteristics of gases, vapours or mixtures. It measures accurately partial pressure and total cumulative pressure independent of gas composition. This proved particularly suitable in the relative capture cross-

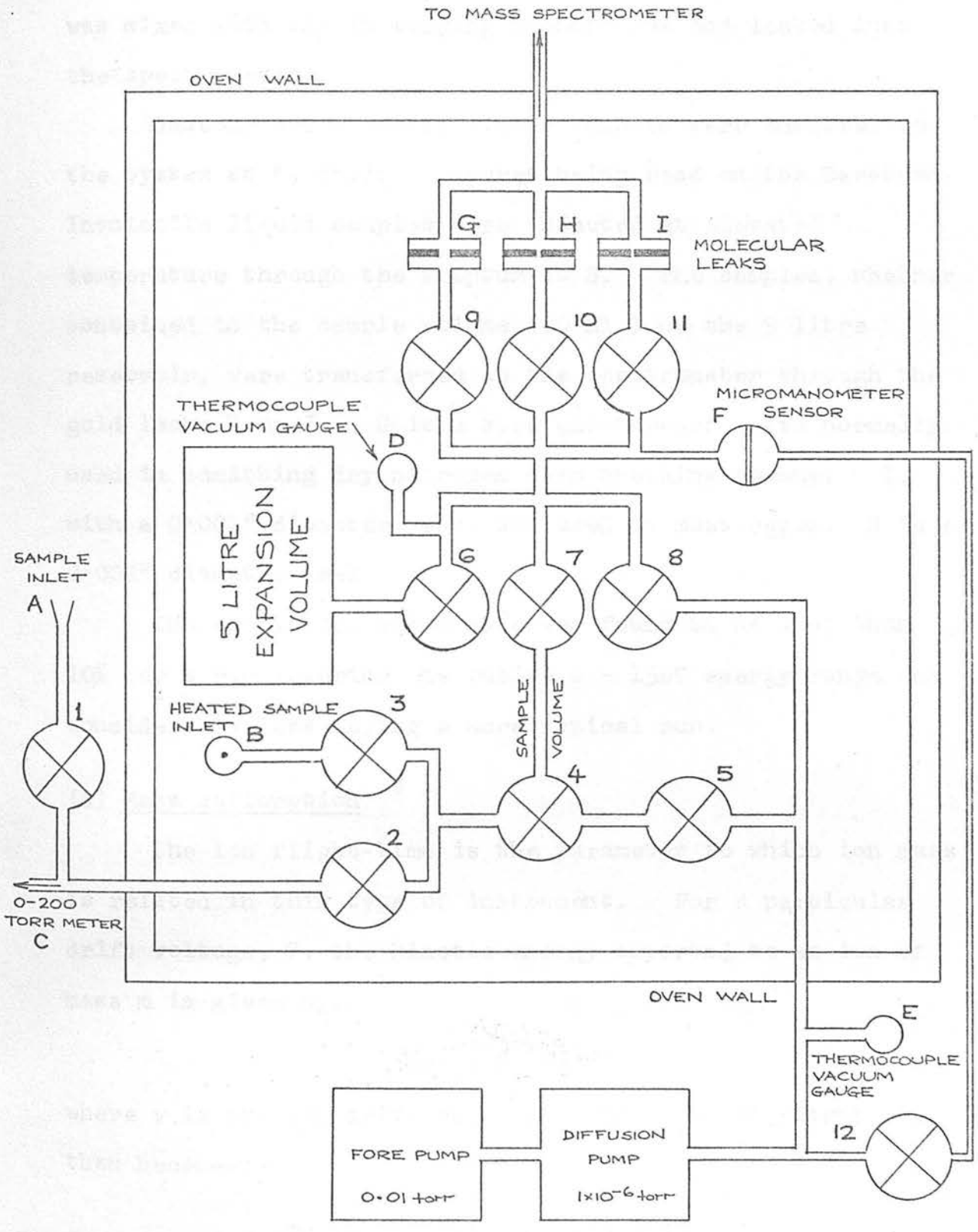

BENDIX HEATED MOLECULAR LEAK UNIT 1072

Fig 3.5

section measurements where the gas under investigation was mixed with SF_6 in varying proportions and leaked into the spectrometer.

Gaseous and volatile liquid samples were admitted to the system at A, their pressures being read on the Baratron. Involatile liquid samples were injected at elevated temperature through the sceptum at B. The samples, whether contained in the sample volume (80 ml.) or the 5 litre reservoir, were transferred to the spectrometer through the gold leaks H or I. G is a straight-through valve normally used in admitting dry nitrogen when breaking vacuum. I, with a 0·001" diameter leak, was used in most cases. H is a 0·002" diameter leak.

The sample depletion rate was found to be less than 10% for a run covering the entire 0 - 15eV energy range and considerably less during a more typical run.

(d) Mass calibration

The ion flight-time is the parameter to which ion mass is related in this type of instrument. For a particular drift voltage, V, the kinetic energy imparted to an ion of mass m is given by:-

$$\tfrac{1}{2}mv^2 = V$$

where v is the ion drift velocity. The time of flight, t, then becomes:-

$$t = \left(\frac{md^2}{2V}\right)^{\frac{1}{2}} = (Km)^{\frac{1}{2}} \quad \text{where } K = \frac{d^2}{2V} \quad \ldots\ldots\ldots (20)$$

where d is the drift-tube length.

If the ion flight time is read directly from an oscilloscope, whose horizontal sweep is synchronised with the ion drawout pulse, then a value of t is obtained which is slightly in error by the time required for the secondary electrons to traverse the multiplier. The straight line plots resulting from a series of measurements repeated at each drift potential provided the values of K required for further mass identification and indicated the insignificance of the multiplier traverse-time contribution.

The alternative method used for mass identification was the construction of a calibration curve for known ions against the mass selector (potentiometer) value. This proved to be both rapid and reliable to 200 a.m.u. after which, in the 200 - 300 a.m.u. range, the rapidly flattening curve provided identification to within $\pm$ 1 a.m.u. and $\pm$ 2 a.m.u. up to 350 a.m.u.

(e) Experimental procedure for mass scans and ionisation efficiency runs.

The multiplier gain was set to maximum, the drift voltage switched on, the electron energy set to 70 volts and the filament current increased to provide a trap current of ~1 μAmp. The sample was fed into the inlet system reservoir to a pressure of between 5 and 10 torr and then leaked into the spectrometer to a drift tube pressure of approximately 5×10^{-6} torr. After the initial focussing procedure the gate pulses were used to locate the ions which were also, in most cases, visible on the oscilloscope. This was followed

by careful focussing of the mass range under investigation and a scan of the spectrum with the gate pulse adjusted to minimum width and the electrometer sensitivity set to register the most abundant ion on scale. The second gate, lagging the first, was used to simultaneously scan the spectrum at a different sensitivity, this procedure being repeated until all ions in the spectrum had been intercalibrated. The relative abundances of the ions were then calculated by measuring the ion peak heights from the scans performed and then normalising to the most abundant ion from a calibration of the sensitivity factors between settings on the electrometers.

Ions selected for energy dependence studies were examined simultaneously using the two available output channels of the electrometers. The most abundant ion was employed as an internal reference and run against all the other ions in the system. The calibration gas was then admitted to the reservoir, the partial pressure being that required to form the calibrant ion with an abundance approximately equal to that of the internal reference used for the energy scale calibration. The energy scale, so calibrated, was usually cross-checked against several ions, especially for those systems in which a substantial spread in appearance potentials was found. This method of internal reference served as a safeguard against any interactions between the sample and calibrant gases which may result in spurious structure. Interactions of this kind were found to interfere to a significant extent in the use of SO_2 for the calibration of the organic systems as a result of charge transfer reactions

between the O^- ion and various organic fragment ions of higher electron affinity. The drift tube pressure was maintained below 1×10^{-5} torr and so precluded such interactions in these systems.

The ions to be investigated were located with the gate pulses and the electron energy decreased to the dissociative resonance capture region of the energy scale. The trap current was switched to the regulated mode and adjusted to the minimum value consistent with a reasonable ion current. Because of the small trap currents employed in the regulated mode (~0·005 μAmp compared to 1 μAmp on the manual position) only those ions with high capture cross-sections could still be seen on the oscilloscope. A scan over the energy range of interest provided a rough idea of the signal intensity to be expected. In order to include the complete resonance peak for ions resulting from thermal or near thermal electron capture a mercury battery (2·6V) was used to bias the filament 'positive' with respect to the source block.

The electron energy was set several volts below the first resonance and the detector sensitivity switched two orders of magnitude above the resonance maximum signal. Using a Solartron LM1620 digital voltmeter to read the electron energy the energy range was examined in 0·1eV increments. The straight line, corresponding to each energy increment, traced out by the recorder depended on the sensitivity range in use, considerable background noise appearing in the lines during use of the 10^{-12} Amp range. This required longer chart running times for the higher

sensitivities, two minutes, at a chart speed of one inch per minute, usually being sufficient to establish the average trace. The ranges above 10^{-10} Amp gave rise to smooth noise-free lines. When electrometer range changes were required, the ion current measured before and after the change provided intercalibration of the ranges. In practice, it was found that the electrometer range multiples (x 2 and x 5) of the instrument were not always the most suitable for accurate measurement and so the gating pulse height was adjusted to provide further signal control. In order to prevent interference between the collecting pulses this method was not employed during the examination of two signals in close proximity, i.e. separated by less than 4 a.m.u.

The charts were analysed by averaging the trace values for each energy increment and measuring the height above the base-line followed by normalisation to the resonance peak maximum. A graph of the normalised ion current against electron energy (ionisation efficiency curve) was then constructed (see Figs. 3.7, 3.8(a) and 3.9(a)).

Each run was repeated at least three times and more often in the case of noisy signals or the presence of uncertain structure.

(f) Experimental procedure for relative attachment cross-sections

The determination of absolute attachment cross-sections involves the measurement of the parameters in the expression:[97]

$$\frac{I_i(E)}{I_e(E)} = \rho.L.\sigma_a(E)$$

where $I_i(E)$ is the ion current generated by single electron

impact, $I_e(E)$ is the current of bombarding electrons of energy E, ρ is the number density of the target gas in the collision region, L is the collision path length over which the measured ion current is collected and $\sigma_a(E)$ is the attachment cross-section for electrons of energy E.

The simple design and linear construction of the total ionisation tube, first introduced by Jones[98] and used for the classic measurements of Smith[99] and Tate and Smith[100] on the inert gases, H_2, N_2, O_2, CO, NO and Hg, has proved to be very successful in this field. A precise knowledge of all the instrument dimensions, the use of accurately known magnetic fields to collimate the electron and ion beams and the location of pressure sensing devices close to the ionisation region resulted in accurate determinations for all the parameters in equation (21). For the present study such determinations were neither practicable nor convenient, the main difficulties arising in the determination of ρ and L. The pressure and temperature conditions in the ionisation region were not known accurately and the effect of contact potentials and the electron energy distribution on the helical path of the electrons were also unknown. However, relative attachment cross-sections, for which a knowledge of $I_e(E)$, ρ and L is not required, could be satisfactorily determined from gas mixtures of the molecule under investigation and another molecule of known cross-section.

Sulphur hexafluoride, which has a large attachment cross-section, was chosen as the reference due to its chemical inertness and the large number of cross-section determinations

reported in the literature. Some of these values, and the methods used, for thermal electron capture by SF_6 are given in Table 3.1.

Table 3.1. $\sigma_a(SF_6)$

σ_a cm.^{2}	Method
$1{\cdot}3 \times 10^{-15}$ (at max.)	Total ionisation[84] (1964)
$3{\cdot}6 \times 10^{-15}$ (average)	Swarm beam[37] (1966)
$2{\cdot}6 \times 10^{-14}$ (average)	Microwave[101] (1966)
$\sim 2 \times 10^{-14}$ (average)	Flowing afterglow[13] (1970)
$1{\cdot}17 \times 10^{-14}$ (0·05eV)	Swarm beam[35] (1971)

The value of $\sigma_a = 1{\cdot}17 \times 10^{-14}$cm.^{2} for the capture of thermal electrons (0·05eV) by SF_6 reported by Christophorou et al.[35] was arbitrarily selected as the standard cross-section and all other values were calculated relative to this using the expression:

$$\sigma_M = \sigma_{SF_6} \left(\frac{P_{SF_6} \cdot I_{M^-}}{P_M \quad I_{SF_6^-}}\right) \quad \ldots\ldots\ldots\ldots \quad (22)$$

where σ_{SF_6} and σ_M are the cross-sections for thermal electron capture by SF_6 and M respectively, P_{SF_6} and P_M are the partial pressures of SF_6 and M in the mixture and $I_{SF_6^-}$ and I_{M^-} are the respective ion currents at the resonance maxima under the same source conditions, i.e., L and I_e.

The capture peak of the ion under investigation was compared to that for SF_6^- being examined simultaneously using the second analog output scanner. Provided that the condition of coincident peak maxima was satisfied the initial

rough mixture of gases was replaced by a mixture of known composition to produce signals of approximately equal intensity. The gases were leaked into the spectrometer to a drift tube pressure not exceeding 2×10^{-6} torr when the mean free path of the molecules is much greater than the instrument dimensions thus precluding anomalous effects from molecular interactions. With the regulated trap current adjusted to maintain a reasonable ion current and the electron energy fixed at the coincident resonance maxima, the ion retarder lens was switched to maximum. The resolved ion and neutral peaks from each parent ion were then scanned simultaneously with the gating pulses adjusted to the minimum width. The sum of the ion and neutral peak heights for each parent ion then gives a measure of the numbers of each parent ion leaving the collision chamber, I_{M^-} and $I_{SF_6^-}$. Non-use of the ion-retarder lens resulted in a partial resolution of the two components (brought about by the discriminative focussing of the ion beam by the optics) so introducing a source of uncertainty into such measurements. It has been assumed that equal detector sensitivity to the components in the mixture prevails over the mass range investigated, 100 - 350 a.m.u.

Although the real ion intensity is represented by the area enclosed by the peaks, time consuming measurements, carried out with a planimeter, showed only a 3% difference in the peak height ratios. The measurement of peak heights was therefore adopted.

Repetition of this procedure for equal partial pressures and also for the attachment of secondary electrons, generated

at high electron energies, gave results in agreement with those obtained for equal signal strengths which were generally reproducible to within ± 25% for source pressures less than 2×10^{-6} torr. Variation of some cross-sections, found for pressures greater than 2×10^{-6}torr, were presumably the result of charge transfer interactions in which the electron affinity of the molecules play a decisive role. Such cases are discussed in Chapter 4.

(g) Experimental procedure for autodetachment lifetimes.

Average autodetachment lifetimes were determined using the method first devised by Edelson et al.[2] The experimental arrangement adopted in this study is shown in Fig. 3.6 and the drift tube dimensions and the retarder lens operating potential given in Fig. 3.3.

Negative parent ions, formed in the ion source as a result of either primary electron capture at thermal electron energies or secondary electron capture at high energies, are accelerated into the drift tube with a variable kinetic energy. If,during passage along the tube, some of the metastable ions undergo autodetachment both the remaining ions and the neutrals formed will continue moving at the same velocity and reach the detector simultaneously, so that they are registered as a single ion packet. If, however, a retarding potential is applied some time after the ions enter the drift tube then the ion packet will be slowed down and the neutrals will pass on unaffected. The detector will therefore respond to two packets separated in time. Variation of the ion drift

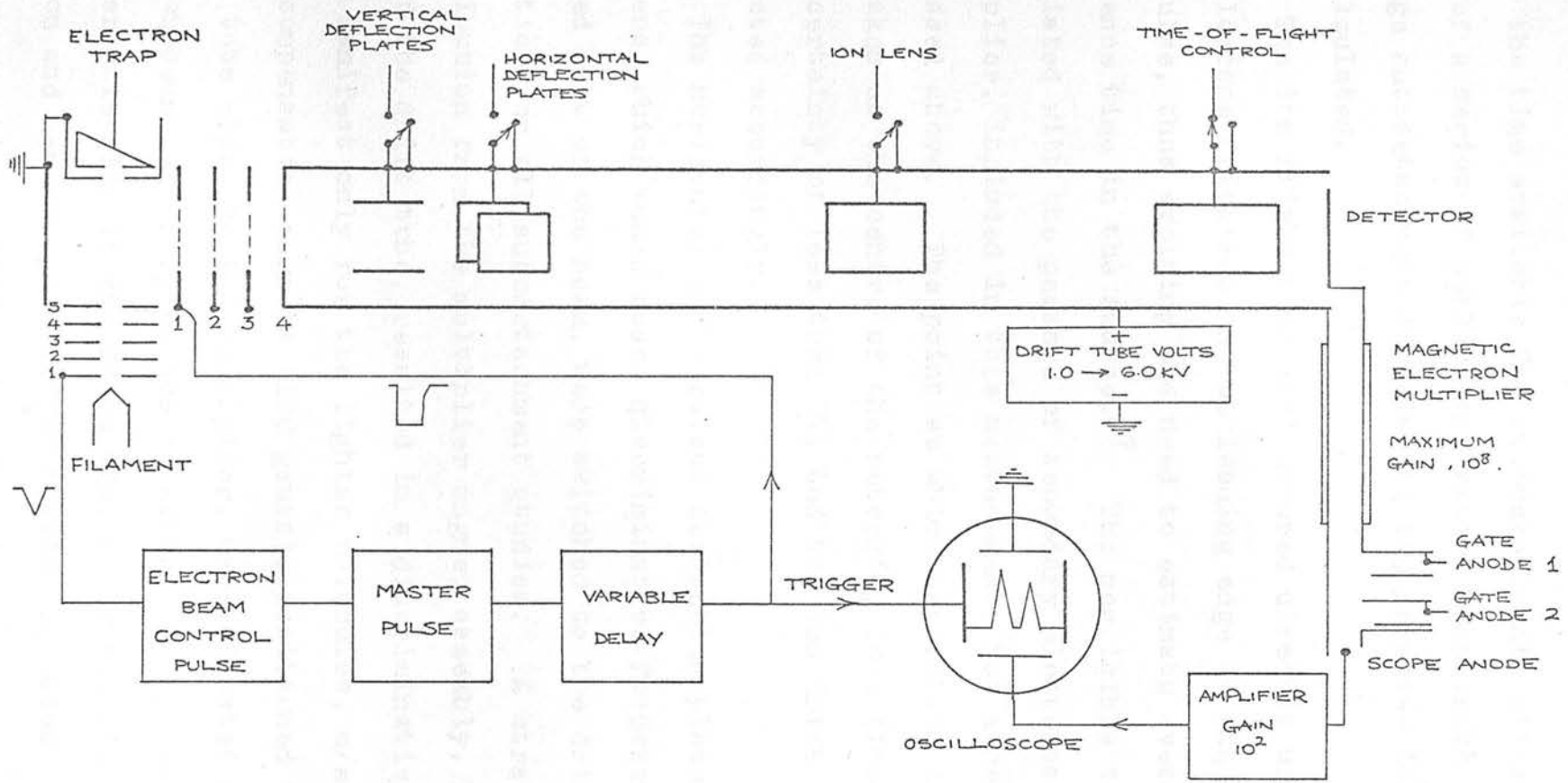

EXPERIMENTAL ARRANGEMENT FOR AUTODETACHMENT STUDIES

Fig 3.6

time, the time available for autodetachment, allows measurement of a series of peak height ratios from which the average autodetachment lifetime of the negative ion state can be calculated.

The ion flight time was measured directly using an oscilloscope triggered on the leading edge of the ion draw-out pulse, thus avoiding the need to estimate average residence time in the source.[37] The negligible time associated with the passage of secondary electrons through the multiplier, included in this measurement, has already been discussed above. The point at which separation is achieved was taken as the centre of the retarding lens (introducing an uncertainty of less than 3%) and the ion drift times were corrected accordingly.

The horizontal and vertical deflection plates and the ion lens, which would cause discriminative focussing of the charged part of the beam, were switched to the drift tube potential for all autodetachment studies. A stray field contribution from the multiplier magnet assembly, bathing the end of the drift tube, resulted in a discriminative effect being manifest only for the lighter molecules, m/e < 150. Weak compensating magnets (100 gauss), positioned on the drift tube close to the multiplier, were adjusted to optimise the ion beam intensity at the detector although for the heavier molecules it was found that no detectable change in the ion and neutral peak height ratios was noted even when the compensating magnets were removed.

After leaking the sample gas into the spectrometer, to

a drift tube pressure not exceeding 2×10^{-6} torr, the apparatus was adjusted as described above and the resolved charged and neutral peaks scanned with the gating pulse on minimum width. The scans were repeated ten to twelve times, first with the trap current regulated at the resonance peak maximum then for secondary capture at 70 volts. This procedure was repeated for all the drift potentials consistent with adequate resolution of the peaks. These measurements revealed no discrepancies between the lifetime at zero volts and 70 volts. Because of increased ion intensities and enhanced filament lifetime, resulting from regulated trap current operation at high electron energies, ions of low capture cross-section were examined exclusively at high energy and no additional errors are anticipated in these results.

The following first order decay law was used to calculate the average autodetachment lifetime (the analogy with the decay of unstable nuclear species is obvious):

$$N_t^- = N_0 \exp(-t/T_a) \quad \ldots\ldots\ldots\ldots \quad (23)$$

where; N_t^- is the number of ions surviving autodetachment after time t.

N_0 is the original number of ions undergoing acceleration and is equal to $N_t^- + N_t^0$, where N_t^0 is the number of neutrals formed as a result of autodetachment after time t.

T_a is the average autodetachment lifetime.

T_a was determined by two methods: (i) direct substitution of N_t^-, $N_0 = N_t^- + N_t^0$ and t into equation (23)

for each drift potential used and (ii) from the reciprocal slope of the plot:

$$\ln(1 - \frac{N_0}{N_t}) \text{ vs. } t$$

determined after a least squares fit of the data. The value, T_a(slope), obtained from this plot, was calculated only in the cases for which three or four drift potentials were used and resulted in complete agreement with $\bar{T}_a$, obtained by direct substitution. This agreement, and the convergence of the straight line plots to the origin, justifies the use of equation (23) and may be taken to indicate that the possible sources of error listed below were not significant in this study:-

(i) Electron detachment by the grids in the path of the ion beam. Compton et al.[37] have shown this to be negligible in similar spectrometers.

(ii) Spontaneous or collision-induced dissociation of the parent negative ions in the drift tube should be negligible. No evidence for spontaneous dissociation of the long-lived negative ions, manifest as fragment peaks slightly displaced from the parent ion peak, was found in this study; collisional stabilisation is too infrequent at the drift tube pressures used ($< 2 \times 10^{-6}$ torr) to affect measurements.

(iii) Collisional detachment and charge transfer in the drift tube should be negligible. These processes were precluded by the use of low pressures, however, experiments with SF_6 indicated the increasing significance of

collisional detachment for drift tube pressures above 1×10^{-5} torr. This resulted in a decrease in the lifetime of SF_6^-, e.g. $T_a = 68$ μsec. for $P = 2 \times 10^{-6}$ torr and $T_a = 60$ μsec. for $P = 5 \times 10^{-5}$ torr.

(iv) The detector sensitivity to charged and neutral particles of the same kinetic energy should be equal. This is partially fulfilled through single-pulse counting techniques.[37] Agreement between $\bar{T}_a$ and T_a(slope), calculated over the drift potential range 2 - 4 KV, indicates that attractive or repulsive effects operating on the ion beam as it approaches the target or a contribution from the extra electron to the secondary electron current are negligible in this study.

With the exception of those ions for which isotope effects or low molecular weight restricted resolution to one drift tube potential or were of exceptionally low cross-section, the autodetachment lifetimes were reproducible to better than ± 10%.

(h) Data processing and energy scale calibration

Electron beams generated from heated filaments possess a Maxwell-Boltzmann distribution of energies of 1 to 2eV. Consequently, when such a beam is used to ionise a gas, the appearance potentials become smeared out and any fine structure in the ionisation efficiency curves is obscured. Early attempts to resolve this problem met with limited success but fine structure in the ionisation curves of some positive ions was observed. Nottingham,[38] using a magnetic

selector observed fine structure in the ionisation efficiency curves of Hg^+. Sugden and Price[39] employed a photoelectron beam in the study of a group of aldehydes and ketones and Clarke[40] obtained a beam spread of 0·2eV using a 127° electrostatic selector enabling fine structure in the curves of N_2^+ and N^+ from nitrogen to be observed.

Two types of velocity selectors have received attention in recent years. Parallel-plate selectors, of the type used by Hutchison,[41] suffer from poor transmission which, although tolerable for positive ion investigations, is unsuitable for negative ion studies. The 127° electrostatic selector, however, was improved by Marmet and Kerwin[42] who obtained a beam of 10^{-7} Amp with an energy spread of 0·02eV. This selector was successfully applied by Marmet and Morrison[43] and the difficulties they experienced have now been largely overcome in the advanced design of Brion et al.[44]

The most widely employed method is the Retarding Potential Difference (R.P.D.) technique of Fox et al.[45] In this, an extra slit, the retarding electrode, is added to the conventional electron gun and is biased slightly negative (~0·5eV) with respect to the filament resulting in a sharp, low energy cut-off in the beam profile. This bias is then increased by a small amount ΔV (typically 0·1eV), resulting in the removal of a further energy slice of width ΔV. The resulting change in ion current Δi, which occurs when ΔV is applied, is then attributed to the band of electrons homogeneous in energy to within ΔVeV.

Significant improvements by Cloutier and Schiff[46] and later by Stockdale, Compton and Reinhardt[47] have removed the tedium from R.P.D. operation. Stockdale et al.[47] applied a modulated voltage to the retarder slit and the current of mass identified ions was de-modulated using a lock-in amplifier allowing a continuous recording of difference ion current as a function of electron energy with an energy resolution of ~0·1eV.

Although the R.P.D. approach provides a simple method for obtaining a quasi-monoenergetic electron source frequent ambiguities arise in data interpretation. Marmet[48] has pointed out that, once past the retarder slit, the sharp energy cut-off in the electron beam may undergo complete or partial relaxation as a result of space charge effects. The ionisation efficiency curves would then be compounded of the true curve plus some unknown fraction of its derivative. Anomalous effects, including negative difference currents, first reported by Fox et al.,[45] non-linear variation of ion signal with electron energy and spurious maxima in ionisation efficiency curves noted by Frost and McDowell,[49,50] and resonance focussing described by Simpson,[51] have all been attributed to maladjusted source potentials and poor magnet alignment. These anomalies are discussed by Gordon, Haarhoff and Krige[52] in terms of a theoretical model developed for the R.P.D. gun. They conclude that the basic capabilities of the R.P.D. technique have been exceeded in the past and suggest a modified technique for tuning an R.P.D. gun for optimum operation.

Despite the modifications introduced, R.P.D. still requires long and careful adjustment to the ion source and suffers from a low signal to noise ratio that imposes a limit on the negative ion studies which can be reasonably undertaken.

Another approach has been the use of analytical methods to remove or reduce the energy spread of the beam. Morrison,[53] who applied this technique to positive ion formation showed, from tests on several artificial examples and two actual cases, that the method was promising and suggested structure in the ionisation efficiency curves of the inert gases and oxygen. Morrison considered two methods for the deconvolution operation each possessing some advantages and disadvantages. The first method which used the iterative equations of van-Cittert,[102] results in a rapid convergence to the correct solution but is unsatisfactory when the initial function, i(V), contains regions of uniform amplitude or the solution, I(E), contains abrupt changes in level. The second method, using Fourier transforms, can result in unpredictable noise amplification which does not influence the entire curve to the same extent. In both cases iterative smoothing of the original function was found to be essential to the recovery of quantitative data.

Ioup and Thomas[54] investigated the relative merits of these two methods and found the iterative (Morrison - van-Cittert) method preferable for the analysis of data which may be noisy and for the cases in which the position of the function on the energy axis is required. The Fourier method

proved particularly suitable to the treatment of very smooth data but single stage unfolding was found to result in a sudden, disastrous increase in the noise level. Deconvolution by the iterative method is accompanied by a gradual build up of noise with each successive step, termination before the noise becomes restrictive is then possible. Similar conclusions as to the superiority of the iterative approach over Fourier transforms had been arrived at in the course of the unfolding of negative ion data by MacNeil and Thynne. These authors[55] carried out exhaustive tests on the reliability of this method using both artificially constructed functions and real systems. Besides an accurate recovery of appearance potentials, resonance peak maxima and peak widths they also found that the amount of random noise which could be introduced into the artificial systems without an adverse effect or data recovery far exceeded that expected in data acquisition.

This method of data analysis was used exclusively in this work, the computer programmes written by MacNeil[113] being used to perform the iterative smoothing and deconvolution procedures. A summary of the Morrison - van-Cittert method as applied in this study is as follows:-

Thermionically emitted electrons possess an energy distribution such that the probability of an electron having an energy in the range U to U + ΔU is given by m(U), where:

$$\sum_{U=0}^{\infty} m(U)\Delta U = 1 \quad \ldots\ldots\ldots \quad (24)$$

Before impact the electrons are accelerated by a

potential difference V, and emerge from the electron gun with an energy E, where E = U + V. If the probability for the formation of a particular ion by an electron of energy E is a function of E, namely I(E), then the probability for formation of the ion by a beam of electrons of nominal energy V, is i(V) where:

$$i(V) \propto \sum_{U=0}^{\infty} I(V+U)\, m(U)\Delta U \quad \ldots\ldots \quad (25)$$

The experimental procedure is to sample the ion current i(V) at equal intervals of V and to find the corresponding values of I(E), which satisfy equation (25).

When the electron energy distribution m(U) is known at the same intervals of energy, and i(V) and m(U) are bounded by zero at the upper and lower ends of the energy range, it is possible to obtain unique solutions for I(E) at comparable intervals in E.

The method of van-Cittert is used for this solution:

$$I(E)_{calc(n+1)} = I(E)_{calc(n)} + i(V) - \sum_{U=0}^{\infty} I(E)_{calc\ n}\, m(U)\Delta U \quad (26)$$

where the set of iterative equations tends to I(E) as n increases.

This method takes a trial function for I(E), convolutes with the electron energy distribution and compares the results with the original i(V). The difference is then used as a correction to the trial functions and the procedure is repeated. The original trial function used is the set of i(V) itself, i.e. when n = 0,

$$I(E)_{calc(n)} = i(V)$$

However, if this process is applied to actual experimental data, the solution obtained for I(E) is almost so obscured by noise as to be effectively useless. Smoothing of the original data is necessary before the deconvolution operation may be performed. The following iterative process removes the random scatter very effectively:

$$i(V)_{calc(1)} = \sum_{U=0}^{\infty} i(V)_{obs}\, m(U)\Delta U.$$

$$i(V)_{calc(n+1)} = i(V)_{calc(n)} + \sum_{U=0} [i(V)_{obs} - i(V)_{calc(n)}]m(U)\Delta U \quad \ldots\ (27)$$

In addition, if at any stage in these operations (26) and (27), I(E) goes negative then it may be set equal to zero.

Empirical testing of the number of smoothing and unfolding operations needed to obtain good quality data showed that 15 smoothing and 20 unfolding iterations enabled satisfactory recovery of appearance potentials, resonance peak maxima and peak widths to be made from the basic experimental data.

The uncertainty in the determination of the onset of ionisation caused by the 'smearing' effect of the electron energy distribution has been largely removed by the deconvolution technique described. However, the electron energy scale must be reliably established before accurate appearance potential data can be obtained. The ideal situation of a field-free ionisation region is impossible to realize in practice. Contact potentials and electric field penetration into the source region results in a discrepancy between the electron beam energy displayed on the voltmeter and the real energy of the beam. Accordingly, the energy scale was calibrated using ions with known appearance potentials.

Three separate calibrants were used to establish the energy scale for negative ion studies; the SF_6^- ion from SF_6, the O^- ion from SO_2 and the O^- ion from CO. The positive ion data were calibrated using the spectroscopically determined appearance potential for A^+/Argon[15] (15·76eV) or CO^+/CO (14·01eV).[23]

Sulphur hexafluoride has been the subject of many mass spectrometric investigations.[1,6,7-13] Using the R.P.D. technique, with the energy scale calibrated by electron retarding curves, Hickham and Fox,[9] and later Fox and Curran,[11] showed the SF_6^- ion to onset at zero energy and the SF_6^- peak profile to reflect the electron energy distribution. Later work by Stamatovic and Schulz[34] has shown that the SF_6^- resonance width still reflects the electron energy distribution for a velocity selected electron beam of 0·02eV width.

The resonance threshold at 0·0eV for SF_6^- ion formation[9,11] was taken as an energy scale reference point in this work and the electron attachment cross-section profile, reversed on the energy scale, provided the electron energy distribution used in the deconvolution procedure. The direct and deconvoluted SF_6^- capture peak observed with this instrument are shown together in Fig. 3.7. The unfolded curve shows an onset at 0·0eV (calibration point), a peak width of 0·4eV at half height and a base line width of 0·8eV.

Schulz[61] has remarked that the energy scale established with SF_6^- may, under certain conditions, be erroneous. Alinearity of the potential distribution along the path of the electron beam (from contact potentials or field

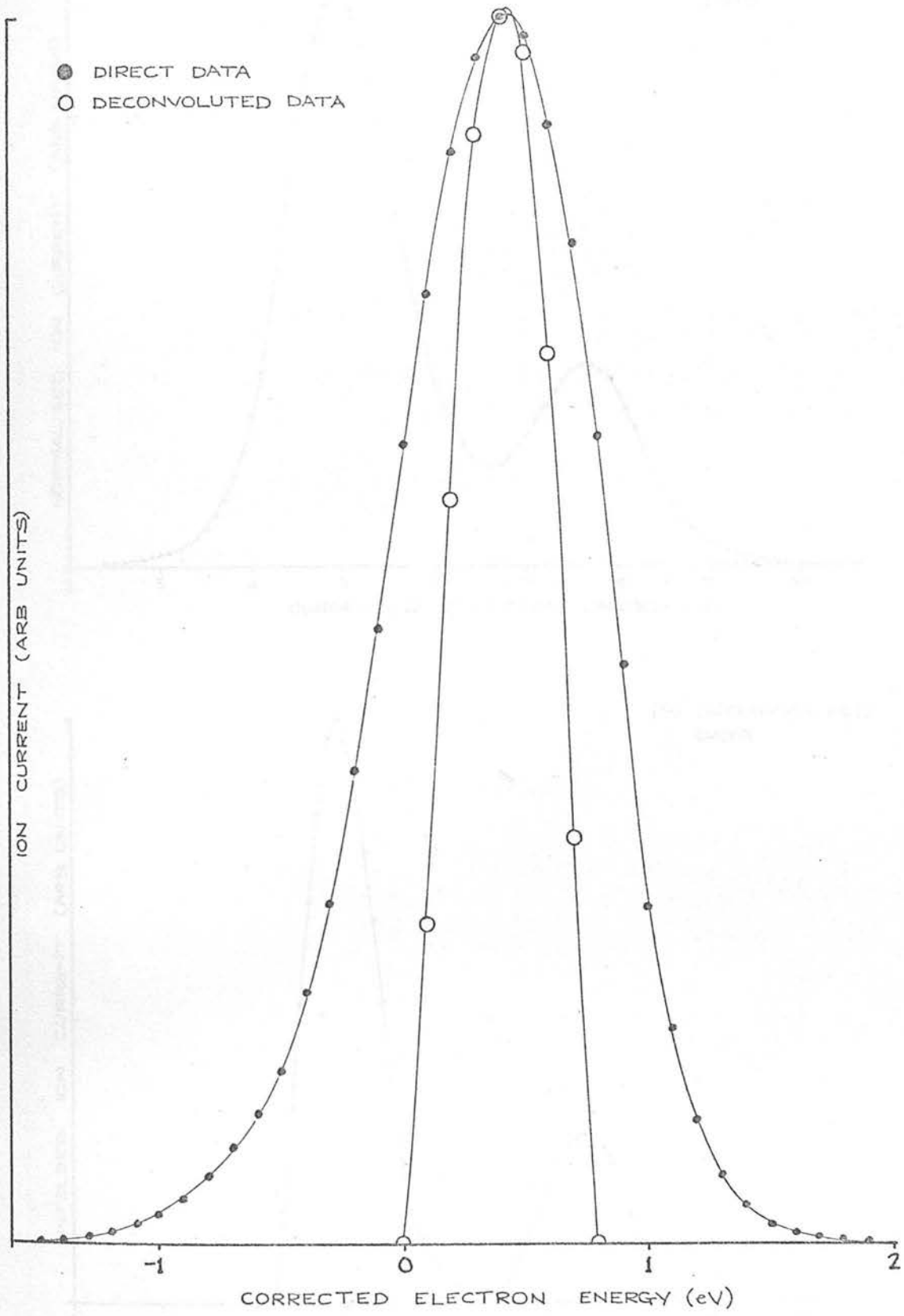
SF_6^- / SF_6
DIRECT DATA
DECONVOLUTED DATA
ION CURRENT (ARB UNITS)
-1
0
1
2
CORRECTED ELECTRON ENERGY (eV)

Fig 3.7

O^- / SO_2

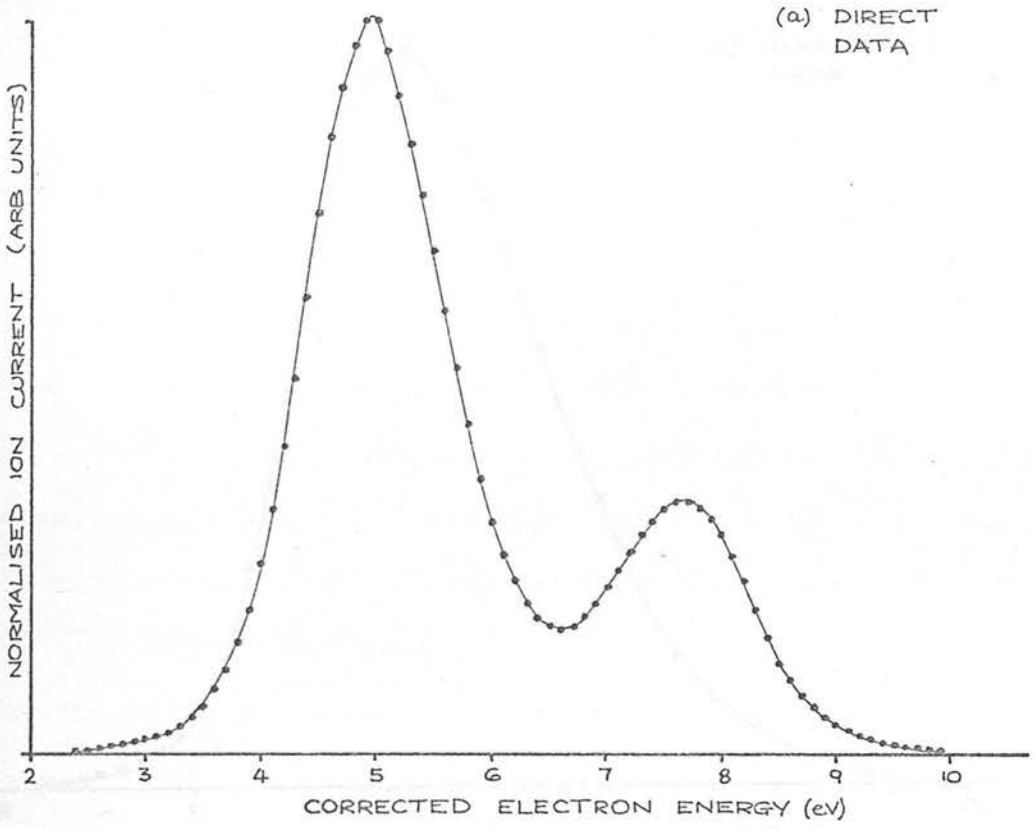
(a) DIRECT DATA
NORMALISED ION CURRENT (ARB UNITS)
2
3
4
5
6
7
8
9
10
CORRECTED ELECTRON ENERGY (eV)

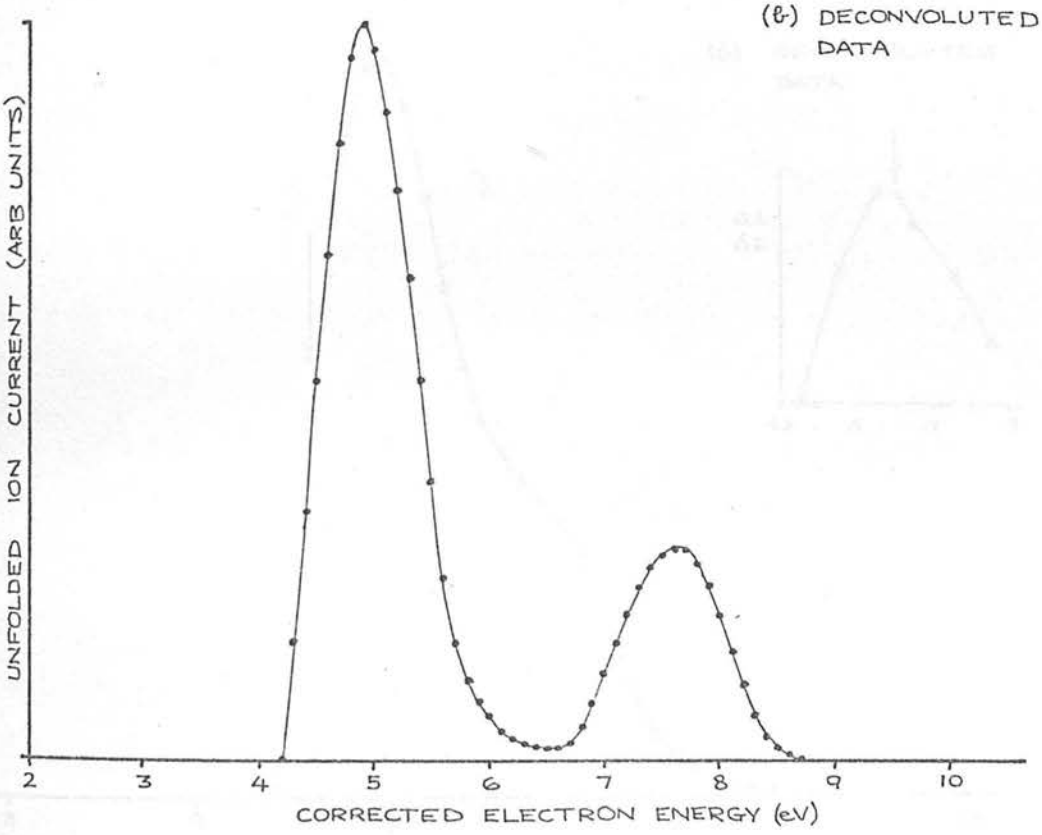
(b) DECONVOLUTED DATA
UNFOLDED ION CURRENT (ARB UNITS)
2
3
4
5
6
7
8
9
10
CORRECTED ELECTRON ENERGY (eV)

Fig 3.8

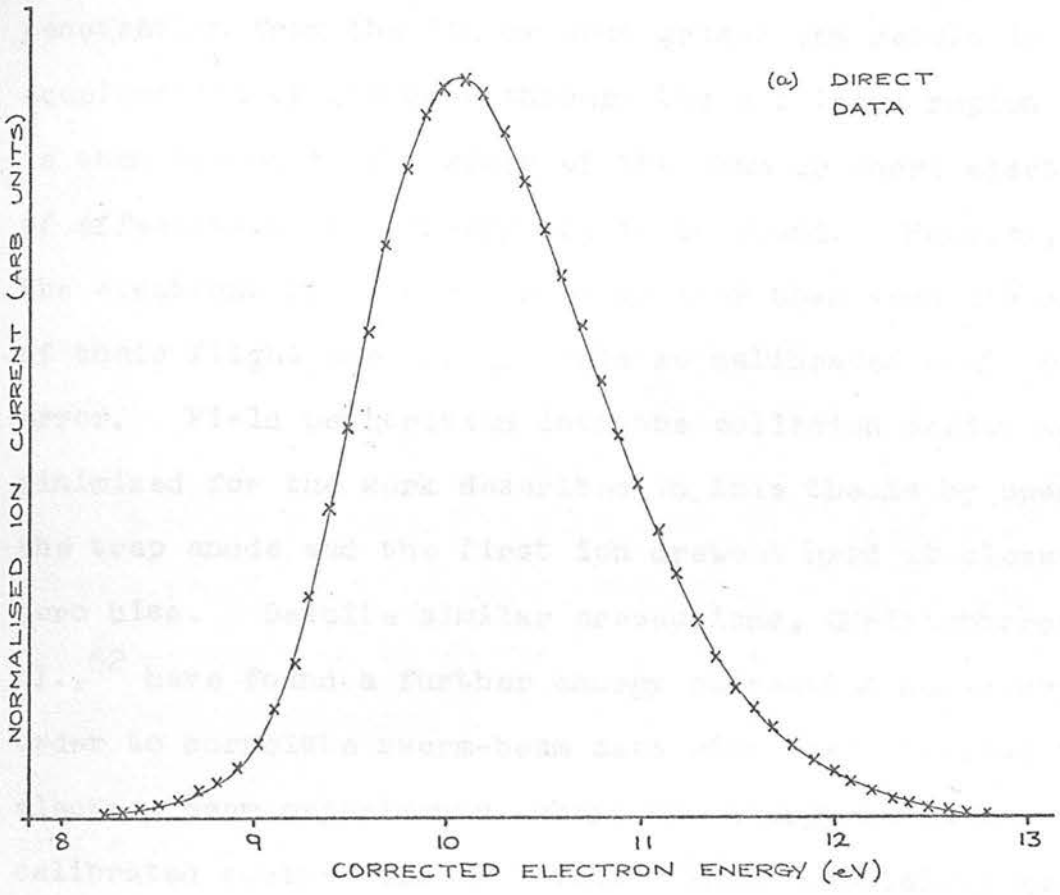
(a) DIRECT DATA
NORMALISED ION CURRENT (ARB UNITS)
8
9
10
11
12
13
CORRECTED ELECTRON ENERGY (eV)

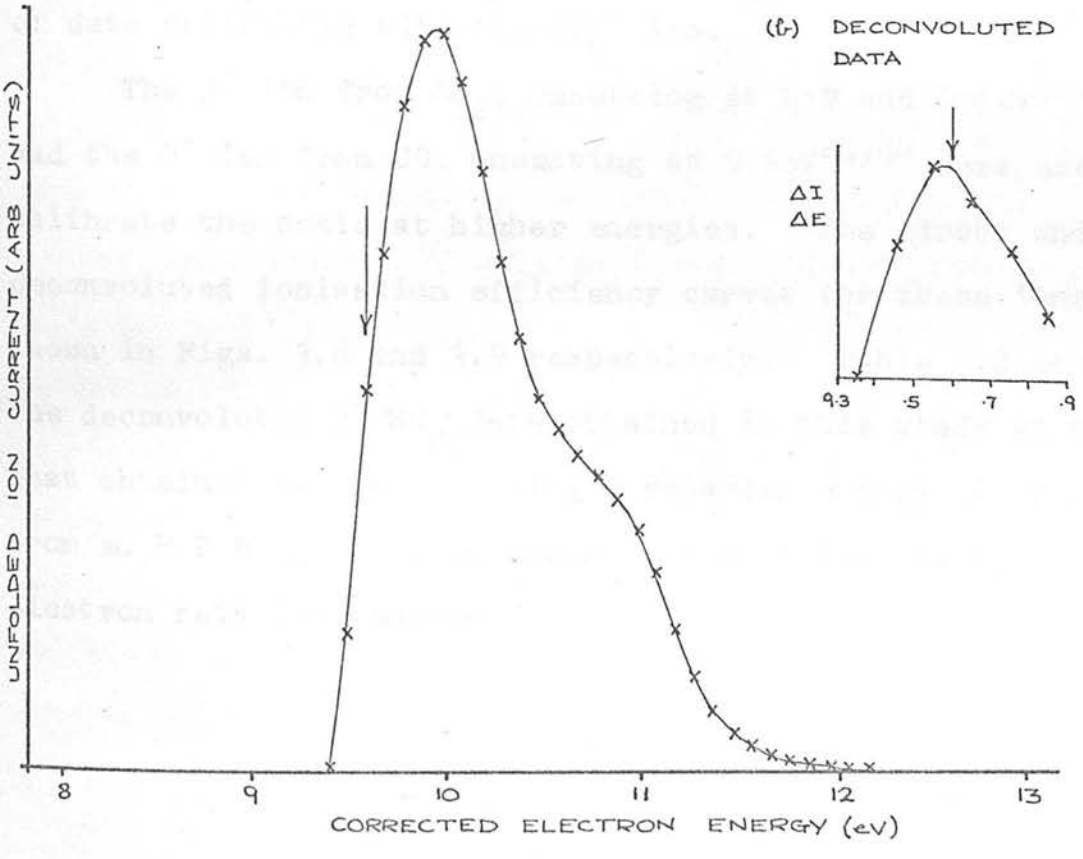
(b) DECONVOLUTED DATA
ΔI
ΔE
9·3
·5
·7
·9
UNFOLDED ION CURRENT (ARB UNITS)
8
9
10
11
12
13
CORRECTED ELECTRON ENERGY (eV)

Fig 3.9

penetration from the ion drawout grids) can result in acceleration of the beam through the collision region. SF_6^- is then formed at the edges of the chamber where electrons of effectively zero energy are to be found. However, as the electrons possess energies greater than zero for most of their flight the energy scale so calibrated would be in error. Field penetration into the collision region was minimised for the work described in this thesis by operating the trap anode and the first ion drawout grid at close to zero bias. Despite similar precautions, Christophorou et al.,[62] have found a further energy correction necessary in order to correlate swarm-beam data with that obtained in electron beam experiments, where the energy scale was calibrated against the SF_6^- ion. This uncertainty must therefore be taken into account when assessing the reliability of data calibrated with the SF_6^- ion.

The O^- ion from SO_2, onsetting at 4·2 and 6·6eV[55,63] and the O^- ion from CO, onsetting at 9·6eV[24,46] were used to calibrate the scale at higher energies. The direct and deconvoluted ionisation efficiency curves for these ions are shown in Figs. 3.8 and 3.9 respectively. Table 3.2 compares the deconvoluted O^-/SO_2 data obtained in this study with that obtained by Kraus[63] using a retarded energy distribution from an R.P.D. gun and an energy scale calibrated by electron retarding curves.

Table 3.2. O^-/SO_2

	This work	Kraus[63]
Appearance Potential (eV)	4·2(calibrant)	4·2
Peak Maximum (eV)	4·9 ± 0·1	4·7 ± 0·1
Appearance Potential (eV)	6·6 ± 0·1	6·6
Peak Maximum (eV)	7·7 ± 0·1	8·0

Similar agreement is also found for the peak parameters taken from the O^-/CO deconvoluted curve shown in Fig. 3.9(b) and those reported by Chantry[24] using R.P.D. and an energy scale calibrated against the appearance potential of the CO^+ ion from CO at 14·0eV. It is apparent that any change in the electron energy distribution as the filament temperature changes over the energy range of interest has negligible effect on the operation of the unfolding procedure and on the accuracy of the results so obtained.

The O^- ion from CO was shown by Chantry to exhibit a very sharp onset, probably vertical, occurring at the theoretical threshold energy of 9·62eV for the process $CO + e \longrightarrow O^- + C(^3P)$. A second peak, corresponding to formation of the carbon atom fragment in the ^1D state, $CO + e \longrightarrow O^- + C^*(^1D)$, was also found at the theoretically predicted threshold of 10·88eV. This second peak is only partially resolved in Fig. 3.9(b). For the purpose of calibration in this work it was assumed that the O^-/CO cross-section behaves as a step function between threshold and maximum. The true threshold for the process, taken as the

point of maximum gradient on the onset edge of the experimental peak, was then set equal to 9·6eV.

(i) Materials

With the exception of the substances listed separately below all of the materials employed in this work were supplied by the following firms and generally used without further purification:-

Air Products, Stoke-on-Trent.

British Drug Houses, Poole.

Cambrian Chemicals Ltd., London.

K & K Laboratories Inc., Plainview, NY, U.S.A.

Pierce Chemical Company, Illinois, U.S.A.

SF_5Cl; supplied as a gift by Dr. H.L. Roberts of I.C.I. (Mond Division).

Mass spectrometric analysis indicated the presence of only a trace (< 0·1%) of SF_6.

CF_3CHO, C_2F_5CHO and CF_3COCF_3; supplied by K & K Laboratories Inc. as the hydrates were dehydrated over a P_2O_5/H_2SO_4 paste at 80°C and the impurities, CF_3H, C_2F_6 and CO_2, removed by prolonged pumping on a vacuum line at -130°C.

GeF_4; this was prepared in the department by Dr. S. Cradock by heating barium hexafluorogerminate to 600°C on a vacuum line. Infra-red analysis of the distilled germanium tetrafluoride revealed no traces of impurity.

PF_2CN, PF_2NCO and PF_2NCS were prepared in the department by Dr. D. Rankine by the following method;

$PF_2Br(gas) \xrightarrow{\text{over solid Ag X at } 300^\circ K} PF_2X$ condensed at $-96^\circ C$

where X = CN, NCO or NCS. The product PF_2X is trapped out at $-96^\circ C$, the unreacted PF_2Br passing straight through the trap. Distillation of the product followed by infra-red analysis, immediately after preparation and periodically during the work reported in Chapter 6, showed no traces of impurity in PF_2CN or PF_2NCS. The PF_2NCO samples, however, were found to oxidise to PF_2OPF_2 on prolonged standing at room temperature and so several samples were used in the course of the work reported in Chapter 6.

CHAPTER 4

AUTODETACHMENT LIFETIMES, ATTACHMENT CROSS-SECTIONS AND ELECTRON AFFINITIES

The methods used in the measurement of autodetachment lifetimes and attachment cross-sections have already been discussed in Chapter 3 and the calculation of electron affinities in Chapter 2. In this chapter the results will be presented and discussed in four sections: (a) fluorocarbons, (b) nitrobenzenes, (c) inorganic and miscellaneous molecules and (d) the electron affinity calculations.

It will be of value, before presentation of the results, to review briefly the energy dependence of formation and the cross-section profiles found for the molecular negative ions investigated during the course of this work. The SF_6^- ion is known to peak at an electron energy less than 0·03eV[84] and the experimental width of the resonance has been found to reflect the energy distribution of the electron beam for a velocity selected beam of 0·02eV width.[34] The use, in this work, of a thermionically generated electron beam with a width of ~1eV therefore determined the width of the SF_6^- capture peak and the reflection of the SF_6^- capture peak observed on the energy scale provided a measure of the electron energy distribution used in the deconvolution procedure.

The energy dependence of all the molecular negative ion capture cross-sections, with the possible exception of $C_6F_{11}.CF_3^-$, were found to be closely equivalent to that of

SF_6^-. This similarity is apparent from the following examples; SF_4^- Fig. 5.1, $C_4F_6(CF_3)_2^-$ Fig. 7.9, $CF_3COCF_3^-$ Fig. 8.6 and $CF_3CF = CFCF_3^-$ and $C_6F_{11}.CF_3^-$ shown in Fig. 4.1. Two previous investigations[84,85] have indicated that the $C_6F_{11}.CF_3^-$ capture peak width is greater than that of SF_6^-, a width of ~0·27eV being reported by Naff et al.[85] using an R.P.D. source with an electron beam width of ~0·1eV. This being the case then the apparent small difference in the cross-section profile observed in this study (Fig. 4.1) may be instrumental, the measurement of ionisation efficiency curves around the zero of electron energy being thwart with many experimental difficulties.

It may therefore be concluded that, for the molecules investigated, the capture cross-sections attain their maximum values at $\leq 0{\cdot}5 \pm 0{\cdot}1$eV with a threshold at 0eV and a width not exceeding that of the electron energy distribution.

(a) Fluorocarbons

Evidence for the existence of long-lived negative ion states in fluorocarbons was first presented by Rajbenbach[104] based on a radiolysis study of c-C_4F_8, C_6F_6, C_6F_{12} and $C_6F_{11}CF_3$ in which electron scavenging was found to take place. Naff et al.[85] measured the energy dependence for electron attachment and the autodetachment lifetimes (T_a) of the molecular negative ions formed by eight fluorocarbons. These results are compared to those measured in this study for the same group of fluorocarbons in Table 4.1.

ATTACHMENT CROSS-SECTION PROFILE FOR $C_4F_8^-$ AND $C_6F_{11}CF_3^-$ RUN WITH SF_6^-

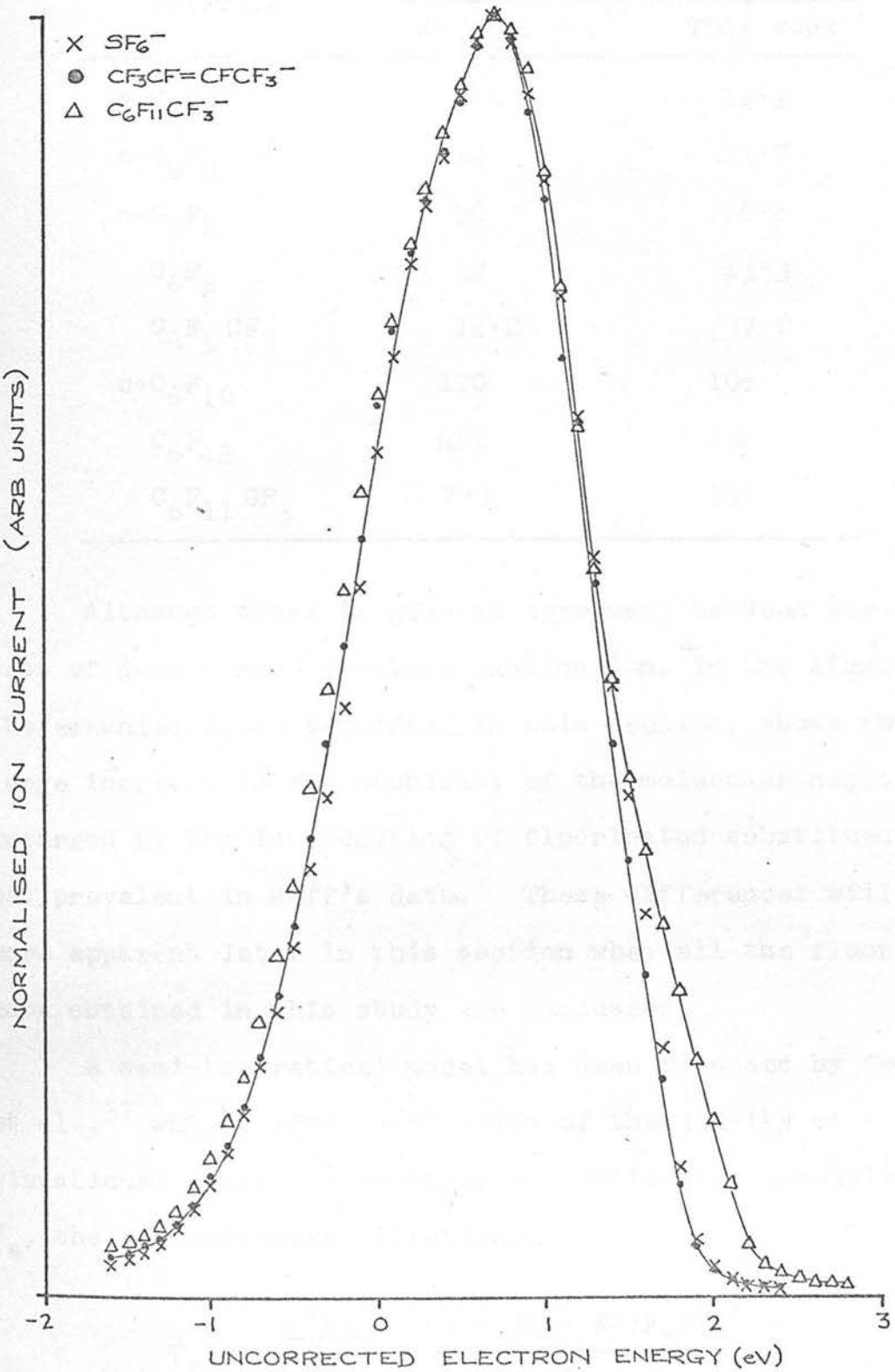

Fig 4.1

Table 4.1.

Fluorocarbon Molecule	$\bar{T}_a$ μsec.	
	Naff et al.[85]	This work
c-C_4F_6	6·9	11·2
c-C_4F_8	12	14·7
c-C_5F_8	50	26·2
C_6F_6	12	13·3
$C_6F_5CF_3$	12·2	37·8
c-C_6F_{10}	120	106
C_6F_{12}	450	236
$C_6F_{11}CF_3$	799	757

Although there is general agreement between the two sets of data a more detailed examination, in the light of the extended study presented in this section, shows that the large increase in the stability of the molecular negative ion incurred by the introduction of fluorinated substituents is not prevalent in Naff's data. These differences will become more apparent later in this section when all the fluorocarbon data obtained in this study are discussed.

A semi-theoretical model has been proposed by Compton et al.,[37] which, after evaluation of the density of vibrational states,[88] provides the following expression for T_a, the autodetachment lifetime;

$$T_a = \frac{2\pi^2\hbar^3}{m^2v^2\sigma_a} \frac{[\epsilon + (1 - \beta\omega)E_z]^{N-1}}{(N-1)! \prod_{i=1}^{N} h\nu_i} \quad \ldots\ldots\ldots (13)$$

On the assumption that σ_a (the attachment cross-section), and the electron affinity, the dominant parameter in the term contained in square brackets, do not vary greatly for these molecules and that the attaching velocity, v, is essentially that of a thermal electron ($\sim 10^7$cm./sec.) in each case, equation (13) predicts an approximately linear dependence of $\ln T_a$ on N, the number of vibrational degrees of freedom in the ion (molecule).

$\ln \bar{T}_a$, the average value for the autodetachment lifetime, is plotted against N for Naff's data in Fig. 4.2 and from the data obtained in this study in Fig. 4.3. From these figures it is apparent that an approximately straight line plot is obtained. Taking the regression line of $\ln \bar{T}_a$ on N, the linear correlation co-efficient r, was calculated from the following expression:

$$r = \frac{n\Sigma N \ln T_a - \Sigma N \Sigma \ln T_a}{[n\Sigma(\ln T_a)^2 - (\Sigma \ln T_a)^2]^{\frac{1}{2}}[n\Sigma N^2 - (\Sigma N)^2]^{\frac{1}{2}}} \quad \ldots\ldots\ldots (28)$$

where n is the number of data points. This gave a value of 0·91 for the results of Naff et al.[85] compared with a value of 0·98 for the same compounds studied in this work ($r = \pm 1$ for perfect correlation). Naff et al.,[85] by taking the CF_3 side chain in $C_6F_5CF_3$ and $C_6F_{11}CF_3$ as single atom groups reduced the number of active vibrational modes to 30 and 48 respectively yielding a better correlation of all points (Fig. 4.2). It can be seen from Fig. 4.3 that such an assumption is not required and this work shows that for

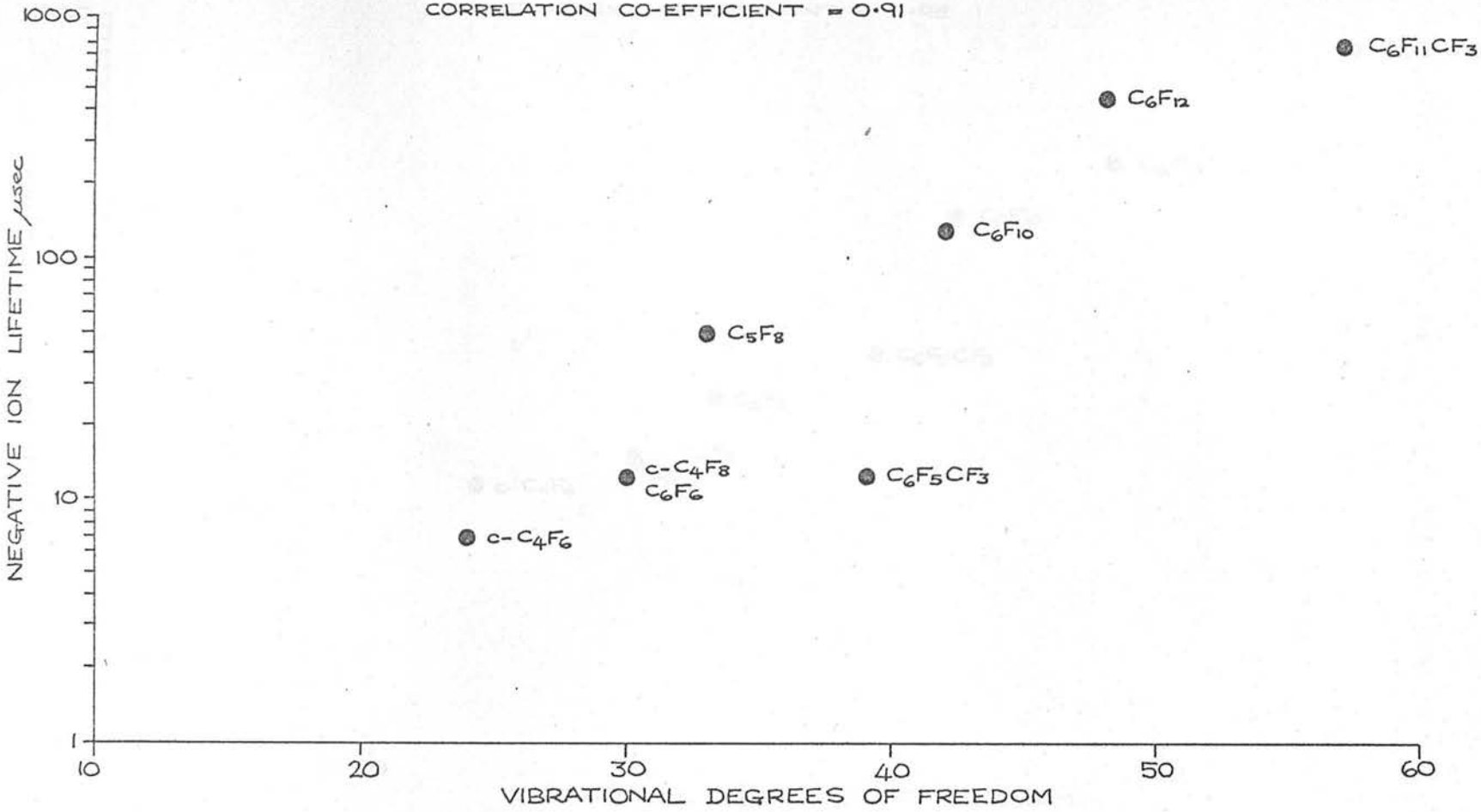
ln $\overline{T}_a$ vs N (NAFF et al)
CORRELATION CO-EFFICIENT = 0·91
NEGATIVE ION LIFETIME/μsec
1000
100
10
1
10
20
30
40
50
60
VIBRATIONAL DEGREES OF FREEDOM
$C_6F_{11}CF_3$
C_6F_{12}
C_6F_{10}
C_5F_8
c-C_4F_8
C_6F_6
$C_6F_5CF_3$
c-C_4F_6

Fig 4.2

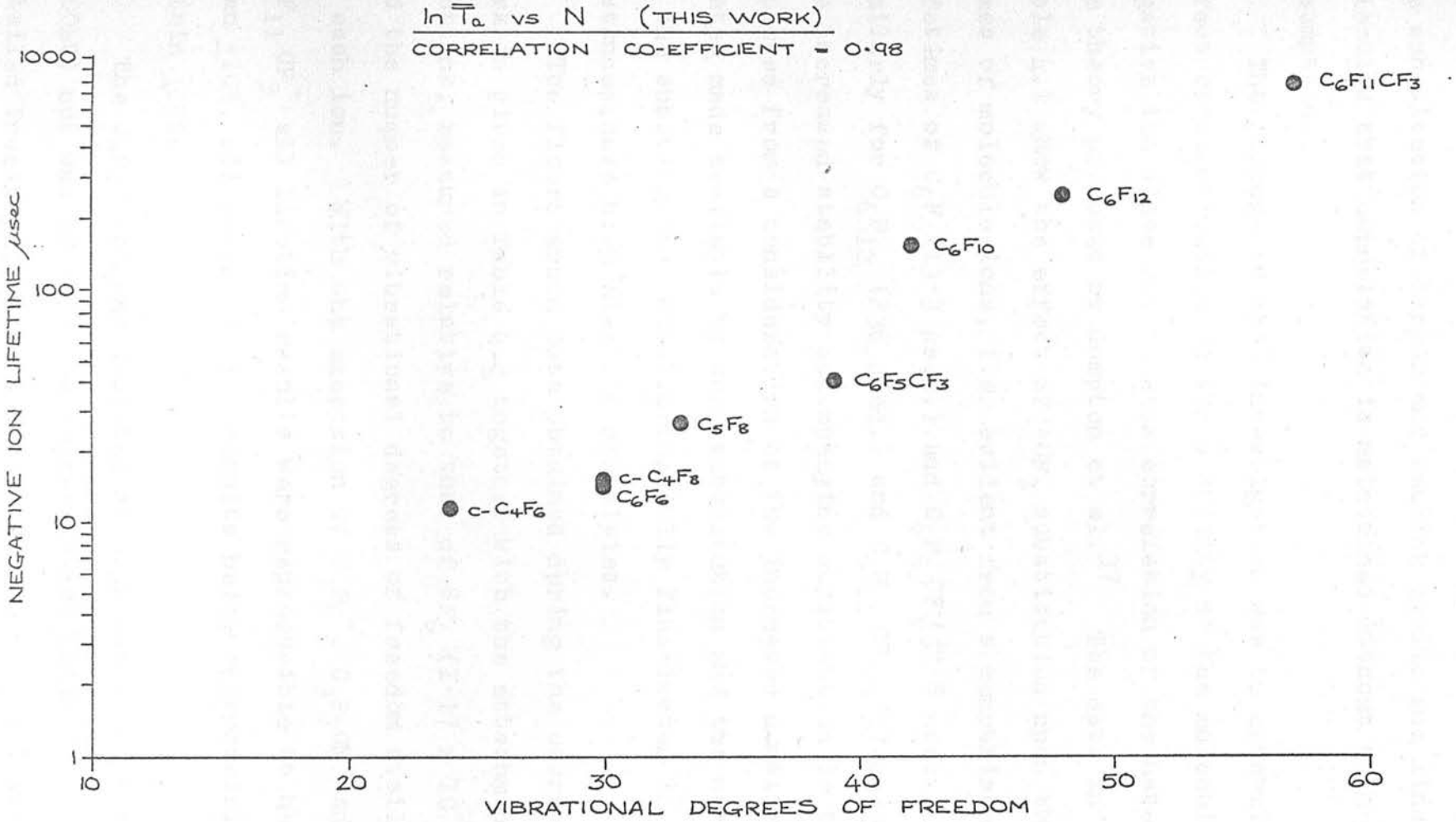
ln $\bar{\tau}_a$ vs N (THIS WORK)
CORRELATION CO-EFFICIENT = 0·98
NEGATIVE ION LIFETIME μsec
1000
100
10
1
10
20
30
40
50
60
VIBRATIONAL DEGREES OF FREEDOM
$C_6F_{11}CF_3$
C_6F_{12}
C_6F_{10}
$C_6F_5CF_3$
C_5F_8
c-C_4F_8
C_6F_6
c-C_4F_6

Fig 4.3

the substitution of larger and smaller cyclic and linear molecules that correlation is maintained without such an assumption.

The purpose of this investigation was to determine the effect of substitution on the stability of the molecular negative ion state and to seek correlation of the data with the theory proposed by Compton et al.[37] The data in Table 4.1 show the effect of $-CF_3$ substitution upon the lifetimes of molecule-ions, i.e. evident from a comparison of the lifetimes of C_6F_6(13·3 μsec.) and $C_6F_5CF_3$(37·8 μsec.) and similarly for C_6F_{12} (236 μsec.) and $C_6F_{11}CF_3$ (757 μsec.). The increased stability accompanying substitution is to be expected from a consideration of the increased density of states made available by such substitution and the nature of the substituents which,being fully fluorinated in these instances,have high electron affinities.

The fluorocarbon data obtained during the course of this work is given in Table 4.2 together with the attachment cross-sections, measured relative to that of SF_6 ($1{\cdot}17 \times 10^{-14}$cm.^{2}),[35] and the number of vibrational degrees of freedom available to each ion. With the exception of $C_3F_6^-$, $C_3F_7CN^-$ and $C_6F_{11}CF_3^-$ all lifetime results were reproducible to better than ±10%, all cross-section results being reproducible to within ±25%.

The $C_3F_6^-$ ion was detected at high electron energies (100eV) but was of very low cross-section which precluded a detailed investigation. A lower limit of 2 μsec. was therefore imposed on the lifetime, this being equivalent to the

TABLE 4.2 $\bar{\tau}_a$ AND $\bar{\sigma}_a$ FOR FLUOROCARBONS

FLUOROCARBON (AB^{-*})	τ_a μsec FOR VARIOUS ION ENERGIES				$\bar{\tau}_a$ μsec	$\bar{\sigma}_a$ cm²	N
	2·0 KV	2·5 KV	3·0 KV	3·5 KV			
C_3F_6	—	—	—	—	>2	—	21
C_3F_7CN	18·6	—	—	—	18·6	—	30
C_4F_6 [−≡−]	16·4	16·0	16·4	—	16·3	6.6×10^{-16}	24
c-C_4F_6	—	11·2	11·7	10·8	11·2	1.0×10^{-16}	24
o-$C_4F_6(CF_3)_2$	110·9	111·9	108·3	—	110·4	2.8×10^{-14}	48
C_4F_8 [∿]	30·7	29·2	31·7	—	30·6	1.0×10^{-15}	30
c-C_4F_8	15·1	13·8	15·1	15·1	14·7	1.3×10^{-16}	30
n-C_4F_{10}	12·4	13·0	—	—	12·7	—	36
C_5F_8 [⬠]	25·4	26·5	26·8	—	26·2	6.8×10^{-15}	33
n-C_5F_{12}	32·6	35·9	34·3	—	34·3	1.9×10^{-15}	45
C_6F_6	—	13·0	14·0	13·0	13·3	4.4×10^{-16}	30
C_6F_{10} [⬡]	107·2	104·6	—	—	105·9	1.3×10^{-14}	42
c-C_6F_{12}	236·5	217·6	255·4	—	236·5	—	48
n-C_6F_{14}	—	96·2	91·8	93·6	93·9	4.0×10^{-15}	54
C_6F_5CN	47·3	49·2	—	—	48·2	9.7×10^{-15}	33
$C_6F_5CF_3$	40·0	38·6	41·4	—	40·0	2.6×10^{-15}	39
p-$C_6F_4(CF_3)_2$	425·1	483·6	441·5	—	450·0	1.0×10^{-14}	48
$C_6F_{11}CF_3$	501	871	902	—	757	5.0×10^{-14}	57
$C_6F_{11}C_2F_5$					~5000	5.1×10^{-14}	66
o-$C_6F_{10}(CF_3)_2$						6.4×10^{-14}	66
m-$C_6F_{10}(CF_3)_2$						3.8×10^{-14}	66
p-$C_6F_{10}(CF_3)_2$						7.8×10^{-14}	66
C_7F_{14} [⩚]	—	230·0	227·0	228·9	229·0	1.8×10^{-15}	57

ion residence time in the source prior to drawout. The $C_3F_7CN^-$ ion, also of low cross-section, could only be successfully resolved for one drift tube potential but the value measured for T_a was reproducible. The long lifetime of the $C_6F_{11}CF_3^-$ ion resulted in a very small neutral peak which was partially immersed in the background noise for the 2KV drift potential measurement. $\bar{T}_a$ was determined over all three values but it is probable that the measurement at 2KVis low.

The perfluoro di-methyl substituted cyclohexanes and perfluoro p-ethyl cyclohexane are shown in Table 4.2 with an approximate lifetime of 5 milliseconds. In all these cases the neutral peak was so small in comparison with the ion peak that measurements could not be made accurately over the limited energy range consistent with resolution. In order to accommodate the molecular negative ions on the time scale at the lower drift potentials (2,2·5KV) the operating frequency of the spectrometer was reduced to 10MHz with a corresponding reduction in ion current and signal to noise ratio, both adversely affecting measurement of the neutral component. The weight of several determinations over a period of months, however, favoured a value of ~5 milliseconds for these species. These results lie on the line extrapolated through the data plotted in Fig. 4.5.

The average autodetachment lifetime values shown in Tables 4.1 and 4.2 are those averaged over the individual drift tube potentials for which measurements were practicable. A further method of determining the average value is from

the reciprocal slope of the plot, ln N_0^-/N_t^- against t, where N_0^-, the number of molecular negative ions initially entering the drift tube, is equal to $N_t^- + N_t^0$ where N_t^- is the number of ions surviving autodetachment after time t and N_t^0 is the number of neutral molecules formed after time t. A series of such plots is shown in Fig. 4.4 where the straight lines indicate least squares fits to the data points. Extrapolation of these lines through the origin validates the use of a first order exponential decay law for the treatment of autodetachment. A comparison of $\bar{T}_a$ and T_a(slope) is made in Table 4.3.

Table 4.3.

Molecule	$\bar{T}_a$ μsec.	T_a(slope) μsec.
c-C_4F_6	11·2	10·6
c-C_4F_8	14·7	13·0
C_4F_8-2	30·6	34·0
$C_4F_6(CF_3)_2$	110·4	115·8
c-C_5F_8	26·2	19·2
n-C_5F_{12}	34·3	26·3
C_6F_6	13·3	11·9
$C_6F_5CF_3$	40·0	33·0
$C_6F_4(CF_3)_2$	450	390

The results obtained by the two methods are in good accord and would probably show closer correlation with an increase in the number of data points, only 3 or 4 being possible for the molecules examined in this work.

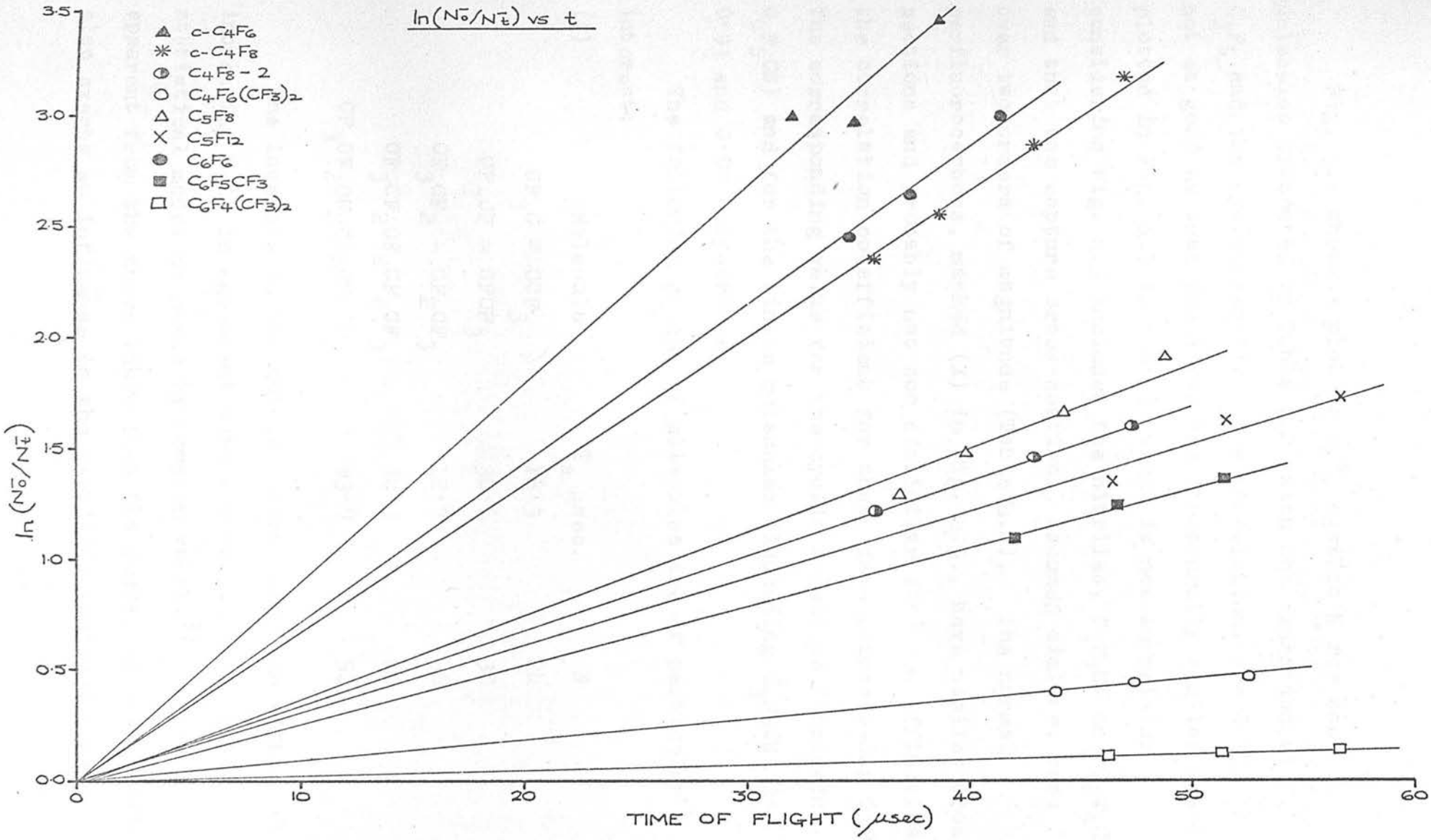
$\ln(N_0^-/N_t^-)$ vs t
c-C4F6
c-C4F8
C4F8 - 2
C4F6(CF3)2
C5F8
C5F12
C6F6
C6F5CF3
C6F4(CF3)2
$\ln(N_0^-/N_t^-)$
TIME OF FLIGHT (μsec)
0.0
0.5
1.0
1.5
2.0
2.5
3.0
3.5
0
10
20
30
40
50
60

Fig 4.4

Fig. 4.5 shows a plot of $\ln\bar{T}_a$ against N for the molecules presented in Table 4.2 (with the exception of C_3F_6 and the cyclohexanes). The correlation, r = 0·92, is not as good as that found for the structurally similar species plotted in Fig. 4.3 (r = 0·98) which is not surprising considering Fig. 4.3 includes the nitriles, C_3F_7CN and C_6F_5CN, and that the capture cross-sections, assumed similar, vary over two orders of magnitude (Table 4.2). The normal perfluorocarbons, marked (X) in Fig. 4.5., have similar cross-sections and probably not too dissimilar electron affinities, the correlation co-efficient for these data points being 0·99. The corresponding value for the cyclic molecules (including C_6F_5CN) and for the linear molecules (including C_3F_7CN) is 0·93 and 0·92 respectively.

The following groups of molecules are of particular interest:

(i)

Molecule	$\bar{T}_a$ μsec.	N
$CF_3C \equiv CCF_3$	16·3	24
$CF_3CF = CFCF_3$	30·6	30
$CF_3CF_2 - CF_2CF_3$	12·7	36
$CF_3CF_2CF_2CF_2CF_3$	34·3	45
$CF_3CF_2CF_2CF_2CF_2CF_3$	93·9	54

The increase in the autodetachment lifetime with increasing N is in agreement with the predictions of the statistical model proposed by Compton et al.[37] It is also apparent from the above table that the degree of unsaturation also exerts an influence on the stability (autodetachment

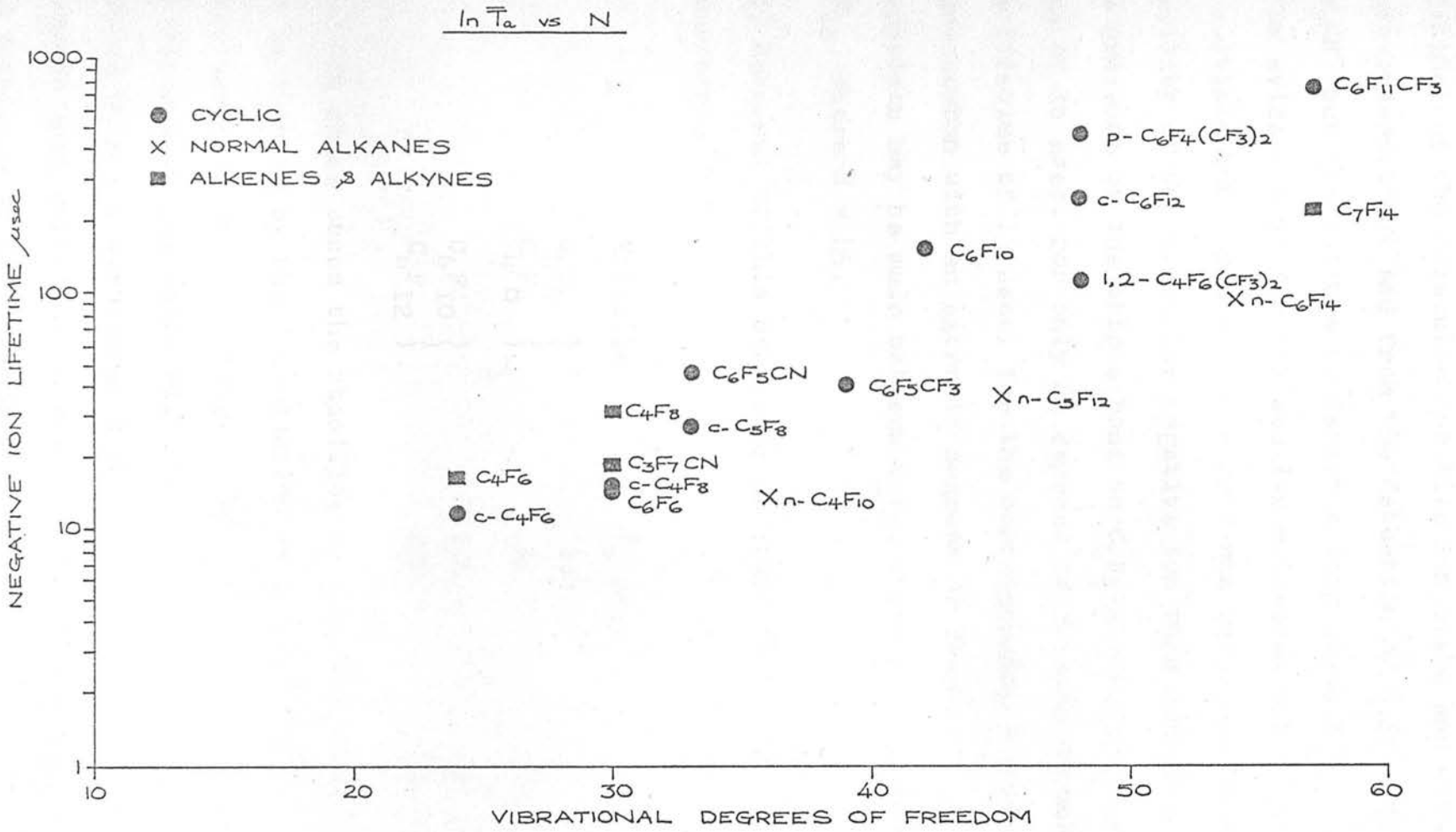
ln $\bar{\tau}_a$ vs N
CYCLIC
NORMAL ALKANES
ALKENES & ALKYNES
NEGATIVE ION LIFETIME /μsec
1000
100
10
1
10
20
30
40
50
60
VIBRATIONAL DEGREES OF FREEDOM
$C_6F_{11}CF_3$
p-$C_6F_4(CF_3)_2$
c-C_6F_{12}
C_7F_{14}
C_6F_{10}
1,2-$C_4F_6(CF_3)_2$
n-C_6F_{14}
C_6F_5CN
$C_6F_5CF_3$
n-C_5F_{12}
C_4F_8
c-C_5F_8
C_3F_7CN
C_4F_6
c-C_4F_8
C_6F_6
n-C_4F_{10}
c-C_4F_6

Fig 4.5

lifetime) of the molecular negative ion state and from the above observations and from the detection of $C_3F_6^-$ and $C_3F_7CN^-$ but the failure to detect a long lived $C_3F_8^-$ ion, it is evident that for the smaller molecules the presence of multiple bonding has a more profound influence on the stability of the molecular negative ion than does N e.g. the presence of the triple bond in C_4F_6-2 results in a lifetime of 16 μsec. for only 24 degrees of freedom compared to the lifetime of 13 μsec. for the corresponding saturated fluorocarbon with an extra 12 degrees of freedom. A similar comparison may be made between C_4F_8, where N = 30, and C_5F_{12}, where N = 45.

(ii) Reversal of this behaviour is found in the cyclic perfluorocarbons;

Molecule	$\bar{T}_a$ μsec.	N
C_4F_6)	11·2	24
C_4F_8)	14·7	30
C_6F_{10})	105·9	42
C_6F_{12})	236·5	48

In these cases the stability of the molecular negative ion is reduced by the introduction of a double bond (unsaturation) into the ring. This effect may be the consequence of the extra rigidity (increased ring stain) imposed upon the structure by unsaturation. It is therefore apparent that substitution exerts two opposing influences on the stability of perfluorocarbon molecular negative ions

(i) an increase due to a lowering of the energy of the unoccupied molecular orbitals[112] accessible to the captured electron and (ii) a decrease resulting from a decrease in the number of vibrational degrees of freedom over which the excess energy associated with capture (incident electron kinetic energy plus molecular electron affinity) may be distributed. The latter effect appears to predominate for the ring structures and the former for the aliphatic molecules.

The substitution of electronegative side chains into these small ring compounds is found to have a profound effect on the stability of the molecular negative ion state and the large increase in $\bar{T}_a$ with substitution, illustrated by the examples in the table below, correlate with the corresponding increase in N.

Molecule	$\bar{T}_a$ μsec.	N
c-C_4F_6	11·2	24
c-C_4F_8	14·7	30
o-$C_4F_6(CF_3)_2$	110·4	48
C_6F_6	13·3	30
$C_6F_5CF_3$	40·0	39
C_6F_5CN	48·2	33
p.$C_6F_4(CF_3)_2$	450·0	48
C_6F_{12}	236·5	48
$C_6F_{11}CF_3$	757	57
$C_6F_{10}(CF_3)_2$	~5000	66
c-C_4F_6	11·2	24
c-C_5F_8	26·2	33
c-C_6F_{10}	105·9	42

The effect of substitution and of increasing ring size on the autodetachment lifetime is seen to correlate with N from the examples presented. However, the effect of CF_3 substitution and CN substitution into the perfluorobenzene ring is of particular interest. The enhanced stability incurred by nitrile substitution, which exceeds that anticipated from a consideration of N alone, is due to the conjugation of the nitrile group with the benzene ring thereby providing an extra vacant low-lying π-electronic orbital.[112] The effect of nitrile substitution was also illustrated above by the detection of a long-lived $C_3F_7CN^-$ ion but not of a $C_3F_8^-$ ion.

From the plot of $\ln\sigma_a$ against N shown in Fig. 4.6. it is apparent that the correlation is not as good as that found from the plots of $\ln T_a$ against N. This is not surprising in view of the spread in the autodetachment lifetimes of the ions plotted in Fig. 4.6, e.g. c-C_4F_6(11·2 μsec.) and $C_6F_{11}CF_3$ (757 μsec.), almost three orders of magnitude. A further plot in Fig. 4.7 shows $\ln\bar{T}_a\sigma_a$ against N. Again the correlation is not particularly good possibly reflecting an appreciable spread in the electron affinities for these molecules. Evidence supporting such a variation in E came to light during the measurement of attachment cross-sections at various drift tube pressures. The following examples illustrate this point:

ln σc vs N
CYCLIC
NORMAL ALKANES
ALKENES & ALKYNES
$C_6F_{11}CF_3$
1,2 - $C_4F_6(CF_3)_2$
p. $C_6F_4(CF_3)_2$
C_6F_{10}
$C_6F_5CF_3$
C_5F_8
C_4F_8
C_6F_6
C_4F_6
c-C_4F_8
c-C_4F_6
n-C_6F_{14}
n-C_5F_{12}
ATTACHMENT CROSS-SECTION $\times 10^{16} cm^2$
1000
100
10
1
10
20
30
40
50
60
VIBRATIONAL DEGREES OF FREEDOM

Fig 4.6

$\ln(\bar{T}_a \sigma_a)$ vs N
CYCLIC
NORMAL ALKANES
ALKENES & ALKYNES
P- $C_6F_4(CF_3)_2$
1,2- $C_4F_6(CF_3)_2$
C_6F_{10}
n- C_6F_{14}
C_5F_8
$C_6F_5CF_3$
n- C_5F_{12}
C_4F_8
C_6F_6
C_4F_6
c- C_4F_8
c- C_4F_6
$\sigma_a \times \bar{T}_a$ (Å² sec. cm⁻²) (×10¹⁶)
VIBRATIONAL DEGREES OF FREEDOM
10
20
30
40
50
60
10^2
10^3
10^4
10^5

Fig 4.7

Molecule	Pressure range (torr)	σ_a cm.^{2}
n.C_6F_{14}	7×10^{-7}	$4{\cdot}0 \times 10^{-15}$
	$2{\cdot}5 \times 10^{-5}$	$3{\cdot}7 \times 10^{-15}$
$C_4F_6(CF_3)_2$	6×10^{-7}	$2{\cdot}8 \times 10^{-14}$
	1×10^{-5}	$3{\cdot}2 \times 10^{-14}$
o-$C_6F_{10}(CF_3)_2$	8×10^{-7}	$6{\cdot}4 \times 10^{-14}$
	2×10^{-5}	$11{\cdot}0 \times 10^{-14}$
p-$C_6F_{10}(CF_3)_2$	4×10^{-7}	$7{\cdot}8 \times 10^{-14}$
	2×10^{-5}	$11{\cdot}1 \times 10^{-14}$

Conclusions regarding the electron affinities of these molecules (relative to that of SF_6 = 1·43eV,[4] SF_6 being the second component in the gas mixture) can be drawn from these studies i.e. n-C_6F_{14} and $C_4F_6(CF_3)_2$ must have similar electron affinities to that of SF_6 whilst the opposite is true for ortho and para-$C_6F_{10}(CF_3)_2$ where preferential electron transfer from SF_6 was found with increasing collision frequency in the source,

i.e. $SF_6^- + C_6F_{10}(CF_3)_2 \longrightarrow C_6F_{10}(CF_3)_2^- + SF_6$.

A similar investigation using mixtures of SF_6 with $C_6F_5CF_3$, $C_6F_4(CF_3)_2$ and C_4F_6 indicated that the measured attachment cross-sections were independent of pressure and hence that the electron affinity of each of these molecules is similar to that of SF_6. Mixtures of SF_6 with $C_6F_{11}.C_2F_5$ and m-$C_6F_{10}(CF_3)_2$ however, showed a rapid increase in fluorocarbon cross-section with source pressure indicating larger electron affinities than SF_6.

The observation that some fluorocarbons exhibit both long

lifetimes (up to 5 m.sec.) and large capture cross-sections (up to 8×10^{-14}cm.^{2}) may be of some significance in the development of less expensive and more efficient substitutes for SF_6 (T_a = 0·7 m.sec., $\sigma_a = 1 \times 10^{-14}$) in the insulation of high voltage power transmission lines and switches. Until large scale tests can be carried out on the conductivity of the decomposition products which may result from a violent discharge in such fluorocarbon gases, the possibilities remain speculative. However, it is highly probable that such products, if formed to any large extent, would be non-conducting polymers of the teflon variety. The limiting factor in such an application would ultimately be the volatility of the fluorocarbon in relation to its cost and efficiency relative to that of SF_6.

(b) Nitrobenzenes

The nitrobenzene molecular negative ion was amongst the first long-lived species to be investigated, a lifetime of 40 μsec.[37] being reported. In an attempt to examine the effect of substitution on the stability of the molecular negative ion, nitrobenzene and the derivatives shown in Table 4.4 were investigated.

In all cases the capture cross-sections were so low as to preclude accurate measurements at the resonance peak energy (~0eV for all molecules) and all measurements were made using the high energy secondary electron capture method (Chapter 3). The interference of the $(M-1)^-$ ion (where M is the molecular weight of the molecule) formed at high energies was overcome by reversal of the retarder lens bias

TABLE 4.4 $\bar{T}_a$ FOR NITROBENZENES

MOLECULE (AB^{-*})	T_a μsec FOR VARIOUS ION ENERGIES				$\bar{T}_a$ μsec	DIPOLE MOMENT (Debyes)	N
	2.0 KV	2.5 KV	3.0 KV	3.5 KV			
$C_6H_5NO_2$	46.4	48.3	48.2	—	48.6	4.3	36
o- $C_6H_4(CH_3)NO_2$	29.9	31.1	—	—	30.5	3.6	45
m- $C_6H_4(CH_3)NO_2$	24.9	21.8	21.7	—	22.8	4.2	45
2,3-$(CH_3)_2C_6H_3NO_2$	20.2	21.7	22.0	19.9	21.0	4.3	54
2,4-$(CH_3)_2C_6H_3NO_2$	21.5	21.4	25.2	20.4	21.1	4.5	54
2,6-$(CH_3)_2C_6H_3NO_2$	16.5	19.4	18.4	—	18.1	3.9	54
p- $C_6H_4(C_2H_5)NO_2$	26.9	28.7	31.0	—	28.8	4.9	54
4-F, o-$C_6H_3(CH_3)NO_2$	22.9	20.2	19.0	—	20.7	2.5	45
2,4-$(F)_2C_6H_3NO_2$	46.0	47.7	46.1	—	46.6	3.5	36
2,5-$(F)_2C_6H_3NO_2$	47.8	46.2	44.9	—	46.4	4.3	36

TABLE 4.5 $\bar{T}_a$ AND $\bar{\sigma}_a$ FOR INORGANIC AND MISCELLANEOUS MOLECULES

MOLECULE (AB^{-*})	$\bar{T}_a$ μsec FOR VARIOUS ION ENERGIES					$\bar{T}_a$ μsec	$\bar{\sigma}_a$ cm^2	N
	2.0 KV	2.5 KV	3.0 KV	3.5 KV	4.0 KV			
SF_4	16.0	16.5	—	—	—	16.2	1.1×10^{-16}	9
SF_6	67.2	67.2	70.0	—	—	68.1	$(1.17 \times 10^{-14})^{35}$	15
WF_6	24.6	32.2	—	—	—	28.4	—	15
SiF_4						>2	—	9
GeF_4						>2	—	9
PF_2CN						>2	—	9
$(CH_3CO)_2$	—	—	—	6.5	6.3	6.4	—	30
$(CF_3)_2NO$	660±100	650±50	—	—	—	650±100	—	24

thus achieving separation of the ion and neutral components through the preferential acceleration of the ion beam instead of the retardation procedure used in the work described in section (a). In this way the $(M-1)^-$ ion did not overlap the neutral component on operation of the retarder lens but was similarly accelerated to arrive at the detector before M^-, which arrives before M neutral.

It is apparent from Table 4.4 that the dependence of $\ln \bar{T}_a$ upon N, which was found for the perfluorocarbon study, is not observed for these nitrocompounds e.g. $\bar{T}_a(C_6H_5NO_2)$ = 48·6 μsec. for N = 36 whilst $\bar{T}_a$ $(2,3\text{-}(CH_3)_2C_6H_3NO_2)$ = 21·0 μsec. when N = 54. It can be seen from Table 4.4 that the introduction of a methyl group (electron donating substituent) into the benzene ring reduces the stability of the molecular ion and that the introduction of a second such group reinforces this effect. Although not immediately apparent these observations are consistent with the factors which were found to influence the stability of the fluorocarbon molecular negative ions. The electro-negative nitro group has the effect of depleting the charge density in the benzene ring and consequently of lowering the energy of the two lowest (degenerate) unoccupied π-electronic orbitals which are involved in negative ion formation. The unoccupied p-orbitals of the nitro group serve to extend the conjugation and so provide an additional vacant low-lying π-electronic orbital[106,112] which will be strongly influenced by the addition of electropositive substituents into the benzene ring. Such groups will serve to replenish electron density and to

offset the influence of the nitro group.

The influence of substituents on the benzene ring is partially reflected in the electric dipole moments of the molecules which have been calculated for Table 4.4 from group contributions.[105] It would however, be erroneous to associate the dipole moment with the stability of the molecular negative ion as the values given in Table 4.4 make no account of the mesomeric effect characteristic of halogen substituents. Mesomeric charge transfer operates against the inductive effect of the electronegative substituent and by extending the conjugation it exerts an influence on the molecular orbitals. Only in the case of mono-substituted derivatives of benzene is the dipole moment a true representation of the inductive effect of the substituent, this comparison being used in a recent paper by Naff et al.[106] to correlate an increase in lifetime with electronegativity of the substituent.

Introduction of fluorine substituents into the benzene ring is not found to influence the stability of the molecular negative ion to the degree which would have been anticipated through a consideration of its inductive effect alone. Therefore it must be concluded that the resonance effect, which is the dominant effect on chemical reactivity and electronic spectra, must be a strong perturbation on the vacant π-electronic orbitals in the substituted nitrobenzene, this effect being reflected in the stability of the molecular negative ion.

Nitrobenzene has been examined previously by Compton

et al.[37] and a value of 40 μsec. reported for the auto-detachment lifetime. A second examination by the same group of workers[106] has resulted in a revised value of 17·5 μsec, which does not compare favourably with the value found in this study (48·6 μsec.). Naff et al.[106] have attributed this correction to the high cross-section for stabilisation exhibited by nitrobenzene in the source which was overlooked in the earlier work. However, the source pressures employed in this study preclude the collisional stabilisation and charge transfer found in Naff's[106] investigation and therefore the discrepancy between the two values remains unresolved.

(c) Inorganic and miscellaneous molecules.

The inorganic molecular negative ions detected are given in Table 4.5. Because of low capture cross-sections and isotope effects the lifetimes of the molecular negative ions of SiF_4, GeF_4 and PF_2CN could not be determined and they have thus been given a lower limit of 2 μsec. (the ion residence time in the source prior to drawout).

The SF_4^- ion from sulphur tetrafluoride could only be resolved at two drift tube potentials but the average lifetime of 16·2 μsec. is probably accurate to within ±10% and that of WF_6^- to within ±25%. The inorganic fluorides and PF_2CN are the smallest molecules (on a number of atoms basis) which were found to exhibit long-lived molecular negative ion states, only 9 degrees of freedom being available for absorption of the excess energy resulting from electron capture i.e. the kinetic energy of the incident electron and

the molecular electron affinity. The fluorocarbon with a comparable lifetime to SF_4^- (16·2 μsec.) is n-C_4F_{10} (12·7 μsec.) which has 36 vibrational degrees of freedom whilst the fluorocarbon with 9 degrees of freedom, CF_4 does not form a long-lived molecular negative ion.

The stability of these molecular ions probably reflects the ease with which the captured electron may be accommodated in the unoccupied d-orbitals and the increasing polarisability of the heavier inorganic molecules.

SF_6^-, being of commercial significance for the insulation of high voltage power installations and transmission lines, has been the subject of three previous time-of-flight investigations[2,37,66] and an ion-cyclotron resonance investigation.[14] The results of these investigations are shown below in Table 4.6. Although the work of Edelson et al.[2] was exploratory and not designed to produce an accurate value it has been included in the Table for the sake of completeness.

Table 4.6. $T_a(SF_6)$

T_a μsec.	Group
~10	Edelson, Griffiths and McAfee,[2] 1965.
25	Compton, Christophorou, Hurst and Reinhardt,[37] 1966.
32	Collins, Christophorou and Carter,[66] 1970.
68	This study 1970/71.
~500	Henis and Mabie,[14] 1970.

The differences between the lifetimes reported, both the time-of-flight measurements and the ion-cyclotron

resonance value, may be only partially explained on the grounds of different ion source conditions and neutral and ion focussing properties prevalent in the individual experiments. These differences may arise, at least in part, from differences in the total energy of the system. Klots[89] has pointed out that SF_6^- ions, even when formed by mono-energetic electrons, will have a range of energies reflecting the thermal distribution of the original neutral molecules and therefore no unique detachment lifetime can be expected of such an ensemble; his calculations suggest that as the total excess energy of the system increases from 0·01eV to 0·1eV above the threshold the autodetachment life-time should change by an order of magnitude. Clearly small changes in the average energy of the attaching electron could represent substantial changes in the total excess energy of the system and therefore show large changes in the ion lifetimes. This might at least explain some of the differences although the I.C.R. value seems too high to reconcile even when the effects of excess energy differences are taken into account.

Klots[89] has also shown, that from a consideration of the micro-wave cross-section data for SF_6 ($2{\cdot}8 \times 10^{-14}$cm.^{2}, Mahan and Young[101]) in conjunction with the assumption of an exponential decay for the negative ion state, a lower limit of 55 μsec. would be expected for $T_a(SF_6)$. He further pointed out that treatment of the electron swarm data predicts a longer lifetime and that reconciliation of Compton's[37] data may be achieved only on the assumption that the electron

affinity of SF_6 is approximately 1·2eV. Substituting the value of $T_a(SF_6)$ found in this study and the latest electron swarm cross-section data[35] into equation (13) a value of 1·44eV is calculated for $E(SF_6)$ which compares more favourably with the value of 1·43eV reported using the magnetron technique.[4]

Diacetyl, which was also one of the first molecular negative ions to be investigated, has been the subject of two previous studies. The results reported are compared to the value measured in this work in Table 4.6. The short lifetime of this species (N = 30) is probably the result of the electron donating effect of the methyl groups on the π-electronic orbitals of the carbonyl groupings.

Table 4.6. $T_a((CH_3CO)_2)$

$\bar{T}_a$ μsec.	Group
12	Compton, Christophorou, Hurst and Reinhardt,[37] 1965.
3·3	Compton and Bouby,[107] 1967.
6·4	This study, 1970/71.

Bis-trifluoromethylnitroxide, $(CF_3)_2NO$, is a stable free radical and as such it is not surprising that, despite only 24 vibrational degrees of freedom, it formed an unusually stable molecular negative ion, $\bar{T}_a \simeq 650$ μsec. The inductive effect of the trifluoromethyl groups would also provide a stabilising influence on the negative ion state. Ion formation by this molecule will be discussed in Chapter 8.

(d) Electron affinities

The statistical theory of electron attachment proposed by Compton et al.[37] (see Chapter 2) provides the following expression:

$$\epsilon + (1 - \beta\omega)E_z = [T_a\sigma_a\, 4\pi m^2 v^2 (N-1)! \prod_{i=1}^{N} h\nu_i . h^{-3}]^{1/N-1} \quad \ldots(14)$$

where ϵ, the energy of the molecule (ion) in excess of the zero point energy E_z, equals $E + e_{ke} + f(E)dE$ where E is the molecular electron affinity, e_{ke} the kinetic energy of the incident electron and $f(E)dE$ the average vibrational energy of the molecule above the zero point energy.

Substitution of the $\bar{T}_a$ and σ_a values, determined above, into equation (14) yields a value for ϵ from which E, the dominant parameter, may be deduced. The kinetic energy of the electron has been taken as 0·05eV and the average thermal (300·16°K) vibrational energy of the molecule was taken as the maximum point in the vibrational energy distribution calculated using equation (9) and represented graphically in Fig. 4.8. for SF_4, SF_6 and C_6F_6.

The electron affinities calculated are given in Table 4.7 together with the literature values and the vibrational frequencies employed in the calculations. The value calculated for $E(SF_4)$, 1·24eV, is in good accord with the value (~1·2eV) deduced from a reconciliation of the SF_4^- appearance potential data from SF_5Cl and SF_6 (Chapter 5) with the reactions which were energetically possible. There are no literature values with which this result may be compared. The value calculated for $E(SF_6)$, 1·44eV, is in

TABLE 4.7 ELECTRON AFFINITIES

MOLECULE	VIBRATIONAL FREQUENCIES cm^{-1}	E_z (eV)	$f(E)dE$ (eV)	ϵ' (eV)	$\bar{\tau}_a$ μsec	σ_a cm^2	E_{calc} (eV)	E_{lit} (eV)
SF_4	889, 867, 728, 645, 557, 532, 463, 239, 235. Ref 111	0·319	0·039	4·19	16·2	$1·1 \times 10^{-16}$	1·24	—
SF_6	965 (3), 772, 642 (2), 617 (3), 525 (3), 370 (3). Ref 88	0·588	0·056	2·65	68·1	$(1·17 \times 10^{-14})^{35}$	1·44	1·43[4]
C_6F_6	1655 (2), 1530 (2), 1490, 1323, 1235, 1157 (2), 1000 (2), 714, 691, 640, 559, 595 (2), 443 (2), 370 (2), 315 (2), 264 (2), 249, 215, 208, 175 (2). Ref 110	1·385	0·147	0·29	13·7	4×10^{-16}	0·19	1·2[4]
$(CF_3)_2CO$	1807, 1360, 1340, 1274, 1250, 1247, 1219, 971, 778, 766, 718, 633, 547, 530, 508, 470, 368, 312, 273, 257, 193, 160, 30(2) Ref 109	1·056	0·126	0·34	(60)[66]	2×10^{-16}	0·17	—
C_5F_{12}	1290 (6), 640 (6), 225 (4), 1150 (6), 560 (6) 345 (6), 895 (4), 382 (3), 300 (2), 30 (2)	1·858	0·243	<0·17	34·3	$1·9 \times 10^{-15}$	< 0	—
	replacement of last two frequencies by 15 (2)						< 0	
	last two frequencies omitted						0·14	
C_6F_{14}	1290 (6), 640 (6), 225 (4), 560 (8), 345 (8), 895 (5), 382 (4), 200 (3), 30 (2)	2·204	0·299	<0·16	93·9	4×10^{-15}	< 0	—
	replacement of last two frequencies by 15 (2)						< 0	
	last two frequencies omitted						0·07	

COMPUTED THERMAL (300·16°K)
VIBRATIONAL ENERGY DISTRIBUTION
FOR SF4 (●), SF6 (X) AND C6F6 (▲)
RELATIVE ABUNDANCE (ARB UNITS)
VIBRATIONAL ENERGY (Kcals)
0
1
2
3
4
5
6
7
8
9

Fig 4.8

excellent agreement with the value reported by Page and Goode[4] (1·43eV) using the magnetron method. These conclusions suggest that the theoretical approach may successfully be applied in the treatment of small symmetric molecules for which $\epsilon' > 2$ and the vibrational frequencies are accurately known.

The Whitten-Rabinovitch empirical correction factor $(1 - \beta\omega)$,[88] which was initially assumed to be unity in these calculations and approached through iteration about ϵ, deviates significantly from unity for $\epsilon' < 2$. It is also primarily for molecules with less than 30 degrees of freedom when an error of only a few percent results from its use. Both these conditions are fulfilled in SF_4 and SF_6 where $\epsilon' = 4{\cdot}2$ and $2{\cdot}6$ and N = 9 and 15 respectively. These factors may be responsible for the discrepancy between the electron affinity calculated for C_6F_6, 0·19eV, compared to the literature value of 1·2eV[4] measured by the magnetron technique. If this is the case then the value of 0·17eV calculated for the electron affinity of hexafluoroacetone may also be a lower limit but there are no other reported values with which a comparison could be made.

The main difficulty encountered in the use of this treatment to study the fluorocarbons, for which there is no information on electron affinities except that deduced from the cross-section studies discussed above, lies in the lack of available vibrational frequency data for these molecules. The frequency values listed in Table 4.7 were estimated using the general approach developed by Pitzer[108] for hydrocarbons

and applied to the data reported for C_3F_8 and CF_3COCF_3[109] to estimate frequency contributions for the CF_3 group, the CF_2 group and for the C-C stretch and bend frequencies in perfluoroalkanes. The following values were deduced:

CF_3 group 1290cm.$^{-1}$(3) 640cm.$^{-1}$(3) 225cm.$^{-1}$(2)
CF_2 group 1150cm.$^{-1}$(2) 560cm.$^{-1}$(2) 345cm.$^{-1}$(2)
(n - 1) C-C stretch frequencies at 895cm.$^{-1}$
(n - 2) C-C-C bend frequencies at 382cm.$^{-1}$

where n is the number of skeletal carbon atoms in the fluorocarbon chain. The use of this method provides all but two of the fundamental vibrational frequencies; the two missing frequencies lie below 30cm.$^{-1}$ and consequently exercise considerable influence on the density of states pertinent to this application. The three values of $E(C_5F_{12})$ and $E(C_6F_{14})$ calculated in Table 4.7 are those computed by setting the two missing frequencies to (a) 30cm.$^{-1}$, (b) 15cm.$^{-1}$ and (c) omitting and correspondingly adjusting N. The failure of this approach to provide a sensible answer for the electron affinities of the two fluorocarbons examined may well be due to the estimations involved in the compilation of the vibrational frequency data and the uncertainties resulting from the calculation of $(1 - \beta\omega)$ when $\varepsilon' < 2$.

In conclusion it may be said that the successful application of the Compton model[37] to the molecular negative ion states of small polyatomic molecules holds some promise in the task of developing a theory to account for the internal

behaviour of complex molecules and that extension of vibrational frequency data and computational techniques will undoubtedly aid in the application of this approach to more complex polyatomic systems.

CHAPTER 5

THE INORGANIC FLUORIDES: SF_4, SF_6, SF_5Cl, GeF_4 and WF_6.

In this and the following chapters negative ion formation in selected groups of inorganic and organic molecules are presented and discussed. Inorganic systems are described in Chapters 5 and 6 and the remaining chapters are devoted to organic systems.

(a) Sulphur Tetrafluoride, SF_4.

Negative ion formation in sulphur tetrafluoride has not been previously investigated. The ions detected at 70eV are shown in Table 5.1 and those detected and measured at low electron energies were F^-, F_2^-, SF_3^- and SF_4^- which were formed with relative abundances in the ratio 1000·0:0·1:2·6:6·0 at their respective capture maxima.

Table 5.1. Negative ion mass spectrum of SF_4 at 70eV.

m/e	Ion	Abundance
19	F^-	1000·0
32	S^-	1·9
38	F_2^-	2·4
51	SF^-	1·4
70	SF_2^-	0·6
89	SF_3^-	1·8
108	SF_4^-	45·8

The experimental ionisation efficiency curves for the ions observed are shown in Figs. 5.1 and 5.2(a) and the deconvoluted data in Fig. 5.2(b). The energy scales are calibrated against the appearance potential at 0·0eV for the SF_6^- ion from SF_6. From the figures it can be seen that ion formation was restricted to low electron energies, the ion current falling to zero at energies above ~4eV.

Sulphur tetrafluoride undergoes associative electron capture,

$$SF_4 + e \xrightarrow{1} SF_4^-$$

the cross-section exhibiting the same energy dependence as that found for SF_6^- formation (Fig. 5.1). Using mixtures of SF_4 and SF_6 of known composition the relative ion currents resulting from competitive electron scavenging were used, in conjunction with the known capture cross-section of SF_6,[35] to estimate a value of $1{\cdot}1 \pm 0{\cdot}2 \times 10^{-16}$ cm.^{2} for the capture cross-section of SF_4 (Chapter 4). The average autodetachment lifetime of the SF_4^- ion was also measured and found to be 16·2 μsec. This value may be compared to the value of 68·1 μsec. found for SF_6^- in which an additional six vibrational degrees of freedom are available for absorbing the kinetic energy associated with the captured electron.

F^- ion formation from SF_4 is shown in Fig. 5.2 and the appearance potential data are summarised in Table 5.2. The error limits represent the mean differences of several repeated determinations for each ion.

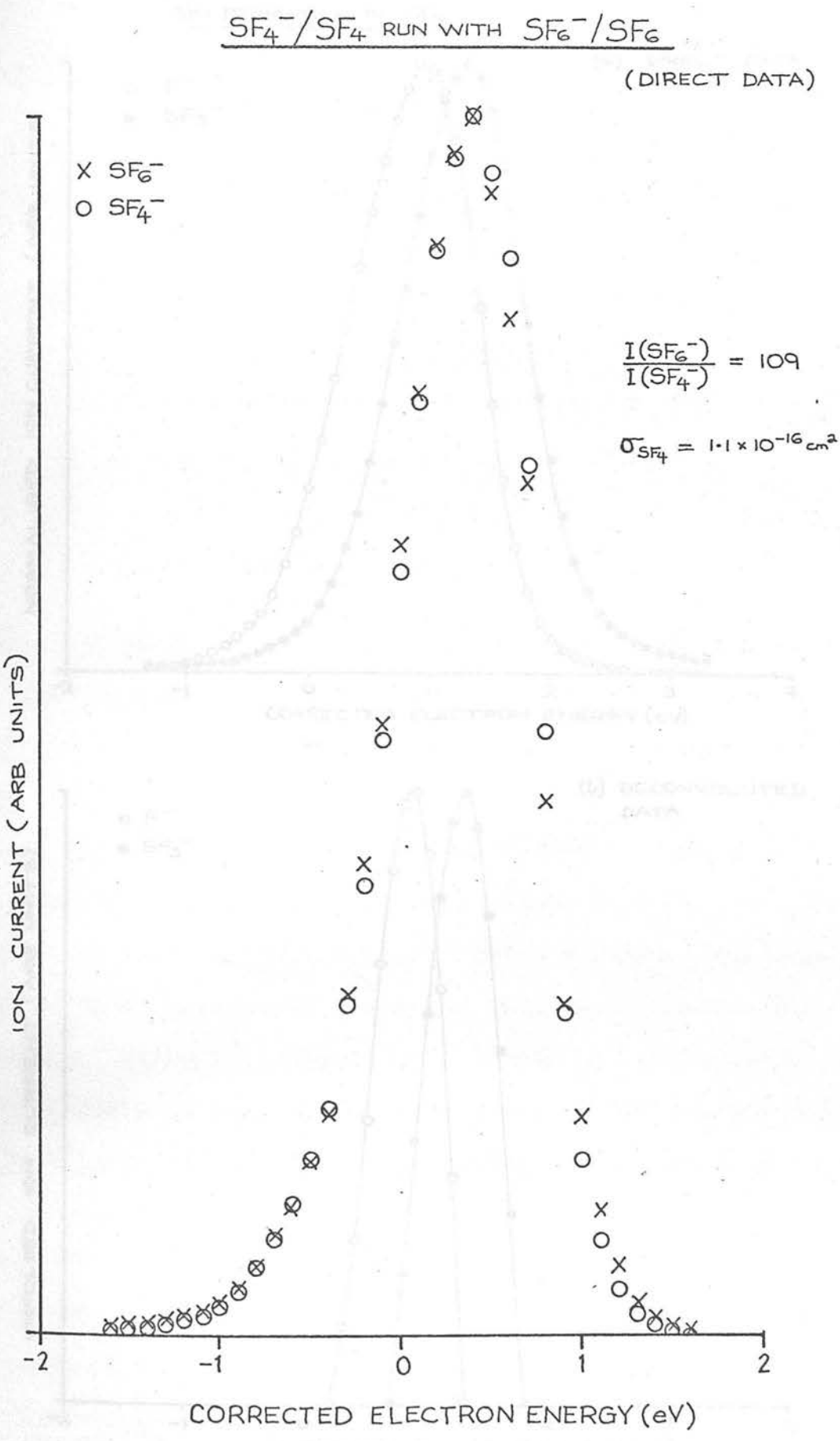
SF_4^-/SF_4 RUN WITH SF_6^-/SF_6
(DIRECT DATA)
X SF_6^-
O SF_4^-
$\frac{I(SF_6^-)}{I(SF_4^-)} = 109$
$\sigma_{SF_4^-} = 1.1 \times 10^{-16} cm^2$
ION CURRENT (ARB UNITS)
-2
-1
0
1
2
CORRECTED ELECTRON ENERGY (eV)

Fig 5.1

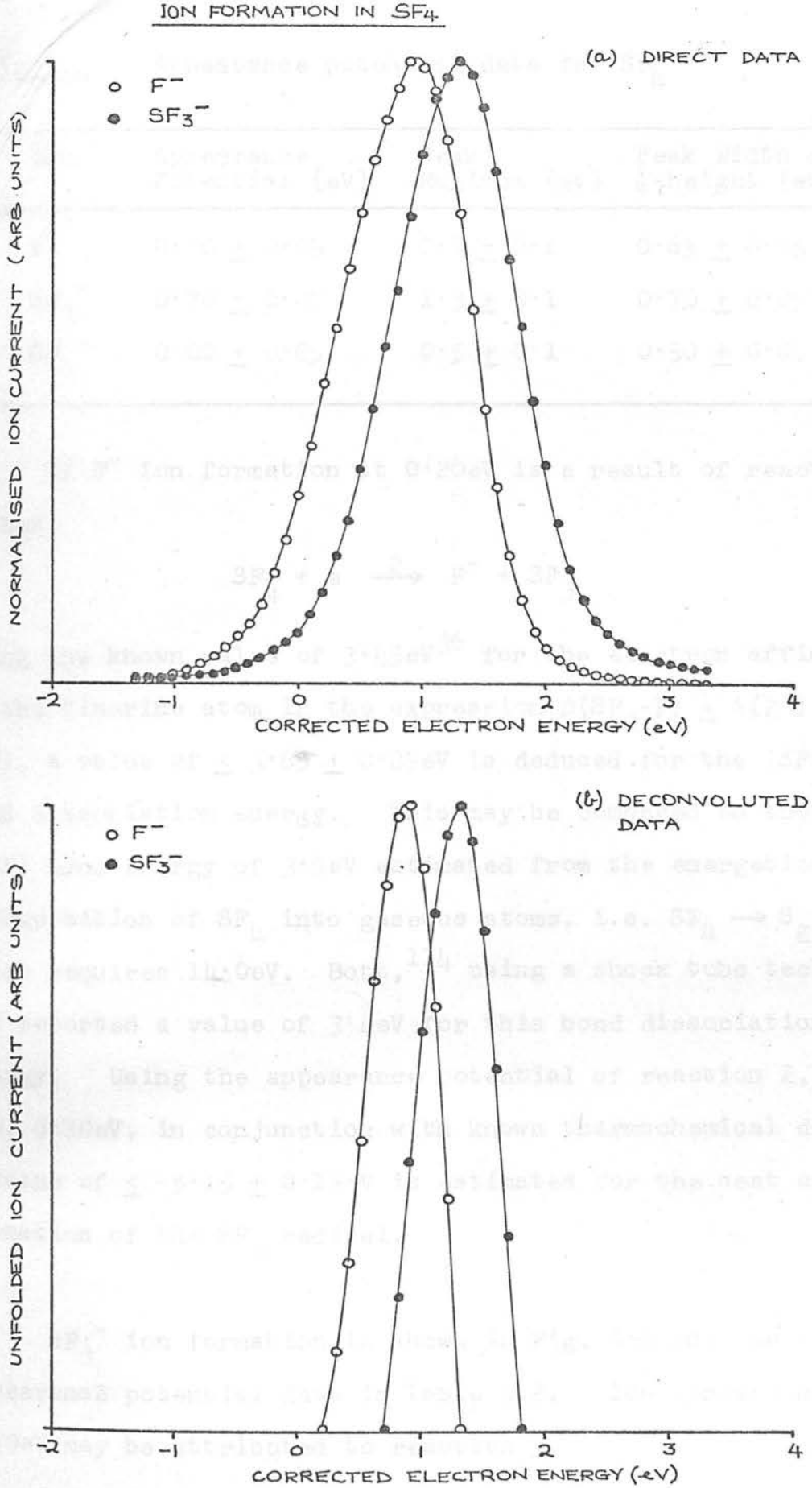
ION FORMATION IN SF_4
(a) DIRECT DATA
o F^-
● SF_3^-
NORMALISED ION CURRENT (ARB UNITS)
-2
-1
0
1
2
3
4
CORRECTED ELECTRON ENERGY (eV)
(b) DECONVOLUTED DATA
o F^-
● SF_3^-
UNFOLDED ION CURRENT (ARB UNITS)
-2
-1
0
1
2
3
4
CORRECTED ELECTRON ENERGY (eV)

Fig 5.2

Table 5.2. Appearance potential data for SF_4

Ion	Appearance Potential (eV)	Peak Maximum (eV)	Peak Width at $\frac{1}{2}$-height (eV)
F^-	0·20 ± 0·05	0·9 ± 0·1	0·65 ± 0·05
SF_3^-	0·70 ± 0·05	1·3 ± 0·1	0·70 ± 0·05
SF_4^-	0·00 ± 0·05	0·5 ± 0·1	0·50 ± 0·05

If F^- ion formation at 0·20eV is a result of reaction 2 then,

$$SF_4 + e \xrightarrow{2} F^- + SF_3$$

using the known value of 3·45eV[36] for the electron affinity of the fluorine atom in the expression $D(SF_3\text{-}F) \leq A(F^-) + E(F)$, a value of $\leq 3{\cdot}65 \pm 0{\cdot}05$eV is deduced for the $(SF_3\text{-}F)$ bond dissociation energy. This may be compared to the mean (S-F) bond energy of 3·5eV estimated from the energetics of decomposition of SF_4 into gaseous atoms, i.e. $SF_4 \longrightarrow S_g + 4F$, which requires 14·0eV. Bott,[114] using a shock tube technique, has reported a value of 3·4eV for this bond dissociation energy. Using the appearance potential of reaction 2, i.e. 0·20eV, in conjunction with known thermochemical data,[29] a value of $\leq -5{\cdot}15 \pm 0{\cdot}15$eV is estimated for the heat of formation of the SF_3 radical.

SF_3^- ion formation is shown in Fig. 5·2 and the appearance potential data in Table 5.2. Ion formation at 0·70eV may be attributed to reaction 3,

$$SF_4 + e \xrightarrow{3} SF_3^- + F$$

Assuming the absence of excess energy in reactions 2 and 3 the following relationship is obtained:

$$A(F^-) + E(F) = A(SF_3^-) + E(SF_3)$$

The electron affinity of SF_3 is therefore estimated to be $2{\cdot}95 \pm 0{\cdot}1$eV. This value is in reasonable agreement with the value of $2{\cdot}71$eV reported by Page and Goode[4] using the magnetron technique.

F_2^- ion formation was also observed at low electron energies, ~0eV. Formation of this ion must be attributed to surface ionisation on the hot filament since, using the known values of $E(F_2) = 2{\cdot}9 \pm 0{\cdot}2$eV[65] and $\Delta H_f(SF_2) = -2{\cdot}9$eV,[64] the minimum enthalpy requirement for reaction 4 is ~$2{\cdot}2$eV.

$$SF_4 + e \xrightarrow{4} F_2^- + SF_2$$

No such ionisation process was noted in this energy region.

(b) Sulphur hexafluoride, SF_6.

This molecule has been the subject of many mass-spectrometric investigations[116,7-13] and because of this the molecule-ion, SF_6^-, is well established as an energy scale calibrant (Chapter 3). The 70eV mass spectrum of SF_6 is given in Table 5.3. The ions detected at low electron energies in this study were F^-, F_2^-, SF_3^-, SF_4^-, SF_5^- and SF_6^-; of these the ions amenable to a detailed investigation

were F^-, SF_3^-, SF_4^-, SF_5^- and SF_6^- which were formed with abundances in the ratio 112:<1:1:253:1000 at their respective capture maxima.

Table 5.3. Negative ion mass spectrum of SF_6 at 70eV.

m/e	Ion	Abundance
19	F^-	160·0
32	S^-	3·0
38	F_2^-	1·0
51	SF^-	5·6
70	SF_2^-	0·4
89	SF_3^-	0·2
108	SF_4^-	0·2
127	SF_5^-	13·6
146	SF_6^-	1000·0

Typical experimental ionisation efficiency data for the ions investigated are shown in Figs. 5.3(a) and 5.4(a); the deconvoluted data are shown in Figs. 5.3(b) and 5.4(b). The energy scale was internally calibrated for the low energy work using the onset at 0·0eV of the SF_6^- ion. This was cross-checked with the calibration of the high energy data where the appearance potentials at 4·2 and 6·6eV for O^- ion formation from SO_2 were used as the energy scale reference points. The unfolded data are compared to appearance potential data reported by other workers in Table 5.4; in general the agreement is reasonable. The SF_3^- and SF_4^-

ION FORMATION IN SF_6 AT LOW ENERGIES

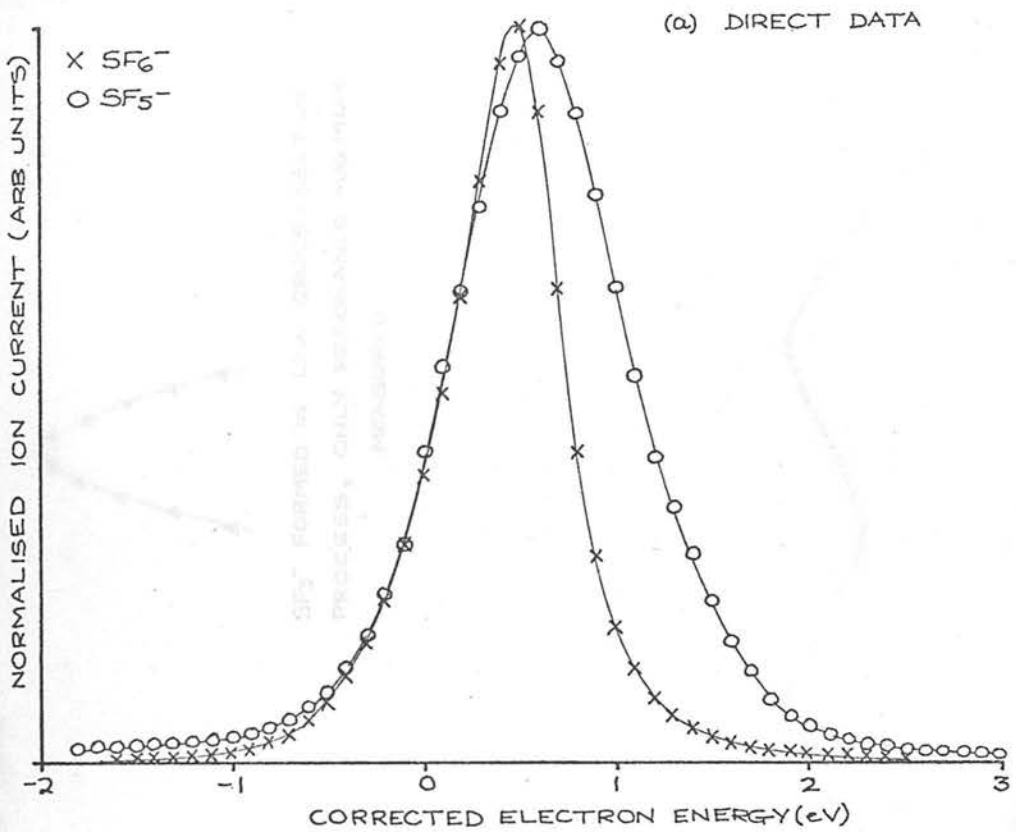

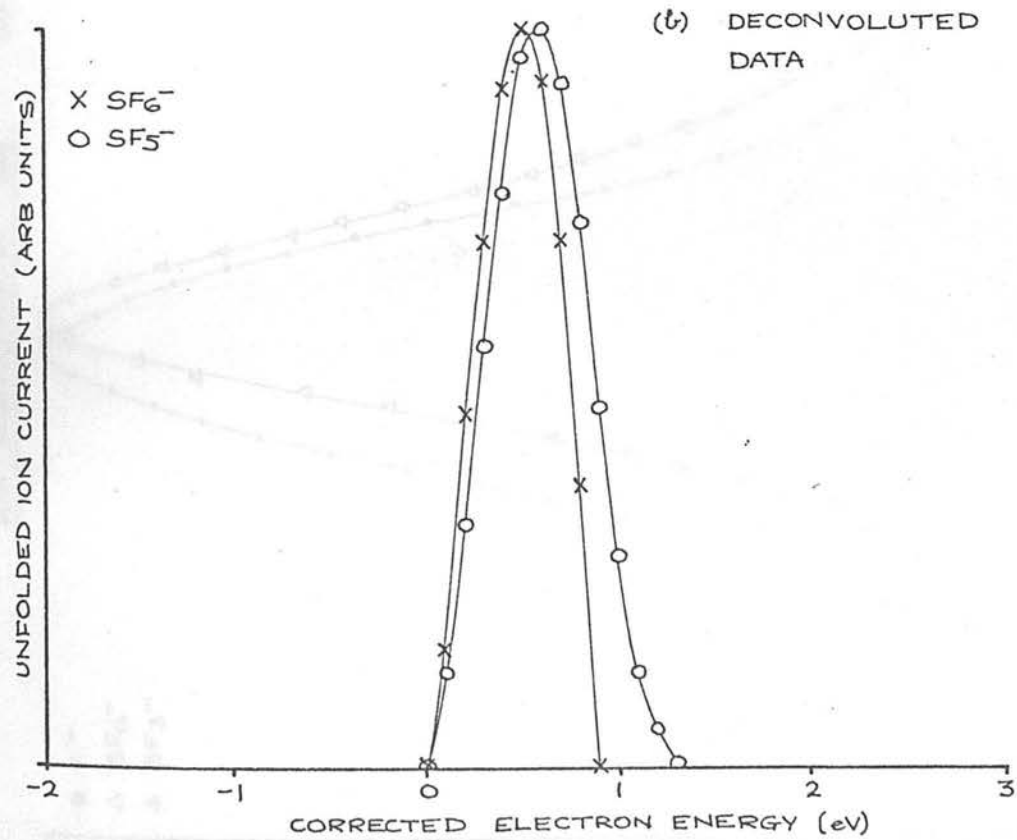

Fig 5.3

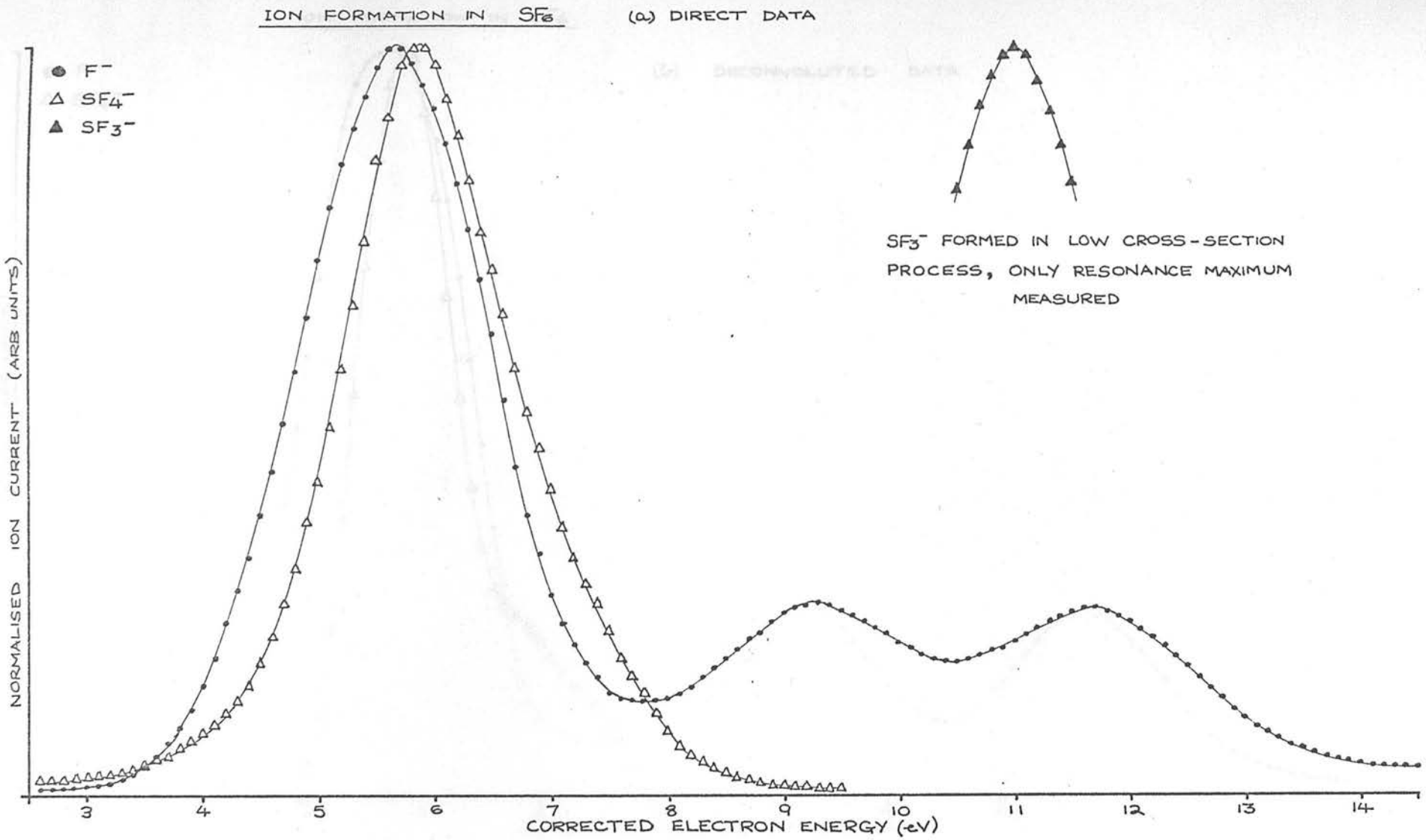
ION FORMATION IN SF_6
(a) DIRECT DATA
F^-
SF_4^-
SF_3^-
NORMALISED ION CURRENT (ARB UNITS)
3
4
5
6
7
8
9
10
11
12
13
14
CORRECTED ELECTRON ENERGY (eV)
SF_3^- FORMED IN LOW CROSS-SECTION PROCESS, ONLY RESONANCE MAXIMUM MEASURED

Fig 5.4

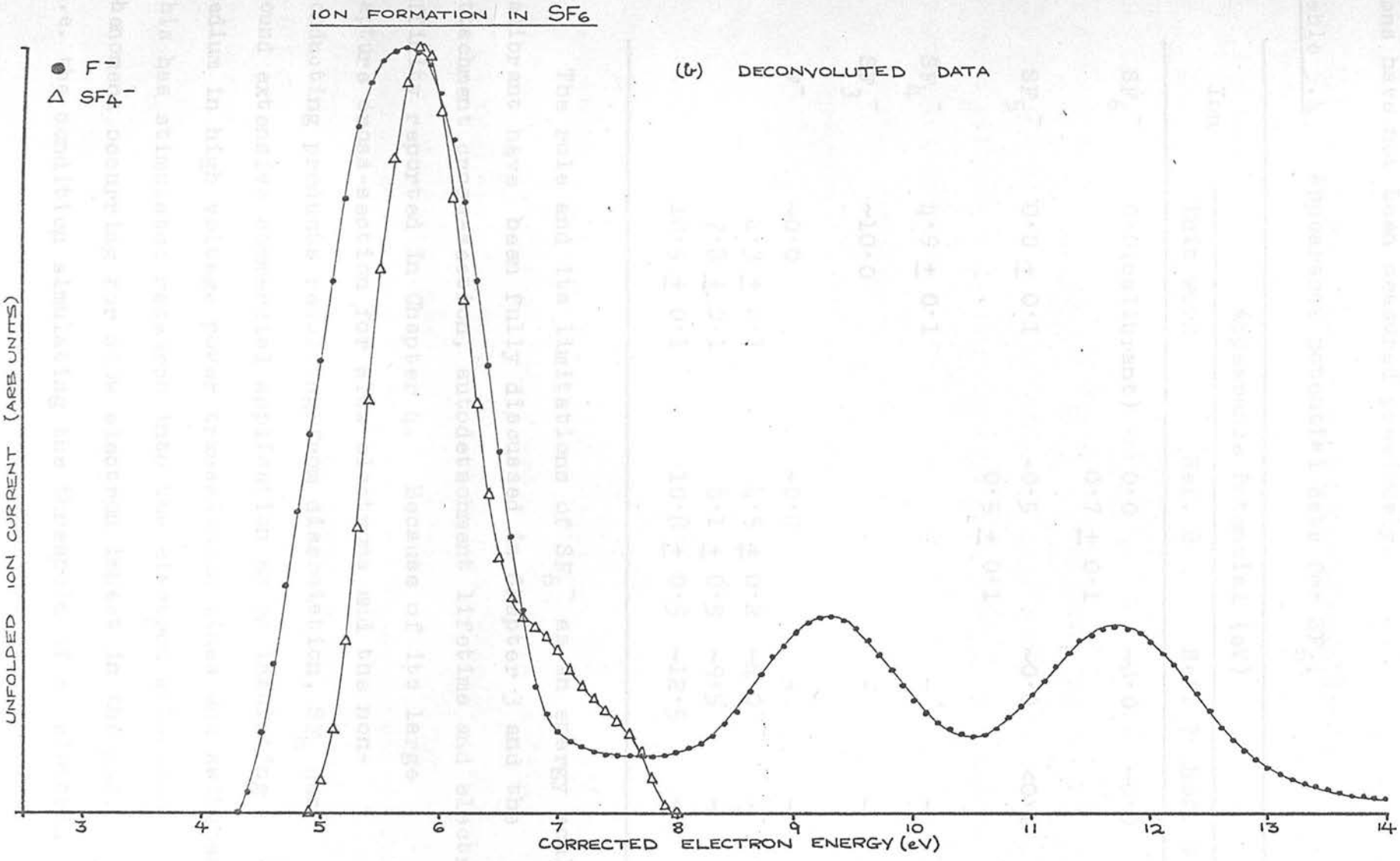
ION FORMATION IN SF_6
(c) DECONVOLUTED DATA
● F^-
△ SF_4^-
UNFOLDED ION CURRENT (ARB UNITS)
3
4
5
6
7
8
9
10
11
12
13
14
CORRECTED ELECTRON ENERGY (eV)

Fig 5.4

ions have not been measured previously.

Table 5.4 Appearance potential data for SF_6.

Ion	Appearance Potential (eV)			
	This work	Ref. 8	Ref. 7	Ref. 9
SF_6^-	0·0(calibrant)	0·0	~0·0	~0·0
		0·7 ± 0·1		
SF_5^-	0·0 ± 0·1	-0·5	~0·0	<0·1
		0·5 ± 0·1		
SF_4^-	4·9 ± 0·1	-	-	-
SF_3^-	~10·0	-	-	-
F^-	~0·0	~0·0	-	-
	4·3 ± 0·1	4·5 ± 0·2	~4·0	-
	7·8 ± 0·1	8·1 ± 0·5	~9·5	-
	10·5 ± 0·1	10·8 ± 0·5	~12·5	-

The role and its limitations of SF_6^- as an energy scale calibrant have been fully discussed in Chapter 3 and the attachment cross-section, autodetachment lifetime and electron affinity reported in Chapter 4. Because of its large capture cross-section for slow electrons and the non-conducting products resulting from dissociation, SF_6 has found extensive commercial application as an insulating medium in high voltage power transmission lines and switches. This has stimulated research into the electron attachment phenomena occurring for slow electron impact in the gas, i.e. the condition simulating the threshold of an electron

avalanche. A discussion of the intermediate compound negative ion states involved in these processes is only possible through a comparison of the results obtained by several experimental approaches. In an attempt to do this the low energy observations made in this study are examined in the light of previous mass spectrometric studies,[1,6,7-11] the temperature variable study of Fehsenfeld[13] using the flowing afterglow technique and the experiments of Brion[12] using a velocity selected electron beam with a very narrow energy distribution.

Within experimental error the present value for $A(SF_5^-)$ is in agreement with those reported previously. Recently Brion,[12] using a 100mV electron energy distribution, showed that the SF_5^- ion was formed as a sharp peak at 0·0eV followed by a broader resonance at ~0·5eV. The SF_5^- peak, found in this work and shown in Fig. 5.3, is considerably broader than the electron energy distribution (Fig. 3.7). Resolution of the broad peak, observed by Brion at 0·5eV, has not been achieved by the deconvolution procedure although its presence is suggested in the trailing edge of the resonance peak.

SF_5^- ion formation, found to occur abundantly at $0{\cdot}0 \pm 0{\cdot}1$eV, may be the result of both dissociative electron capture (reaction 5) and spontaneous dissociation (reaction 7)

$$SF_6 + e \longrightarrow SF_6^{-*}(T_a \sim 10^{-13}\text{sec}) \xrightarrow{5} SF_5^- + F$$

$$SF_6 + e \longrightarrow SF_6^{-*}(T_a \text{ up to } 10^{-6}\text{sec}) \xrightarrow{6} SF_6 \text{ (or } SF_6^*) + e$$

$$\downarrow 7$$

$$SF_5^- + F$$

The distinction between reactions 5 and 7 lies in the description of the parent ion potential surface in the Franck-Condon region of the ground state neutral SF_6 molecule. The intermediate compound ion state involved in dissociative capture (reaction 5) can be described as a virtual state of the ion and is represented by a repulsive surface in the Franck-Condon region. Such a state can exist for only a single vibrational time period, $\sim 10^{-13}$ second, before decaying by autodetachment or dissociative capture. The potential surface representing the compound ion state in reaction 7 exhibits a potential well in the Franck-Condon region, the weakly bound negative ion state thus surviving autodetachment for times up to 10^{-5} second.

The SF_6^- ion was found in this work to be a long lived species exhibiting an average autodetachment lifetime of 68 μsec. and an electron affinity calculated to be 1·4eV. Spontaneous dissociation from this long lived state by reaction 7 would be endothermic by approximately 1·2eV therefore suggesting a low probability for this dissociation channel. However, under different source conditions, when higher temperatures may prevail, higher vibrationally excited states of the ion may be formed and consequently spontaneous dissociation cannot be excluded. Ahearn and Hannay,[7] using a magnetic deflection instrument, have reported a metastable ion peak with an apparent m/e = 110·6 which they have attributed to reaction 7. The SF_5^- ion current detected in this study may therefore result from both reactions 5 and 7 where vibrationally excited states are responsible for the

latter. The spontaneous dissociation of such species is expected to be very rapid and as the time lag between ion formation and drawout in the time-of-flight mass spectrometer is 1 - 2 μsec. the products of such a reaction would be detected as dissociative capture products.

The low intensity F^- ion peak, observed by Curran[10] and Brion[12] as a facsimile of the SF_6^- peak at zero energy, was also detected in this study with a similar cross-section, i.e. $\leq$ 1% SF_6^- intensity. The appearance at 0·0eV for the F^- ion signal may be used in conjunction with the known electron affinity of 3·45eV[36] for the fluorine atom to estimate a value of $\leq$ 3·45eV for the SF_5-F bond dissociation energy. This is very close to the value of ~3·4eV calculated for the average S-F bond energy in SF_6 from the energetics of decomposition; $SF_6 \longrightarrow S_g + 6F$.

Work reported on the temperature dependence of SF_5^- ion formation from SF_6[13,19] has shown the rate constant to increase rapidly with rising temperature and hence an increasing population of vibrationally excited SF_6 molecules. Fehsenfeld[13] constructed an Arrhenius plot over the temperature range 0 - 300°C and obtained a value of 0·4eV for the activation energy, suggesting that the lowest dissociating level of SF_6^{-*} cuts through the SF_6 curve at about the 4th or 5th vibrational level. Consequently SF_5^- ion formation below 0·4eV indicates that vertical transitions from the small population of vibrationally excited SF_6 molecules present are sufficient to produce a substantial SF_5^- current. Collectively the above information allows a simple

qualitative two-dimensional picture of the potential energy surfaces to be constructed, as shown in Fig. 5.5(a). The surface labelled (i) corresponds to the ground state configuration of SF_6^-, that labelled (ii) to one of the many vibrationally excited SF_6^{-*} states and (iii) and (iv) represent two of the possible non-bonding surfaces.

At room temperature, formation of a long lived (T_a = 68 μsec.) SF_6^- state occurs with the highest probability, SF_5^- ion formation being formed to about 25% of this. At elevated temperatures the increased population of vibrationally excited molecules is accompanied by a higher transition probability to such surfaces as those labelled (iii) and (iv), this being manifest in the rapidly increasing SF_5^- ion current.

If the surfaces leading to the dissociative capture products F^- and SF_5^- are separated in the Franck-Condon region, then it would be expected that only the lower of the two surfaces would be involved and consequently only one ion would result from dissociative capture. This situation corresponds to the surface labelled (iii) in Fig. 5.5(a) which lies below the lowest surface resulting in F^- ion formation. If the two surfaces (leading to SF_5^- + F and F^- + SF_5) were coincident in the Franck-Condon region however, the factor determining the electron capture between the two receding fragments (i.e. SF_5 and F) will be the relative depths of the potential wells which the electron 'sees', that is the electron affinities of the fragments. As $E(SF_5)$[4] > $E(F)$[36] a predominant SF_5^- current would be

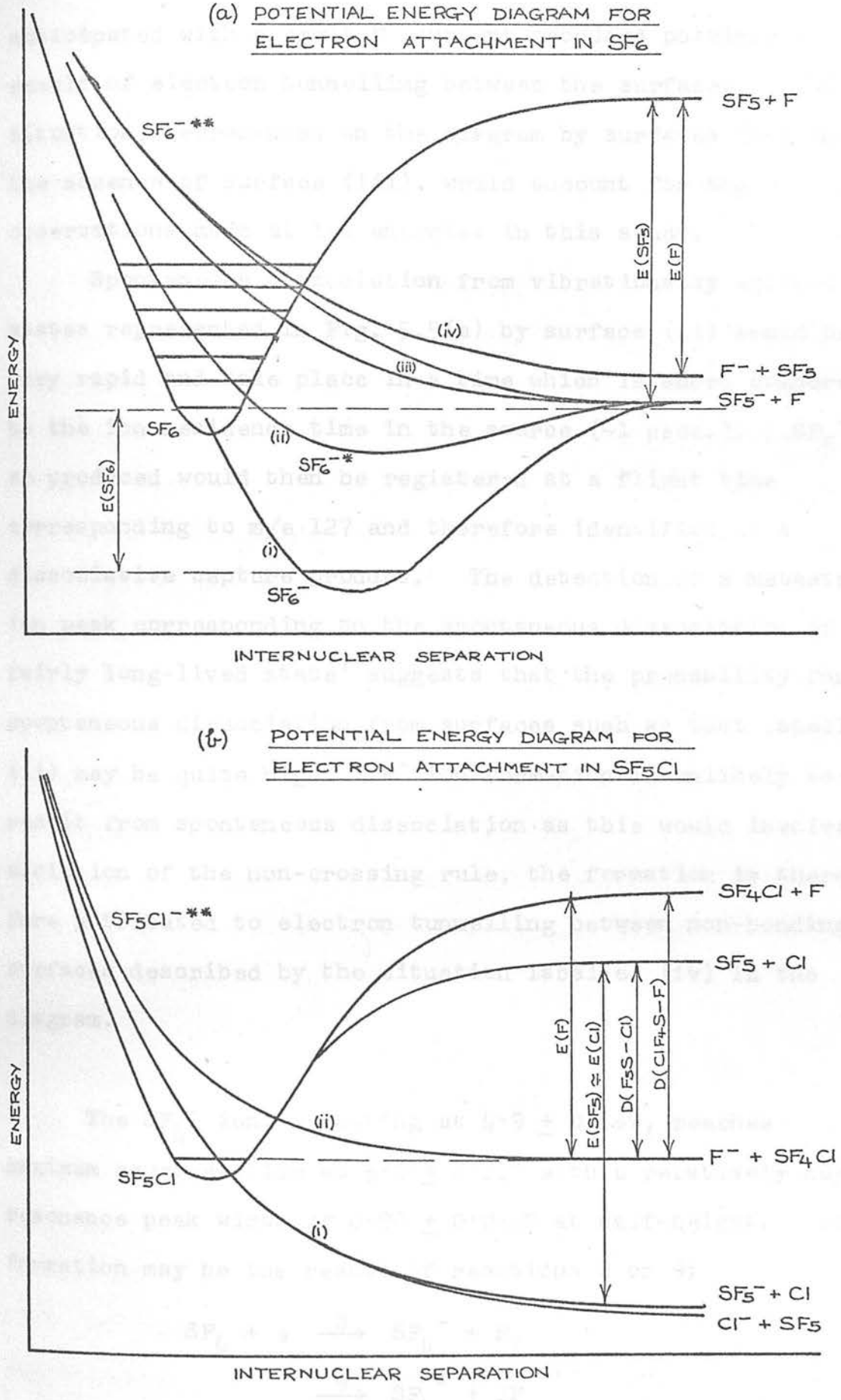
(a) POTENTIAL ENERGY DIAGRAM FOR ELECTRON ATTACHMENT IN SF_6
SF_6^{-**}
$SF_5 + F$
E(SF5)
E(F)
(iv)
(iii)
$F^- + SF_5$
$SF_5^- + F$
ENERGY
SF_6
(ii)
SF_6^{-*}
E(SF6)
(i)
SF_6^-
INTERNUCLEAR SEPARATION
(b) POTENTIAL ENERGY DIAGRAM FOR ELECTRON ATTACHMENT IN SF_5Cl
SF_5Cl^{-**}
$SF_4Cl + F$
$SF_5 + Cl$
E(F)
E(SF5) ≈ E(Cl)
D(F5S-Cl)
D(ClF4S-F)
(ii)
$F^- + SF_4Cl$
SF_5Cl
(i)
$SF_5^- + Cl$
$Cl^- + SF_5$
ENERGY
INTERNUCLEAR SEPARATION

Fig 5.5

anticipated with a small F^- current produced possibly as the result of electron tunnelling between the surfaces. This situation, represented on the diagram by surfaces (iv) in the absence of surface (iii), would account for the observations made at low energies in this study.

Spontaneous dissociation from vibrationally excited states represented in Fig. 5.5(a) by surface (ii) would be very rapid and take place in a time which is short compared to the ion residence time in the source (~1 μsec.). SF_5^- so produced would then be registered at a flight time corresponding to m/e 127 and therefore identified as a dissociative capture product. The detection of a metastable ion peak corresponding to the spontaneous dissociation of a fairly long-lived state[7] suggests that the probability for spontaneous dissociation from surfaces such as that labelled (ii) may be quite high. F^- ion formation is unlikely to result from spontaneous dissociation as this would involve violation of the non-crossing rule, the formation is therefore attributed to electron tunnelling between non-bonding surfaces described by the situation labelled (iv) in the diagram.

The SF_4^- ion, onsetting at 4·9 ± 0·1eV, reaches maximum cross-section at 5·8 ± 0·1eV with a relatively narrow resonance peak width of 0·90 ± 0·05eV at half-height. Ion formation may be the result of reactions 8 or 9;

$$SF_6 + e \xrightarrow{8} SF_4^- + F_2$$

$$\xrightarrow{9} SF_4^- + 2F$$

Using known thermochemical data[23] and the value of 1·2eV for $E(SF_4)$ calculated in Chapter 4, the minimum enthalpy requirements for 8 and 9 are 3·3 and 4·9eV respectively. It is therefore reasonable to accept reaction 9 as that responsible for SF_4^- ion formation. Exact agreement between ΔH_{min} and $A(SF_4^-)$ would then indicate the absence of excess energy and provides confirmation for the value of $E(SF_4)$ = 1·2eV calculated from the statistical model of electron attachment. Assuming that the SF_4^- appearance potential is the minimum enthalpy requirement for reaction 9, $E(SF_4)$ = 1·2eV and the SF_5-F bond dissociation energy is $\leq$ 3·45eV, the SF_4-F bond dissociation energy is estimated to be $\leq$ 2·65eV.

The structure in the trailing edge of the SF_4^- peak, Fig. 5.4(b), although reproducible on the energy scale was not reproducible in shape due to the low ion currents involved and the low signal to noise ratio at the baseline. Ion formation at this energy must be attributed to reaction 9 in which excess energy is involved. The onset of this shoulder at ~6·6eV indicates that ~1·7eV of excess energy must be partitioned between the fragments.

The SF_3^- ion was formed with a very low cross-section (Fig. 5.4(a)) which prevented a detailed investigation of its energy dependence. The capture maximum, however, was found to be at 11·0 $\pm$ 0·1eV and a rough investigation revealed the resonance peak shape to show a close resemblance to that observed for the SF_4^-/SF_6 ion. The appearance potential was therefore estimated to be at approximately 10eV, although

this does not exclude the possibility that a resonance of lower cross-section precedes the major peak. Using the values $\Delta H_f(SF_3) \leq -5{\cdot}15$eV and $E(SF_3) = 2{\cdot}9$eV obtained earlier the minimum enthalpy requirement for reaction 10 is estimated to be 6·9eV.

$$SF_6 + \xrightarrow{10} SF_3^- + 3F$$

This leads to the tentative suggestion that, in the absence of an undetected resonance at lower energy, ~3eV of excess energy is associated with SF_3^- ion formation.

Appearance potential data for F^- ion formation is given in Table 5.4 and the direct and deconvoluted ionisation efficiency curves are shown in Figs. 5.4(a) and (b) respectively. Within experimental error the present values are in reasonable agreement with those reported by Marriott.[8] Three resonance processes are evident (excluding the process at 0·0eV which has been discussed above) ion formation onsetting at 4·3, 7·8 and 10·5eV with their cross-section ratios being approximately 4:1:1.

$$SF_6 + e \xrightarrow{11} F^- + SF_4 + F$$
$$\xrightarrow{12} F^- + SF_3 + 2F$$
$$\xrightarrow{13} F^- + SF_2 + 3F$$

Reactions 11, 12 and 13 involve the successive stripping of fluorine atoms from the molecule and may be responsible for the onsets at 4·3, 7·8 and 10·5eV. If this is so the SF_4-F bond dissociation energy $\leq 2{\cdot}65$eV, estimated from the

SF_4^- data above, suggests that $\geq$ 1·65eV of excess energy is associated with reaction 11. Assuming that no excess energy is associated with 12 and 13 then the SF_3-F and SF_2-F bond dissociation energies are estimated to be 3·5 $\pm$ 0·3 and 2·7 $\pm$ 0·4eV respectively. The value of 3·5 $\pm$ 0·3eV deduced for the SF_3-F bond energy is in good agreement with the value of 3·65 $\pm$ 0·05eV obtained from the sulphur tetrafluoride work and this suggests that there is little or no excess energy associated with reaction 12.

The following bond dissociation energies have been deduced:

Bond	Bond Strength (eV)
SF_5-F	$\leq$ 3·45
SF_4-F	$\leq$ 2·65
SF_3-F	3·5 $\pm$ 0·3 (3·65 $\pm$ 0·05 from SF_4 work)
SF_2-F	2·7 $\pm$ 0·4

Complete dissociation of SF_6 into gaseous atoms, $SF_6 \longrightarrow S_g + 6F$, requires 20·3eV, using this in conjunction with the values above implies that;

$$D(SF\text{-}F) + D(S\text{-}F) \geq 7{\cdot}85 \pm 0{\cdot}45\text{eV}.$$

The appearance of the SF_2^- and SF^- ions in the negative ion mass spectrum at 70eV shows that these ions are stable to the following decomposition reactions;

$$SF_2^- \xrightarrow{14} SF + F^-$$
$$SF^- \xrightarrow{15} S + F^-$$

From the known value for E(F) = 3·45eV[36] and E(SF) = 0·9 ± 0·2eV[64] reaction 15 can be used to provide a lower limit of 2·55 ± 0·2eV for the S-F bond dissociation energy which, on subtraction from 7·85 ± 0·45eV obtained above for D(SF-F) + D(S-F), results in a value of 5·3 ± 0·65eV for the SF-F bond dissociation energy.

(c) Pentafluorosulphur Chloride, SF_5Cl

Pentafluorosulphur chloride was studied in order to investigate the effect of the chlorine atom upon negative ion formation by fluorine containing sulphur compounds and its possible effect on the stability of the negative molecule-ion. Neither positive nor negative ion formation from SF_5Cl has been investigated previously. The 70eV positive ion mass spectra of SF_5Cl and SF_6 are presented for comparison in Table 5.6 (page 104).

Both molecules readily form doubly charged fragment positive ions containing sulphur and fluorine but for SF_5Cl no doubly charged ions containing S, F and Cl are observed and the singly charged ions containing all three elements are generally of low abundance. This reflects the relative weakness of the S-Cl bond compared to the S-F bond in SF_5Cl. A molecule-ion of very low intensity is formed in SF_5Cl but no parent ion was observed for SF_6, in agreement with the observations of Dibeler and Mohler.[116]

The positive ion appearance potential data shown in Table 5.7 were obtained using the semi-logarithmic plot method[117] referenced to an energy scale calibrated against

Table 5.6. Positive ion mass spectra of SF_5Cl and SF_6 at 70eV.

	SF_5Cl		SF_6	
m/e	Ion	Abundance	Ion	Abundance
16	S^{2+}	0·1	S^{2+}	< 0·1
19	F^+	0·4	F^+	0·4
32	S^+	3·1	S^+	1·4
35	Cl^+	2·0		
	SF_2^{2+}	1·5	SF_2^{2+}	0·7
37	Cl^+	0·7		
44·5	SF_3^{2+}	< 0·1	SF_3^{2+}	< 0·1
51	SF^+	6·1	SF^+	4·6
54	SF_4^{2+}	0·4	SF_4^{2+}	0·4
63·5	SF_5^{2+}	< 0·1		
67	SCl^+	1·6		
70	SF_2^+	6·8	SF_2^+	4·7
86	$SFCl^+$	0·6		
89	SF_3^+	36·8	SF_3^+	18·0
105	SF_2Cl^+	0·2		
108	SF_4^+	5·3	SF_4^+	3·2
124	SF_3Cl^+	< 0·1		
127	SF_5^+	100·0	SF_5^+	100·0
143	SF_4Cl^+	11·0		
162	SF_5Cl^+	< 0·1		

the spectroscopic appearance potential of A^+ (15·76eV).[15] The appearance potential data for SF_6 has been previously reported by Dibeler and Mohler.[116]

Table 5.7. Positive ion appearance potential data for SF_5Cl

m/e	Ion	Appearance Potential (eV)
19	F^+	33·8 ± 0·3
32	S^+	33·2 ± 0·5
35/37	Cl^+	20·8 ± 0·3
127	SF_5^+	13·2 ± 0·2
143/145	SF_4Cl^+	15·9 ± 0·1

For dissociation into gaseous atoms SF_6 and SF_5Cl require 20·3 and 18·9eV respectively. Assuming the S-F bonds to have a constant energy then $D(SF_5\text{-}F) - D(SF_5\text{-}Cl) =$ 1·4eV and, using the value of $\leq$ 3·45eV deduced for the SF_5-F bond dissociation energy from the SF_6 data, $D(SF_5\text{-}Cl)$ is estimated to be $\leq$ 2·05eV. This relatively low bond strength is compatible with the observation that SF_5Cl undergoes thermal decomposition at about 200°C.[16]

The appearance potential of the SF_5^+ ion from SF_5Cl at 13·2 ± 0·2eV, arising from reaction 16, may be compared with the value of 15·9 ± 0·2eV for SF_5^+ formation from SF_6 reported by Dibeler and Mohler[116] as a result of reaction 17.

$$SF_5Cl + e \xrightarrow{16} SF_5^+ + Cl + 2e$$

$$SF_6 + e \xrightarrow{17} SF_5^+ + F + 2e$$

Neglecting possible excess energy contributions, $D(SF_5\text{-}F) - D(SF_5\text{-}Cl) = 2{\cdot}7 \pm 0{\cdot}4$eV which is only in reasonable accord with the difference of $1{\cdot}4$eV deduced from the energetics of decomposition above.

The most probable ionisation processes leading to Cl^+ ion formation at $20{\cdot}8 \pm 0{\cdot}3$eV are reactions 18 and 19;

$$SF_5Cl + e \xrightarrow{18} Cl^+ + SF_5 + 2e$$

$$\xrightarrow{19} Cl^+ + SF_4 + F + 2e$$

Assuming $D(SF_5\text{-}Cl) \simeq 2{\cdot}0$eV, then the minimum enthalpy requirements for 18 and 19 are ~16 and ~19eV respectively. This suggests that reaction 19 is that responsible for Cl^+ ion formation at $20{\cdot}8 \pm 0{\cdot}3$eV.

In addition to the appearance potential for the F^+ ion measured at $33{\cdot}8 \pm 0{\cdot}3$eV, breaks in the F^- and Cl^- ionisation efficiency curves were noted at $32{\cdot}8$ and $33{\cdot}5$eV respectively.

$$SF_5Cl + e \xrightarrow{20} F^+ + S + 4F + Cl + 2e$$

$$\xrightarrow{21} F^+ + F^- + S + 3F + Cl + e$$

$$\xrightarrow{22} F^+ + Cl^- + S + 4F + e$$

Reactions 20, 21 and 22 have minimum enthalpy requirements of $37{\cdot}1$, $33{\cdot}7$ and $33{\cdot}5$eV respectively, it would therefore appear that the appearance potential of F^+ at $33{\cdot}8$ together

with the observed breaks in the F^- and Cl^- curves, suggests that both ion-pair processes 21 and 22 contribute to F^+ ion formation.

The appearance potential for the S^+ ion at 33·2 ± 0·5eV is in reasonable agreement with the calculated energy requirement of 32·2eV for reaction 23.

$$SF_5Cl + e \xrightarrow{23} S^+ + SF + Cl + 2e$$

Any ion pair processes would have an energy requirement at least 3·4eV lower than this, since it would involve F^- or Cl^- ion formation. S^+ ion formation may therefore be attributed to reaction 23.

$$SF_5Cl + e \xrightarrow{24} SF_4Cl^+ + F + 2e$$

If it is assumed that $D(SF_4Cl - F)$ is the same as the SF_5-F bond dissociation energy, ~3·4eV, then using the appearance potential of 15·9 ± 0·1eV measured for the SF_4Cl^+ ion, an upper limit of 12·5 ± 0·2eV is estimated for $I(SF_4Cl)$, the ionisation potential of SF_4Cl. There is no other reported value.

Pentafluorosulphur chloride was an abundant source of negative ions, the total cross-section for negative ion formation being greater, under comparable source conditions, than for SF_4 or SF_6. The 70eV negative ion mass spectrum is presented in Table 5.8.

Despite a thorough search at low and high electron energies, that is in regions of primary and secondary electron capture, SF_5Cl^- was not detected. This is in contrast to the situation in SF_6 and

$$SF_5Cl + e \xrightarrow{25} SF_5Cl^-_{gd\ st} \quad (T_a \sim 10^{-6}\ \text{sec.})$$

indicates that reaction 25 does not occur.

Table 5.8 Negative ion mass spectrum of SF_5Cl at 70eV.

m/e	Ion	Abundance
19	F^-	1000·0
32	S^-	0·7
35/37	Cl^-	100·0
38	F_2^-	< 0·1
51	SF^-	8·0
54	FCl^-	2·0
70	SF_2^-	0·6
89	SF_3^-	16·2
108	SF_4^-	3·3
127	SF_5^-	24·1

Parent ion formation along a potential surface such as that labelled (ii) in Fig. 5.5(a) would not be detected directly due to the short lifetimes of such excited states. Fragment ion formation as a result of the spontaneous dissociation of such states would be detected as dissociative capture products hence the observation of the fragment ions F^-, Cl^-

and SF_5^- at zero electron energy does not therefore preclude the possibility of short-lived SF_5Cl^- ion states. The dissociative

$$SF_5Cl + e \longrightarrow SF_5Cl^{-*} (\tau \sim 10^{-13} \text{sec.}) \xrightarrow{26} SF_5^- + Cl$$
$$\xrightarrow{27} Cl^- + SF_5$$
$$\xrightarrow{28} F^- + SF_4Cl$$

capture reactions 26, 27 and 28 however, are all exothermic to thermal electron capture. Excluding the surfaces just discussed, Fig. 5.5(b) may be used to represent this system for thermal electron capture; the repulsive surface, drawn through the ground state configuration of SF_5Cl, labelled (i), represents a non-bonding excited state of SF_5Cl^{-*} decaying in a vibrational time period ($\sim 10^{-13}$ sec.) via auto-detachment to ground state SF_5Cl or dissociative capture to the fragments shown. F^- ion formation is described by dissociation of the excited SF_5Cl^{-*} ion along the surface labelled (ii), this channel being open only on condition that $D(SF_4Cl\text{-}F)$ is less than $E(F)$.

As SF_5Cl^{-**} dissociates along the surface labelled (i), the electron will be resonating between the receding fragments, and as the potential wells 'seen' by the electron are of comparable depth, i.e. $E(Cl)^{36} \simeq E(SF_5)$,[4] equal localisation probabilities might be anticipated. Separation of the surfaces, representing $SF_5^- + Cl$ and $Cl^- + SF_5$ formation, in the Franck-Condon region would lead to a predominance of the ion formed along the lower surface with

the other ion, formed along the upper surface, in an amount determined by the extent of electron tunnelling between the surfaces.

Precise measurements on the relative abundances of the dissociative capture ions at zero electron energy could not be made because of the signal contributions arising from surface ionisation of fragments following pyrolysis of SF_5Cl on the hot filament. The signal resulting from 'thermal' ion formation was found to decay rapidly with decreasing filament temperature (i.e. with increasing electron energy). The appearance of ions of thermal origin in the drift tube may be explained as follows: at 'negative' electron energies, any ions formed on the filament are prevented from reaching the collision chamber and from being detected by the repulsion of the electron slits. As this bias is decreased and becomes attractive, ions are drawn through the electron slits and trace out an intensity curve which is similar to that for electrons under the same conditions. However, the simple sigmoidal function is modified by the concurrent decay of filament temperature and a peak in intensity is observed. Thermal ions are therefore dependent upon operating conditions and reproducible results are difficult to obtain.

The negative ions detected and measured in SF_5Cl were F^-, Cl^-, FCl^-, SF_3^-, SF_4^- and SF_5^-. Pressure dependence measurements showed them all to be of primary origin, including FCl^-. Experimental and unfolded ionisation efficiency curves for some of the ions, measured at electron

energies greater than 2eV, are shown in Figs. 5.6(a) and (b). The SF_4^- ion has not been included as the low cross-section for ion formation resulted in data of inferior quality. The energy scale is calibrated against the appearance potentials at 4·2 and 6·6eV for the O^- ion formed from SO_2. The appearance potential data for the ions formed by SF_5Cl are shown in Table 5.9.

The SF_5^- ion resonance peak has a width of 0·8 ± 0·1eV at half-height and the unfolded experimental data shows the onset to be at 0·1 ± 0·1eV. Since $E(SF_5) = 3·6eV$[4] and $D(SF_5\text{-}Cl)$ has been estimated above to be ~2·0eV, then the SF_5^- ion should be formed at ~0eV; this was found to be so experimentally.

Table 5.9. Appearance potential data for SF_5Cl.

Ion	Appearance Potential (eV)	Peak Maximum (eV)	Peak Width at ½-height (eV)
SF_5^-	0·1 ± 0·1	0·6 ± 0·1	0·8 ± 0·1
SF_4^-	4·1 ± 0·2	5·8 ± 0·3	~1·5
SF_3^-	7·4 ± 0·1	8·8 ± 0·1	1·4 ± 0·1
FCl^-	7·5 ± 0·1	8·9 ± 0·1	1·7 ± 0·1
Cl^-	~0·0	-	-
	4·9 ± 0·1	-	-
	unresolved ion current between 5·0 - 7·5eV		
	7·6 ± 0·2	8·9 ± 0·1	1·7 ± 0·1
F^-	~0·0	-	-
	2·9 ± 0·1	4·7 ± 0·1	1·3 ± 0·1
	7·6 ± 0·1	9·0 ± 0·1	1·5 ± 0·1

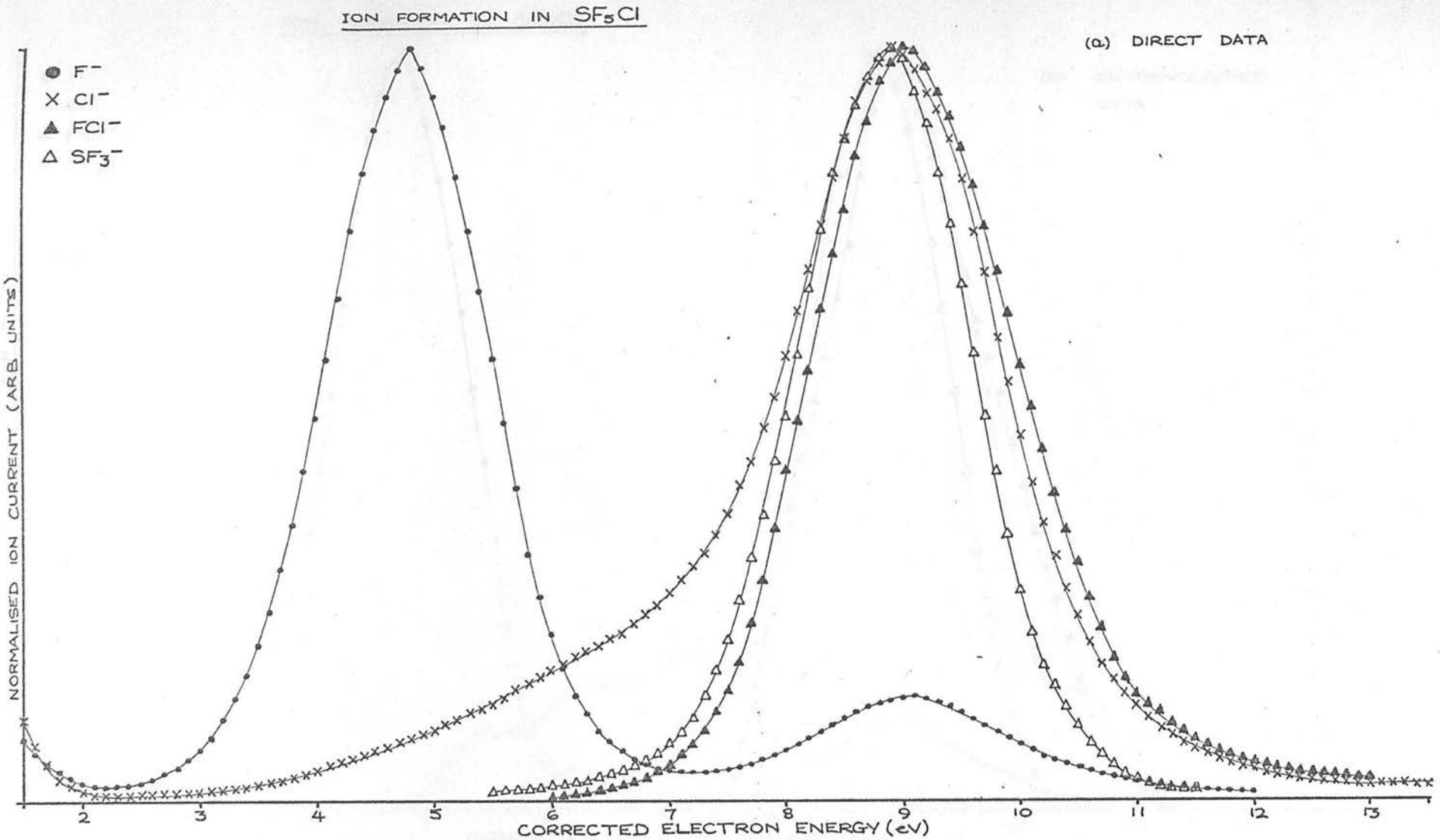
ION FORMATION IN SF_5Cl
(a) DIRECT DATA
F^-
Cl^-
FCl^-
SF_3^-
NORMALISED ION CURRENT (ARB. UNITS)
2
3
4
5
6
7
8
9
10
11
12
13
CORRECTED ELECTRON ENERGY (eV)

Fig 5.6

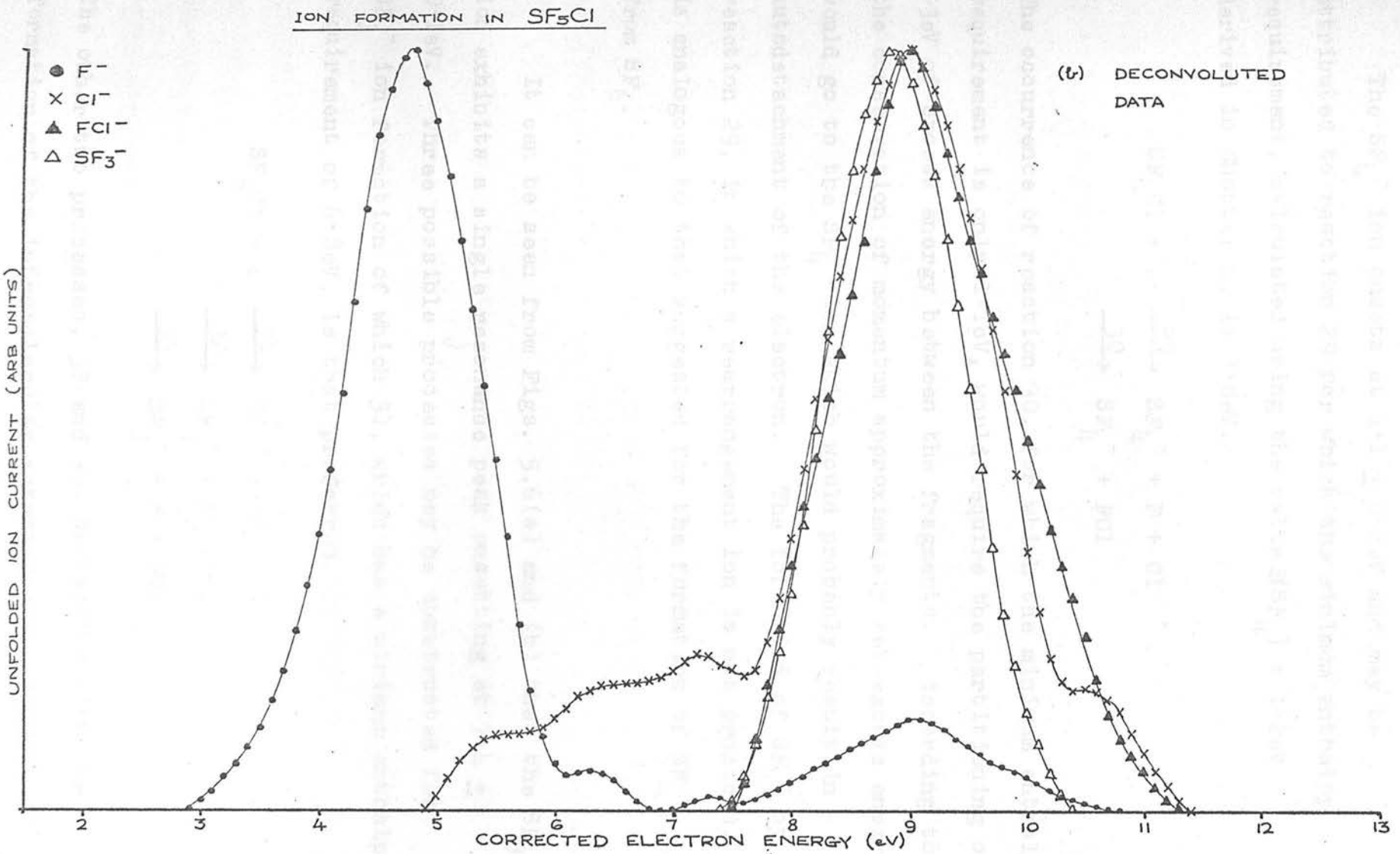
ION FORMATION IN SF_5Cl
F^-
Cl^-
FCl^-
SF_3^-
(t) DECONVOLUTED DATA
UNFOLDED ION CURRENT (ARB UNITS)
2
3
4
5
6
7
8
9
10
11
12
13
CORRECTED ELECTRON ENERGY (eV)

Fig 5.6

The SF_4^- ion onsets at 4·1 ± 0·2eV and may be attributed to reaction 29 for which the minimum enthalpy requirement, calculated using the value $E(SF_4) = 1·2eV$ derived in Chapter 4, is 3·8eV.

$$SF_4Cl + e \xrightarrow{29} SF_4^- + F + Cl$$
$$\xrightarrow{30} SF_4^- + FCl$$

The occurrence of reaction 30, for which the minimum enthalpy requirement is only 1·1eV, would require the partitioning of ~3eV of excess energy between the fragments. According to the conservation of momentum approximately 2eV excess energy would go to the SF_4^- ion which would probably result in autodetachment of the electron. The formation of SF_4^- by reaction 29, in which a rearrangement ion is not produced, is analogous to that suggested for the formation of SF_4^- from SF_6.

It can be seen from Figs. 5.6(a) and (b) that the SF_3^- ion exhibits a single resonance peak onsetting at 7·4 ± 0·1eV. Three possible processes may be constructed for SF_3^- ion formation of which 31, which has a minimum enthalpy requirement of 6·8eV, is that preferred.

$$SF_5Cl + e \xrightarrow{31} SF_3^- + 2F + Cl$$
$$\xrightarrow{32} SF_3^- + F_2 + Cl$$
$$\xrightarrow{33} SF_3^- + F + FCl$$

The other two processes, 32 and 33, proceeding with the formation of the intramolecular rearrangement fragments F_2

and FCl respectively, would involve the release of 2·2 and 2·3eV of excess energy since they have minimum enthalpy requirements of 5·2 and 5·1eV respectively.

Pressure dependence measurements at the resonance peak maximum of the FCl^- ion onsetting at 7·5 ± 0·1eV, showed it to be a primary ion.

$$SF_5Cl + e \xrightarrow{34} FCl^- + SF_3 + F$$

Assuming no excess energy is involved in reaction 34, and using $\Delta H_f(SF_3) = -5·1eV$, a value of $E(FCl) = 1·5 \pm 0·4eV$ is calculated. Since FCl^- is stable against the decomposition reaction $FCl^- \longrightarrow Cl^- + F$, the electron affinity (using $E(Cl) = 3·6eV$[36] and $D(F-Cl) = 2·56eV$[18]) is estimated to be $\geq 1·04eV$. There is no other value reported for E(FCl) but values of 2·9 ± 0·2 and 2·5 ± 0·2eV[65] have been reported for $E(F_2)$ and $E(Cl_2)$ respectively.

Cl^- ion formation occurs extensively throughout the energy range 0 - 15eV. The appearance of Cl^- at thermal electron energies has already been discussed and attributed to the dissociative capture reaction 27 and also to surface ionisation on the filament. The unfolded ionisation efficiency curve shown in Fig. 5.6(b) exhibits complex structure between the onset at 4·9 ± 0·1eV and the major peak onsetting at 7·6 ± 0·2eV. The small bump on the trailing edge of the major peak was not reproducible and is believed to result from ineffective unfolding over the broad

tail of the resonance.

The following reactions, with their respective minimum anthalpy requirements, ΔH_{min}, may be suggested to account for Cl^- ion formation:

		ΔH_{min} (eV)
$SF_5Cl + e \xrightarrow{35}$	$Cl^- + SF_4 + F$	1·2
$\xrightarrow{36}$	$Cl^- + SF_3 + F_2$	3·1
$\xrightarrow{37}$	$Cl^- + SF_3 + 2F$	4·8
$\xrightarrow{38}$	$Cl^- + SF_2 + F_2 + F$	6·4
$\xrightarrow{39}$	$Cl^- + SF_2 + 3F$	8·0

Some Cl^- ion formation from 35 could possibly be a contributing factor to the increasing ion current observed below 2eV which has been partly attributed to reaction 27. It is not unreasonable to attribute ion formation at 4·9 ± 0·1eV to reaction 37 and suggest tentatively that reactions 38 and 39 may account for the ion current around 6·5eV and that maximising at 8·9 ± 0·1eV respectively. Reaction 36 does not, therefore, appear to contribute to Cl^- ion formation.

The appearance of F^- in the zero electron energy region has already been discussed in terms of surface ionisation on the filament and the dissociative capture reaction 28. An upper limit of 3·45eV, i.e. E(F),[36] can therefore be placed on the SF_4Cl-F bond dissociation energy. The following reactions, with their respective minimum enthalpy requirements, may be suggested to account for further F^- formation:

		ΔH_{min} (eV)
$SF_5Cl + e \xrightarrow{40}$	$F^- + SF_4 + Cl$	1·5
$\xrightarrow{41}$	$F^- + SF_3 + FCl$	2·5
$\xrightarrow{42}$	$F^- + SF_3 + F + Cl$	5·1
$\xrightarrow{43}$	$F^- + SF_2 + FCl + F$	6·6
$\xrightarrow{44}$	$F^- + SF_2 + F_2 + Cl$	6·6
$\xrightarrow{45}$	$F^- + SF_2 + 2F + Cl$	8·3

Reaction 40 may contribute to the F^- ion current observed below 2eV. The broad resonance onsetting at 2·9 ± 0·1eV may be attributed initially to reaction 41 with reaction 42 also contributing. In view of the uncertainty associated with the thermochemical data used in the calculations it is tentatively suggested that one or both of reactions 43 and 44 are responsible for the small peak in the tail of the major F^- resonance peak and that reaction 45 may be partially responsible for the broad, low cross-section, resonance onsetting at 7·6 ± 0·2eV.

(d) Germanium tetrafluoride, GeF_4.

The existence of the SiF_5^- ion has been demonstrated by the formation of tetraphenylarsonium pentafluorosilicate in the reaction of tetraphenylarsonium chloride and silicon dioxide in aqueous methanolic hydrogen fluoride.[20] It was suggested, in that work, on the basis of infra-red spectra, that use of germanium dioxide may have yielded a compound containing the GeF_5^- ion but no more definite evidence for the formation of this ion could be obtained.

MacNeil and Thynne[21] examined negative ion formation in SiF_4 and found that, with ion source pressures above 10^{-5} torr,

SiF_5^- was produced as a result of the ion-molecule reaction:

$$SiF_3^- + SiF_4 \xrightarrow{46} SiF_5^- + SiF_2$$

The relative ease of formation of such ions in the gas phase suggested that a comparable study with germanium tetrafluoride might yield information regarding the GeF_5^- ion and permit a comparison to be made between ion formation in SiF_4 and GeF_4.

A positive ion study of GeF_4 was also undertaken in order to establish an approximate Ge-F bond energy and to extend the range of ionisation potentials. In Table 5.10 the 70eV positive ion mass spectrum of GeF_4 is compared to the spectra of CF_4 and SiF_4 reported by Dibeler and Mohler.[116] The table is so constructed that only the ions from GeF_4 are listed in order of increasing molecular weight.

Table 5.10. Positive ion mass spectra of CF_4, SiF_4 and GeF_4 at 70eV.

Ion	X = C[116]	X = Si[116]	X = Ge
F^+	49·0	17·2	17·2
XF^{++}	4·9	7·2	<0·5
XF_2^{++}	49·4	37·7	7·3
XF_3^{++}	16·8	11·5	<0·5
X^+	84·4	41·5	27·1
XF^+	40·0	38·7	16·5
XF_2^+	128·4	6·9	4·4
XF_3^+	1000·0	1000·0	1000·0
XF_4^+	-	17·8	-

The ionic abundances in the GeF_4 mass spectrum are the values summed over all the germanium isotopes.

There are several points of interest arising from a comparison of these mass spectra; (i) CF_4^+ and GeF_4^+ were not detected, (ii) relatively high abundances of doubly charged ions appear in all three spectra, (iii) for SiF_4 and GeF_4 the XF_2^{++} ion current is greater than that of the corresponding singly charged ion, (iv) the abundance of ions which have an odd number of fluorine atoms is greater than those which have an even number and (v) the abundance of all ions relative to the abundance of XF_3^+ (the most abundant ion in each spectrum) decreases in traversing the series CF_4 to SiF_4 to GeF_4.

The semi-logarithmic plot method of Lossing et al.[117] was used to determine the appearance potentials of all the singly charged ions in the GeF_4 mass spectrum. The energy scale was calibrated against the appearance potential of the CO^+ ion from CO at 14·0eV[23] and the results are presented in Table 5.11.

Table 5.11. Appearance potential data for the positive ions of GeF_4.

Ion	Appearance Potential (eV)
F^+	33·0 ± 0·3
Ge^+	29·4 ± 0·2
GeF^+	22·7 ± 0·2
GeF_2^+	20·6 ± 0·3
GeF_3^+	15·7 ± 0·2

If the minimum enthalpy requirement for reaction 47 is set equal to the appearance potential of the Ge^+ ion, 29·4 ± 0·2eV,

$$GeF_4 + e \xrightarrow{47} Ge^+ + 4F + 2e$$

then, using the published value of 7·9eV[22] for the ionisation potential of Ge, the average Ge-F bond energy is estimated to be ~5·4eV. This may be compared to the average bond energies of 4·1 and 5·4eV calculated for CF_4 and SiF_4 respectively.

If the ionisation processes taking place in GeF_4 proceed by the successive splitting of fluorine atom fragments then reactions 48, 49 and 50 may be postulated to account for the appearance potentials at 15·7, 20·6 and 22·7eV for the GeF_3^+, GeF_2^+ and GeF^+ ions respectively.

$$GeF_4 + e \xrightarrow{48} GeF_3^+ + F + 2e$$
$$\xrightarrow{49} GeF_2^+ + 2F + 2e$$
$$\xrightarrow{50} GeF^+ + 3F + 2e$$

On the basis of these processes, and using the average Ge-F bond energy obtained from reaction 47, 5·4eV, the ionisation potentials of GeF_3, GeF_2 and GeF may be estimated to be $\leq$ 10·3, $\leq$ 9·8 and $\leq$ 6·5eV respectively. GeF_2 is the only species in this system for which thermochemical data have been established.[25] Using $\Delta H_f(GeF_2) = -5·9 \pm 0·1eV$[25] and the value of $\leq$9·8eV for $I(GeF_2)$, suggested on the basis of reactions 47 and 49, then a lower limit of -15·1eV may be

estimated for the heat of formation of GeF_4. In the absence of a direct determination this value can be used in rough calculations in order to indicate the feasibility of possible negative ion processes.

F^+ ion formation at $33{\cdot}0 \pm 0{\cdot}3$eV may be the consequence of reaction 51 in which x + 1 (Ge - F) bonds are broken,

$$GeF_4 + e \xrightarrow{51} F^+ + GeF_{4-(x+1)} + xF + 2e$$

using the relationship $(x+1)D(Ge\text{-}F) \leq 33{\cdot}0 - I(F)$, where $I(F) = 17{\cdot}4$eV[22] and $D(Ge\text{-}F)_{average} \simeq 5{\cdot}4$eV, then a value of 3 is found for (x+1), so the process responsible for F^+ ion formation may be written as, $GeF_4 + e \longrightarrow F^+ + GeF + 2F + 2e$.

Negative ion formation occurs extensively in germanium tetrafluoride. The ions detected and measured at low electron energies were F^-, F_2^-, GeF_2^-, GeF_3^-, GeF_4^- and GeF_5^-; all primary except GeF_5^- which was shown by pressure studies to be secondary. Several digermanium ions were also detected both at high and low electron energies but with intensities too low for a detailed examination to be made. The 70eV negative ion mass spectrum measured at a source pressure of 1×10^{-5} torr is shown in Table 5.12.

Table 5.12. Negative ion mass spectrum of GeF_4 at 70eV.

Ion	Abundance
F^-	1000·0
F_2^-	<1·0
GeF_2^-	<1·0
GeF_3^-	48·0
GeF_4^-	443·0
GeF_5^-	6·2
$Ge_2F_2^-$	0·8
$Ge_2F_4^-$	1·0
$Ge_2F_6^-$	0·2
$Ge_2F_8^-$	<0·1

The $Ge_2F_x^-$ ions were of very low intensity and attempts at pressure dependence measurements were unsuccessful. At low electron energies the ions $Ge_2F_2^-$ and $Ge_2F_4^-$ were detected in the same region as the GeF_4^- ion (zero volts) suggesting an origin at the surface of the filament which is particularly hot at this energy range. The additional possibility of ion formation as a result of ion-molecule interactions is discussed below.

Typical experimental results for some of the primary ions are presented in Figs. 5.7(a) and (b) and Fig. 5.8(a) and the deconvoluted data in Fig. 5.8(b). In order to prevent crowding in Fig. 5.8 the GeF_2^- ionisation efficiency curve has not been included; it showed an exactly similar

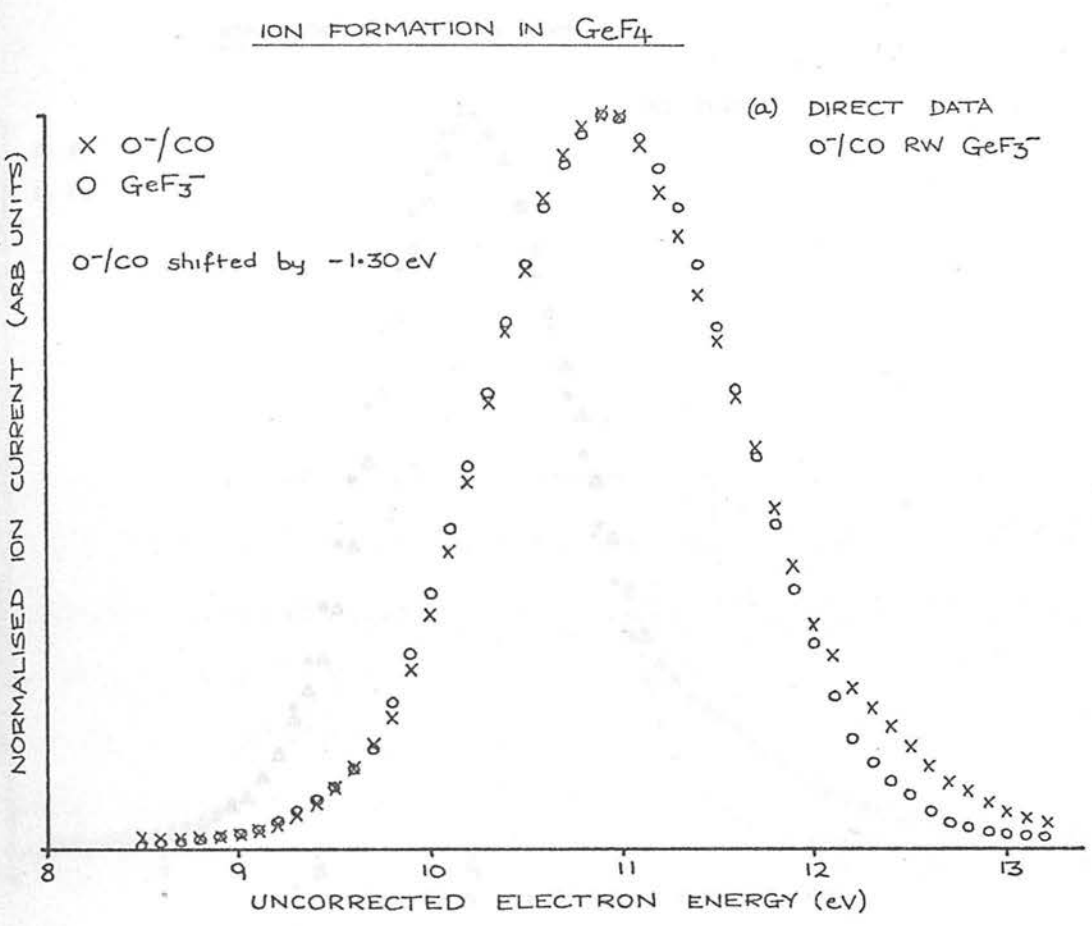
ION FORMATION IN GeF4
(a) DIRECT DATA
O⁻/CO RW GeF3⁻
× O⁻/CO
○ GeF3⁻
O⁻/CO shifted by −1·30 eV
NORMALISED ION CURRENT (ARB UNITS)
8
9
10
11
12
13
UNCORRECTED ELECTRON ENERGY (eV)

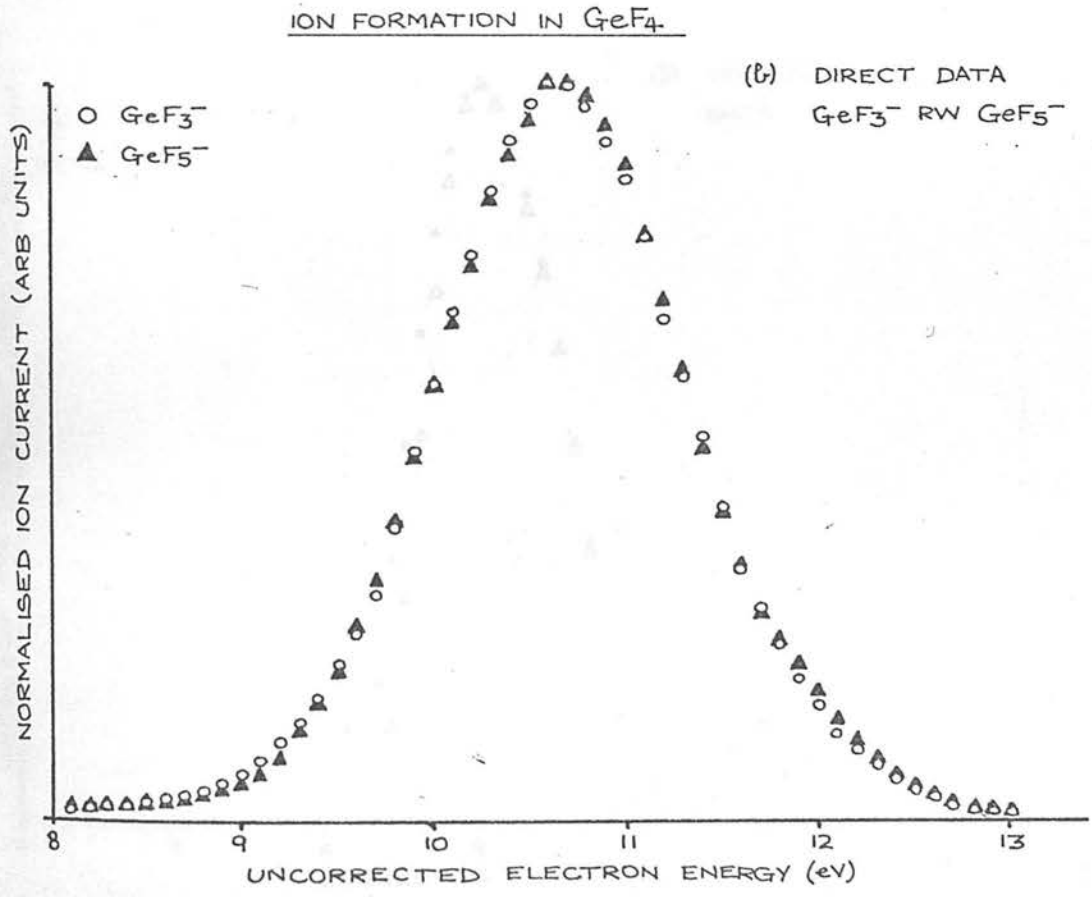
ION FORMATION IN GeF4
(b) DIRECT DATA
GeF3⁻ RW GeF5⁻
○ GeF3⁻
▲ GeF5⁻
NORMALISED ION CURRENT (ARB UNITS)
8
9
10
11
12
13
UNCORRECTED ELECTRON ENERGY (eV)

Fig 5.7

ION FORMATION IN GeF_4

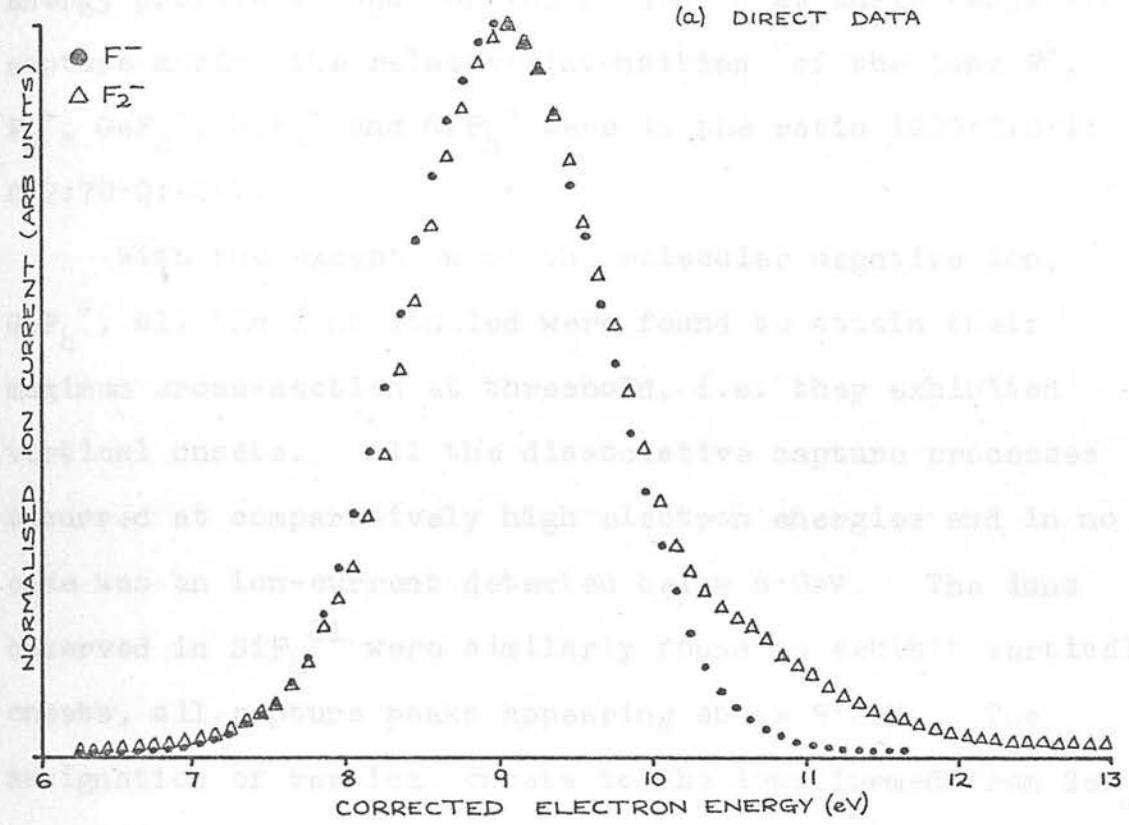

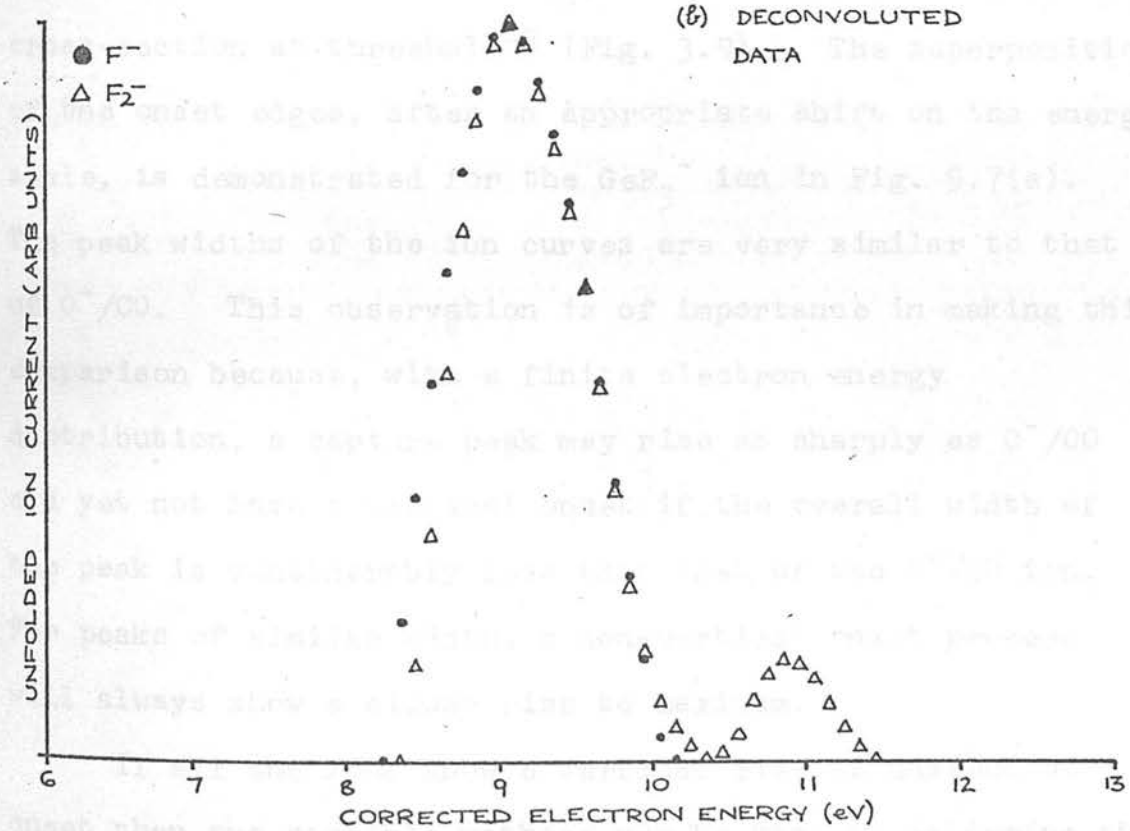

Fig 5.8

energy profile to that of the F^- ion. At their respective capture maxima the relative intensities of the ions F^-, F_2^-, GeF_2^-, GeF_3^- and GeF_4^- were in the ratio 1000·0:0·1: 0·2:70·0:<0·1.

With the exception of the molecular negative ion, GeF_4^-, all the ions studied were found to attain their maximum cross-section at threshold, i.e. they exhibited vertical onsets. All the dissociative capture processes occurred at comparatively high electron energies and in no case was an ion-current detected below 6·0eV. The ions observed in SiF_4[21] were similarly found to exhibit vertical onsets, all capture peaks appearing above 9·0eV. The assignation of vertical onsets to the ions formed from GeF_4 was made by comparing the normalised capture peak profiles with that of the O^- ion from CO which itself attains maximum cross-section at threshold[24] (Fig. 3.9). The superposition of the onset edges, after an appropriate shift on the energy scale, is demonstrated for the GeF_3^- ion in Fig. 5.7(a). The peak widths of the ion curves are very similar to that of O^-/CO. This observation is of importance in making this comparison because, with a finite electron energy distribution, a capture peak may rise as sharply as O^-/CO and yet not have a vertical onset if the overall width of the peak is considerably less than that of the O^-/CO ion. For peaks of similar width, a non-vertical onset process will always show a slower rise to maximum.

If all the ions show a vertical rise to maximum at onset then two possible methods may be used to determine this

energy. In one method, the point of maximum gradient on the onset edge of the unfolded peak may be compared with that for O^-/CO which is at 9·62eV.[24] The selection of this point is inexact to ± 0·1eV and leads to a maximum uncertainty of ± 0·2eV in calculating a difference. However, from Fig. 5.7(a), it is clear that the leading edges of the curves may be superimposed and so the experimental energy shifts required to achieve this present a second and more accurate determination of the onset energies, the uncertainty being ± 0·05eV. Both methods were used to establish the onset energies and both methods gave the same result within their respective experimental errors.

Table 5.13 shows the measured onset energies for the negative ions from GeF_4.

Table 5.13. Appearance potential data for the negative ions of GeF_4.

Ion	Appearance Potential		Peak Width at ½-height eV
	Superposition of edges (eV)	Δ Maximum gradient (eV)	
F^-	8·60 ± 0·05	8·5 ± 0·2	1·0 ± 0·1
F_2	8·70 ± 0·05	8·7 ± 0·2	1·0 ± 0·1
GeF_2^-	8·70 ± 0·10	8·8 ± 0·2	1·1 ± 0·1
GeF_3^-	8·30 ± 0·05	8·4 ± 0·2	1·1 ± 0·1
GeF_5^-	8·30 ± 0·05	8·4 ± 0·2	1·1 ± 0·1
GeF_4^-	Non-vertical onset ~0·0		0·5 ± 0·1

The GeF_4^- ion was also detected at high electron energies (10 - 100eV) as a result of secondary electron capture; at zero electron energy the cross-section for primary electron capture exhibited the same energy dependence as that for SF_6^- (Fig. 3.7). This enabled a value of $1{\cdot}5 \pm 0{\cdot}4 \times 10^{-16}$cm.^{2} to be estimated for the attachment cross-section of GeF_4 relative to that of SF_6, $1{\cdot}17 \times 10^{-14}$cm.^{2}.[35] A molecular negative ion was also detected in SiF_4, however, the cross-section was much less than that of GeF_4 and it was not measured. In both cases the low attachment cross-sections prevented estimations of the average autodetachment lifetimes, such measurements were also complicated by the presence of several isotopes of germanium which made accurate evaluation of the neutral component impossible.

Following the observation of digermanium ions in the mass spectrum of GeF_4 at 70eV a search for these and similar ions was carried out at low electron energies. Mass analysis at zero electron energy revealed only the ions $Ge_2F_2^-$ and $Ge_2F_4^-$. The possible thermal origin of these ions at this energy has been discussed above. Using very high trap currents (~0·5 μAmp) and source pressures in the range 2-5 x 10^{-5} torr, traces of digermanium ions and GeF_4^- were detected in the energy region close to the GeF_3^- capture peak. Ion-molecule reactions may therefore be taking place under these conditions and GeF_3^- and GeF_4^- (probably formed as a result of secondary and scattered electron

capture) are possible precursors. Reactions 52, 53 and 54 are of the type envisaged;

$$GeF_3^- + GeF_4 \xrightarrow{52} Ge_2F_4^- + 3F \text{ (or } F_2 + F)$$

$$GeF_4^- + GeF_4 \xrightarrow{53} Ge_2F_6^- + 2F \text{ (or } F_2)$$

$$GeF_5^- + GeF_4 \xrightarrow{54} Ge_2F_8^- + F$$

Germanium compounds containing two germanium atoms have been isolated by Margrave;[25] a GeF_2/GeF_4 adduct, Ge_2F_6, thought to originate from the complex $(GeF_2)_3GeF_4$ was isolated as a white solid. Raman investigations of $(GeF_2)_3GeF_4$ failed to reveal any Ge-Ge frequencies. In the light of Margrave's observations, fluorine atom bridged structures may be envisaged for the digermanium ions observed in this study so that three, four and five co-ordination of the germanium is maintained in reactions 52, 53 and 54 respectively;

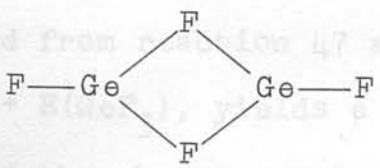

(52)

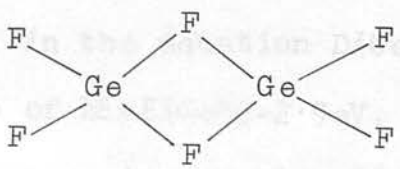

(53)

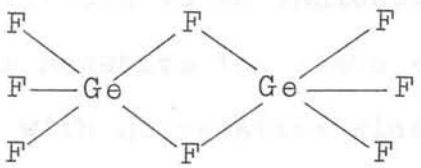

(54)

The formation of complex ions in the gas phase does not imply that, necessarily, the ion will exist in a solid. The factors affecting the stability of the ion in the two states are different, for example, in the solid state the lattice energy term is an important parameter. Nevertheless, detection of such ions in the gas phase might well be used to stimulate research in certain areas aimed at forming such inorganic complexes.

The GeF_3^- ion has an appearance potential of 8·30 ± 0·05eV, the reaction attaining maximum cross-section at threshold. Formation of this ion may be attributed to reaction 55,

$$GeF_4 + e \xrightarrow{55} GeF_3^- + F$$

The lack of thermochemical information for this ion precludes a detailed examination of the energetics of reaction 55, however, use of the average bond energy, $\bar{D}(Ge\text{-}F) = 5{\cdot}4eV$, deduced from reaction 47 above, in the equation $D(GeF_3\text{-}F) \leq 8{\cdot}3 + E(GeF_3)$, yields a value of $EE = E(GeF_3) + 2{\cdot}9eV$. This assumes the absence of kinetic energy in reaction 55. A vertical onset for an ion resulting from the bond cleavage of a diatomic molecule is an indication of a potential well in the molecular negative ion state and hence the formation of the products with no relative kinetic energy at onset (see Fig. 2.2(a)). If GeF_3-F can be treated as a 'diatomic-like' system then reaction 55 would not be expected to involve excess kinetic energy at onset and the value of EE =

$E(GeF_3)$ + 2·9eV would only be uncertain within the inaccuracy of the estimated Ge-F bond energy assumed equal to the GeF_3-F bond dissociation energy. Some justification for this assumption can be found in the work of Collins and Christophorou[66] where it was found that for (C-Br) bond cleavage in a series of aliphatic bromides (C_2H_5Br to $C_8H_{17}Br$) the isotope effect on the peak parameters could only be reconciled by consideration of RBr as a diatomic system where R = C_2H_5 to C_8H_{17}.

Two possible processes may be responsible for the vertical onset at 8·70 ± 0·10eV for the GeF_2^- ion, reactions 56 and 57.

$$GeF_4 + e \xrightarrow{56} GeF_2^- + F_2$$
$$\xrightarrow{57} GeF_2^- + 2F$$

As there is no value reported for $E(GeF_2)$ the energy requirements of reactions 56 and 57 cannot be estimated; GeF_2^- ion formation cannot therefore be assigned to either.

F_2^- ion formation is shown in Fig. 5.8, the appearance potential of the main peak being at 8·70 ± 0·05eV. The intensity of this ion showed a linear pressure dependence; it is therefore formed by an intramolecular rearrangement reaction of the type shown in 58 and 59

$$GeF_4 + e \xrightarrow{58} F_2^- + GeF_2$$
$$\xrightarrow{59} F_2^- + F + GeF$$

The study in SiF_4,[21] for which thermochemical data were available, indicated the process analogous to 58 to be responsible for F_2^- ion formation, the process analogous to 59 being energetically unfavourable. The processes established for negative ion formation in CF_4 and SiF_4[21] indicate a close similarity for these fluorides; if this constitutes a trend within the Group 4 fluorides then reaction 58 may be predicted as that responsible for F_2^- ion formation in GeF_4. Using the values $E(F_2) = 2{\cdot}9 \pm 0{\cdot}2eV$[65] and $\Delta H_f(GeF_2) = -5{\cdot}9 \pm 0{\cdot}1eV$,[25] an upper limit to the heat of formation of GeF_4 may therefore be calculated to be $-17{\cdot}5 \pm 0{\cdot}4eV$. This can be compared to the lower limit of $-15{\cdot}1eV$ calculated on the basis of reactions 47 and 49 and to the values of $-9{\cdot}6$[23] and $-16{\cdot}7eV$[23] for $\Delta H_f(CF_4)$ and $\Delta H_f(SiF_4)$ respectively.

Unfolding the F_2^- ion data revealed a second peak of lower cross-section, onsetting at $10{\cdot}4 \pm 0{\cdot}1eV$, which may correspond to F_2^- ion formation by reaction 59.

The F^- ion curve shows a single sharp resonance onsetting at $8{\cdot}6 \pm 0{\cdot}05eV$, the peak having a width of $1{\cdot}0 \pm 0{\cdot}1eV$ at $\frac{1}{2}$-height.

$$GeF_4 + e \xrightarrow{60} F^- + GeF_3$$
$$\xrightarrow{61} F^- + F + GeF_2$$

Reaction 61 is analogous to that suggested for F^- ion formation in CF_4 and SiF_4. Using $E(F) = 3{\cdot}4eV$[36] in the expression $D(Ge\text{-}F)_{av} \leq 8{\cdot}6 + E(F)$, results in $D(Ge\text{-}F)_{av} \leq$

12·0eV, thus, on the assumption of reaction 61, D(Ge-F) $\leq$ 6·0eV, which is in reasonable agreement with the average value over all four bonds, ~5·4eV, deduced from reaction 47.

F^- ion formation by reaction 60 would involve ~6eV of excess energy to be distributed between the fragments. As already indicated, the vertical onset implies the products of a diatomic molecule to be formed with zero relative kinetic energy at onset, hence if 'diatomic-like' behaviour can be assumed the excess energy would be used in exciting internal modes within the GeF_3^- ion, which might well result in electron detachment. F^- ion formation is therefore attributed to reaction 61.

Ionisation efficiency curves for the GeF_3^- and GeF_5^- ions obtained by simultaneously monitoring both ions are shown in Fig. 5.7(b); they clearly have similar profiles and indicate that GeF_3^- is the precursor to formation of the secondary GeF_5^- ion. The ion-molecule reaction 62 can be written to account for GeF_5^- ion formation. This also follows similar

$$GeF_3^- + GeF_4 \xrightarrow{62} GeF_5^- + GeF_2$$

behaviour in SiF_4, where reaction 46 was shown to occur.

(e) Tungsten hexafluoride, WF_6.

The relative abundances of negative ions formed from WF_6 at 70eV are shown in Table 5.14; the relative abundances are those summed over all isotopes using the following isotope

ratios:[22]

m/e	180	182	183	184	186
%	0·14	26·29	14·31	30·66	28·60

Because of incomplete resolution of m/e 183 in this work all measurements were made on the isotope of m/e = 186 followed by reference to the percentage abundance table above.

Table 5.14. Negative ion mass spectrum of WF_6 at 70eV and a source pressure of 1 x 10^{-5} torr.

Ion	Abundance
F^-	1000·0
F_2^-	<0·1
WF_4^-	10·0
WF_5^-	252·0
WF_6^-	2·1
WF_7^-	0·7

Pressure dependence measurements showed WF_6^- and WF_7^- to be secondary species, however, WF_6^- only shows a second order pressure dependence at high electron energies due to its formation by the capture of slow secondary electrons whereas WF_7^- must originate from an ion-molecule reaction, possibly of the type; $WF_5^- + WF_6 \longrightarrow WF_7^- + WF_4$.

The ions detected and measured at low electron energies were F^-, WF_4^- and WF_5^- in the ratio 1000:4:55, at their respective capture maxima. WF_6^- was detected at zero electron

energy as a primary ion but with a very low capture cross-section, whereas WF_7^- was not detected at low energies, even with a flight tube pressure of 5×10^{-5} torr.

The average autodetachment lifetime for the WF_6^- ion was estimated using the secondary electron capture method at 100eV. Only two drift tube potentials, 2·0 and 2·5KV, proved satisfactory for a suitable resolution of WF_6^- (m/e = 186) and WF_6 neutral (m/e = 182). The isotope ratios above were then used to calculate the total charged and neutral contributions, from which values of 25 and 32 μsec. were calculated for $T_a(WF_6)$ at 2·0 and 2·5KV respectively. The uncertainty involved in these values far exceeds that normally expected for lifetime measurements but the average value of ~28 μsec. is believed to be accurate to within 25%.

Typical experimental and unfolded ionisation efficiency data are shown in Figs. 5.9(a) and (b) respectively. The electron energy scale is calibrated against the appearance potentials of the O^- ion from SO_2 at 4·2 and 6·6eV. Appearance potential data for the ions investigated are given in Table 5.15.

Table 5.15. Appearance potential data for WF_6

Ion	Appearance Potential (eV)	Peak Maximum (eV)	Peak Width at ½-height (eV)
F^-	1·8 ± 0·1	2·8 ± 0·1	1·1 ± 0·1
	5·3 ± 0·1	6·1 ± 0·2	-
	6·5 ± 0·2	7·5 ± 0·2	-
	7·6 ± 0·2	9·3 ± 0·1	1·8 ± 0·1
WF_4^-	8·3 ± 0·1	9·6 ± 0·1	1·2 ± 0·1
WF_5^-	4·4 ± 0·1	5·9 ± 0·1	1·4 ± 0·1
WF_6^-	~0·0		

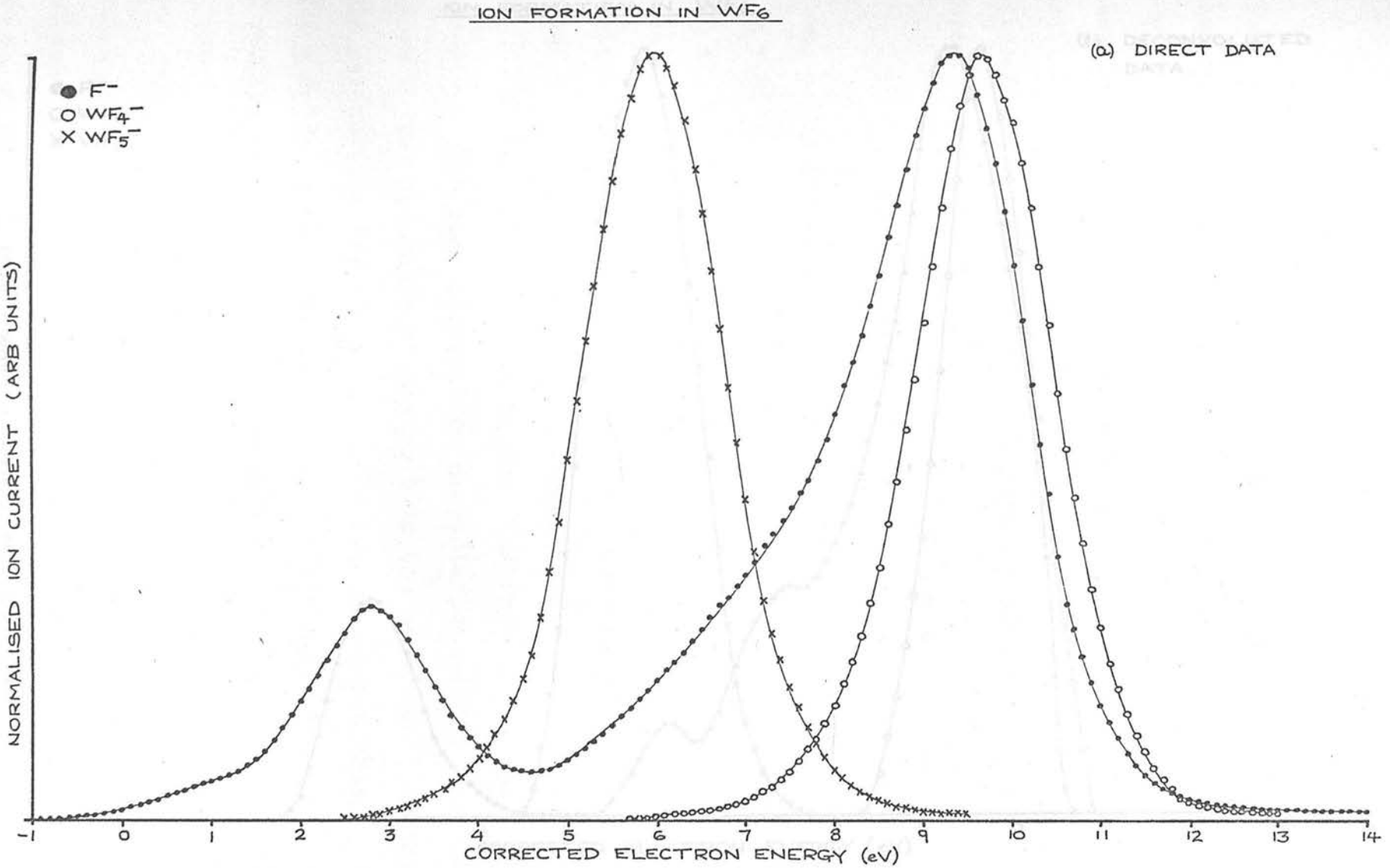
ION FORMATION IN WF6
(a) DIRECT DATA
● F⁻
○ WF4⁻
× WF5⁻
NORMALISED ION CURRENT (ARB UNITS)
-1
0
1
2
3
4
5
6
7
8
9
10
11
12
13
14
CORRECTED ELECTRON ENERGY (eV)

Fig 5.9

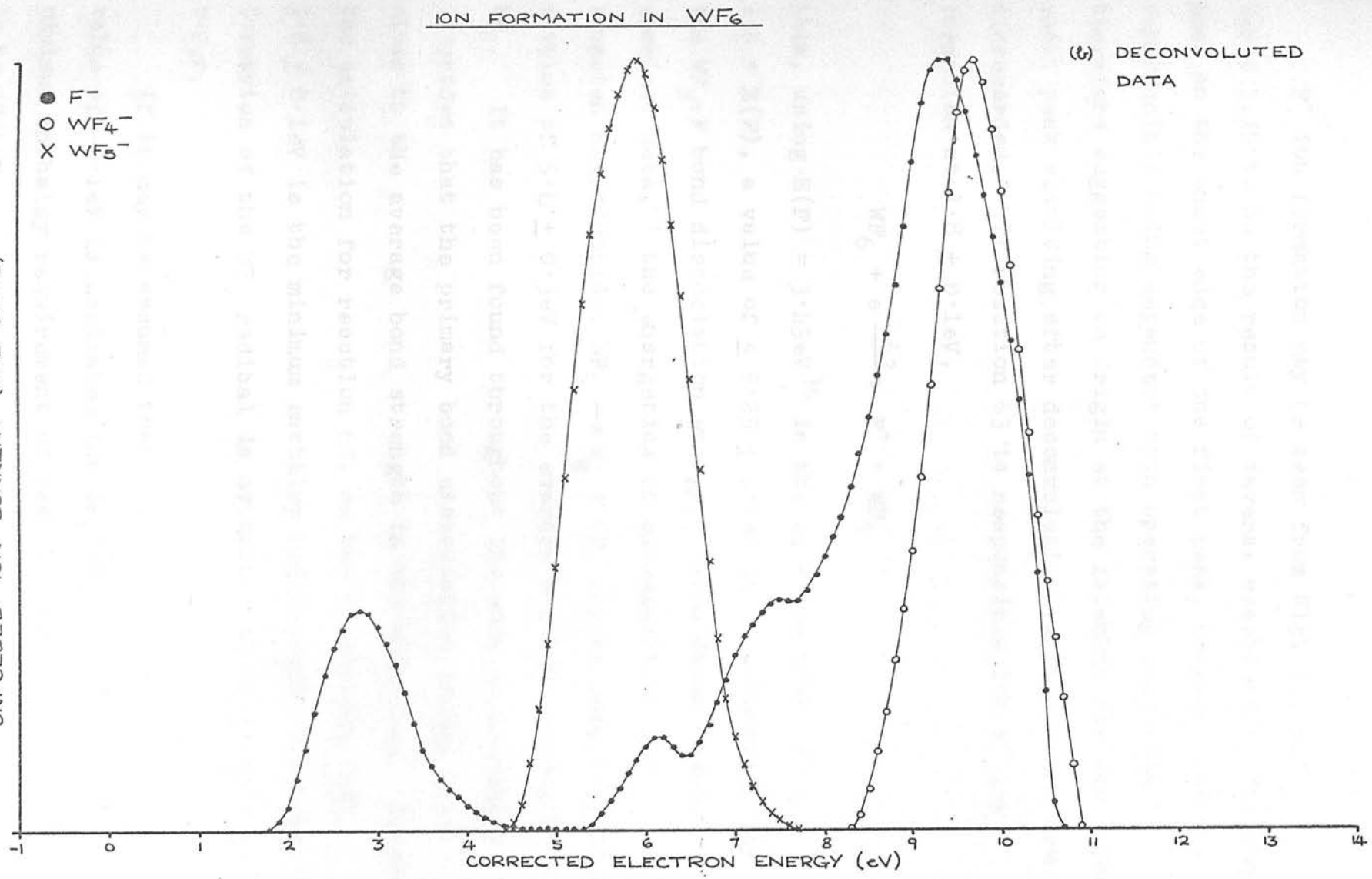
ION FORMATION IN WF6
(f) DECONVOLUTED DATA
F⁻
WF4⁻
WF5⁻
UNFOLDED ION CURRENT (ARB UNITS)
CORRECTED ELECTRON ENERGY (eV)
-1
0
1
2
3
4
5
6
7
8
9
10
11
12
13
14

Fig 5.9

F^- ion formation may be seen from Fig. 5.9 and Table 5.15 to be the result of several reactions. The small hump on the onset edge of the first peak, however, was not reproducible being dependent upon operating conditions therefore suggesting an origin at the filament surface. The small peak resulting after deconvolution has therefore been disregarded. If reaction 63 is responsible for F^- ion formation at $1{\cdot}8 \pm 0{\cdot}1$eV,

$$WF_6 + e \xrightarrow{63} F^- + WF_5$$

then, using $E(F) = 3{\cdot}45$eV[36] in the equation $D(WF_5\text{-}F) \leq 1{\cdot}8 + E(F)$, a value of $\leq 5{\cdot}25 \pm 0{\cdot}1$eV may be estimated for the WF_5-F bond dissociation energy. From known thermochemical data,[27] the energetics of decomposition for tungsten hexafluoride, $WF_6 \longrightarrow W_g + 6F$, may be used to estimate a value of $5{\cdot}4 \pm 0{\cdot}3$eV for the average W-F bond strength in WF_6. It has been found throughout the work on inorganic fluorides that the primary bond dissociation energy lies close to the average bond strength in the molecule. Reversing the calculation for reaction 63, on the assumption that $1{\cdot}8 \pm 0{\cdot}1$eV is the minimum enthalpy requirement, the heat of formation of the WF_5 radical is estimated to be $\leq -13{\cdot}9 \pm 0{\cdot}2$eV.

If it may be assumed that $D(WF_5\text{-}F) \simeq D(WF_4\text{-}F)$ then a value of $-9{\cdot}1$eV is estimated for $\Delta H_f(WF_4)$ from which the minimum enthalpy requirement of reaction 64 is calculated to be $\sim 7{\cdot}4$eV.

$$WF_6 + e \xrightarrow{64} F^- + F + WF_4$$

Reaction 64 is therefore suggested for F^- ion formation at $7{\cdot}6 \pm 0{\cdot}2$eV. Reversing this argument and assuming the appearance potential for reaction 64 is also the minimum enthalpy requirement, this allows an estimation of the WF_4-F bond dissociation energy to be made, i.e. $D(WF_4\text{-}F) = 7{\cdot}6 \pm 0{\cdot}2 - 1{\cdot}8 \pm 0{\cdot}1 = 5{\cdot}8 \pm 0{\cdot}3$eV. Applying the same argument i.e. $D(WF_4\text{-}F) \simeq D(WF_3\text{-}F)$, $\Delta H_f(WF_3)$ is estimated to be $\simeq -4{\cdot}6$eV and the minimum enthalpy requirement for the next least energetically demanding process, 65, is calculated to be 11·1eV.

$$WF_6 + e \xrightarrow{65} F^- + F_2 + WF_3$$

Since the F^- ion current falls to zero above 11·0eV reaction 65 does not appear to contribute to ion formation.

After deconvolution, the shoulder on the onset edge of the major F^- ion peak indicated two resonance processes, onsetting at 5·3 and 6·5eV, in addition to the main peak which onsets at 7·6eV. The assignation of reactions 63 and 64 to the onsets at 1·8 and 7·6eV on the basis of the above calculations suggest that the onsets at 5·3 and 6·5eV must result from reaction 63 in which 3·5 and 4·7eV of excess energy are involved respectively. In the absence of a translational energy analysis of the fragments the excess energy cannot be quantitatively attributed to either excitation of the WF_5 radical and/or kinetic energy of the fragments.

WF_5^- ion formation onsets at $4{\cdot}4 \pm 0{\cdot}1$eV, only one capture peak being observed. Assuming that $D(WF_5\text{-}F) \leq 5{\cdot}25 \pm 0{\cdot}1$eV in the equation $5{\cdot}25 \leq 4{\cdot}4 + E(WF_5)$ for reaction 66, a value of

$$WF_6 + e \xrightarrow{66} WF_5^- + F$$

$E(WF_5) \geq 0{\cdot}85 \pm 0{\cdot}2$eV is estimated.

Reactions 67 and 68 are the only two reactions which may result in WF_4^- ion formation.

$$WF_6 + e \xrightarrow{67} WF_4^- + F_2$$
$$\xrightarrow{68} WF_4^- + 2F$$

From the energetics of decomposition discussed above $\Delta H_f(WF_4)$ has been estimated as $\sim -9{\cdot}1$eV, hence reactions 67 and 68 have calculated minimum enthalpy requirements of $9{\cdot}2 - E(WF_4)$eV and $10{\cdot}8 - E(WF_4)$eV respectively. From the appearance potential for WF_4^- ion formation at $8{\cdot}3 \pm 0{\cdot}1$eV, alternative lower limits of $0{\cdot}9$ and $2{\cdot}5$eV are estimated for $E(WF_4)$. The reactions leading to SF_4^- ion formation in both SF_6 and SF_5Cl are analogous to reaction 68 above so, on the assumption that the trend in the dissociative capture reactions observed in the other inorganic systems applies to WF_6, it is tentatively suggested that reaction 68 is responsible for WF_4^- ion formation and consequently that $E(WF_4) \gtrsim 2{\cdot}5$eV.

(f) Summary

The electron affinities, bond dissociation energies and heats of formation deduced in the course of this chapter are presented and discussed in Chapter 9.

The following points result from a comparison of this work with previous investigations of inorganic fluorides;

With the exception of SF_5Cl, all the fluorides examined in this study formed stable molecular negative ions and in each case the attachment cross-section profile was similar to that exhibited by SF_6^- thereby indicating a true resonance width less than or equal to the width of the electron energy distribution. Work on the fluorides of the row one elements, BF_3,[103] CF_4[21] and NF_3,[30] has shown that molecular negative ions are not formed whereas work on the second and third row group 4 fluorides, SiF_4[21] and GeF_4, and the group 6 fluorides, SF_4, SF_6 and WF_6, has revealed long-lived molecular ions. These observations probably reflect the ease with which the captured electron may be accommodated in the unoccupied d-orbitals of these molecules and the increasing polarisability of the heavier molecules.

The inorganic tetrafluorides are the smallest molecules (on a number of atoms basis) for which stable molecular negative ions were detected, only 9 internal degrees of freedom being available for absorption of the translational energy of the incident electron. The perfluorocarbon with a comparable lifetime to SF_4^- (T_a = 16·2 μsec.) is n-C_4F_{10} (T_a = 12·7 μsec.) which has 36 internal degrees of freedom.

A distinct trend was found in the dissociative capture processes occurring in the group 4 tetrafluorides. The following ion formation reactions occurring in GeF_4 are compared to those found in SiF_4[21] where vertical onsets at relatively high electron energies were also a feature of the observed behaviour:

F^- ion formation

$$GeF_4 + e \xrightarrow{61} F^- + F + GeF_2$$
$$SiF_4 + e \longrightarrow F^- + F + SiF_2$$

F_2^- ion formation

$$GeF_4 + e \xrightarrow{58} F_2^- + GeF_2$$
$$SiF_4 + e \longrightarrow F_2^{2-} + SiF_2$$

secondary ion formation

$$GeF_3^- + GeF_4 \xrightarrow{62} GeF_5^- + GeF_2$$
$$SiF_3^- + SiF_4 \xrightarrow{46} SiF_5^- + SiF_2$$

In contrast to the group 4 fluorides, the fluorides of group 6, SF_4, SF_6, SF_5Cl and WF_6, were found to undergo dissociative electron capture processes by the successive stripping of fluorine atoms from the molecule, e.g., F^- ion formation in SF_6

$$SF_6 + e \xrightarrow{69} F^- + SF_5$$
$$\xrightarrow{11} F^- + SF_4 + F$$
$$\xrightarrow{12} F^- + SF_3 + 2F$$
$$\xrightarrow{13} F^- + SF_2 + 3F$$

In no case were there clear examples of processes involving the formation of neutral intramolecular rearrangement fragments (F_2 or FCl), although the corresponding ions were detected in each system.

CHAPTER 6

THE FLUOROPHOSPHINES; PF_3, PF_2CN, PF_2NCO and PF_2NCS

A recent study of negative ion formation in PF_3 by MacNeil and Thynne[103] showed that, with the exception of F^- (formed by a non-resonance process), all ions were formed at high electron energies (>10eV) with vertical onsets. The availability of thermo-chemical data for PF_3 and possible fragment species enabled analysis of the negative ion data to be satisfactorily carried out although no positive ion study was made.

There are no values reported for the heats of formation of PF_2CN, PF_2NCO or PF_2NCS and the thermochemical data for the nitrile and isothiocyanate fragments are reported with large uncertainties, there being no value reported for the isocyanate radical. A positive ion study of PF_3 was therefore undertaken in order to determine values for the ionisation potentials of PF_2 and PF which could then be used in the interpretation of the positive ion studies of the PF_2X compounds.

The positive ion data will be presented first, each molecule being discussed separately. This will be followed by a brief comparison of the positive ion data for each molecule, the same procedure then being repeated for the negative ion studies.

(a) Positive ion formation

(i) Phosphorus trifluoride, PF_3

The positive ion mass spectrum of PF_3 measured at 70eV is shown in Table 6.1. Although doubly charged ions were observed they have been omitted from the spectrum as a detailed investigation of this molecule was not carried out.

Table 6.1. Positive ion mass spectrum of PF_3 at 70eV.

m/e	Ion	Abundance
19	F^+	11
31	P^+	67
50	PF^+	56
69	PF_2^+	1000
88	PF_3^+	378

The ionisation efficiency curves for the singly charged ions of interest, PF_3^+, PF_2^+ and PF^+, are shown in Fig. 6.1. and the appearance potential data, calibrated against the spectroscopic appearance potential of argon (15·76eV),[15] are listed in Table 6.2.

Table 6.2. Appearance potential data for the positive ions of PF_3.

m/e	Ion	Appearance Potential (eV)
50	PF^+	21·2 ± 0·5
69	PF_2^+	15·4 ± 0·4
88	PF_3^+	11·3 ± 0·2

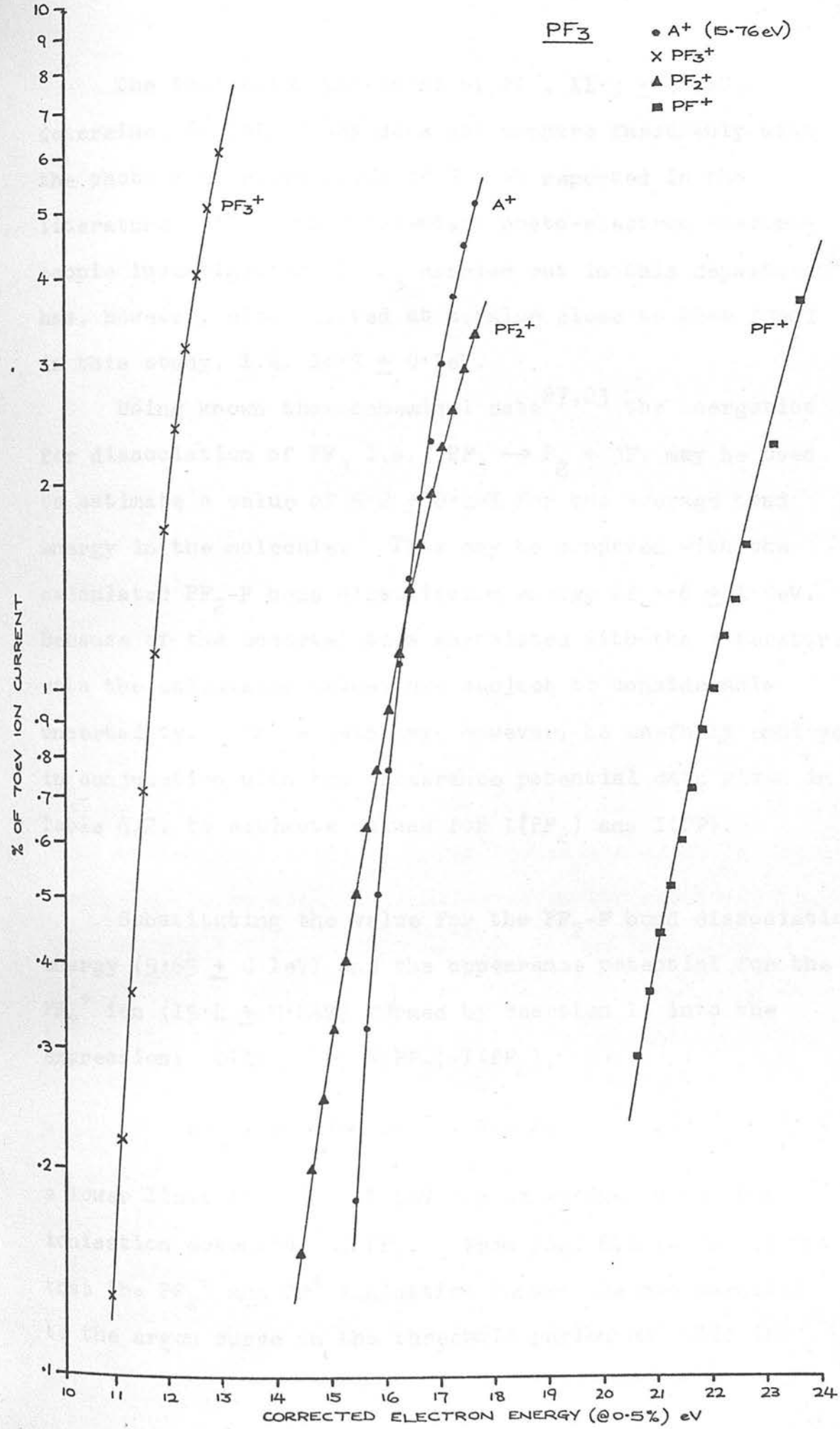
PF3
• A+ (15·76 eV)
× PF3+
▲ PF2+
■ PF+
PF3+
A+
PF2+
PF+
% OF 70eV ION CURRENT
10
9
8
7
6
5
4
3
2
1
·9
·8
·7
·6
·5
·4
·3
·2
·1
10
11
12
13
14
15
16
17
18
19
20
21
22
23
24
CORRECTED ELECTRON ENERGY (@0·5%) eV

Fig 6.1

The ionisation potential of PF_3, 11·3 ± 0·2eV, determined in this study does not compare favourably with the photo-ionisation value of 9·71eV reported in the literature.[22,23] An independent photo-electron spectroscopic investigation of PF_3 carried out in this department[56] has, however, also arrived at a value close to that found in this study, i.e. 11·5 ± 0·1eV.

Using known thermochemical data[27,23] the energetics for dissociation of PF_3 i.e., $PF_3 \longrightarrow P_g + 3F$, may be used to estimate a value of 5·2 ± 0·4eV for the average bond energy in the molecule. This may be compared with the calculated PF_2-F bond dissociation energy of 5·6 ± 1·0eV. Because of the uncertainties associated with the literature data the calculated values are subject to considerable uncertainty. These data may, however, be usefully employed in conjunction with the appearance potential data given in Table 6.2. to estimate values for $I(PF_2)$ and I(PF).

Substituting the value for the PF_2-F bond dissociation energy (5·65 ± 0·1eV) and the appearance potential for the PF_2^+ ion (15·4 ± 0·4eV) formed by reaction 1, into the expression: $D(PF_2\text{-}F) \leq A(PF_2)\text{-}I(PF_2)$,

$$PF_3 + e \xrightarrow{1} PF_2^+ + F + 2e$$

a lower limit of 9·75 ± 1·4eV may be estimated for the ionisation potential of PF_2. From Fig. 6.1 it is evident that the PF_2^+ and PF^+ ionisation curves are not parallel to the argon curve in the threshold region and this is

responsible for the large uncertainties that have been attributed to those appearance potentials which were compared at 0·5% of the 70eV ion current.

For reaction 2, using $D(PF_2\text{-}F) = 5{\cdot}65 \pm 0{\cdot}1$eV and the D(PF-F) bond energy in PF_2 calculated from thermochemical data to be $4{\cdot}8 \pm 0{\cdot}7$eV

$$PF_3 + e \xrightarrow{2} PF^+ + 2F + 2e$$

in conjunction with the PF^+ appearance potential measured to be $21{\cdot}2 \pm 0{\cdot}5$eV, a value of $\geq 10{\cdot}7 \pm 2{\cdot}2$eV is estimated for I(PF). There are no other reported values with which $I(PF_2)$ or I(PF) can be compared.

(ii) Cyanodifluorophosphine, PF_2CN.

The positive ion mass spectrum of PF_2CN measured at 70eV is given in Table 6.3. Typical ionisation curves for the selected positive ions investigated are shown in Fig.6.2. where the energy scale is referenced to the spectroscopic appearance potential of the CO^+ ion formed from CO at $14{\cdot}01$eV.[23] A carbon monoxide/PF_2CN mixture was used in the calibration of the energy scale for both the positive and negative ion studies as there was not sufficient PF_2CN available for the preparation of several calibration mixtures. From Fig. 6.2 it is apparent that the ionisation curves are almost parallel to the CO^+ curve in the 3 to 0·3% threshold region and all appearance potentials, listed in Table 6.4, were reproducible to better than $\pm 0{\cdot}3$eV.

TABLE 6.3

POSITIVE ION MASS SPECTRUM OF PF_2CN AT 70eV

m/e	ION	ABUNDANCE
12	C^+	2.5
14	N^+	0.5
19	F^+	1.5
25	PF^{++}	0.4
26	CN^+	33.1
28.5	PCN^{++}	1.2
31	P^+	58.8
34.5	PF_2^{++}	0.3
38	$PFCN^{++}$	2.2
43	PC^+	8.1
45	PN^+	4.3
47.5	PF_2CN^{++}	4.3
50	PF^+	91.9
57	PCN^+	9.1
62	PFC^+	0.3
69	PF_2^+	1000.0
76	$PFCN^+$	91.9
95	PF_2CN^+	216.9

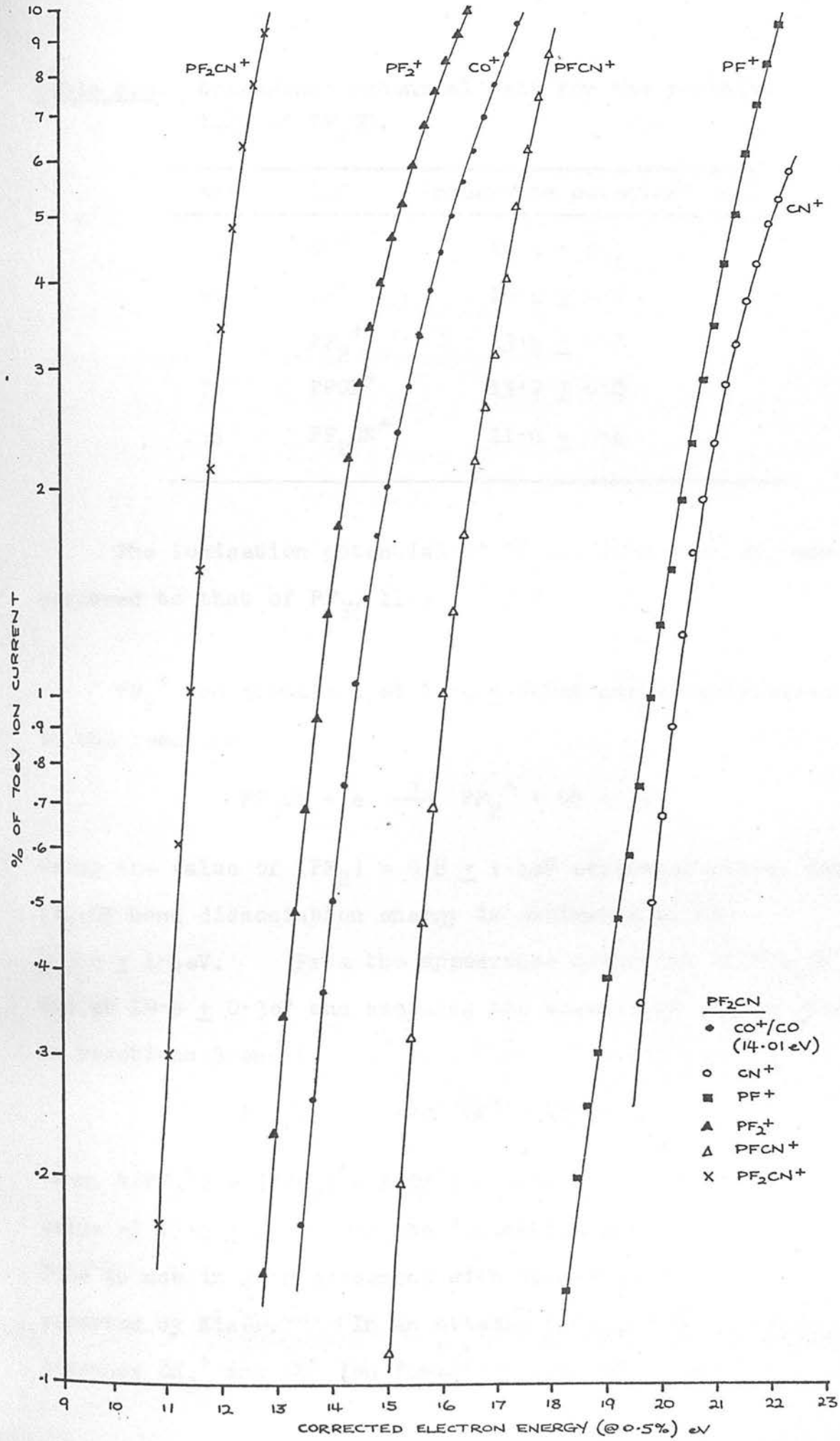
PF2CN+
PF2+
CO+
PFCN+
PF+
CN+
% OF 70eV ION CURRENT
CORRECTED ELECTRON ENERGY (@0·5%) eV
PF2CN
CO+/CO (14·01 eV)
CN+
PF+
PF2+
PFCN+
PF2CN+

Fig 6.2

Table 6.4. Appearance potential data for the positive ions of PF_2CN.

m/e	Ion	Appearance potential (eV)
26	CN^+	19·6 ± 0·3
50	PF^+	19·4 ± 0·2
69	PF_2^+	13·4 ± 0·2
76	$PFCN^+$	15·7 ± 0·2
95	PF_2CN^+	11·6 ± 0·2

The ionisation potential of PF_2CN, 11·6 ± 0·2eV, may be compared to that of PF_3, 11·3 ± 0·2eV.

PF_2^+ ion formation at 13·4 ± 0·2eV may be attributed to the reaction

$$PF_2CN + e \xrightarrow{3} PF_2^+ + CN + 2e$$

Using the value of (PF_2) = 9·8 ± 1·4eV estimated above, the PF_2-CN bond dissociation energy is estimated to be ≤ 3·6 ± 1·6eV. From the appearance potential of the CN^+ ion at 19·6 ± 0·3eV and assuming the absence of excess energy in reactions 3 and 4,

$$PF_2CN + e \xrightarrow{4} CN^+ + PF_2 + 2e$$

then, $A(PF_2^+) - I(PF_2) = A(CN^+) - I(CN)$, resulting in a value of 16·4 ± 2·0eV for the ionisation potential of CN. This is not in good agreement with the value of 14·2eV reported by Kiser.[22] In an attempt to resolve this discrepancy CH_3^+ and CN^+ ion formation from CH_3CN were

investigated and the appearance potentials were measured to be 16·7 ± 0·2eV and 23·4 ± 0·4eV respectively. Using these values in conjunction with the ionisation potential of the methyl radical, 9·8eV,[23] a value of 16·5 ± 0·6eV may be estimated for I(CN). McDowell and Warren[57] have shown that the CN^+ ion from CH_3CN is formed with excess kinetic energy, in accord with Stevenson's Rule,[115] from which they concluded that an upper limit to I(CN) must be 15·8eV. Combining this value with the appearance potential of the CN^+ ion from PF_2CN formed by reaction 4, a value of $D(PF_2\text{-}CN) \leq 3·8 \pm 0·6$eV is deduced; in good accord with the value estimated from reaction 3, $\leq 3·6 \pm 1·6$eV. This agreement also serves to reconcile the value for $I(PF_2)$, estimated from the PF_3 work, and suggests that the uncertainty associated with that value (9·75 ± 1·4eV) as a result of the thermochemical data used in the calculations, is not a realistic representation of the uncertainty. In view of this, parameters estimated as a result of further calculations involving the use of $I(PF_2)$ or I(PF), will not be written with large uncertainties.

If reaction 5 is responsible for PF^+ ion formation at 19·4 ± 0·2eV then, assuming that the strength of the P-F bond

$$PF_2CN + e \xrightarrow{5} PF^+ + F + CN + 2e$$

ruptured in the course of reaction 5 is equal to the PF-F bond energy in PF_2, calculated from thermochemical data to

be $4{\cdot}8 \pm 0{\cdot}7$eV, and the ionisation potential of PF is taken to be $\simeq 10{\cdot}7$eV, substitution into the expression; $D(P\text{-}F) + D(P\text{-}CN) \leq A(PF^+) - I(PF)$, results in a value of $\lesssim 3{\cdot}9$eV for the P-CN bond energy. This is in good agreement with the values of $\lesssim 3{\cdot}6$ and $\lesssim 3{\cdot}8$eV estimated above.

$PFCN^+$ ion formation at $15{\cdot}7 \pm 0{\cdot}2$eV can be attributed to reaction 6,

$$PF_2CN + e \xrightarrow{6} PFCN^+ + F + 2e$$

Assuming $D(PFCN\text{-}F) \simeq 4{\cdot}8$eV (the PF—F bond dissociation energy in PF_3) a value of $\gtrsim 10{\cdot}9$eV is estimated for the ionisation potential of PFCN. There are no other values with which this can be compared.

(iii) Difluoro(isocyanato)phosphine, PF_2NCO.

There is a close similarity between the relative ionic abundances in the positive ion mass spectrum of PF_2NCO at 70eV, shown in Table 6.5, and that of PF_2CN shown in Table 6.3. Typical ionisation data for the selected positive ions of PF_2NCO investigated are presented in Fig. 6.3. The energy scale is calibrated against the spectroscopic appearance potential of A^+/argon (15·76eV) and the appearance potentials measured are shown in Table 6.6.

TABLE 6.5

POSITIVE ION MASS SPECTRUM OF PF_2NCO AT 70eV

m/e	ION	ABUNDANCE
12	C^+	3.1
14	N^+	5.6
16	O^+	2.2
19	F^+	2.3
25	PF^{++}	0.7
26	CN^+	8.6
28	CO^+	63.4
30	NO^+	3.8
31	P^+	48.6
34.5	PF_2^{++}	0.2
38	$PFNC^{++}$	0.4
42	NCO^+	49.3
43	PC^+	3.6
45	PN^+	50.0
47	PO^+	54.7
50	PF^+	123.9
55.5	PF_2NCO^{++}	12.1
62	PFC^+	0.4
64	PFN^+	27.2
66	PFO^+	0.4
69	PF_2^+	1000.0
73	$PNCO^+$	2.9
76	$PFNC^+$	1.4
83	PF_2N^+	0.5
85	PF_2O^+	0.9
92	$PFNCO^+$	285.3
111	PF_2NCO^+	841.5

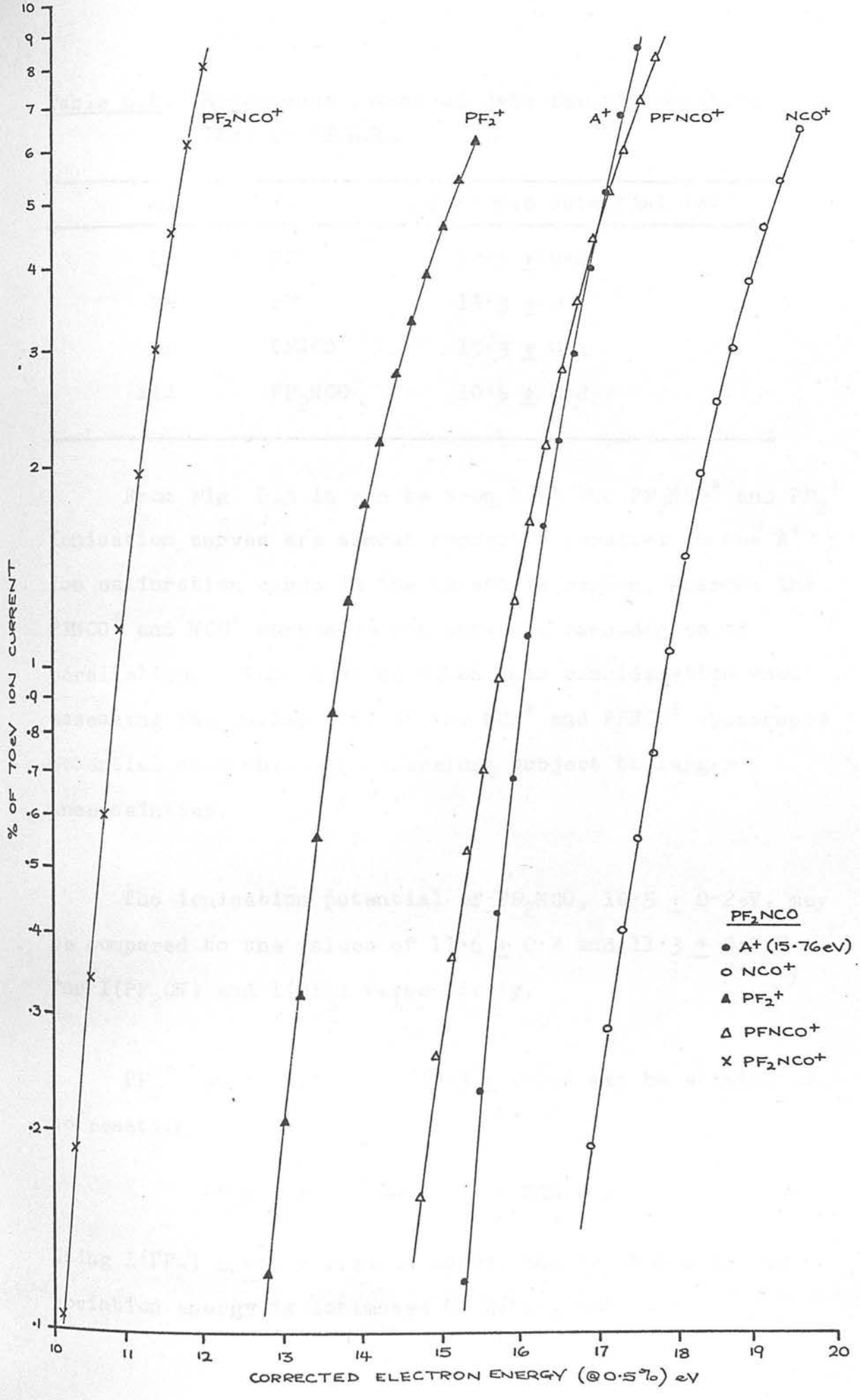
PF2NCO+
PF2+
A+
PFNCO+
NCO+
% OF 70eV ION CURRENT
CORRECTED ELECTRON ENERGY (@0·5%) eV
PF2NCO
A+ (15·76eV)
NCO+
PF2+
PFNCO+
PF2NCO+

Fig 6.3

Table 6.6. Appearance potential data for the positive ions of PF_2NCO.

m/e	Ion	Appearance Potential (eV)
42	NCO^+	17·6 ± 0·4
69	PF_2^+	13·3 ± 0·2
92	$PFNCO^+$	15·3 ± 0·4
111	PF_2NCO^+	10·5 ± 0·2

From Fig. 6.3 it can be seen that the PF_2NCO^+ and PF_2^+ ionisation curves are almost perfectly parallel to the A^+ ion calibration curve in the threshold region, whereas the $PFNCO^+$ and NCO^+ curves do not show the same degree of parallelism. This must be taken into consideration when assessing the reliability of the NCO^+ and $PFNCO^+$ appearance potential data which are therefore subject to larger uncertainties.

The ionisation potential of PF_2NCO, 10·5 ± 0·2eV, may be compared to the values of 11·6 ± 0·2 and 11·3 ± 0·2eV for $I(PF_2CN)$ and $I(PF_3)$ respectively.

PF_2^+ ion formation at 13·3 ± 0·2eV may be attributed to reaction 7,

$$PF_2NCO + e \xrightarrow{7} PF_2^+ + NCO + 2e$$

Using $I(PF_2) \simeq 9{\cdot}8$eV deduced above, the PF_2-NCO bond dissociation energy is estimated to be $\lesssim 3{\cdot}5$eV.

If NCO^+ ion formation at 17·6 ± 0·4eV is a result of reaction 8,

$$PF_2NCO + e \xrightarrow{8} NCO^+ + PF_2 + 2e$$

then on the assumption that both 7 and 8 proceed without excess energy, i.e. $A(PF_2^+) - I(PF_2) = A(NCO^+) - I(NCO)$, then a value of 14·1eV may be estimated for the ionisation potential of NCO. Stevenson's rule states that, for complementary reactions, only in the formation of the ion from the radical with the lowest ionisation potential will the products generally be found in their lowest states or without kinetic energy.[115] The bond dissociation energies estimated from the PF_2^+ appearance potential data are therefore expected to be more accurate than those values estimated from the X^+ data and, for the same reason, the ionisation potential estimated for the isocyanate radical from reaction 8 is only expected to be an upper limit (as shown to be the case for I(CN) estimated from CN^+ ion formation from CH_3CN and PF_2CN).

From the appearance potential for $PFNCO^+$ ion formation by the following reaction,

$$PF_2NCO + e \xrightarrow{9} PFNCO^+ + F + 2e$$

at 15·3 ± 0·4eV and the PFNCO-F bond dissociation energy, assumed to be equal to the PF-F bond energy in PF_2 (4·8eV), a value of ≳ 10·5 eV may be estimated for I(PFNCO). This may be compared to the value ≳ 10·9eV estimated for I(PFCN).

(iv) Difluoro(isothiocyanato)phosphine, PF_2NCS.

The positive ion mass spectrum of PF_2NCS at 70eV which is presented in Table 6.7 may be compared to the spectra of PF_2CN and PF_2NCO given in Tables 6.3 and 6.5 respectively. Typical ionisation data for the positive ions studied in PF_2NCS are shown in Fig. 6.4 in which the energy scale is referenced to the spectroscopic appearance potential of the A^+ ion from argon at 15·76eV.[15] From the figure it is apparent that the behaviour of all ions in the threshold region is similar to that of the A^+ ion, only the NCS^+ ionisation curve deviating from parallelism below 1%. The measured appearance potentials are presented in Table 6.8.

Table 6.8. Appearance potential data for the positive ions of PF_2NCS.

m/e	Ion	Appearance Potential (eV)
58	NCS^+	15·6 ± 0·3
69	PF_2^+	12·5 ± 0·2
108	$PFNCS^+$	14·8 ± 0·2
127	PF_2NCS^+	9·8 ± 0·2

From a comparison of the ionisation potentials of the oxygen and sulphur atoms, 13·6 and 10·3eV respectively, the ionisation potential measured for PF_2NCS, 9·8 ± 0·2eV is in the expected direction with respect to the ionisation potential of PF_2NCO, measured to be 10·5 ± 0·2eV.

TABLE 6.7

POSITIVE ION MASS SPECTRUM OF PF_2NCS AT 70eV

m/e	ION	ABUNDANCE
12	C^+	2.0
14	N^+	0.9
19	F^+	1.3
25	PF^{++}	0.3
26	CN^+	9.2
29	NCS^{++}	3.6
31	P^+	32.7
32	S^+	88.9
34.5	PF_2^{++}	2.7
38	$PFNC^{++}$	1.0
43	PC^+	6.8
44	CS^+	22.5
45	PN^+	3.9
47.5	PF_2NC^{++}	2.0
50	PF^+	113.9
54	$PFNCS^{++}$	3.9
58	NCS^+	116.7
63.5	PF_2NCS^{++}	30.5
64	PFN^+	1.4
69	PF_2^+	1000.0
76	$PFNC^+$	21.8
83	PF_2N^+	5.8
89	$PNCS^+$	1.4
95	PF_2NC^+	2.2
108	$PFNCS^+$	52.8
127	PF_2NCS^+	861.1

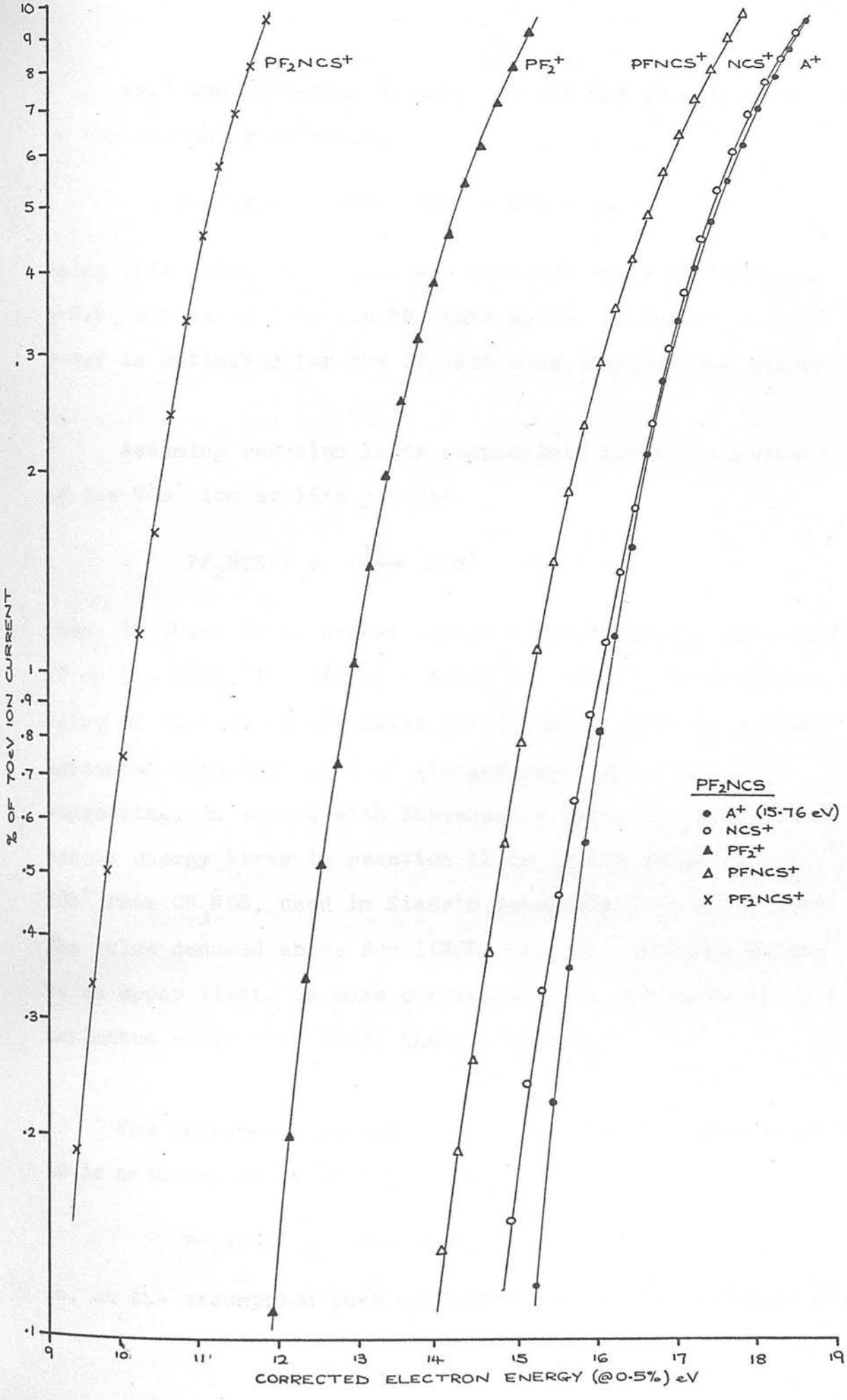
PF2NCS+
PF2+
PFNCS+
NCS+
A+
% OF 70eV ION CURRENT
CORRECTED ELECTRON ENERGY (@0·5%) eV
PF2NCS
A+ (15·76 eV)
NCS+
PF2+
PFNCS+
PF2NCS+

Fig 6.4

PF_2^+ ion formation at 12·5 ± 0·2eV may be attributed to the following reaction,

$$PF_2NCS + e \xrightarrow{10} PF_2^+ + NCS + 2e$$

Using this value in conjunction with the value of $I(PF_2) \simeq$ 9·8eV, estimated from the PF_3 data above, an upper limit of 2·7eV is estimated for the PF_2-NCS bond dissociation energy.

Assuming reaction 11 is responsible for the appearance of the NCS^+ ion at 15·6 ± 0·3eV,

$$PF_2NCS + e \xrightarrow{11} NCS^+ + PF_2 + 2e$$

then, if there is no excess energy associated with reactions 10 or 11, $A(PF_2^+) - I(PF_2) = A(NCS^+) - I(NCS)$, from which a value of ~12·9eV is estimated for I(NCS). This is in poor agreement with the value of ≤10·4eV reported by Kiser[22] suggesting, in accord with Stevenson's rule, the presence of excess energy terms in reaction 11 or in the formation of NCS^+ from CH_3NCS, used in Kiser's determination, or in both. The value deduced above for I(NCS) ~12·9eV, although it may be an upper limit, is more compatible with the value of 14·1 estimated above for I(NCO) than is 10·4eV.

The appearance potential of the $PFNCS^+$ ion from reaction 12 is measured to be 14·8 ± 0·2eV,

$$PF_2NCS + e \xrightarrow{12} PFNCS^+ + F + 2e$$

so, on the assumption that $D(PFNCS\text{-}F) \simeq D(PF_2\text{-}F) \simeq 5{\cdot}65$eV, a

value of $\gtrsim$ 9·2eV is estimated for the ionisation potential of PFNCS. This may be compared to the values of $\gtrsim$ 9·7 and $\gtrsim$ 10·1eV deduced for I(PFNCO) and I(PFCN) respectively.

(v) Discussion of positive ion data

A comparison of the 70eV mass spectra reveals some interesting trends:

(1) Each spectrum exhibits relatively high abundances of doubly charged ions and, although the singly charged PF_2^+ ion is the most abundant species in each case, the doubly charged PF_2^{++} ion is very nearly the least abundant of the doubly charged species. This suggests that I(PF_2^+) is considerably higher than the ionisation potentials of the other singly charged species from which doubly charged ions are formed.

(2) The total cross-section for positive ion formation in these molecules was found to be approximately the same and the abundances of the molecular positive ions relative to PF_2^+, the most abundant ion in all three spectra, were found to reflect the values measured for their respective ionisation potentials.

Molecule, PF_2X	PF_2CN	PF_2NCO	PF_2NCS
PF_2X^+ abundance (arb)	217	840	860
I(PF_2X)eV	11·6	10·5	9·8

(3) Rearrangement ions were evident in each spectrum i.e. PN^+/PF_2CN; PC^+, PO^+, NO^+, PFC^+, PFO^+ and PF_2O^+/PF_2NCO

and PC^+/PF_2NCS. The particularly large variety and high abundance of the 'rearrangement' ions detected in PF_2NCO may be deceptive in light of the oxidation product PF_2OPF_2 detected in the gas after short periods at room temperature, although ions such as PFC^+ and PC^+ cannot be attributed to the fragmentation of this oxidation product.

(4) In each spectrum the abundances of the PF^+ and PF_2^+ ions considerably exceeds those of the PX^+ and PFX^+ ions respectively (where X = CN, NCO and NCS) but with the exception of PFCN, for which the ionisation potential was found to be slightly higher than $I(PF_2)$, the ionisation potentials of the PFX radicals are lower than that of PF_2 (~9·8eV). In order to reconcile this with the relative ionic abundances found it must be concluded that the P-X bonds are weaker than the corresponding P-F bonds in these molecules.

A glance at the appearance potential data for PF_2^+ ion formation in PF_3 (15·4eV), PF_2CN (13·4eV), PF_2NCO (13·3eV) and PF_2NCS (12·5eV) reveals that, if each process proceeds by single bond cleavage and no kinetic energy contributions are involved (supported by Stevenson's rule), the following comparisons may be made;

$$D(PF_2\text{-}F) = D(PF_2\text{-}CN) + 2\cdot0eV$$

$$D(PF_2\text{-}F) = D(PF_2\text{-}NCO) + 2\cdot1eV$$

$$D(PF_2\text{-}F) = D(PF_2\text{-}NCS) + 2\cdot9eV$$

Using the PF_2-F bond dissociation energy calculated from thermochemical data, 5·6eV, values of 3·6, 3·5 and 2·7eV can be estimated for the PF_2-CN, PF_2-NCO and PF_2-NCS bond dissociation energies respectively.

(5) The ionisation potentials (in eV) measured for the molecules PF_2X and deduced for the radicals X are listed below with the spectroscopic ionisation potentials[22] of the nitrogen, oxygen and sulphur atoms for comparison;

N (14·5)	CN (<16·5)	PF_2CN (11·6 ± 0·2)
O (13·6)	NCO (<14·1)	PF_2NCO (10·5 ± 0·2)
S (10·4)	NCS (<12·9)	PF_2NCS (9·8 ± 0·2)

It is evident from these data that the expected trend is maintained.

(b) Negative ion formation

(i) Phosphorus trifluoride, PF_3.

Negative ion formation in PF_3 has been investigated by MacNeil and Thynne[103] and only a brief summary of their findings will be reported here. Dissociative electron capture was found to occur with a low probability, the average capture cross-section being estimated to be two orders of magnitude lower than that for SiF_4 (which was found in this study to be comparable with GeF_4).

At 70eV the ions detected were F^-, F_2^-, PF^- and PF_2^-

with relative abundances in the ratio 1000:6:<1:<1; at their respective capture maxima the ions F_2^-, PF^- and PF_2^- were formed in the ratio 485:590:1000. With the possible exception of PF_2^- these ions were formed with vertical onsets at energies greater than 9eV. F^- ion formation, onsetting ~8eV, was found to rise gradually to a plateau around 16eV. Differentiation of this curve indicated that unresolved resonance processes were probably present in the low energy tail of the curve. The reactions responsible for ion formation in PF_3 are listed in Table 6.9 together with the appearance potentials and the minimum energy requirements calculated for each process.

Table 6.9. Appearance potential data for PF_3 (MacNeil and Thynne[103])

Ion	Appearance Potential (eV)	Reaction, $PF_3 + e \longrightarrow$	ΔH_{min} (eV)
PF_2^-	10·3 ± 0·1	$\xrightarrow{13} PF_2^- + F$	5·6 ± 1·0-E(PF_2)
PF^-	11·4 ± 0·1	$\xrightarrow{14} PF^- + 2F$	10·5 ± 0·4-E(PF)
F_2^-	10·9 ± 0·1	$\xrightarrow{15} F_2^- + P + F$	10·9 ± 0·6

In order to reconcile the measured onset data with those reactions energetically favourable large amounts of excess energy had to be assigned to reactions 13 and 14 i.e., $\geq 3{\cdot}9 \pm 1{\cdot}2 + E(PF_2)$eV and $\geq 0{\cdot}9 \pm 0{\cdot}4 + E(PF)$eV respectively.

(ii) Cyanodifluorophosphine, PF_2CN.

Negative ion formation in PF_2CN, as in PF_3, was found

to occur with a low probability, the average dissociative capture cross-section probably being comparable with that of PF_3. The 70eV mass spectrum of PF_2CN is presented in Table 6.10.

Table 6.10. Negative ion mass spectrum of PF_2CN at 70eV.

m/e	Ion	Abundance
12	C^-	0·5
19	F^-	46·5
26	CN^-	1000·0
31	P^-	0·5
38	F_2^-	0·5
45	FCN^-	0·9
50	PF^-	0·1
57	PCN^-	<0·1
69	PF_2^-	10·2
75	$PFCN^-$	0·8
81	PF_2C^-	0·2
95	PF_2CN^-	6·4

The ions detected and measured at low electron energies were CN^-, PF_2^-, F^- and FCN^- with relative abundances in the ratio 1000:118:11:<1 at their respective major capture maxima. F_2^-, PF^- and the molecular negative ion PF_2CN^- were not detected at low electron energies. With the exception of CN^-, formed abundantly at 0eV, ion formation was restricted to energies greater than 4eV and in contrast to PF_3, for which only single resonance peaks were found,

several resonance processes were noted for all but the FCN^- ion. Ionisation efficiency curves for the F^-, CN^-, FCN^- and PF_2^- ions in the 2-9eV region are shown in Fig. 6.5(a) and (b) and the major F^- peak onsetting ~9eV is shown separately in Fig. 6.6(a) and (b) together with a typical O^-/CO peak included for comparison.

In order to compensate for the low ion intensities observed it was found necessary to use higher than normal trap currents (up to 0·3 μAmp) with a consequent broadening of the electron energy distribution. Since the deconvolution was carried out using the narrower energy distribution measured at low electron trap currents, the unfolded ionisation curves also reflect a broader energy distribution than normal. This is apparent from a comparison of the O^-/CO data obtained under the conditions in this work (Fig. 6.6) with that measured at low trap currents (Fig. 3.9) where the shape of the electron energy distribution is more stable than at high currents. In all experimental runs however, the onset edges of the F^-, CN^-, FCN^- and PF_2^- resonances at ~4eV could be matched with that of the O^-/CO ion measured simultaneously indicating that the ions are formed by processes occurring with a vertical onset.

Appearance potential data for the ions measured are given in Table 6.11, the vertical onsets being determined in two ways as before.

ION FORMATION IN PF_2CN (LOW ENERGY)

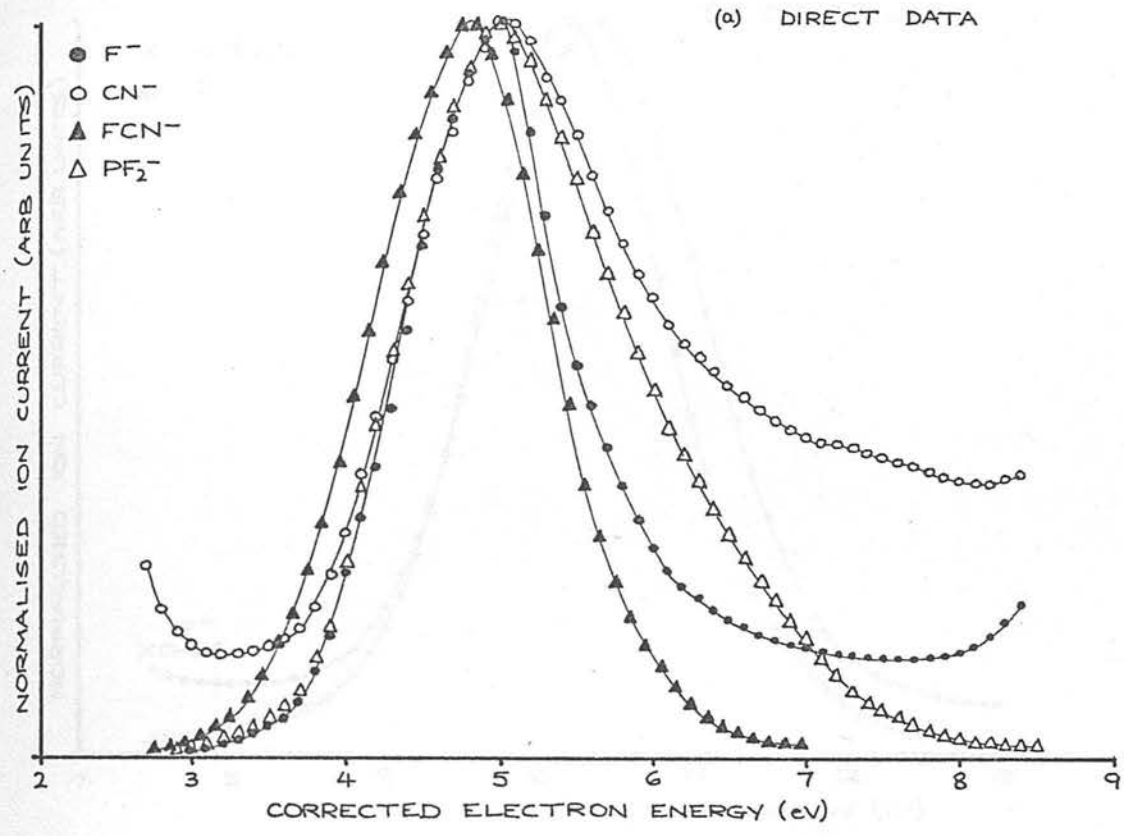

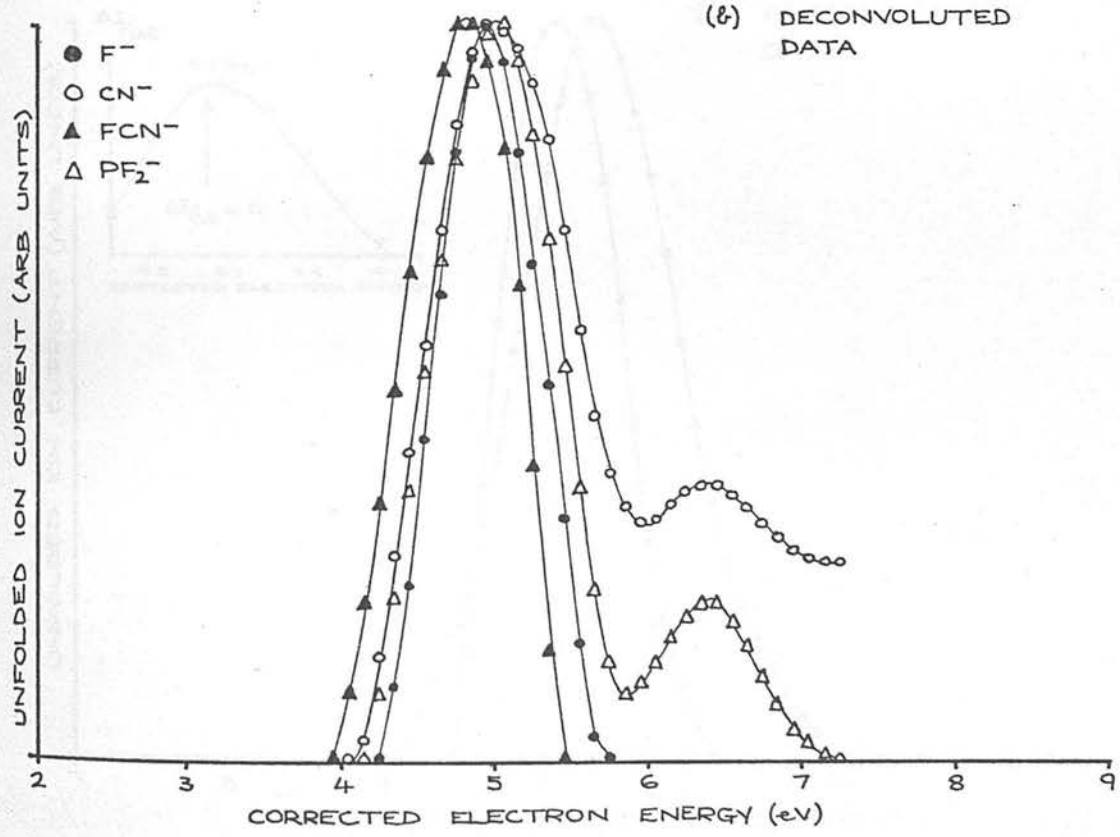

Fig 6.5

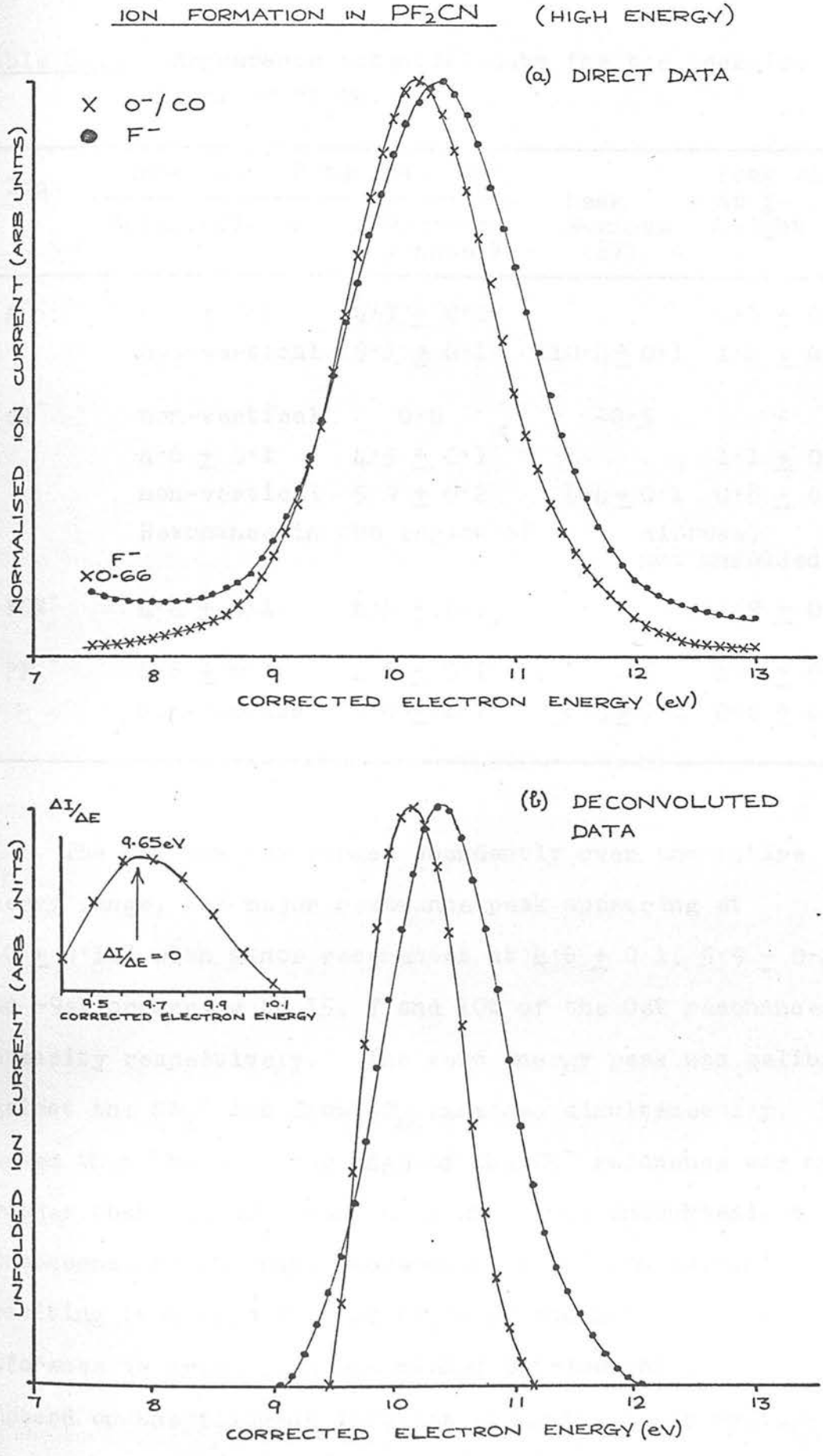
ION FORMATION IN PF_2CN (HIGH ENERGY)
(a) DIRECT DATA
X O^-/CO
● F^-
F^- X0·66
NORMALISED ION CURRENT (ARB UNITS)
7
8
9
10
11
12
13
CORRECTED ELECTRON ENERGY (eV)
(b) DECONVOLUTED DATA
$\Delta I/\Delta E$
9·65eV
$\Delta I/\Delta E = 0$
9·5
9·7
9·9
10·1
CORRECTED ELECTRON ENERGY
UNFOLDED ION CURRENT (ARB UNITS)
7
8
9
10
11
12
13
CORRECTED ELECTRON ENERGY (eV)

Fig 6.6

Table 6.11. Appearance potential data for the negative ions of PF_2CN.

Ion	Appearance Potential (eV)		Peak Maximum (eV)	Peak width at ½-height (eV)
	Superposition	Δ Maximum gradient		
F^-	4·6 ± 0·1	4·7 ± 0·1		0·8 ± 0·1
	non-vertical	9·1 ± 0·1	10·4 ± 0·1	1·2 ± 0·1
CN^-	non-vertical	0·0	~0·5	-
	4·6 ± 0·1	4·5 ± 0·1		1·1 ± 0·1
	non-vertical	5·9 ± 0·2	6·4 ± 0·1	0·8 ± 0·1
	Resonance in the region of 9eV - diffuse; not unfolded.			
FCN^-	4·4 ± 0·1	4·5 ± 0·1		0·9 ± 0·1
PF_2^-	4·6 ± 0·1	4·6 ± 0·1		1·0 ± 0·1
	non-vertical	5·8 ± 0·1	6·4 ± 0·1	0·8 ± 0·1

The CN^- ion was formed abundantly over the entire energy range, the major resonance peak appearing at 0·0 ± 0·1eV with minor resonances at 4·6 ± 0·1, 5·9 ± 0·2 and ~9eV occurring to 15, 7 and 10% of the 0eV resonance intensity respectively. The zero energy peak was calibrated against the SF_6^- ion from SF_6 examined simultaneously. This showed that the trailing edge of the CN^- resonance was much broader than the SF_6^- resonance which was undoubtedly a consequence of the high background of CN^- ion current resulting from pyrolysis of PF_2CN on the hot filament. This inference is drawn from the marked detrimental effect PF_2CN imposed on the filament lifetime (tungsten); an average

filament lifetime was found to be only $2\frac{1}{2}$ hours of which less than 2 hours could be usefully employed in data acquisition. On removal of the filament after this time period it was found to be very brittle and the surface to be covered with a grey substance, possibly tungsten carbide. However, the onset and peak maximum of the zero energy CN^- peak were reproducible and ion formation may be attributed to the following reaction,

$$PF_2CN + e \xrightarrow{16} CN^- + PF_2$$

thus, $D(PF_2\text{-}CN) \leq E(CN)$. The electron affinity of the nitrile radical has been determined by two methods from which the following values have been reported; $3{\cdot}6 \pm 0{\cdot}4$eV from lattice energy calculations[58] and an average value of $3{\cdot}1 \pm 0{\cdot}3$eV measured using the magnetron technique,[4] $D(PF_2\text{-}CN)$ is therefore estimated to be $\leq 3{\cdot}6 \pm 0{\cdot}4$eV or $\leq 3{\cdot}1 \pm 0{\cdot}3$eV respectively, i.e., average of $3{\cdot}4 \pm 0{\cdot}6$eV which is in good agreement with the value of $3{\cdot}6 \pm 1{\cdot}6$eV estimated from the positive ion data above.

The vertical onset at $4{\cdot}6 \pm 0{\cdot}1$eV probably corresponds to CN^- ion formation by reaction 17 and CN^- ion formation at ~9eV to reaction 18,

$$PF_2CN + e \xrightarrow{17} CN^- + PF + F$$

$$\xrightarrow{18} CN^- + P + 2F$$

then, in the absence of excess energy terms and using the magnetron value for E(CN) in the expression, D(P-CN) + D(P-F) = A(CN^-) + E(CN), and since $D(PF_2\text{-}CN) \leq E(CN)$, values

of 4·6 and 4·4eV may be estimated for D(PF-F) and D(P-F) respectively. Although these values are significantly lower than the average bond energy calculated for PF_3, 5·2 ± 0·4eV, the value of 4·6eV deduced for D(PF-F) is in good agreement with the thermochemical value of 4·8eV and the value of 4·4eV estimated for D(P-F) is in excellent agreement with the value of 4·5 ± 1·0eV reported by Gaydon[18] for this bond.

The small CN^- resonance at 5·9 ± 0·2eV must correspond to reaction 18 accompanied by the release of ~1·3eV of excess energy. This may be compared to ion formation in PF_3 where all reactions, except that responsible for F_2^- ion formation, involved considerable excess energy.

The PF_2^- ion appears with a vertical onset at 4·6 ± 0·1eV. From the magnitude of the PF_2-CN bond dissociation energy estimated from reaction 16 above, i.e. $D(PF_2\text{-}CN) \leq E(CN)$,[4] the minimum energy requirement for the reaction,

$$PF_2CN + e \xrightarrow{19} PF_2^- + CN$$

in the absence of excess energy, is 3·1 ± 0·3eV - $E(PF_2)$. Since no such ions are formed below 4·6 ± 0·1eV the excess energy of reaction 19 is ≥ 1·5 ± 0·4eV. A further resonance of lower cross-section onsetting at 5·8 ± 0·1eV may similarly be attributed to the formation of PF_2^- by reaction 19 involving ≥ 2·5 ± 0·6eV of excess energy. The excess energy associated with the analogous reaction in PF_3,

$$PF_3 + e \xrightarrow{13} PF_2^- + F$$

is reported to be $\geq 3{\cdot}9 \pm 1{\cdot}2$eV.[103] Formation of PF_2^- as a result of reaction 20 is not possible energetically in this energy range.

$$PF_2CN + e \xrightarrow{20} PF_2^- + C + N$$

The (C-N) bond energy is reported to be $7{\cdot}8$eV[18] but from reaction 20, assuming that $D(PF_2\text{-}CN) \leq 3{\cdot}1 \pm 0{\cdot}3$eV and that the measured appearance potential, $5{\cdot}8 \pm 0{\cdot}1$eV, is the minimum energy requirement of reaction 20, D(C-N) is estimated to be less than or equal to $2{\cdot}7 + E(PF_2)$eV, which would impose an unreasonably high value on $E(PF_2)$. Reaction 20 does not therefore appear to contribute to PF_2^- ion formation.

From Figs. 6·5 and 6·6 it is apparent that F^- ion formation occurs as the result of two resonance processes. The first onsets vertically at $4{\cdot}6 \pm 0{\cdot}1$eV and is about 66% as intense as the second resonance which onsets non-vertically at $9{\cdot}1 \pm 0{\cdot}1$eV. There are three reactions possible in the energy range in which F^- ion formation is observed.

$$PF_2CN + e \xrightarrow{21} F^- + PFCN$$
$$\xrightarrow{22} F^- + PF + CN$$
$$\xrightarrow{23} F^- + P + F + CN$$

which, on the general assumption that $D(P\text{-}F) \simeq 5$eV and $D(P\text{-}CN) \simeq 3$eV, have minimum energy requirements of ~1·5, ~4·5 and ~9·5eV respectively. It is therefore not unreasonable to assign the onsets at $4{\cdot}6 \pm 0{\cdot}1$ and $9{\cdot}1 \pm 0{\cdot}1$eV

to reactions 22 and 23 respectively. This being the case then from reaction 22, D(PF-F) + D(PF-CN) $\leq$ 4·6 $\pm$ 0·1 + E(F) and from 23, D(PF-F) + D(P-F) + D(P-CN) $\leq$ 9·1 $\pm$ 0·1 + E(F). Using the value of E(F) = 3·4eV[36] and assuming D(P-CN) $\simeq$ 3·1 $\pm$ 0·3eV, values of ~4·9 and ~4·5eV may be estimated for D(PF-F) and D(P-F) respectively, in good agreement with the values of ~4·6 and ~4·4eV estimated above.

Pressure dependence measurements for the formation of the FCN^- ion at 4·4 $\pm$ 0·1eV showed it to be a primary ion and therefore formed by a reaction involving intramolecular rearrangement such as 24 or 25,

$$PF_2CN + e \xrightarrow{24} FCN^- + PF$$

$$\xrightarrow{25} FCN^- + P + F$$

The minimum energy requirement of reaction 24 and 25, estimated using the value of D(C-N) calculated from known thermochemical data[23,123] (5·3 $\pm$ 1·0eV) and the heat of formation of PF_2CN deduced from reaction 16 (-3·5 $\pm$ 1·2eV), are 2·7 $\pm$ 1·6 - E(FCN) and 7·2 $\pm$ 1·6 -E(FCN)eV respectively. As reaction 24 would therefore involve 1·7 + E(FCN)eV of excess energy it is most probable that reaction 25 is that responsible for FCN^- ion formation at 4·4 $\pm$ 0·1eV from which E(FCN) is estimated to be $\geq$ 2·8 $\pm$ 1·7eV. There is no other value reported for this electron affinity but values of 3·45,[36] 3·1 $\pm$ 0·3[4] and 2·9 $\pm$ 0·2eV[65] have been reported for E(F), E(CN) and $E(F_2)$ respectively.

(iii) Difluoro(isocyanato)phosphine, PF_2NCO.

The total electron capture cross-section (PF_2NCO) was found to be less than that of PF_2CN or PF_2NCS (which were approximately equal) by at least an order of magnitude. Unlike PF_2CN and PF_2NCS, which were stable to oxidation under the conditions prevailing in the gas handling system, PF_2NCO was found to contain traces of the oxidation product PF_2OPF_2. An infra-red analysis of the freshly prepared sample showed no traces of PF_2OPF_2 suggesting that oxidation was taking place either during the transfer of the gas into the inlet system or during residence in the inlet system. Despite precautions, i.e. storage of the PF_2NCO at liquid nitrogen temperatures and baking of the inlet system before admission of the sample, the oxidation product could not be entirely eliminated. The ions PF_2O^- and PFO^- present in the 70eV negative ion mass spectrum of a freshly prepared sample shown in Table 6.12 probably originate from this oxidation product. The PF_2O^- ion, which was also present at low electron energies, was therefore investigated as a dissociative capture product of PF_2OPF_2.

Table 6.12. Negative ion mass spectrum of PF_2NCO at 70eV.

m/e	Ion	Abundance
12	C^-	3·2
16	O^-	70·8
19	F^-	607·3
26	CN^-	228·3
31	P^-	4·0
38	F_2^-	2·6
42	NCO^-	1000·0
66	PFO^-	6·9
85	PF_2O^-	132·4

The ions detected at low electron energies were NCO^-, PF_2O^-, F^- and CN^- appearing with relative abundances in the ratio 1000:1:0·3:<0·1 at their respective capture maxima. The CN^- ion was formed at zero energy with a very low capture cross-section, the shape of which was very dependent upon the filament temperature. CN^- ion formation is thus attributed to surface ionisation following the pyrolysis of PF_2NCO at the filament and will not be discussed in any further detail.

Typical ionisation efficiency curves for NCO^- and PF_2O^- are shown in Fig. 6.7(a) and (b) and for F^- and the second peak of PF_2O^- in Fig. 6.8(a) and (b). The second peak of PF_2O^-, which was 50% as intense as the low energy peak, was found to exhibit a vertical rise to maximum at threshold. This is readily seen in Fig. 6.8(b) by a comparison between the deconvoluted onset edges of the PF_2O^- and O^-/CO peaks measured simultaneously. As a consequence of the lower energy PF_2O^- resonance the ion current does not fall to zero in the energy region between the two peaks and so the onset edges do not match quite as closely as usual. However, as the weight of several experimental runs was clearly in favour of closely matched edges this resonance will be treated as having a vertical onset for the discussion below. Appearance potential data for the ions investigated are given in Table 6.13.

ION FORMATION IN PF_2NCO (LOW ENERGY)

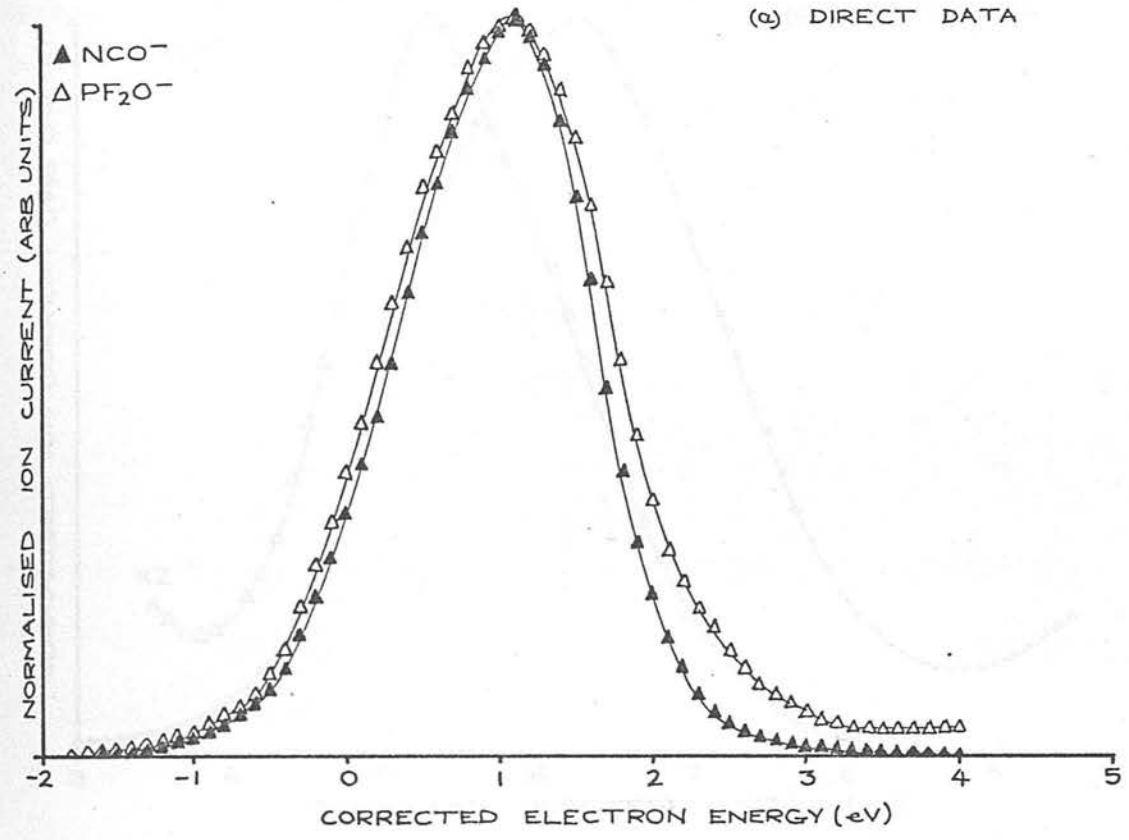

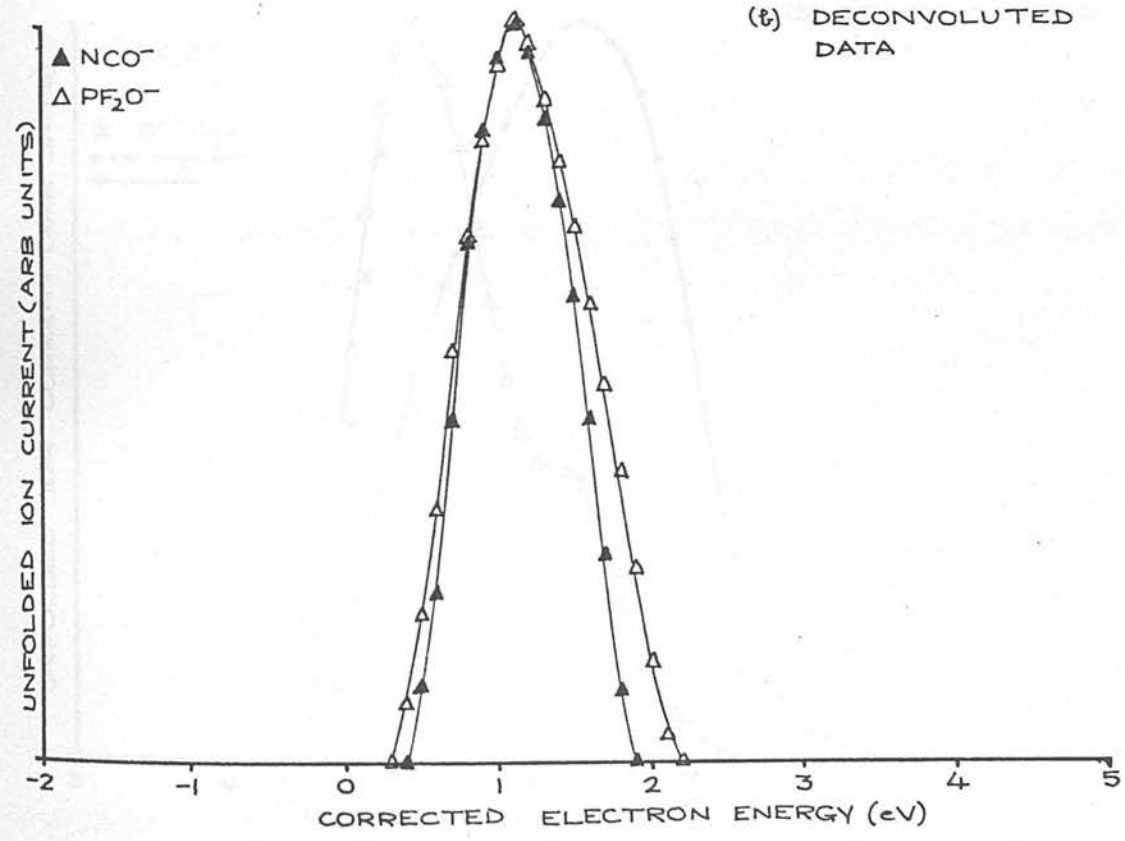

Fig 6.7

ION FORMATION IN PF_2NCO (HIGH ENERGY)

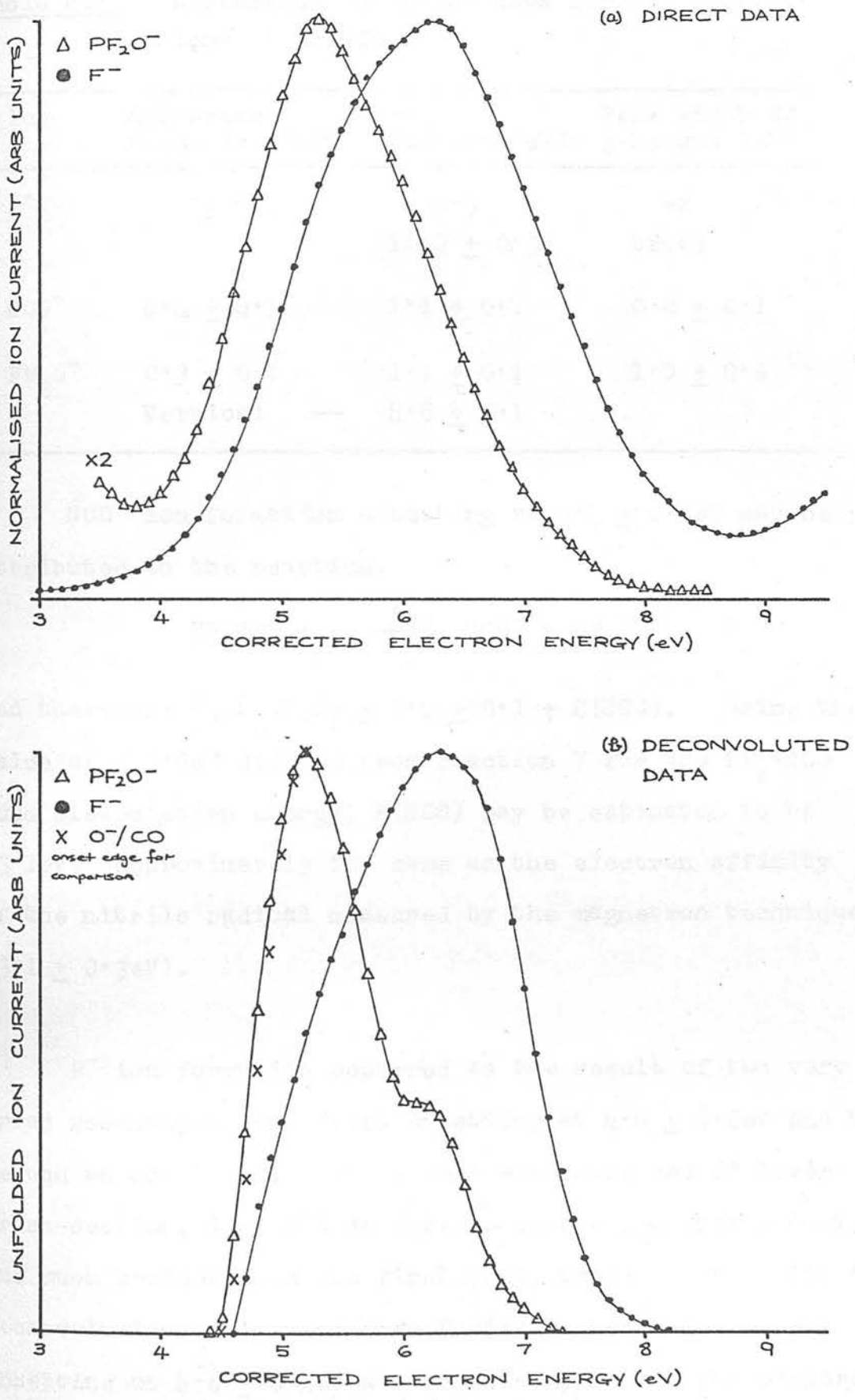

Fig 6.8

Table 6.13. Appearance potential data for the negative ions of PF_2NCO.

Ion	Appearance Potential (eV)	Peak Maximum (eV)	Peak Width at $\frac{1}{2}$-height (eV)
F^-	$4{\cdot}6 \pm 0{\cdot}2$	~6·3	~2
	~9	$11{\cdot}0 \pm 0{\cdot}3$	broad
NCO^-	$0{\cdot}4 \pm 0{\cdot}1$	$1{\cdot}1 \pm 0{\cdot}1$	$0{\cdot}8 \pm 0{\cdot}1$
PF_2O^-	$0{\cdot}3 \pm 0{\cdot}1$	$1{\cdot}1 \pm 0{\cdot}1$	$1{\cdot}0 \pm 0{\cdot}1$
	Vertical —	$4{\cdot}8 \pm 0{\cdot}1$	

NCO^- ion formation onsetting at $0{\cdot}4 \pm 0{\cdot}1$eV may be attributed to the reaction,

$$PF_2NCO + e \xrightarrow{26} NCO^- + PF_2$$

and therefore $D(PF_2\text{-}NCO) \leq 0{\cdot}4 \pm 0{\cdot}1 + E(NCO)$. Using the value of $\leq 3{\cdot}5$eV deduced from reaction 7 for the PF_2-NCO bond dissociation energy, E(NCO) may be estimated to be ~3·1eV; approximately the same as the electron affinity of the nitrile radical measured by the magnetron technique[4] ($3{\cdot}1 \pm 0{\cdot}3$eV).

F^- ion formation occurred as the result of two very broad resonances, the first onsetting at $4{\cdot}6 \pm 0{\cdot}2$eV and the second at about 9eV. The second resonance was of lower cross-section, i.e. 25% as intense as the low energy peak, and much broader than the first peak, hence any attempts at deconvolution would have been futile. Because the peak onsetting at $4{\cdot}6 \pm 0{\cdot}2$eV was broad compared to the electron

energy distribution the profile of the unfolded peak shown in Fig. 6.8(b) may be either the result of an unresolved second resonance (possibly from F^- ion formation in PF_2OPF_2) or of ineffective deconvolution. The onset was reproducible however, and will be treated as representing F^- ion formation by reaction 27, analogous to the reaction (22) responsible for F^- ion formation in PF_2CN.

$$PF_2NCO + e \xrightarrow{27} F^- + PF + NCO$$

From reaction 27, $D(P\text{-}NCO) + D(P\text{-}F) \leq 4{\cdot}6 \pm 0{\cdot}2 + E(F)$ so, using the value of $E(F) = 3{\cdot}45eV$[36] and $D(PF_2\text{-}NCO) \leq 3{\cdot}5 \pm 1{\cdot}6eV$ deduced above, $D(PF\text{-}F)$ is estimated to be $\leq 4{\cdot}5 \pm 1{\cdot}8eV$. This may be compared to the values of ~4·9 and ~4·6eV estimated for the corresponding bond in PF_2CN.

Assuming that reaction 28 is responsible for F^- ion formation at ~9eV

$$PF_2NCO + e \xrightarrow{28} F^- + P + F + NCO$$

a value of ~4·4 is estimated for $D(P\text{-}F)$ which compares favourably with the values of ~4·5 and ~4·4eV estimated for the corresponding bond in PF_2CN and the value of $4{\cdot}5 \pm 1{\cdot}0eV$ quoted by Gaydon.[18]

If PF_2O^- is formed as a dissociative electron capture produce of PF_2OPF_2, reaction 29 may be responsible for the resonance onsetting at $0{\cdot}3 \pm 0{\cdot}1eV$,

$$PF_2OPF_2 \xrightarrow{29} PF_2O^- + PF_2$$

then, $D(PF_2O - PF_2) - E(PF_2O) \leq 0{\cdot}3 \pm 0{\cdot}1eV$. In the absence of any information on either $D(PF_2O-PF_2)$ or $E(PF_2O)$ conclusions cannot be drawn regarding the magnitude of either.

The resonance peak onsetting vertically at $4{\cdot}8 \pm 0{\cdot}1eV$ was found, after deconvolution, to have a second resonance hidden in the trailing edge of the peak and appearing about 6eV. If the onset at $4{\cdot}8 \pm 0{\cdot}1eV$ may be attributed to reaction 30,

$$PF_2OPF_2 + e \xrightarrow{30} PF_2O^- + PF + F$$

the shoulder at ~6eV can be similarly attributed to reaction 30 in which approximately 1eV of excess energy is involved. The formation of PF_2^-/PF_3 and PF_2^-/PF_2CN were also found to involve excess energy. From the onset at $4{\cdot}8 \pm 0{\cdot}1eV$ D(PF-F) is estimated to be $4{\cdot}5 \pm 0{\cdot}2eV$ again in fair agreement with the values of ~4·9 and ~4·6eV deduced from the equivalent bond rupture in PF_2CN and ~4·5eV for that in PF_2NCO.

(iv) Difluoro(isothiocyanato)phosphine, PF_2NCS.

The mass spectrum of PF_2NCS measured at 70eV is shown in Table 6.14. As in the case of PF_2NCO but not PF_2CN, a molecular negative ion was not detected.

The ions formed at low electron energies were NCS^-, S^-, CN^-, F^- and PF_2^- in the ratio 1000:7:5:<0·1:<0·1 at their respective capture maxima. Of these the NCS^-, S^- and CN^- ions were formed at approximately zero electron energy. The S^- and CN^- ions also appeared with vertical onsets around 4eV, i.e. in the same place as the PF_2^- ion. Because of the

Table 6.14. Negative ion mass spectrum of PF_2NCS at 70eV.

m/e	Ion	Abundance
12	C^-	<0·1
19	F^-	1·7
26	CN^-	12·4
31	P^-	<0·1
32	S^-	2·5
38	F_2^-	<0·1
58	NCS^-	1000·0
69	PF_2^-	0·1

low capture cross-section of PF_2NCS (comparable with that of PF_3 and PF_2CN) high trap currents had to be employed thus involving high filament temperatures at the lower electron energies. Surface ionisation was therefore marked during this study and the CN^- and S^- peaks at ~0eV shown in Fig. 6.9(a) and (b) are attributed to this process. The NCS^- ion also appeared at 0eV but in this case the background ion current, which extended over the entire energy range, occurred to a much lesser degree relative to the peak maximum ion current intensity, i.e. <1%, than did the background ion currents of CN^- or S^- (each ~15% of the 0eV ion current) apparent in the trailing edges of the 4eV resonances which do not fall to zero current. Although the NCS^- ion current has been shown in Fig. 6.9 as falling to zero at about 2·5eV this was only for ease of presentation and in fact although the background NCS^- ion current was less than 1%

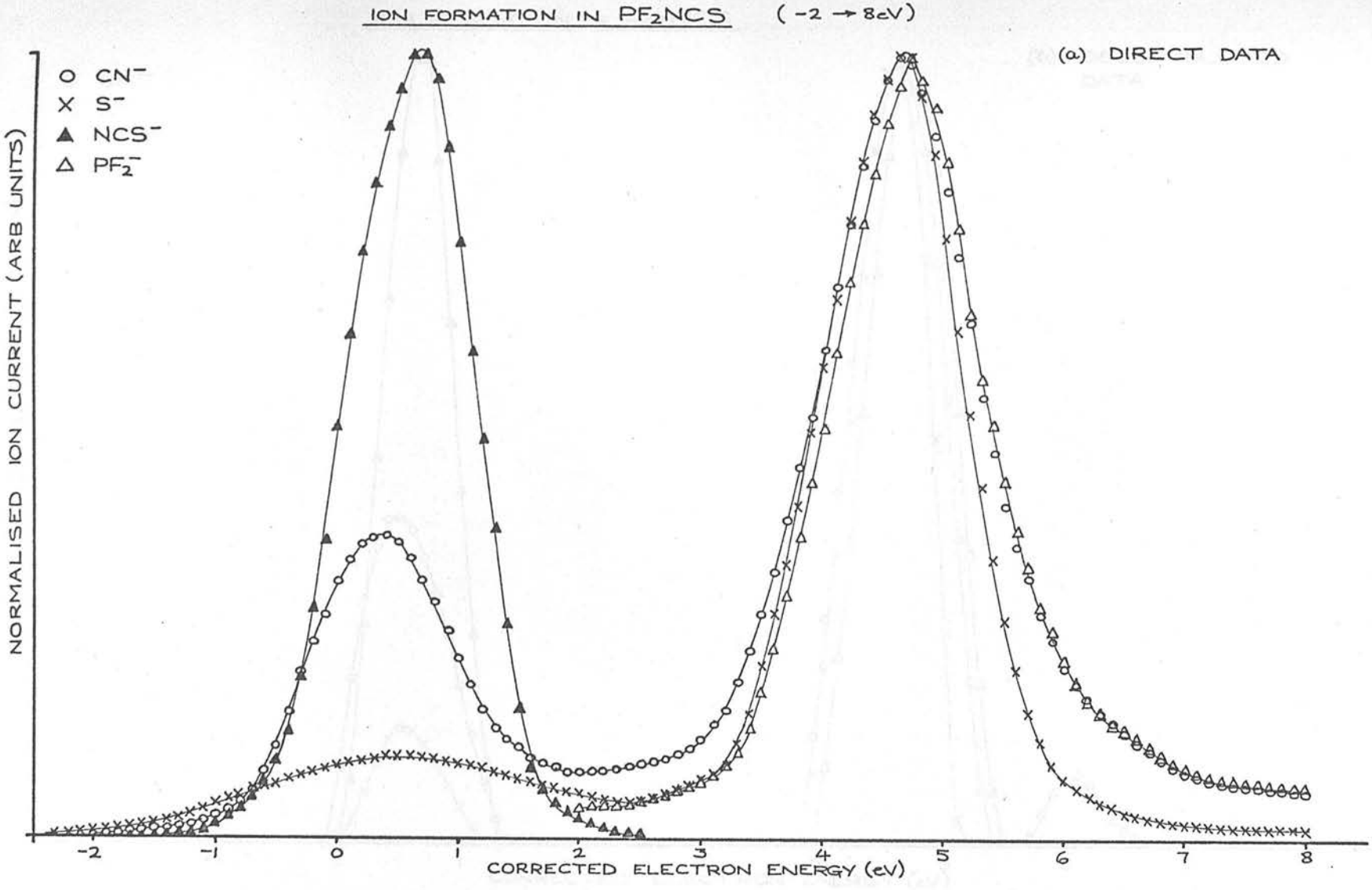
ION FORMATION IN PF_2NCS (-2 → 8eV)
(a) DIRECT DATA
O CN^-
X S^-
▲ NCS^-
△ PF_2^-
NORMALISED ION CURRENT (ARB UNITS)
-2
-1
0
1
2
3
4
5
6
7
8
CORRECTED ELECTRON ENERGY (eV)

Fig 6.9

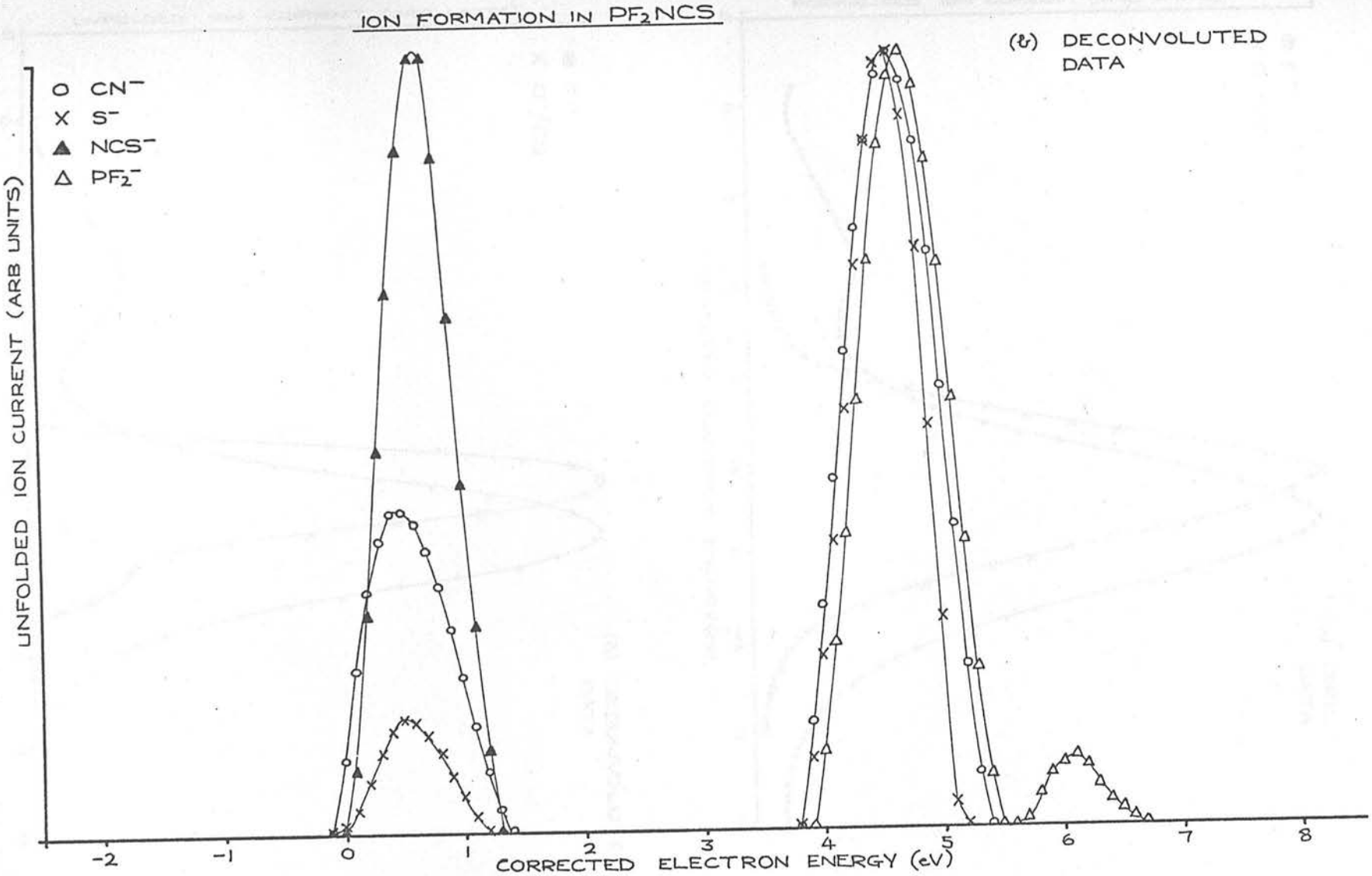
ION FORMATION IN PF_2NCS
(a) DECONVOLUTED DATA
O CN^-
X S^-
▲ NCS^-
△ PF_2^-
UNFOLDED ION CURRENT (ARB UNITS)
-2
-1
0
1
2
3
4
5
6
7
8
CORRECTED ELECTRON ENERGY (eV)

Fig 6.9

ION FORMATION IN PF_2NCS

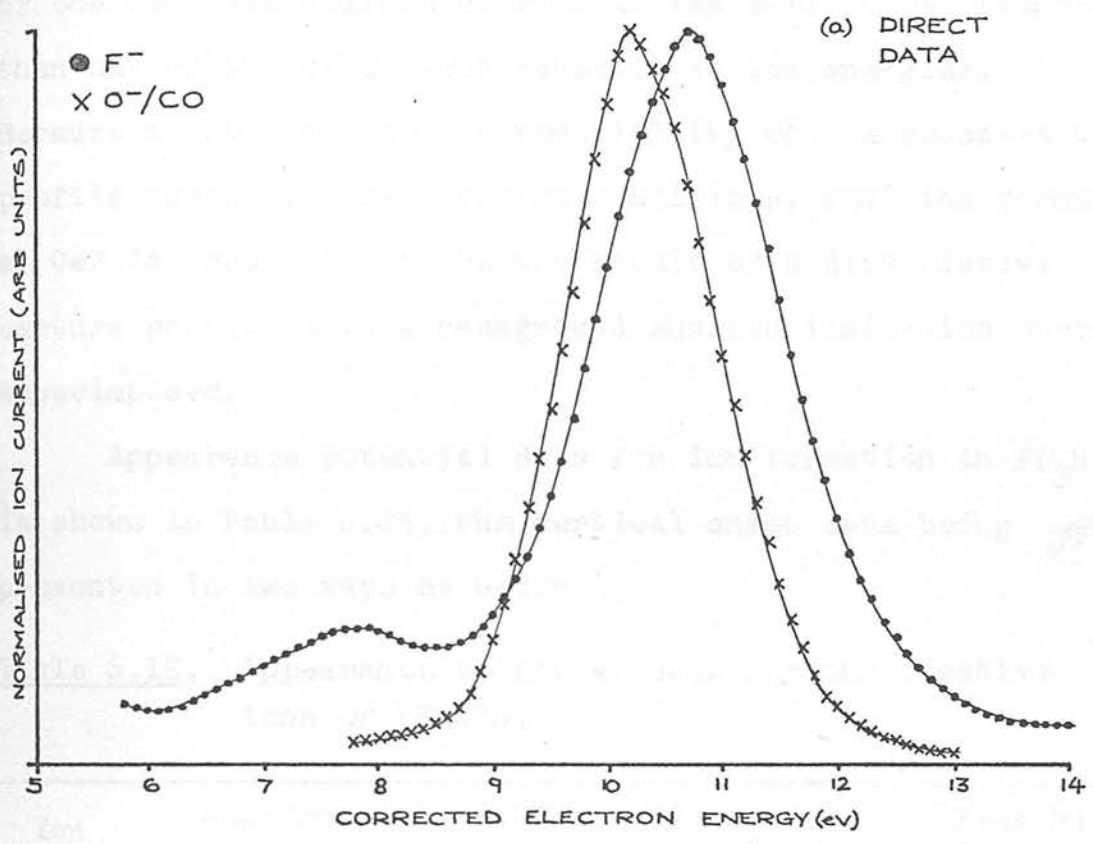

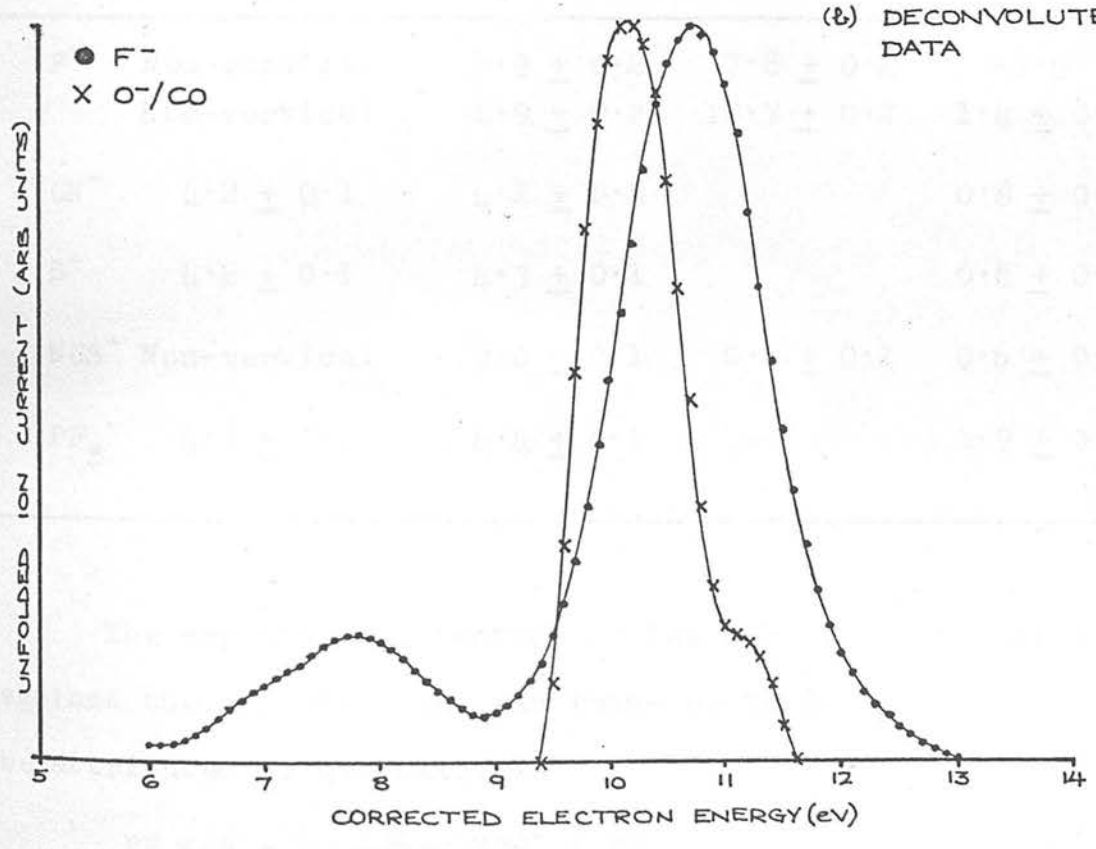

Fig 6.10

of the 0eV peak maximum current it was still more intense than any of the other ions detected at low energies. Because of this and the reproducibility of the cross-section profile under different source conditions, NCS^- ion formation at 0eV is considered to be the result of a dissociative capture process with a background surface ionisation current superimposed.

Appearance potential data for ion formation in PF_2NCS is shown in Table 6.15, the vertical onset data being presented in two ways as before.

Table 6.15. Appearance potential data for the negative ions of PF_2NCS.

Ion	Appearance Potential (eV)		Peak Maximum (eV)	Peak Width at ½-height (eV)
	Superposition of edges	Δ Maximum gradient		
F^-	Non-vertical	6·3 ± 0·2	7·8 ± 0·2	~1·5
	Non-vertical	8·9 ± 0·2	10·7 ± 0·2	1·4 ± 0·1
CN^-	4·2 ± 0·1	4·2 ± 0·1		0·8 ± 0·1
S^-	4·2 ± 0·1	4·3 ± 0·1		0·8 ± 0·1
NCS^-	Non-vertical	0·0 ± 0·1	0·6 ± 0·1	0·6 ± 0·1
PF_2^-	4·3 ± 0·1	4·4 ± 0·1		0·9 ± 0·1

The appearance potential of the NCS^- ion, calibrated against the SF_6^-/SF_6 ion, was found to be 0·0 ± 0·1 and may be attributed to the reaction

$$PF_2NCS + e \xrightarrow{3l} NCS^- + PF_2.$$

From the equation $D(PF_2\text{-}NCS) \leq A(NCS^-) + E(NCS)$, the PF_2-NCS bond dissociation energy is estimated to be $\leq 2{\cdot}2 \pm 0{\cdot}1$eV, that is, the electron affinity of the isothiocyanate radical reported in the literature.[4] This is in fair agreement with the value of 2·7eV estimated for this bond from the positive ion data above (on the assumption that $D(PF_2\text{-}F) = 5{\cdot}6$eV).

PF_2^- ion formation onsets vertically at $4{\cdot}3 \pm 0{\cdot}1$eV and may be the consequence of the reaction

$$PF_2NCS + e \xrightarrow{32} PF_2^- + NCS$$

for which the minimum energy requirement is $2{\cdot}2 \pm 0{\cdot}1 - E(PF_2)$eV. Although this would involve more than $2{\cdot}2 \pm 0{\cdot}1 + E(PF_2)$eV of excess energy it would be in line with PF_2^- ion formation from PF_3 and PF_2CN where more than $3{\cdot}9 \pm 1{\cdot}2$ and $1{\cdot}3 \pm 0{\cdot}5$eV of excess energy accompany the analogous reactions.

From Fig. 6.9(b) it can be seen that a peak of lower cross-section onsetting at $5{\cdot}6 \pm 0{\cdot}1$eV is revealed after deconvolution of the experimental PF_2^- ionisation efficiency curve. Ion formation at this energy may correspond to reaction 32 with an extra $1{\cdot}3 \pm 0{\cdot}1$eV of excess energy or more probably to the following reaction

$$PF_2NCS + e \xrightarrow{33} PF_2^- + NC + S$$

from which, on the assumption that the NC = S bond energy is not too different from the SC = S bond strength reported by

MacNeil and Thynne[60] to be $\leq 5{\cdot}0 \pm 0{\cdot}3$eV, a value of $\geq 1{\cdot}6 \pm 0{\cdot}5$eV is estimated for the electron affinity of the PF_2 radical. although there are no other values with which this can be compared it is generally found that fluorinated radicals exhibit higher electron affinities than the corresponding hydrogenated radicals. This is illustrated in Table 6.16 where the electron affinities reported for various hydrogenated radicals are compared to the corresponding fluorinated species. In view of this trend $E(PF_2) \geq 1{\cdot}6 \pm 0{\cdot}5$eV does not appear to be an unreasonable value. However, assuming that the onset at $4{\cdot}3 \pm 0{\cdot}1$eV is responsible for PF_2^- ion formation by reaction 33 a value of $\geq 2{\cdot}9 \pm 0{\cdot}5$eV may be estimated for $E(PF_2)$ which, by reference to Table 6.16 alone, also appears to be a reasonable value. Therefore, it is not possible using only Table 6.16 to make a choice between these two values, and in turn to decide upon which

Table 6.16. Electron affinities of hydrogenated and fluorinated radicals.

Hydrogenated Radicals	EeV	Fluorinated Radicals	EeV
CH_3[4]	1·08	CF_3[4]	1·89
NH_2[59]	0·74	NH_2[4]	3·00
PH_2[59]	1·26	PF_2	-
CH_3O[4]	0·38	CF_3O[4]	1·35
CH_3S[4]	1·36	CF_3S[4]	1·80

of the two resonances corresponds to ion formation by reaction 33.

A consideration of the dissociative capture behaviour found in the other molecules studied (PF_3, PF_2CN and PF_2NCO) may assist in resolving this problem. Considerable excess energy has to be assigned to the reactions responsible for PF_2^- ion formation in PF_3 and PF_2CN and in each case the resonance is found to attain maximum cross-section at the threshold. It is therefore not unreasonable to assume that ion formation in PF_2NCS might follow the same trend. This being the case then the resonance onsetting vertically at $4{\cdot}3 \pm 0{\cdot}1$eV would be expected to correspond to PF_2^- ion formation by reaction 32 (in which $\geq 2{\cdot}1 \pm 0{\cdot}1$eV of excess energy is involved) and that process onsetting at $5{\cdot}6 \pm 0{\cdot}1$eV to correspond to reaction 33 from which $E(PF_2)$ is estimated to be $\geq 1{\cdot}6 \pm 0{\cdot}5$eV. This explanation appears to be reasonable and as a consequence the PF_2^- onset at $4{\cdot}3 \pm 0{\cdot}1$eV is tentatively attributed to ion formation by reaction 32 and the onset at $5{\cdot}6 \pm 0{\cdot}1$eV to ion formation by reaction 33.

The F^- ionisation efficiency curve is shown in Fig. 6.10(a) and (b). Because this ion is formed with a low capture cross-section abnormally high trap currents had to be employed (up to $0{\cdot}5$ μAmp) and consequently a low signal to noise ratio tolerated. From Fig. 6.10(a) it can be seen that the ion current rises below 6eV and a rough investigation suggested a further resonance at ~4eV, in the same energy region as the PF_2^-, CN^- and S^- resonances. However,

the background signal was so high that the benefits of a detailed investigation of F^- ion formation below 6eV were offset by the unreasonably rapid filament corrosion resulting from the high trap current level necessary for such measurements.

After deconvolution of the experimental data shown in Fig. 6.10(a) the two resonances investigated were found to onset at $6{\cdot}3 \pm 0{\cdot}2$eV and $8{\cdot}9 \pm 0{\cdot}2$eV. Assuming that $D(NC = S)$ is approximately the same as $D(SC = S) \leq 5{\cdot}0 \pm 0{\cdot}3$eV,[60] $D(PF\text{-}F) \simeq 4{\cdot}8$eV and $E(F) = 3{\cdot}4$eV[36] the minimum energy requirements for the following reactions,

$$PF_2NCS + e \xrightarrow{34} F^- + PF + NCS$$
$$\xrightarrow{35} F^- + PFNC + S$$
$$\xrightarrow{36} F^- + P + NCS + F$$

are estimated to be $3{\cdot}6$, $6{\cdot}4$ and $8{\cdot}2$eV respectively. Reaction 34 may therefore correspond to the resonance appearing in the 4eV region, reaction 35 to that onsetting at $6{\cdot}3 \pm 0{\cdot}2$eV and reaction 36 to that at $8{\cdot}9 \pm 0{\cdot}2$eV.

The small CN^- ion peak in the zero electron energy region has already been discussed above and attributed to surface ionisation following pyrolysis of PF_2NCS on the hot filament. The resonance onsetting vertically at $4{\cdot}2 \pm 0{\cdot}1$eV may be formed as the result of the following reaction,

$$PF_2NCS + e \xrightarrow{37} NC^- + S + PF_2$$

Using the upper limit of 2·2 ± 0·1eV deduced from reaction 31 for the PF_2- NCS bond dissociation energy in the following expression, D(PF_2-NCS) + D(NC=S) ≤ 4·2 ± 0·1 + E(CN), where E(CN) is taken as 3·1 ± 0·3eV,[4] a value of ≤ 5·1 ± 0·5eV is estimated for the NC = S bond dissociation energy in the absence of excess energy. This may be compared to the value of ≤ 5·0 ± 0·3eV reported by MacNeil and Thynne[60] for the SC = S bond dissociation energy which has already been used above as an approximation to the NC = S bond strength.

As in the case of CN^- ion formation at zero electron energy, S^- ion formation at zero electron energy is attributed to surface ionisation. The major peak, onsetting vertically at 4·2 ± 0·1eV, may be the result of one of the following reactions,

$$PF_2NCS + e \xrightarrow{38} S^- + PF_2NC$$

$$\xrightarrow{39} S^- + PF_2 + NC$$

Using the known value of E(S) = 2·1eV[59] in conjunction with D(NC = S) estimated above to be ≤ 5·1 ± 0·5eV, the minimum energy requirements of reactions 38 and 39 are calculated to be 3·0 ± 0·5 and 5·2 ± 0·6eV respectively. Reaction 38 is therefore proposed as that responsible for S^- ion formation at 4·2 ± 0·1eV. Reversing the argument and assuming the absence of excess energy in reaction 39 the NC = S bond dissociation energy is estimated to be ≤ 4·1 ± 0·2eV. There is no other value with which this may be

compared besides that of $\leq 5{\cdot}1 \pm 0{\cdot}5$eV deduced above (reaction 37).

(v) Discussion of the negative ion data

The fluorophosphines investigated were all found to exhibit low dissociative capture cross-sections, PF_2NCO being lower than the others by over an order of magnitude. As a consequence of these low cross-sections, high trap currents were employed and the resultant enhanced surface ionisation at low energies (~0eV) tolerated. Despite these difficulties useful dissociative capture data were obtained and reactions have been proposed to account for ion formation.

The 70eV mass spectra, with the exception of PF_2CN shown in Table 6.10, were simple and straightforward. Only in the case of PF_2CN was a molecular negative ion detected and only in PF_2CN was a rearrangement ion, other than F_2^-, detected. From the first observation it is concluded that $T_a(PF_2CN) > 2$ μsec. and from the appearance potential of the FCN^- ion at low energies ($4{\cdot}4 \pm 0{\cdot}1$eV) the electron affinity of the FCN radical is estimated to be $\geq 2{\cdot}8 \pm 1{\cdot}7$eV.

During the course of the positive ion study it was assumed that the PF-F bond dissociation energy in PF_2CN, PF_2NCO and PF_2NCS was approximately similar to the equivalent bond in PF_2, $4{\cdot}8 \pm 0{\cdot}7$eV, which was calculated using known thermochemical data.[23,27] The PF-F bond strengths calculated from the negative ion data justifies this assumption, the average value being 4·6eV and the average P-F bond strength, 4·4eV, comparing favourably with the value of $4{\cdot}5 \pm 1{\cdot}0$eV

reported for this bond in the literature.[18]

Because the electron affinities of the fragments resulting from dissociative electron capture are known accurately, the negative ion data can provide a more reliable estimate of the PF_2 - X bond dissociation energy. The values deduced from the positive ion work were calculated using the ionisation potential of the PF_2 radical and are therefore subject to the large uncertainties associated with the thermochemical data employed in the calculation of $D(PF_2\text{-}F) = 5{\cdot}6 \pm 1{\cdot}0$eV which was used in the estimation of $I(PF_2)$. Table 6.17 lists the PF_2-X bond dissociation energies deduced in the course of this work; those values in the first column are deduced from the positive ion data by a comparison of PF_2^+ ion formation in the three molecules and those values in the second column are estimated for the negative ion data.

Table 6.17. $D(PF_2 - X)$

Bond	Bond Dissociation Energy (eV)	
	Positive ion data	Negative ion data
PF_2-CN	$\leq 3{\cdot}6 \pm 1{\cdot}6$	$\leq 3{\cdot}1 \pm 0{\cdot}3$
PF_2-NCO	$\leq 3{\cdot}5 \pm 1{\cdot}6$	$\leq 3{\cdot}0 \pm 0{\cdot}3$
PF_2-NCS	$\leq 2{\cdot}7 \pm 1{\cdot}6$	$\leq 2{\cdot}2 \pm 0{\cdot}1$

The bond dissociation energies presented in the right hand column of Table 6.17, being accurate within the uncertainties associated with the values reported for E(CN)[4] and E(NCS),[4] are those preferred. The PF_2-NCO bond dissociation energy

was taken as being 0·1eV less than the PF_2-CN bond dissociation energy in accord with the relative appearance potentials of the PF_2^+ ions. In view of this, the electron affinity of the NCO radical, which was estimated using the value of D(PF_2-NCO) deduced from the positive ion data to be ~3·1eV, is now revised to 2·6 ± 0·4eV. There is no other value with which this may be compared.

From Figs. 6·5 and 6·9 it can be seen that most of the negative ions measured exhibit a resonance peak at or very close to the same electron energy. Following Dorman,[118] it may be suggested that this coincidence of peaks is due to the competitive dissociation of a single state of the molecular negative ions, PF_2CN^- and PF_2NCS^-. This situation may be visualised as follows:- an impinging electron with the required energy adds to the neutral molecule into a 'compound-ion' state which is able to dissociate in a number of different ways. Each of the decomposition routes to form F^-, CN^-, FCN^-, and PF_2^- from PF_2CN^{-*} and F^-, CN^-, S^- and PF_2^- from PF_2NCS^{-*} is possible but occurs with varying probability and thus all of the ions are observed close to the same electron energy, which is related[80] to the energy of the 'compound-ion' state, but with an intensity proportional to the probability of the various dissociation paths. Small displacements of some resonances on the electron energy scale, relative to the energy at which most of the fragments appear, may be explained by the population of close upper energy states of the molecular negative ion.

The $4{\cdot}6 \pm 0{\cdot}2$eV F^- ion resonance from PF_2NCO may similarly be the result of such a decomposition, in this case involving an excited state of the PF_2NCO molecular negative ion.

The bond dissociation energies, ionisation potentials and electron affinities deduced in the course of this chapter will be listed separately in Chapter 9.

CHAPTER 7

THE C_3 and C_4 PERFLUOROCARBONS

The formation and relative stability of perfluorocarbon molecular negative ions have been discussed in detail in Chapter 4. As a continuation of a systematic investigation of negative ion formation by perfluorocarbons[17,21,119] the C_3 and C_4 compounds listed in Table 7.1 have been examined.

Table 7.1. The perfluorocarbons investigated

Formula	Name
C_3F_6	perfluoropropylene
C_3F_8	perfluoropropane
C_4F_6-2	hexafluorobutyne-2
C_4F_8-2	octafluorobutene-2
n-C_4F_{10}	perfluoro-normal-butane
c-C_4F_6	perfluoro-cyclo-butene
c-C_4F_8	perfluoro-cyclo-butane
1,2-$C_4F_6(CF_3)_2$	perfluoro-1,2-dimethylcyclobutane

The negative ion mass spectra measured at 70eV are presented in section (a) and discussed in three groups; (i) C_3F_6 and C_3F_8, (ii) C_4F_6-2, C_4F_8-2 and n-C_4F_{10} and (iii) c-C_4F_6, c-C_4F_8 and 1,2-$C_4F_6(CF_3)_2$. The ionisation efficiency data and comparisons with previous investigations, when available, are given in the succeeding sections, each molecule being considered separately. The results are

generally summarised and discussed in the final section including reference to some limited data for hexafluorobutyne-2, C_4F_6-2, perfluorocyclopentene, C_5F_8 and perfluoronormalhexane, C_6F_{14}.

(a) Negative ion mass spectra

(i) C_3F_6 and C_3F_8

The negative ion mass spectra of C_3F_6 and C_3F_8 measured at 70eV are presented in Table 7.2. The F^- ion intensity has been normalised to 1000·0 in each spectrum. The outstanding feature of these spectra is the low relative intensity exhibited by the other ions to that of the F^- ion, a situation which is found for all the lower perfluorocarbons (below C_6). Reconciliation of this observation lies in the high electron affinity of the fluorine atom (3·45eV[36]) and the number of such atoms available in the molecule. In the absence of values for the relative dissociative capture cross-sections for these molecules a direct comparison between the relative ionic abundances in C_3F_6 and C_3F_8 would be unrealistic, each molecule will therefore be discussed separately and the fragmentation behaviour compared.

Perfluoropropylene, C_3F_6.

Complementary ion formation will be considered first as the relative abundance of complementary ions, reflecting the relative probability for that particular dissociative capture channel from the transient molecular negative ion intermediate state involved, should enable relative electron

TABLE 7.2. NEGATIVE ION MASS SPECTRA OF C_3F_6 AND C_3F_8 AT 70eV

m/e	ION	ABUNDANCE	
		$CF_3 \cdot CF = CF_2$	$CF_3CF_2CF_3$
12	C^-	1·1	<0·1
19	F^-	1000·0	1000·0
24	C_2^-	12·2	0·1
31	CF^-	5·2	0·2
36	C_3^-	0·2	<0·1
38	F_2^-	3·3	0·1
43	C_2F^-	12·1	0·1
50	CF_2^-	0·3	<0·1
55	C_3F^-	0·3	
62	$C_2F_2^-$	0·5	<0·1
69	CF_3^-	1·9	22·3
81	$C_2F_3^-$	1·2	<0·1
93	$C_3F_3^-$	1·2	<0·1
112	$C_3F_4^-$	0·1	
119	$C_2F_5^-$		18·6
131	$C_3F_5^-$	11·2	
150	$C_3F_6^-$	0·1*	<0·1
169	$C_3F_7^-$		0·3

* MOLECULAR NEGATIVE ION

affinities of the species to be determined and provide insight into the fragmentation paths favoured. The F^- ion and the complementary ion $C_3F_5^-$ are formed with relative abundances in the ratio 1000 to 11 at 70eV and 1000 to 66 at their respective capture maxima suggesting that E(F) > $E(C_3F_5)$, where E(F) = 3·45eV.[36]

The structure of the $C_3F_5^-$ ion is bound to be speculative, if indeed a unique structure exists. The tertiary C-F bond, located at the central carbon atom, being the weakest, is probably the most favoured candidate for rupture leaving the captured electron to reside in the vacant orbital lying in close proximity to the double bond. At low electron energies the $C_3F_5^-$ ion exhibits a narrow resonance with a sharp onset clearly suggesting formation by a specific process and consequently an ion with a well-defined structure; the formation of $C_3F_5^-$ involving the rupture of primary, secondary and the tertiary C-F bond would result in a smearing of the resonance peak, these bonds having significantly different strengths.[124] The following structure may be tentatively proposed for this ion; $CF_3\text{-}\overline{C} = CF_2$. The effect of the extra electron on the molecular orbitals, particularly in the region of the double bond, is uncertain although it is envisaged that a change in hybridisation on the central carbon atom tending towards a linear ion would take place.

The CF_3^- and $C_2F_3^-$ ions are formed in the ratio 1·9 to 1·2 suggesting an approximately equal probability for formation and equivalent electron affinities. The most probable structure of the $C_2F_3^-$ ion is that formed with retention of the

double bond, i.e. $^{-}CF = CF_2$, and is therefore the lower analogue of $C_3F_5^-$ discussed above. The electron affinity of C_2F_3 formed from C_2F_4 has been reported to be $2{\cdot}0 \pm 0{\cdot}2$eV[119] which, as predicted above, is comparable with the electron affinity of the CF_3 radical which has been reported by several workers; $1{\cdot}9 \pm 0{\cdot}1$,[4] $2{\cdot}1 \pm 0{\cdot}2$[119] and 2·0eV.[17,122]

An important feature of the C_3F_6 spectrum is the absence of ions which would have resulted from cleavage of the double bond i.e. CF_3CF^-, which was not detected, and CF_2^-, detected to only 0·03% of the F^- ion current and which might, at least in part, be formed from the terminal CF_3 group. The relatively high abundances of C_2^- and C_2F^- ions, 12·2 to 12·1, further suggests retention of the double bond, these species being observed abundantly, both in the 70eV spectrum and by dissociative electron capture in CF_2CH_2.[113] Both these species have been reported to have high electron affinities i.e. $E(C_2) = 2{\cdot}8 \pm 0{\cdot}5$,[113] $3{\cdot}1$[120] and $\geq 2{\cdot}9$eV[121] and $E(C_2F) \geq 2{\cdot}2 \pm 0{\cdot}7$[113] and $\geq 3{\cdot}3 \pm 0{\cdot}8$eV.[113]

The rearrangement ion F_2^- is formed relatively abundantly in perfluoropropylene and may originate by a rearrangement about the single C-C bond with perfluoroallene, $CF_2 = C = CF_2$, as the neutral species. The ion $C_3F_4^-$, detected to only 0·01% F^- ion intensity at 70eV, may be the complementary ion in this reaction thus suggesting that $E(C_3F_4) < E(F_2)$ where $E(F_2) = 2{\cdot}9 \pm 0{\cdot}2$eV.[65]

Perfluoronormalpropane, C_3F_8.

The most significant complementary reactions occurring in perfluoropropane are those involving C-F bond cleavage to form F^- and $C_3F_7^-$ and C-C bond cleavage forming CF_3^- and $C_2F_5^-$. At 70eV F^- and $C_3F_7^-$ are formed in the ratio 1000 to 0·3 and at their respective capture maxima in the ratio 1000 to 0·4 suggesting that $E(F) > E(C_3F_7)$ which is confirmed by values reported in the literature i.e. $E(F) = 3{\cdot}45eV$[36] and $E(C_3F_7) = 2{\cdot}0$[4] and 2·4eV.[122] A structure cannot be unequivocally assigned to the perfluoropropyl ion as the C-F bond involved in ion formation may be a primary or a secondary bond. As secondary C-F bond cleavage is favoured energetically the $C_3F_7^-$ ion is tentatively assigned the iso-structure i.e. $CF_3\text{-}\overline{C}F\text{-}CF_3$.

CF_3^- and $C_2F_5^-$ are formed in the ratio 22 to 19 at 70eV and 20 to 22 at their respective capture maxima which suggests approximately equivalent electron affinities for these radicals. This is confirmed from the following values reported in the literature; $E(CF_3) \simeq 2{\cdot}0eV$[4,17,122,119] and $E(C_2F_5) = 2{\cdot}3$[122] and 2·4eV.[17]

The differences between the spectra of perfluoropropylene and perfluoropropane are dominated by the retention of the double bond in the fragmentation behaviour of C_3F_6 and ion formation by the cleavage of successive C-C bonds in the saturated molecule, C_3F_8. The influence of the double bond is further apparent in the formation of a 'long-lived' C_3F_6 molecular negative ion but in the absence of the corresponding

C_3F_8 molecular negative ion and also in the relatively high abundance of C_2 species in the spectrum of C_3F_6.

(ii) C_4F_6-2, C_4F_8-2 and n-C_4F_{10}

The 70eV mass spectra of the C_4 perfluorocarbons investigated are shown in Table 7.3. They have all been normalised to an F^- ion abundance of 1000·0 although absolute ion abundance comparisons between the molecules cannot be made, as explained above.

The effect of unsaturation on ion formation i.e. the retention of multiple bonds in the fragmentation products, which was noted for C_3F_6 is also observed in these spectra. This is particularly evident in the absence of a $CF_3C^-(C_2F_3^-)$ ion from C_4F_6-2 which would result from rupture of the triple bond and electron capture, similarly a $CF_3CF^-(C_2F_4^-)$ ion was not detected from C_4F_8-2. However, a relatively high intensity $C_2F_5^-$ ion was formed from n-C_4F_{10} i.e. F^- to $C_2F_5^-$ is 1000 to 114 at 70eV, the analogous bond ruptured in this case being a saturated C-C bond.

A consideration of complementary reactions in hexafluorobutyne-2 leads to the conclusion that $E(F) > E(C_4F_5)$ and that $E(C_3F_3) > E(CF_3)$ where $E(F) = 3{\cdot}45eV$[36] and $E(CF_3) \simeq 2{\cdot}0eV$[4,17,119,122]. Similarly the results from octafluorobutene-2 suggests that $E(F) > E(C_4F_7)$ and that $E(CF_3) > E(C_3F_5)$ and for perfluoronormalbutane $E(F) > E(C_4F_9)$ and $E(C_3F_7) \simeq E(CF_3)$; $E(C_3F_7)$ has been reported to be $2{\cdot}0^4$ and $2{\cdot}4eV$.[122]

As in the case of the $C_3F_7^-$ ion formed from C_3F_8 the

TABLE 7.3 NEGATIVE ION MASS SPECTRA OF SOME C_4 PERFLUOROCARBONS AT 70eV

m/e	ION	ABUNDANCE					
		C_4F_6-2 —≡—	C_4F_8-2	n.C_4F_{10} 	c-C_4F_6 	c-C_4F_8	$C_4F_6(CF_3)_2$
12	C^-	0·3	0·6	<0·1	1·6	0·7	<0·1
19	F^-	1000·0	1000·0	1000·0	1000·0	1000·0	1000·0
24	C_2^-	6·6	24·3	0·9	26·1	3·1	4·3
31	CF^-	0·2	3·7	1·1	4·1	4·8	2·2
36	C_3^-	0·7	1·3	<0·1	3·2	1·0	1·2
38	F_2^-	1·0	3·2	0·7	1·6	2·0	2·5
43	C_2F^-	2·1	33·5	2·1	25·5	10·7	15·2
48	C_4^-		0·1				0·9
50	CF_2^-	0·7	0·3	0·7	0·6	3·6	1·2
55	C_3F^-		1·5	<0·1	3·5	0·7	3·1
62	$C_2F_2^-$		1·1	0·3	0·8	0·6	2·1
67	C_4F^-						1·2
69	CF_3^-	11·5	6·5	11·5	2·2	7·6	11·7
74	$C_3F_2^-$	3·5	0·8		1·5	0·4	5·6
81	$C_2F_3^-$		0·5	0·3	1·2	1·4	3·3
86	$C_4F_2^-$	0·1	0·1			0·4	0·6
93	$C_3F_3^-$	962·5	4·2	<0·1	51·1	0·6	11·7
100	$C_2F_4^-$						0·3
105	$C_4F_3^-$						0·3
119	$C_2F_5^-$			113·7			2·8
124	$C_4F_4^-$	0·1					
131	$C_3F_5^-$		2·0	<0·1		1·4	4·9
143	$C_4F_5^-$	3·1	0·9		5·2		2·8
150	$C_3F_6^-$			<0·1			
162	$C_4F_6^-$	97·3*	0·9		20·5*		
169	$C_3F_7^-$			8·5			
181	$C_4F_7^-$		0·1			<0·1	37·7
193	$C_5F_7^-$						2·2
200	$C_4F_8^-$		560·0*	0·2		12·4*	
219	$C_4F_9^-$			1·3			
231	$C_5F_9^-$						46·4
238	$C_4F_{10}^-$			<0·1*			
262	$C_6F_{10}^-$						0·6
281	$C_6F_{11}^-$						50·1
300	$C_6F_{12}^-$						3095·0*

* MOLECULAR NEGATIVE ION

$C_4F_9^-$ ion probably has the iso-structure resulting from the rupture of a secondary C-F bond, the energetically favoured process. C_2^- ion formation in C_4F_6-2 and C_2^-, C_2F^- and $C_2F_2^-$ ion formation in C_4F_8-2 lend further support to the preferential retention of multiple bonds.

The relatively high abundance of the F_2^- ion from C_4F_8-2 is interesting in light of F_2^- ion formation in C_3F_6. Following the same argument it is proposed that a terminal CF_3 group and the adjacent tertiary fluorine atom is involved in the intramolecular rearrangement leaving the stable diene species $CF_2 = C = CF\text{-}CF_3$. The $C_4F_6^-$ ion detected in the C_4F_8-2 spectrum may therefore be this diene negative ion. It is not unexpected that this ion is stable in view of the observation that both c-C_4F_6 and C_4F_6-2 form parent ions.

(iii) <u>c-C_4F_6, c-C_4F_8 and 1,2-$C_4F_6(CF_3)_2$</u>

The most surprising feature of these spectra is the appearance of the CF_3^- ion in the spectra of c-C_4F_6 and c-C_4F_8 and also the complementary ions $C_3F_3^-$ and $C_3F_5^-$ respectively. The CF_3^- ion has been previously reported by Reese, Dibeler and Mohler[126] and by Bibby and Carter.[125] Rearrangement ions are also prevalent in the spectrum of $C_4F_6(CF_3)_2$ i.e., $C_2F_5^-$ and the complementary species $C_4F_7^-$. Pressure dependence measurements at the resonance capture peaks of these ions indicated formation by a primary process therefore involving ring cleavage (release of ring stain) and intramolecular rearrangement. The following reaction schemes are therefore proposed to account for CF_3^- and $C_2F_5^-$ ion formation;

CF_3^- from c-C_4F_6

$$c\text{-}C_4F_6 + e \xrightarrow{1} CF_3^- + C_3F_3$$

where the C_3F_3 radical may have the following structure subsequent to further rearrangement; $CF_2{=}C{=}CF$

CF_3^- from c-C_4F_8

$$c\text{-}C_4F_8 + e \xrightarrow{2} CF_3^- + C_3F_5$$

where the C_3F_5 radical may have one of several structures e.g. $CF_3\dot{C}CF_2$, $CF_2{=}CF{-}\dot{C}F_2$ or $CF_3CF{=}\dot{C}F$.

$C_2F_5^-$ from $C_4F_6(CF_3)_2$

$$C_4F_6(CF_3)_2 + e \xrightarrow{3} C_2F_5^- + C_4F_7$$

again several canonical forms may be written for the C_4F_7 radical; $CF_3.CF_2\dot{C}{=}CF_2$, $CF_3CF{=}CF.\dot{C}F_2$, $CF_3CF{=}\dot{C}.CF_3$ and so on.

Similarly the same reactions may be written to represent the formation of the complementary ions $C_3F_3^-$, $C_3F_5^-$ and $C_4F_7^-$ respectively. All of these ions were detected at low electron energies and comparisons of electron affinities, estimated on the assumption that the complementary reactions proposed above take place, with values derived for the same radicals formed in simple dissociative capture reactions lend support to these proposals.

The following limits are suggested for the electron affinities of the complementary rearrangement ions discussed above; $E(C_3F_3) > E(CF_3)$ from reaction 1, $E(CF_3) > E(C_3F_5)$ from reaction 2 and $E(C_4F_7) > E(C_2F_5)$ from reaction 3 where

$E(CF_3)$ = 2·0eV,[4,17,119,122] $E(C_2F_5)$ = 2·3,[122] 2·4eV[17] and from the C_3F_6 and C_4F_8-2 spectra $E(C_3F_3) > E(CF_3)$ and $E(CF_3) > E(C_3F_5)$ respectively, in agreement with the above conclusions.

In $C_4F_6(CF_3)_2$ the most abundant ion was the molecular negative ion, $C_6F_{12}^-$. The fragment ions expected from the removal of a CF_3 substituent group, CF_3^- and the complementary ion $C_5F_9^-$, are both present although surprisingly no $C_4F_6^-$ ion (which would be formed by the loss of two CF_3 groups) was detected. The relative abundances of the CF_3^- and $C_5F_9^-$ ions are in the ratio 12 to 46 at 70eV and 2:100 at their respective capture maxima suggesting that $E(C_5F_9) > E(CF_3)$.

A comparison of the F^- ion and $(parent-F)^-$ ion currents in these perfluorocyclic compounds suggests that $E(C_4F_5)$, $E(C_4F_7)$ and $E(C_6F_{11}) < E(F)$ where these fluorocarbon species may be cyclic or linear.

In conclusion three distinct types of spectra may be identified;

(i) the spectra of the saturated linear perfluorocarbons, where fragmentation is dominated by successive C-C bond cleavage, the abundances of the possible alkyl ion fragments being determined by their relative electron affinities,

(ii) the spectra of the unsaturated linear perfluorocarbons where the successive splitting of carbon-carbon bonds is terminated at the multiple bond, these spectra showing an abundance of ions containing the multiple bond unit,

(iii) the spectra of saturated and unsaturated cyclic perfluorocarbons are similar in that they both exhibit

relatively high intensity rearrangement ions, involving opening of the ring and fluorine atom transfer. Retention of the double bond as in the unsaturated linear perfluorocarbons is also prevalent in the fragments produced from c-C_4F_6.

(b) Perfluoropropylene, C_3F_6.

The cross-section for dissociative electron capture in C_3F_6 (as represented by total ion current) was found to be over an order of magnitude less than in C_3F_8 under comparable ion source conditions. Consequently, of the ions detected at low electron energies, F^-, CF_3^-, $C_3F_3^-$ and $C_3F_5^-$, which were formed in the ratio 1000:5:17:66 at their respective capture maxima, only the F^- and $C_3F_5^-$ ions were formed with cross-sections amenable to a detailed investigation. Typical experimental data are shown in Figs. 7.1(a) and 7.2(a) and the deconvoluted curves in Figs. 7.1(b) and 7.2(b). The energy scale is calibrated against the appearance potentials of the O^- ion formed from SO_2 at 4·2 and 6·6eV.

In a previous investigation of ion formation in C_3F_6, Bibby and Carter[124] reported F^- ion formation with an appearance potential of 1·9 ± 0·1eV. The experimental ionisation efficiency curve shown in Bibby's thesis for this ion is in close agreement with that shown in Figs. 7.1(a) and 7.2(a) and the peak maxima, as taken from Bibby's curve; 3·5, 7·2, 12·0 and 14·0eV, are in good agreement with the values found in this study, namely, 3·3, 6·9, 12·1 and ~14·5eV.

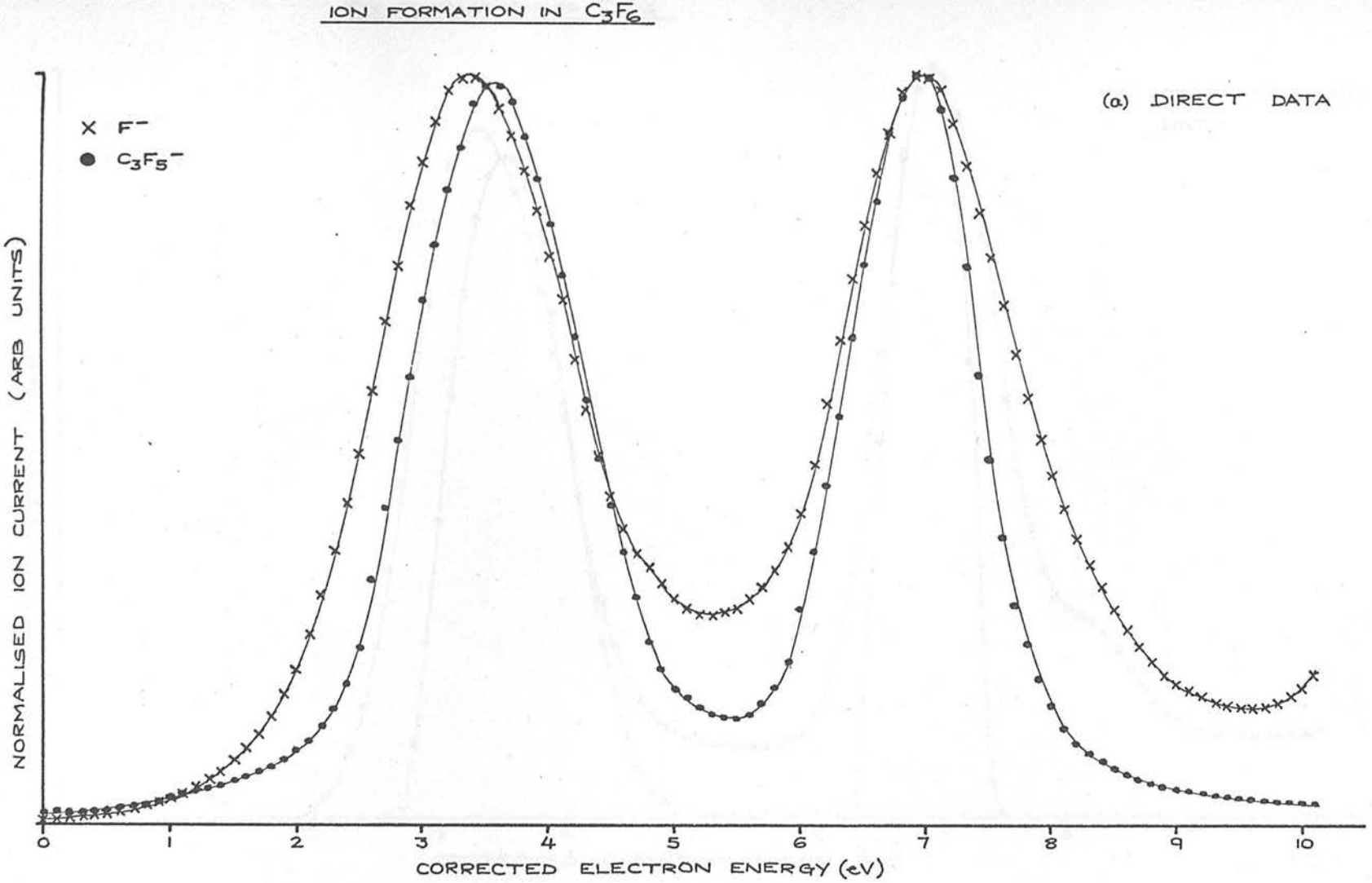
ION FORMATION IN C_3F_6
(a) DIRECT DATA
× F^-
● $C_3F_5^-$
NORMALISED ION CURRENT (ARB UNITS)
0
1
2
3
4
5
6
7
8
9
10
CORRECTED ELECTRON ENERGY (eV)

Fig 7.1

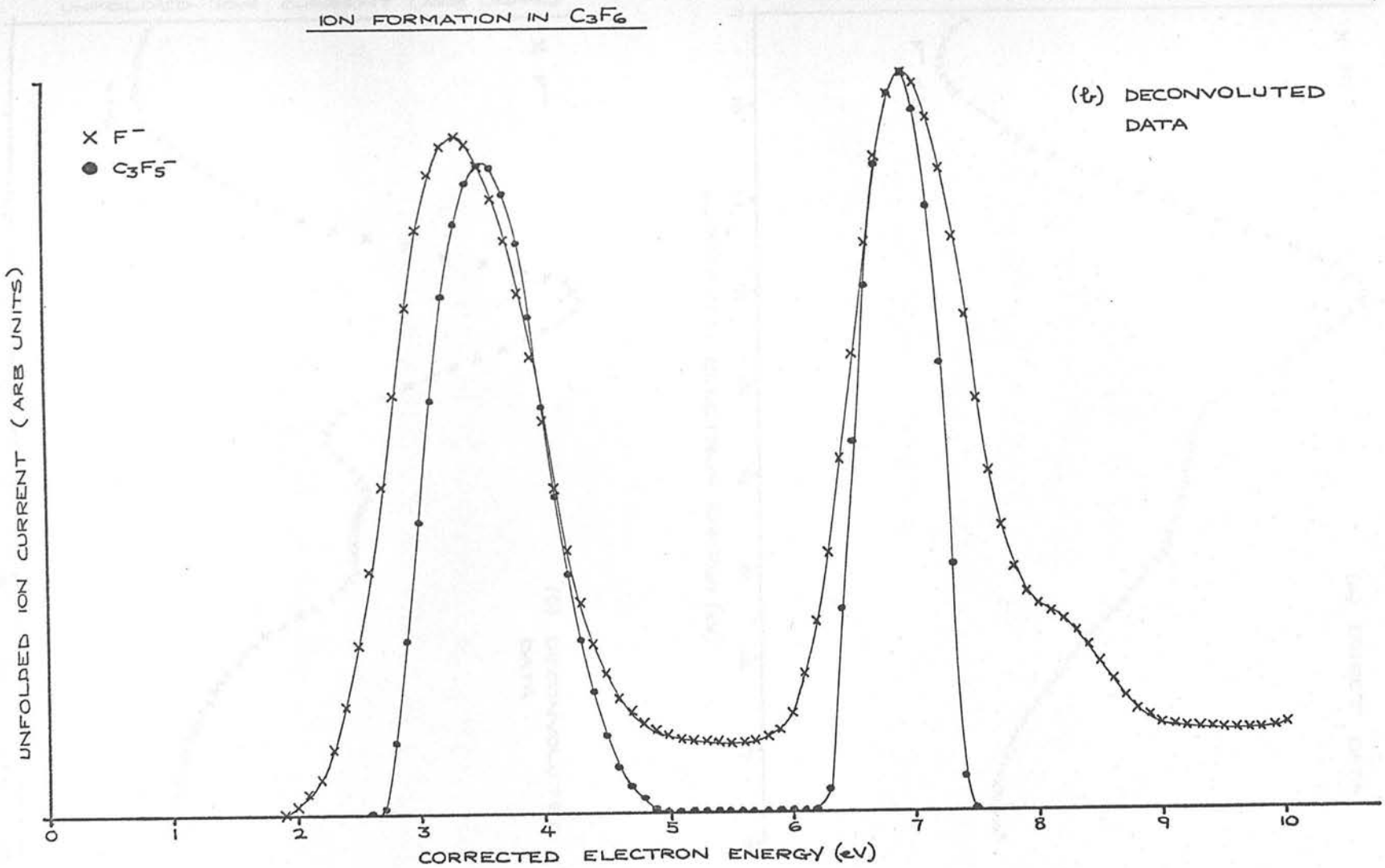
ION FORMATION IN C_3F_6
(b) DECONVOLUTED DATA
× F^-
● $C_3F_5^-$
UNFOLDED ION CURRENT (ARB UNITS)
0
1
2
3
4
5
6
7
8
9
10
CORRECTED ELECTRON ENERGY (eV)

Fig 7.1

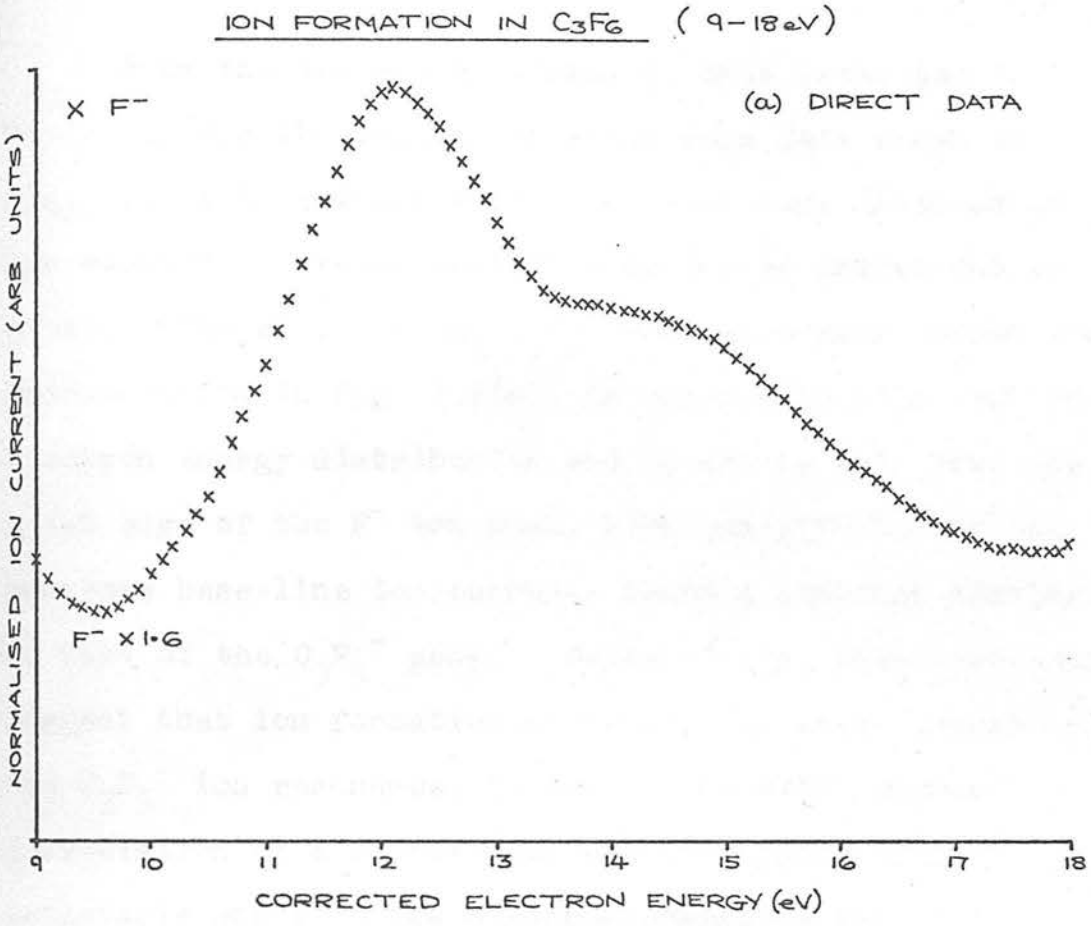
ION FORMATION IN C_3F_6 (9 – 18 eV)
X F^-
(a) DIRECT DATA
NORMALISED ION CURRENT (ARB UNITS)
F^- X 1·6
9
10
11
12
13
14
15
16
17
18
CORRECTED ELECTRON ENERGY (eV)

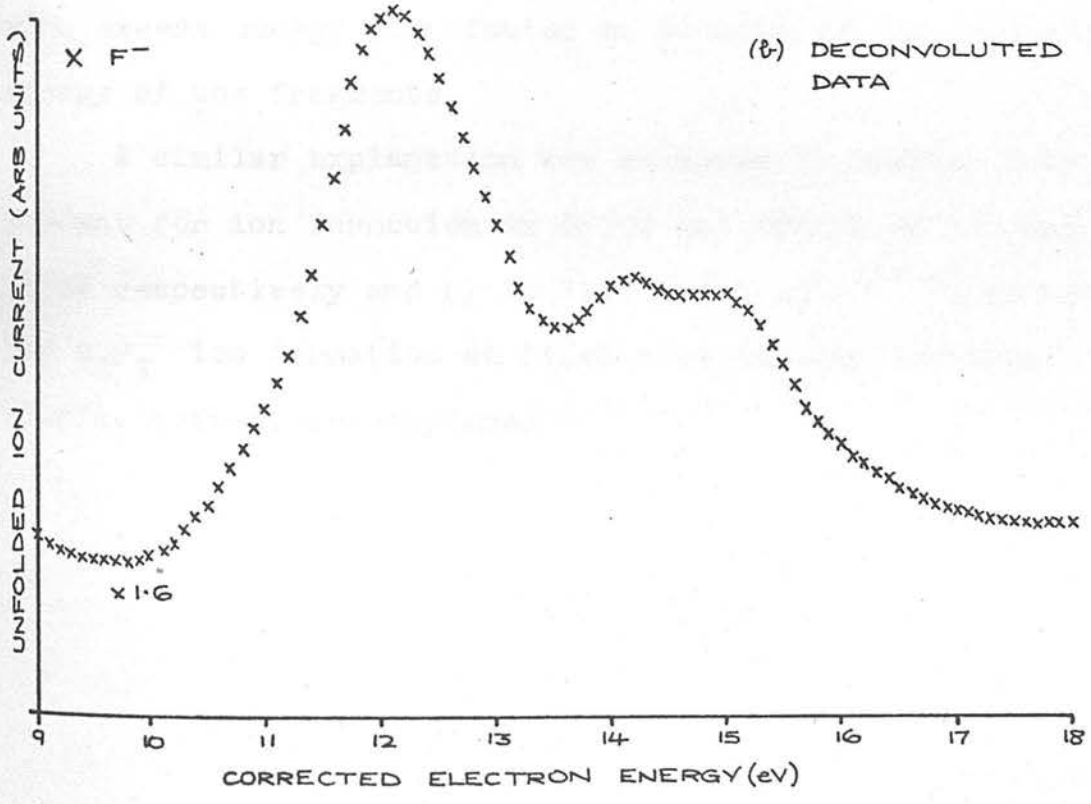
X F^-
(b) DECONVOLUTED DATA
UNFOLDED ION CURRENT (ARB UNITS)
X 1·6
9
10
11
12
13
14
15
16
17
18
CORRECTED ELECTRON ENERGY (eV)

Fig 7.2

From the appearance potential data presented in Table 7.4 and the ionisation efficiency data shown in Fig. 7.1 it is evident that all of the ions observed at low electron energies exhibit a resonance maximising at 6·9eV. The width of the $C_3F_5^-$ resonance peak, shown after deconvolution in Fig. 7.1(b), is comparable with that of the electron energy distribution and it can be seen that the onset edge of the F^- ion peak, although affected by the non-zero base-line ion current, bears a distinct similarity to that of the $C_3F_5^-$ peak. Collectively, these observations suggest that ion formation at 6·2eV, the onset energy of the $C_3F_5^-$ ion resonance, is due to the multi-channel dissociation of a short-lived electronically excited metastable state of the molecular negative ion;

$$C_3F_6 + e_{6\cdot2eV} \xrightarrow{4} C_3F_6^{-*} \longrightarrow F^-,\ CF_3^-,\ C_3F_3^-\ \&\ C_3F_5^-.$$

with excess energy distributed as kinetic and/or excitation energy of the fragments.

A similar explanation was advanced in Chapter 6 to account for ion formation in PF_2CN and PF_2NCS at 4·6 and 4·2eV respectively and by MacNeil and Thynne[119] to account for $C_2F_3^-$ ion formation at 6·4eV from another perfluoro-olefin, tetrafluoroethylene.

Table 7.4. Appearance potential data for C_3F_6

Ion	Appearance Potential(eV)	Peak Maximum(eV)	Peak Width at ½-height(eV)
F^-	1·9 ± 0·1	3·3 ± 0·1	1·4 ± 0·1
	5·7 ± 0·2	6·9 ± 0·1	1·1 ± 0·1
	7·8 ± 0·2	shoulder	-
	9·8 ± 0·3	12·1 ± 0·2	~2
	13·6 ± 0·3	~14·5	-
$C_3F_5^-$	2·65 ± 0·1	3·55 ± 0·1	0·9 ± 0·1
	6·2 ± 0·1	6·9 ± 0·1	0·7 ± 0·1
CF_3^-	~6	6·9	-
$C_3F_3^-$	4·7 ± 0·2	5·7 ± 0·2	1·4 ± 0·2
	shoulder	6·9 ± 0·2	-

Assuming that the initial appearance potential for F^- ion formation, 1·9 ± 0·1eV, corresponds to the reaction,

$$C_3F_6 + e \xrightarrow{5} F^- + C_3F_5$$

then, using E(F) = 3·45eV,[36] a value of ≤ 5·35 ± 0·1eV may be estimated for the C_3F_5-F bond dissociation energy. This may be compared with other C-F bond dissociation energies reported in the literature i.e. $D(C_2F_3\text{-}F) \leq 5{\cdot}25 \pm 0{\cdot}1$eV,[119] $D(C_2F_5\text{-}F) \leq 5{\cdot}2$eV[17] and $D(CF_3\text{-}F) = 5{\cdot}3$eV.[130] Using this value in conjunction with known thermochemical data,[127,129] the heat of formation of the C_3F_5 radical may be estimated to be ≤ -6·8 ± 0·2eV. This species was tentatively assigned the structure $CF_3\text{-}C{=}CF_2$ in section (a).

Although five specific appearance potentials for F^- ion formation have been listed in Table 7.4 it is evident from Figs. 7.1 and 7.2 that ion formation is occurring extensively throughout the energy range above the first appearance potential at 1·9 ± 0·1eV. Because of this, and the generally poor quality of the thermochemical data available for fragment species, it is difficult to assign specific processes to each of these peaks, however, the minimum enthalpy requirements for some of the possible F^- ion forming reactions have been estimated below:

	ΔH_{min}(eV)
$C_3F_6 + e \xrightarrow{6} F^- + CF_3 + CFCF$	1·6, 3·8
$\xrightarrow{7} F^- + CF_3 + CCF_2$	-
$\xrightarrow{8} F^- + CF_2 + CFCF_2$	4·9
$\xrightarrow{9} F^- + CF_3CF + CF$	6·4
$\xrightarrow{10} F^- + F + CF_3 + C_2F$	7·5
$\xrightarrow{11} F^- + CF + 2CF_2$	7·6
$\xrightarrow{12} F^- + 2CF + CF_3$	8·8
$\xrightarrow{13} F^- + F_2 + C_2F + CF_2$	9·8
$\xrightarrow{14} F^- + 2F + C_2F + CF_2$	11·4
$\xrightarrow{15} F^- + F + 2CF + CF_2$	12·7

These minimum enthalpy values are subject to appreciable uncertainty, in some cases > 0·5eV. The two values shown for reaction 5 are those calculated using the two values reported for $\Delta H_f(FC_2F)$ i.e. -2·2 ± 0·7[27] and ~0eV[129] respectively. The latter and more recent value is preferred. Thermochemical data suggest that $D(CF_3CF{=}CF_2)$~2·8eV, so

reactions involving cleavage of this bond are to be expected and have been included in the above list i.e. reactions 9, 11, 12 and 15. Evidence from the mass spectrum, however, was clearly in favour of the retention of the double bond following fragmentation thus suggesting that $D(CF_3CF{=}CF_2) > D(CF_3\text{-}CFCF_2)$, where this latter bond is calculated to be 4·4eV from thermochemical data.

Fig. 7.1(b) shows that the first F^- ion peak onsetting at 1·9 ± 0·1eV is broader than the other peaks and it is suggested that reaction 6 contributes to the trailing edge of this resonance. The resonance onsetting at 5·7 ± 0·2eV has been discussed above in relation to the decomposition of a metastable state of the molecular negative ion. The actual process involved, however, cannot be unequivocally identified although reaction 9, with a minimum enthalpy requirement of 6·4eV, and reaction 5, involving translational energy and/or internal excitation of the C_3F_5 radical and which is the complementary reaction to that resulting in $C_3F_5^-$ ion formation by this mechanism, are favoured. The low intensity resonance seen on the trailing edge of this peak (Fig. 7.1(b)), with an appearance potential at 7·8 ± 0·2eV, may correspond to reactions 10 or 11 and any or all of reactions 13, 14 and 15 may be responsible for the onset at 9·8 ± 0·3eV and at higher energies respectively.

Although this method of process assignment is inevitably speculative it remains the most useful approach in the absence of more accurate thermochemical data.

Two dissociative capture processes are noted for $C_3F_5^-$ ion formation; the process at 6·2eV has been discussed above in relation to decomposition of a short-lived state of the molecular negative ion, i.e.

$$C_3F_6 + e_{6\cdot2eV} \xrightarrow{4} C_3F_6^{-*} \xrightarrow{16} C_3F_5^{-*} + F^*$$

where the excess energy is distributed as internal excitation of the $C_3F_5^-$ ion and/or translational energy of both fragments.

Ion formation at 2·65 ± 0·1eV must be the result of the following reaction,

$$C_3F_6 + e \xrightarrow{17} C_3F_5^- + F$$

Assuming the absence of excess energy in reactions 5 and 17 then, $A(F^-) + E(F) = A(C_3F_5^-) + E(C_3F_5)$. Using the reported value of 3·45eV[36] for E(F) the electron affinity of the C_3F_5 radical is estimated to be 2·7 ± 0·2eV. There is no other value with which this may be compared.

The CF_3^- ion intensity was too low to facilitate a detailed investigation; the maximum ion current was recorded at 6·9eV with an estimated appearance potential of approximately 6eV. Reactions 18 or 19 may be expected to be responsible for CF_3^- ion formation at this energy

$$C_3F_6 + e_{6\cdot3eV} \xrightarrow{4} C_3F_6^{-*} \xrightarrow{18} CF_3^- + CF + CF_2$$
$$\xrightarrow{19} CF_3^- + F + CCF_2$$

Assuming $E(CF_3) = 2\cdot0eV$[4,17,119,122] reaction 18 has minimum enthalpy requirements of 5·1eV. The energy requirements of Reaction 19, involving retention of the double bond,

cannot be estimated in the absence of a value for $\Delta H_f(CCF_2)$. If it is now assumed, in the light of the 70eV evidence, that reaction 19, involving retention of the double bond, is the favoured reaction path then, using $6{\cdot}2 \pm 0{\cdot}1$eV as the minimum energy requirement of reaction 19, a value of $\leq +1{\cdot}0 \pm 0{\cdot}3$eV is estimated for $\Delta H_f(CCF_2)$ which may be compared to the following values:

$\Delta H_f(C_2F) = 2{\cdot}86 \pm 0{\cdot}43$,[131] $\Delta H_f(FC_2F) = \sim 0$eV[128] and $-2{\cdot}2 \pm 0{\cdot}7$eV,[27] and $\Delta H_f(HC_2F) = 0 \pm 0{\cdot}5$eV.[113]

Two appearance potentials were noted for the $C_3F_3^-$ ion, the principal peak appearing at $4{\cdot}7 \pm 0{\cdot}2$eV; the second process could be seen as a low intensity resonance on the trailing edge of the first peak and was attributed to the decomposition of the metastable molecular negative ion mentioned above,

$$C_3F_6 + e_{6{\cdot}2eV} \xrightarrow{4} C_3F_6^{-*} \xrightarrow{20} C_3F_3^- + 3F \text{ (or } F_2 + F)$$

There are insufficient thermochemical data to enable calculations to be made for the initial appearance potential of this ion which, at 4·7eV, is probably formed by reaction 20 involving F atom or molecular F_2 formation and less excess energy than at 6·2eV.

(c) Perfluoronormalpropane, C_3F_8

At low electron energies the following ions were observed to be formed by dissociative capture processes; F^-, F_2^-, CF_3^-, $C_2F_5^-$ and $C_3F_7^-$ in the ratio 1000:0·1:19·8:22·5:0·4

at their respective capture maxima. Typical experimental ionisation efficiency curves for these ions, with the exception of F_2^-, are shown in Fig. 7.3(a) and the deconvoluted curves in Fig. 7.3(b). The energy scale was calibrated against the appearance potentials of the O^- ion formed from SO_2 at 4·2 and 6·6eV and the SF_6^- ion from SF_6 at 0·0eV.

There have been three previous negative ion studies of perfluoropropane[122,124,132] although, of these, only Lifshitz and Grajower[122] have previously observed $C_3F_7^-$; F_2^- has not been reported previously. The appearance potential data measured in this study are compared to the values reported from previous investigations in Table 7.5.

Table 7.5. Comparison of appearance potential data for C_3F_8.

Ion	Appearance Potential (eV)			
	This study	Greenhaus[132]	Bibby[124]	Lifshitz[122]
F^-	1·8 ± 0·1	1·63 ± 0·09	1·7 ± 0·1	1·35 ± 0·1
F_2^-	2·2 ± 0·2	-	-	-
CF_3^-	2·25 ± 0·1	2·07 ± 0·09	2·5 ± 0·1	2·0 ± 0·1
$C_2F_5^-$	2·45 ± 0·1	1·99 ± 0·09	2·2 ± 0·1	1·7 ± 0·1
$C_3F_7^-$	2·9 ± 0·1	-	-	2·4 ± 0·1

In general the agreement is not particularly good, especially with the results of Lifshitz and Grajower.[122] Examination of their data, particularly for the appearance potential of the F^- ion which was obtained by drawing a linear section through a semi-logarithmic plot of the onset

ION FORMATION IN C_3F_8

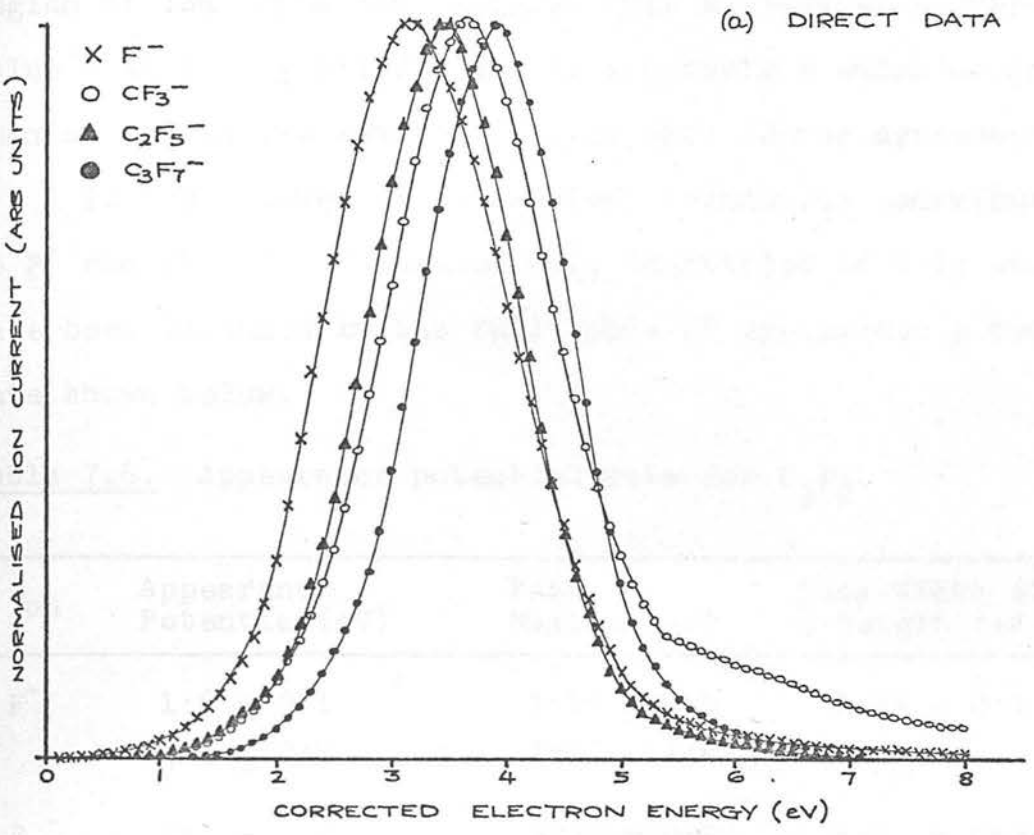

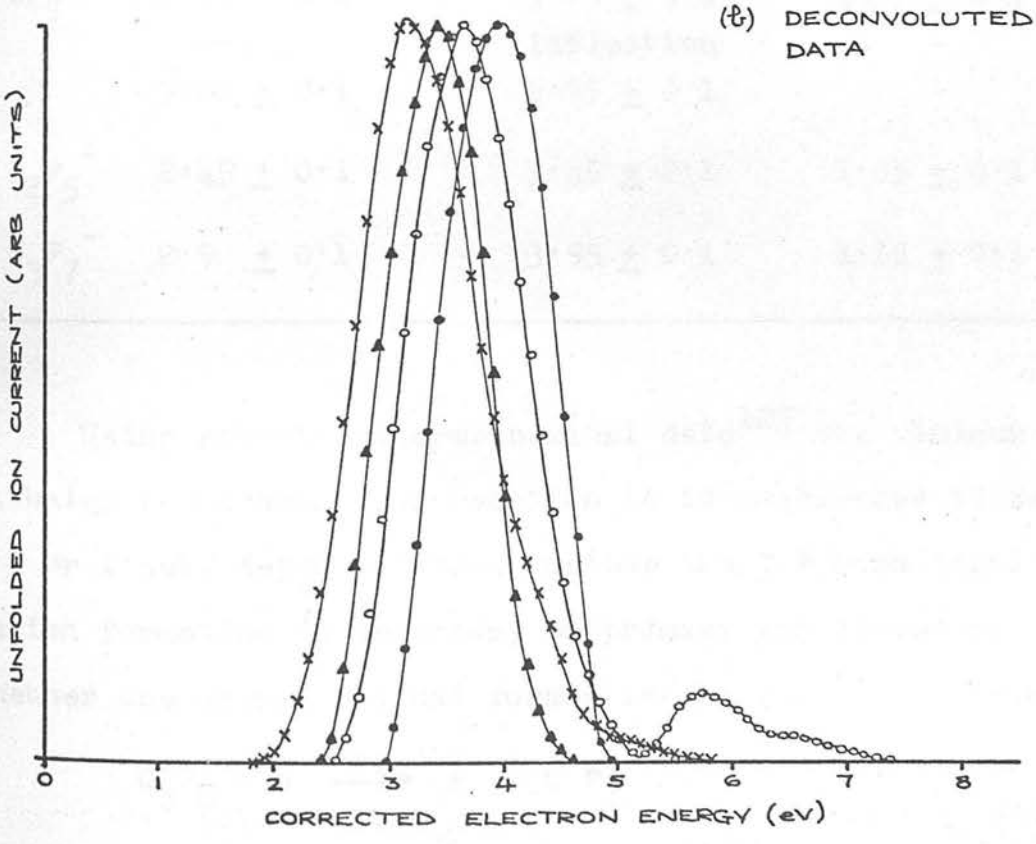

Fig 7.3

region of ion formation, suggest that a somewhat higher value than 1·35 ± 0·1eV might be appropriate which would then bring the two sets of results into better agreement.

Further, lower cross-section, resonances contributing to F^- and CF_3^- ion formation were identified in this study and have been included in the full table of appearance potential data shown below.

Table 7.6. Appearance potential data for C_3F_8.

Ion	Appearance Potential(eV)	Peak Maximum(eV)	Peak Width at ½-height (eV)
F^-	1·8 ± 0·1	3·15 ± 0·1	1·25 ± 0·1
	4·0 ± 0·2	inflection	-
F_2^-	2·2 ± 0·2	3·35 ± 0·2	1·6 ± 0·2
CF_3^-	2·55 ± 0·1	3·65 ± 0·1	1·25 ± 0·1
	~4·5	inflection	-
	5·25 ± 0·1	5·75 ± 0·1	-
$C_2F_5^-$	2·45 ± 0·1	3·45 ± 0·1	1·05 ± 0·1
$C_3F_7^-$	2·9 ± 0·1	3·95 ± 0·1	1·15 ± 0·1

Using reported thermochemical data[127] the minimum enthalpy requirement for reaction 21 is calculated to be 1·3 or 1·9eV, depending upon whether the C-F bond involved in ion formation is secondary or primary and therefore whether the propyl radical formed is the iso- or normal-variety.

$$C_3F_8 + e \xrightarrow{21} F^- + C_3F_7$$

As the C_3F_7 fragment cannot be identified as being of either structure and no break in the ionisation efficiency curve was observed, which might suggest that both fragments may be formed at different electron energies, the following relationship; $D(F\text{-}C_3F_7) \leq A(F^-) + E(F)$, where $E(F) = 3{\cdot}45eV$,[36] may be used to estimate an upper limit of $5{\cdot}25 \pm 0{\cdot}1eV$ for the C_3F_7-F bond dissociation energy. This value compares favourably with other C-F bond dissociation energies which usually lie in the range $5{\cdot}0$ - $5{\cdot}4eV$ e.g. $D(F - C_3F_5) \leq 5{\cdot}35 \pm 0{\cdot}1$ (above) and $D(F - C_2F_3) \leq 5{\cdot}25 \pm 0{\cdot}1eV$.[119]

From Fig. 7.3(b) it is apparent that a second process onsetting at $4{\cdot}0 \pm 0{\cdot}2eV$ is appearing as an inflection on the trailing edge of the F^- resonance peak. Reactions 22 and 23, which have minimum enthalpy requirements of $4{\cdot}2$ and $4{\cdot}7eV$ respectively, may account for the ion current observed in this energy range.

$$C_3F_8 + e \xrightarrow{22} F^- + CF_2 + C_2F_5$$
$$\xrightarrow{23} F^- + F + C_3F_6$$

CF_3^- ion formation appears initially at $2{\cdot}55 \pm 0{\cdot}1eV$ with a second low cross-section resonance onsetting at $5{\cdot}25 \pm 0{\cdot}1$. The main peak is found to be asymmetric and the deconvoluted runs indicated an inflection on the trailing edge of this peak at $\sim 4{\cdot}5eV$.

$$C_3F_8 + e \xrightarrow{24} CF_3^- + C_2F_5$$
$$\xrightarrow{25} CF_3^- + CF_2 + CF_3$$
$$\xrightarrow{26} CF_3^- + F + C_2F_4$$

Reactions 24, 25 and 26, which have minimum enthalpy requirements of 1·7, 4·5 and 5·3eV respectively, are proposed to account for the CF_3^- ion formation observed. The enthalpy requirement for reaction 24 has been calculated on the assumption that the strength of the C-C bond broken in the process is 3·7eV, the same as the equivalent bond in C_3H_8.[133] Assuming that 2·55 ± 0·1eV is the minimum energy requirement for reaction 24, and taking the electron affinity of the CF_3 radical to be 2·0 ± 0·1eV,[4,17,119] the CF_3-C_2F_5 bond dissociation energy is estimated to be ≤ 4·55 ± 0·2eV. Although this value appears to be unreasonably high compared with the hydrocarbon it compares favourably with the CF_3-C_2F_3 bond dissociation energy which is calculated to be 4·4eV from thermochemical data. Reconciliation of a lower value for $D(CF_3\text{-}C_2F_5)$ with the observed data would involve the assignation of excess energy to reaction 24.

If $C_2F_5^-$ ion formation at 2·45 ± 0·1eV occurs by reaction 27, the complementary process to reaction 24,

$$C_3F_8 + e \xrightarrow{27} C_2F_5^- + CF_3$$

then, $A(CF_3^-) + E(CF_3) = A(C_2F_5^-) + E(C_2F_5)$ and a value of 2·1 ± 0·2eV may be deduced for $E(C_2F_5)$. As this value compares favourably with others reported in the literature i.e. 1·8 ± 0·2,[124] 1·95 ± 0·2,[124] 2·3[122] and 2·4eV,[17] it is suggested that either (i) reactions 24 and 27 proceed without excess energy, in which case $D(C_2F_5 - CF_3) \leq 4·55 \pm$ 0·2eV or (ii) both reactions involve approximately the same

amount of excess energy. In either case the electron affinity of the pentafluoroethyl radical so estimated is expected to be accurate to within the uncertainty shown.

The $C_3F_7^-$ ion, detected previously only by Lifshitz and Grajower,[122] was formed with a very low cross-section. Data for this ion are shown in Fig. 7.3 and a value of $2{\cdot}9 \pm 0{\cdot}1$eV measured for the appearance potential.

$$C_3F_8 + e \xrightarrow{28} C_3F_7^- + F$$

From reactions 21 and 28 and assuming no excess energy involvement the electron affinity of the heptafluoropropyl radical is calculated to be $2{\cdot}35 \pm 0{\cdot}2$eV. This may be compared with previously reported values of $2{\cdot}0^4$ and ~$2{\cdot}4$eV.[122]

F_2^- ion formation occurred with a very low cross-section. Measurements at the resonance peak maximum showed a linear dependence of ion current on source pressure indicating that ion formation occurs as the result of an intramolecular rearrangement process such as in reactions 29 and 30,

$$C_3F_8 + e \xrightarrow{29} F_2^- + C_3F_6$$
$$\xrightarrow{30} F_2^- + (CF_3)_2C$$

The first of these processes involves adjacent carbon atoms and the second involves only the secondary C-F bonds and results in the formation of the $(CF_3)_2C$ diradical.

Using known thermochemical data,[127] reconciliation of

reaction 29 with the F_2^- appearance potential at 2·2 ± 0·2eV would require that $E(F_2) \geq 4{\cdot}3 \pm 0{\cdot}2$eV. This value is inconsistent with values reported in the literature i.e. 2·9 ± 0·2[65] and ≥ 2·8 ± 0·3eV[55] and it is suggested that reaction 29 does not contribute to ion formation. In the absence of thermochemical data for $(CF_3)_2C$, calculations for reaction 30 cannot be undertaken but this process is tentatively proposed to account for the ion formation observed.

(d) Octafluorobutene-2, C_4F_8.

Octafluorobutene-2 was found to be a prolific source of negative ions at low electron energies and the following ions were detected and measured; F^-, F_2^-, CF_3^-, $C_3F_3^-$, $C_3F_5^-$, $C_4F_7^-$ and $C_4F_8^-$ formed in the ratio 1000:1:9:6:21:6:26 at their respective capture maxima. Typical experimental and deconvoluted ionisation efficiency data are shown in Fig. 7.4 and 7.5 where the energy scales are calibrated against the appearance potential of the SF_6^- ion from SF_6 at 0·0eV and the O^- ion from SO_2 at 4·2 and 6·6eV respectively.

It can be seen from Fig. 7.5 that all ions, with the exception of $C_4F_7^-$ which may have been formed with a cross-section below that amenable to detection, exhibit coincident resonances onsetting at 4·0 ± 0·2, 7·8 ± 0·2 and possibly at 9·8 ± 0·2eV. This is consistent with the formation and subsequent multi-channel dissociation of metastable molecular negative ion states at these energies;

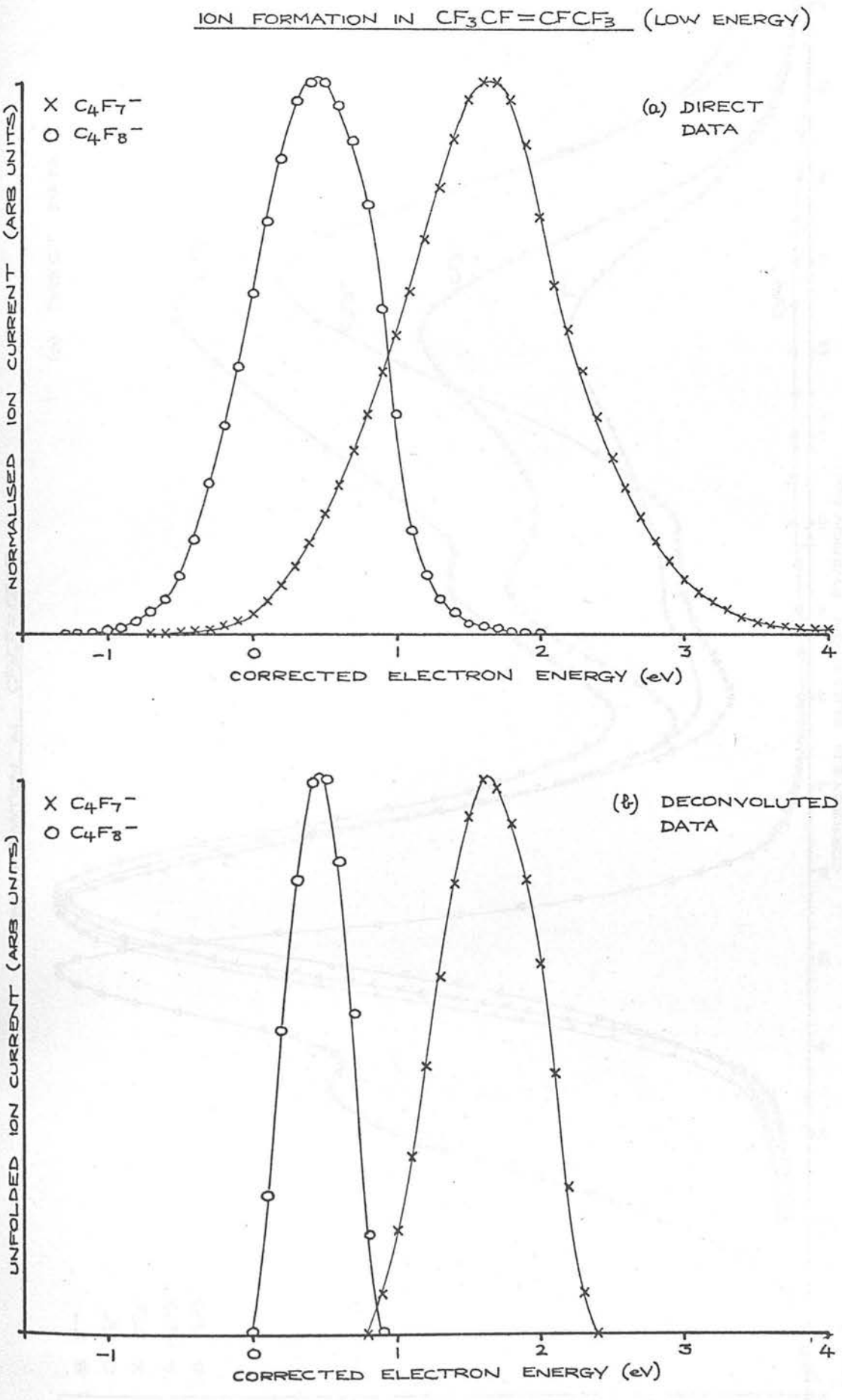
ION FORMATION IN $CF_3CF=CFCF_3$ (LOW ENERGY)
X $C_4F_7^-$
O $C_4F_8^-$
(a) DIRECT DATA
NORMALISED ION CURRENT (ARB UNITS)
-1
0
1
2
3
4
CORRECTED ELECTRON ENERGY (eV)
X $C_4F_7^-$
O $C_4F_8^-$
(b) DECONVOLUTED DATA
UNFOLDED ION CURRENT (ARB UNITS)
-1
0
1
2
3
4
CORRECTED ELECTRON ENERGY (eV)

Fig 7.4

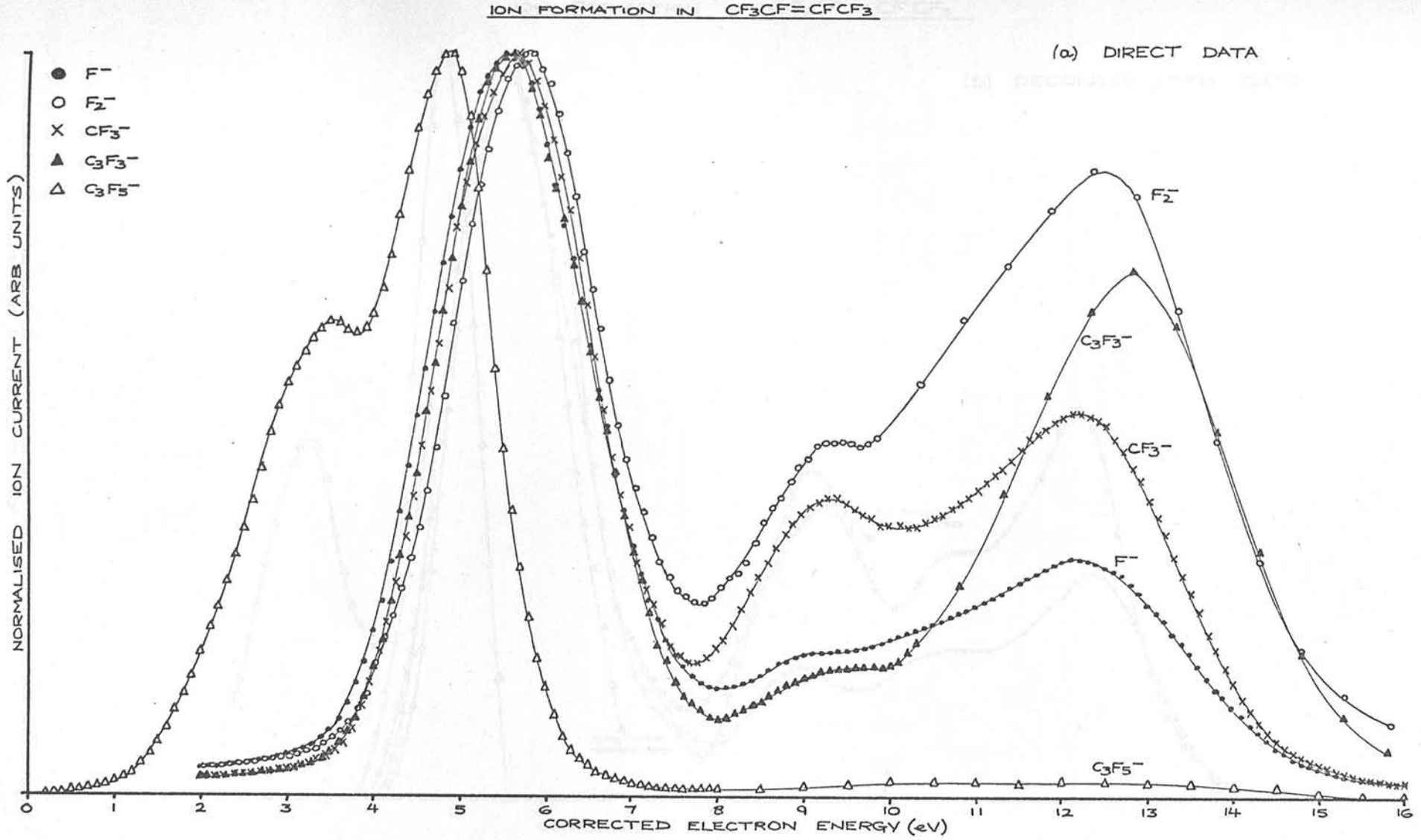
ION FORMATION IN $CF_3CF=CFCF_3$
(a) DIRECT DATA
F^-
F_2^-
CF_3^-
$C_3F_3^-$
$C_3F_5^-$
NORMALISED ION CURRENT (ARB UNITS)
CORRECTED ELECTRON ENERGY (eV)
0 1 2 3 4 5 6 7 8 9 10 11 12 13 14 15 16

Fig 7.5

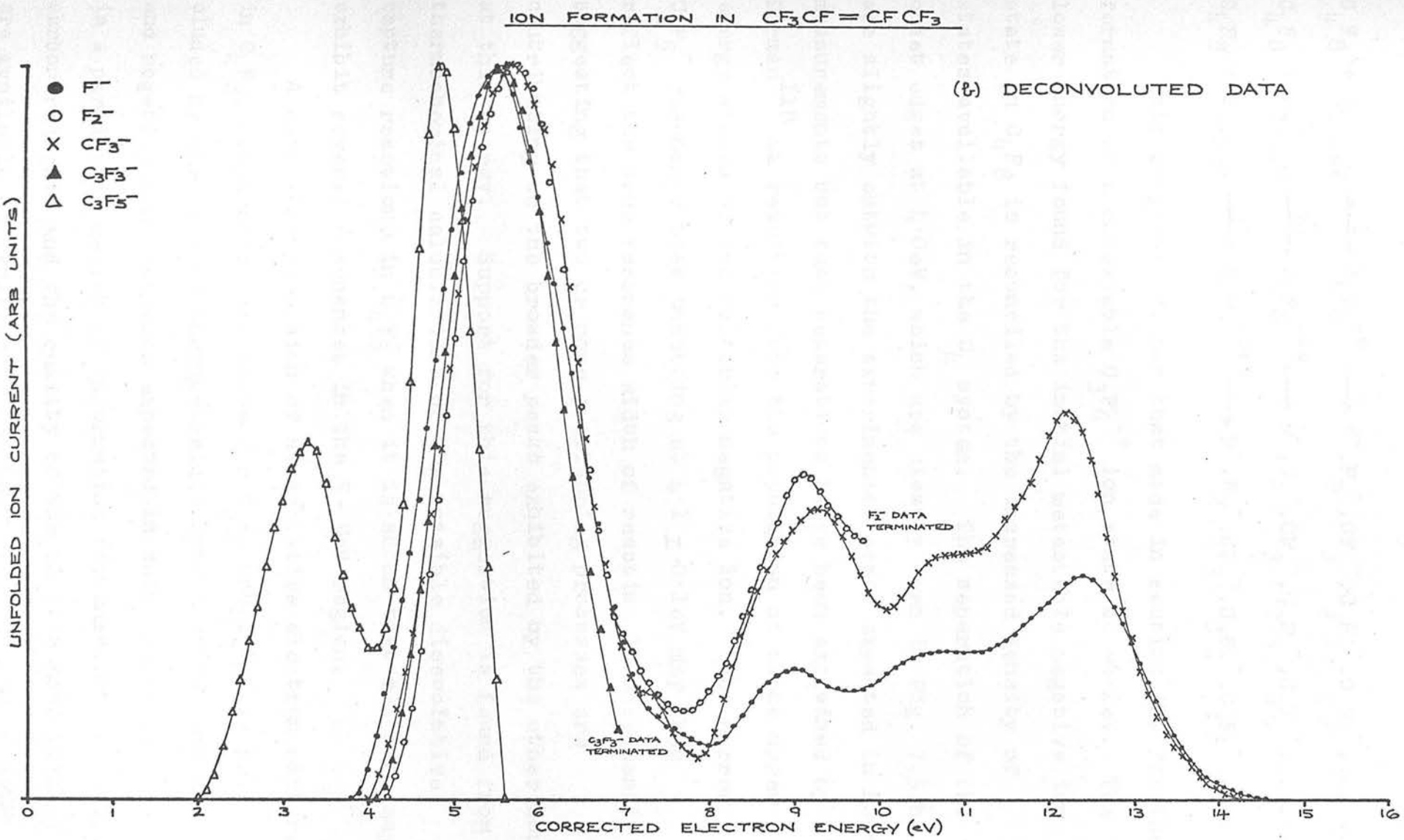
ION FORMATION IN $CF_3CF=CFCF_3$
(b) DECONVOLUTED DATA
F^-
F_2^-
CF_3^-
$C_3F_3^-$
$C_3F_5^-$
UNFOLDED ION CURRENT (ARB UNITS)
F_2^- DATA TERMINATED
$C_3F_3^-$ DATA TERMINATED
0 1 2 3 4 5 6 7 8 9 10 11 12 13 14 15 16
CORRECTED ELECTRON ENERGY (eV)

Fig 7.5

$$C_4F_8 + e_{4\cdot0eV} \xrightarrow{31} C_4F_8^{-*} \longrightarrow F^-, F_2^-, CF_3^-, C_3F_3^-, C_3F_5^-, \ldots\ldots$$

$$C_4F_8 + e_{7\cdot8eV} \xrightarrow{32} C_4F_8^{-**} \longrightarrow F^-, F_2^-, CF_3^-, C_3F_3^-, C_3F_5^-, \ldots\ldots$$

$$C_4F_8 + e_{9\cdot8eV} \xrightarrow{33} C_4F_8^{-***} \longrightarrow F^-, F_2^-, CF_3^-, C_3F_3^-, C_3F_5^-, \ldots\ldots$$

This proposal follows that made in section (b) for the formation of a metastable $C_3F_6^{-*}$ ion state at ~6·2eV. The lower energy found for the initial metastable negative ion state in C_4F_8 is reconciled by the increased density of states available in the C_4 system. The separation of the onset edges at 4·0eV, which are clearly seen in Fig. 7.5(b), are slightly outwith the experimental error expected in these measurements but such separations ha ve been explained by Dorman[118] as resulting from the population of close upper energy states of the molecular negative ion. The narrow $C_3F_5^-$ resonance peak onsetting at $4\cdot1 \pm 0\cdot1$eV may then reflect the true resonance width of reaction 1 consequently suggesting that two or more overlapping processes are contributing to the broader peaks exhibited by the other ions at this energy. Support for this suggestion is found from thermochemical calculations of the possible dissociative capture reactions in C_4F_8 when it is shown that all ions may exhibit several resonances in the 5 - 9eV region.

A detailed discussion of dissociative electron capture in C_4F_8, comparable with those for C_3F_6 and C_3F_8, is precluded by the lack of thermochemical data for the neutral and negative ion fragments expected in such reactions. There is a particular dearth of information for unsaturated fluorocarbon radicals and the quality of the limited data which are available as typified by the heat of formation of CFCF

reported in the literature; 0eV[128] and -2·2 ± 0·7eV.[27] In the light of these difficulties an attempt will be made to elucidate reaction mechanisms by interpolating bond energies and heats of formation of structurally similar species deduced above or available in the literature.

The appearance potential data measured for this molecule are shown in Table 7.7.

Table 7.7. Appearance potential data for C_4F_8.

Ion	Appearance Potential(eV)	Peak Maximum(eV)	Peak Width at ½-height(eV)
F^-	3·9 ± 0·1	5·5 ± 0·1	2·0 ± 0·1
	8·0 ± 0·2	9·0 ± 0·2	-
	9·7 ± 0·2	10·7 ± 0·2	-
	11·2 ± 0·2	12·4 ± 0·2	-
F_2^-	4·2 ± 0·1	5·7 ± 0·1	1·8 ± 0·1
	7·8 ± 0·2	9·1 ± 0·2	-
	9·7 ± 0·2	-	-
CF_3^-	4·0 ± 0·1	5·6 ± 0·1	1·8 ± 0·1
	7·8 ± 0·2	9·2 ± 0·2	-
	10·0 ± 0·2	10·8 ± 0·2	-
	11·1 ± 0·3	12·1 ± 0·3	-
$C_3F_3^-$	4·1 ± 0·1	5·6 ± 0·1	1·7 ± 0·1
	8·0 ± 0·2	-	-
	9·8 ± 0·3	-	-
$C_3F_5^-$	2·0 ± 0·1	3·3 ± 0·1	1·1 ± 0·1
	4·1 ± 0·1	4·85 ± 0·1	0·9 ± 0·1
	Further processes ~9 and ~12eV		
$C_4F_7^-$	0·8 ± 0·1	1·65 ± 0·1	0·8 ± 0·1
$C_4F_8^-$	0·0 ± 0·1	0·45 ± 0·1	0·5 ± 0·1

A small F^- ion current was detected from the initial resonance onsetting at $3{\cdot}9 \pm 0{\cdot}1$eV down to ~0eV but the intensity was too small to enable a specific resonance to be identified. The minimum enthalpy requirement of reaction 34 would be expected to lie in the range 1·7 to 2·0eV i.e. corresponding to a C-F bond dissociation energy of 5·1 to 5·4eV.

$$C_4F_8 + e \xrightarrow{34} F^- + C_4F_7$$

The occurrence of this reaction may be partially responsible for the F^- ion current detected below 3eV.

The next least energetically demanding processes, 35 and 36, have minimum enthalpy requirements of approximately 5·1 and 5·4eV respectively. ΔH_{min} reaction 36 was calculated on the assumption that $\Delta H_f(CF_3CFCF)$

$$C_4F_8 + e \xrightarrow{35} F^- + F + C_4F_6\text{-}2$$
$$\xrightarrow{36} F^- + CF_2 + C_3F_5$$

$\simeq \Delta H_f(CF_3CCF_2)$ which was found to be $\leq -6{\cdot}8 \pm 0{\cdot}2$eV from section (b). This being the case, it is concluded that the onset at $3{\cdot}9 \pm 0{\cdot}1$eV, discussed above in terms of reaction 31, corresponds to reaction 34 in which approximately 2eV of excess energy is involved.

Reactions 38, 39 and 40 have estimated minimum enthalpy requirements of 7·3, 9 and 9·9eV respectively and all or some of these may contribute to ion formation,

$$C_4F_8 + e \xrightarrow{37} F^- + CF_3C + CFCF_3$$
$$\xrightarrow{38} F^- + CF_2 + CFCF + CF_3$$
$$\xrightarrow{39} F^- + F + CF_3C_2 + CF_3$$
$$\xrightarrow{40} F^- + CF_2 + CF + CFCF_3$$

The heat of formation of the CF_3C_2 species was estimated from the appearance potential found for the $C_3F_3^-$ ion from hexafluorobutyne-2 at $0{\cdot}7 \pm 0{\cdot}2$eV.

$$C_4F_6 + e \xrightarrow{41} CF_3C_2^- + CF_3$$

Using known thermochemical data[134] the heat of formation of the $C_3F_3^-$ ion is calculated to be $\leq -4{\cdot}1 \pm 0{\cdot}4$eV. If the strength of the C-C bond broken in the reaction is ~4eV, the electron affinity of the CF_3C_2 radical is estimated to be about $3{\cdot}3$eV (consistent with mass spectrum prediction) and therefore $\Delta H_f(CF_3C_2) \simeq -0{\cdot}8$eV.

Many such reactions may be constructed to account for F^- ion formation but the uncertainty associated with the thermochemical data used in the calculations precludes the unequivocal identification of specific reactions, particularly at high energies.

Pressure dependence measurements showed that F_2^- ion formation occurred by primary processes throughout the energy range shown in Fig. 7.5. Therefore the following processes, with the estimated minimum enthalpy requirements indicated, may be responsible,

		ΔH_{min}(eV)
$C_4F_8 + e \xrightarrow{42}$	$F_2^- + CF_3CCCF_3$	$3{\cdot}0$
$\xrightarrow{43}$	$F_2^- + CF_2CCFCF_3$	-
$\xrightarrow{44}$	$F_2^- + 2CF_3C$	-
$\xrightarrow{45}$	$F_2^- + CF + C_3F_5$	$9{\cdot}3$
$\xrightarrow{46}$	$F_2^- + CF_2C + CF_3CF$	$9{\cdot}9$

The onset at 4·2 ± 0·1eV, already discussed in terms of reaction 31, may correspond to ion formation by reactions 42 or 43 accompanied by the corresponding amount of excess energy i.e. ~1·2eV in the case of reaction 42 which, involving the loss of both tertiary fluorine atoms, is that preferred. The reactions responsible for the remaining appearance potentials cannot be identified unambiguously although reactions 45 and/or 46 may be tentatively suggested as possible decomposition channels corresponding to reaction 33.

After formation of the CF_3^- ion the accompanying fragment, C_3F_5, presumably has the structure CF_3CFCF. Although the heat of formation of this particular fragment is unknown it may be assumed to be not too different from $\Delta H_f(CF_3CCF_2)$, which was deduced in section (b) to be $\leq$ -6·8 ± 0·2eV. Because thermochemical data is also available for all combinations resulting from the fragmentation of CF_3CFCF the minimum enthalpy requirements (± ~0·5eV) for the most probable reactions have been calculated;

		ΔH_{min}(eV)
$C_4F_8 + e \xrightarrow{47}$	$CF_3^- + CFCFCF_3$	2·8
$\xrightarrow{48}$	$CF_3^- + CFCF + CF_3$	4·8
$\xrightarrow{49}$	$CF_3^- + CF + CFCF_3$	7·4
$\xrightarrow{50}$	$CF_3^- + F + C_2F + CF_3$	8·5
$\xrightarrow{51}$	$CF_3^- + CFCF + CF_2 + F$	8·7
$\longrightarrow$	$CF_3^- + 2CF + CF_3$	9·8

As there is insufficient energy available at 4·0 ± 0·1eV to facilitate reaction 48 (assuming $\Delta H_f(CFCF) \sim 0eV$[128]) it is concluded that reaction 47, involving ~1·2eV of excess energy, must be responsible for CF_3^- ion formation from reaction 31 at 4·0 ± 0·1eV. Reactions 48 and/or 49 may be responsible for ion formation at 7·8 ± 0·2eV, i.e. from reaction 32, but as reaction 48 would involve over 3eV of excess energy reaction 49 is preferred; for the same reasons ion formation by reaction 52 at 9·8eV is tentatively proposed as the CF_3^- forming dissociation channel of reaction 33. The remaining reactions are not excluded and the possibility of several processes contributing to the initial resonance peak onsetting at 4·0 ± 0·1 has already been suggested.

Although $C_3F_3^-$ ion formation occurs extensively (Fig. 7·5) the ionic structure involved need not necessarily be consistent over the energy range investigated. In the absence of rearrangement the following four structures are possible; CF_3CC, CF_2CFC, CF_2CCF and CFCFCF, and there are no thermochemical data available for any of these species, except the value of -0·8eV estimated for $\Delta H_f(CF_3C_2)$ above. Thus, any attempt at process identification is futile.

From Fig. 7.5 the $C_3F_5^-$ ionisation efficiency curve is seen to exhibit a peak at lower energies than the other ions. If reaction 53 is responsible for ion formation at 2·0 ± 0·1eV

$$C_4F_8 + e \xrightarrow{53} C_3F_5^- + CF_3$$

then, assuming $D(C_3F_5\text{-}CF_3)$ is not too different from the analogous bonds in C_3F_6 and C_3F_8 (which were calculated and deduced to be 4·4 and $\leq$ 4·55 $\pm$ 0·2eV respectively) a value of $\geq$ 2·4 $\pm$ 0·3eV may be estimated for the electron affinity of the C_3F_5 radical. This may be compared to the value of 2·7 $\pm$ 0·2eV deduced for the C_3F_5 radical formed from C_3F_6.

Using available thermochemical data[134,128,129] and assuming that 2·0 $\pm$ 0·1eV is the minimum enthalpy requirement for reaction 53 the heat of formation of the $C_3F_5^-$ ion is calculated to be $\leq$ -9·7 $\pm$ 0·3eV. Subtracting the electron affinity, $\geq$ 2·4 $\pm$ 0·3eV, the heat of formation of the C_3F_5 radical is estimated to be $\leq$ -7·3 $\pm$ 0·6eV which is similar to the value deduced for the same species from C_3F_6 above, $\leq$ -6·8 $\pm$ 0·2eV. Using $\Delta H_f(C_3F_5^-) \leq$ -9·7 $\pm$ 0·3eV the minimum enthalpy requirements for reactions 54, 55 and 56 are estimated to be 5·9 $\pm$ 0·5, 9·4 $\pm$ 0·5 and 11·0 $\pm$ 0·5eV respectively.

$$C_4F_8 + e \xrightarrow{54} C_3F_5^- + CF_2 + F$$
$$\xrightarrow{55} C_3F_5^- + CF + F_2$$
$$\xrightarrow{56} C_3F_5^- + CF + 2F$$

It is not unreasonable to suggest that all of these reactions may contribute to ion formation and particularly reaction 55 which is suggested as the decomposition channel of reaction 33.

The $C_4F_7^-$ and $C_4F_8^-$ curves, measured simultaneously, are shown in Fig. 7.4. If the $C_4F_7^-$ onset at 0·8 $\pm$ 0·1eV may be attributed to the following reaction,

$$C_4F_8 + e \xrightarrow{57} C_4F_7^- + F$$

then, if $D(C_4F_7\text{-}F)$ ~5·2eV a value of $\geq$ 4·4eV may be deduced for $E(C_4F_7)$. This value is undoubtedly high which inevitably reflects on the choice of 5·2eV for the C-F bond dissociation energy involved in reaction 57. The tertiary C-F bonds, being the weakest, are the most likely to partake in ion formation and Lifshitz et al.[135] used this assumption to estimate values of 3·5 and 3·9eV for the electron affinities of the C_6F_{11} and C_7F_{13} radicals respectively. In the same article a value of 3·1eV was estimated for $E(C_5F_9)$ and as it has been generally found that the electron affinity of perfluoro radicals increases as the series are ascended the value deduced above for $E(C_4F_7)$ appears to be seriously in error. Lifshitz estimated that the tertiary C-F bond energy was in fact close to 4·3eV.and using this value in conjunction with the $C_4F_7^-$ appearance potential the electron affinity is revaluated to be ~3·5eV. When viewed in relation to the electron affinities measured for the lower olefinic radicals in the series; C_2F_3 and C_3F_5, i.e. $E(C_2F_3) = 2·0 \pm 0·2$[119] and $E(C_3F_5) = 2·7 \pm 0·2$eV deduced from reaction 17, this value appears to be of the expected magnitude.

The C_4F_8 molecular negative ion, shown in Fig. 7.4, has already been discussed in Chapter 4 where the ionisation efficiency curve, measured using a tungsten filament with a regulated trap current of 0·1 μAmp, is shown in Fig. 4.1. The more recent data shown in Fig. 7.4 was obtained with a

rhenium filament and a regulated trap current of only 0·01 μAmp which resulted in a sharper more stable electron energy distribution.

(e) Perfluoronormalbutane, C_4F_{10}.

The ions detected and measured at low electron energies in C_4F_{10} were F^-, CF_3^-, $C_2F_5^-$, $C_3F_7^-$, $C_4F_9^-$ and $C_4F_{10}^-$ which were formed with relative abundances in the ratio 1000:4:103:13:1:<1 at their respective capture maxima. All of these ions were identified in a previous study of C_4F_{10} by Greenhaus;[132] Bibby and Carter,[124,125] however, reported only the F^-, CF_3^-, $C_2F_5^-$ and $C_3F_7^-$ ions. Typical ionisation efficiency data measured in this study are shown in Fig. 7.6, where the energy scale is calibrated against the appearance potentials of the O^- ion formed from SO_2 at 4·2 and 6·6 eV. The appearance potentials measured are compared with those of previous studies in Table 7.8.

Table 7.8. Comparison of appearance potential data for C_4F_{10}

Ion	Appearance Potential (eV)		
	This work	Greenhaus[132]	Bibby & Carter[124,125]
F^-	2·0 ± 0·1 3·8 ± 0·1	1·6 ± 0·07	1·8 ± 0·1
CF_3^-	2·3 ± 0·1 3·8 ± 0·2	4·0 ± 0·3	2·6 ± 0·1
$C_2F_5^-$	2·1 ± 0·1 3·8 ± 0·2	2·6 ± 0·3	1·85 ± 0·1
$C_3F_7^-$	2·1 ± 0·1	3·6 ± 0·3	2·0 ± 0·1
$C_4F_9^-$	2·2 ± 0·2	2·2 ± 0·3 ~4	-
$C_4F_{10}^-$	0·0 ± 0·1	0·32 ± 0·3	-

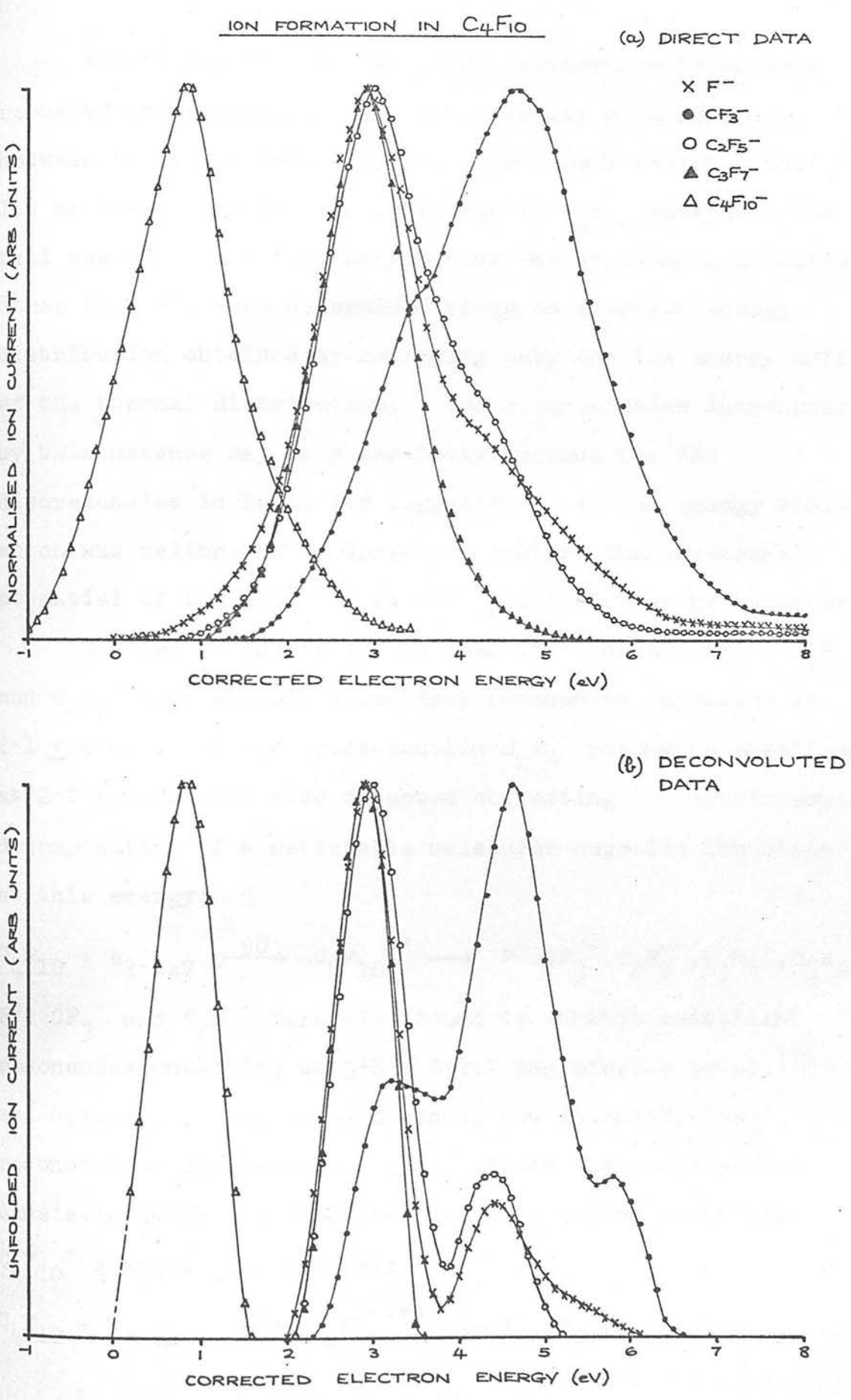
ION FORMATION IN C_4F_{10}
(a) DIRECT DATA
X F^-
● CF_3^-
O $C_2F_5^-$
▲ $C_3F_7^-$
△ $C_4F_{10}^-$
NORMALISED ION CURRENT (ARB UNITS)
-1
0
1
2
3
4
5
6
7
8
CORRECTED ELECTRON ENERGY (eV)
(b) DECONVOLUTED DATA
UNFOLDED ION CURRENT (ARB UNITS)
-1
0
1
2
3
4
5
6
7
8
CORRECTED ELECTRON ENERGY (eV)

Fig 7.6

Except for the CF_3^- and $C_3F_7^-$ appearance potentials reported by Greenhaus, there is generally good agreement between the three sets of data. Greenhaus reported that the low cross-section for ion formation in C_4F_{10} precluded the full use of the RPD method and that the appearance potentials, other than F^-, were determined using an electron energy distribution obtained by retarding only the low energy half of the thermal distribution. The uncertainties introduced by this measure may only partially account for the discrepancies in Table 7.8 suggesting that the energy scale, which was calibrated by Greenhaus against the appearance potential of the SF_6^- ion at 0·05 ± 0·03eV, may be in error.

In Fig. 7.6(b) it can be seen that the F^-, CF_3^-, $C_2F_5^-$ and $C_3F_7^-$ ions exhibit coincident resonances onsetting at 2·1 ± 0·2eV. A low cross-section $C_4F_9^-$ resonance onsetting at 2·2 ± 0·2eV was also detected suggesting the multichannel decomposition of a metastable molecular negative ion state at this energy;

$$C_4F_{10} + e_{2\cdot1eV} \xrightarrow{58} C_4F_{10}^{-*} \longrightarrow F^-, CF_3^-, C_2F_5^-, C_3F_7^-, C_4F_9^-$$

F^-, CF_3^- and $C_2F_5^-$ were also found to exhibit coincident resonances onsetting at 3·8 ± 0·2eV and Dibeler et al.[126] and Greenhaus[132] reported a second low intensity $C_4F_9^-$ resonance at approximately 4eV. These observations are consistent with the decomposition of a second metastable $C_4F_{10}^-$ state at 3·8 ± 0·2eV;

$$C_4F_{10} + e_{3\cdot8eV} \xrightarrow{59} C_4F_{10}^{-**} \longrightarrow F^-, CF_3^-, C_2F_5^-, C_4F_9^-, \ldots\ldots$$

Again this follows similar proposals in Chapter 5 and in sections (b) and (d) above for a metastable $C_3F_6^-$ state at 6·2eV and metastable $C_4F_8^-$ states at 4·0, 7·8 and 9·8eV. The appearance of such states at lower energies in C_4F_{10} is in the expected direction (as mentioned in section (d)).

The appearance potential data measured for C_4F_{10} are tabulated below,

Table 7.9. Appearance potential data for C_4F_{10}.

Ion	Appearance Potential(eV)	Peak Maximum(eV)	Peak Width at ½-height(eV)
F^-	2·0 ± 0·1	2·9 ± 0·1	0·9 ± 0·1
	3·8 ± 0·1	4·4 ± 0·1	0·9 ± 0·1
CF_3^-	2·3 ± 0·1	3·2 ± 0·1	-
	3·8 ± 0·2	4·65 ± 0·1	1·2 ± 0·1
$C_2F_5^-$	2·1 ± 0·1	3·0 ± 0·1	0·9 ± 0·1
	3·8 ± 0·2	4·4 ± 0·1	0·9 ± 0·1
$C_3F_7^-$	2·1 ± 0·1	2·9 ± 0·1	0·8 ± 0·1
$C_4F_9^-$	2·2 ± 0·2	low cross-section	
$C_4F_{10}^-$	0·0 ± 0·1	low cross-section	

It is apparent from Fig. 7.6 that F^- ion formation occurs by two resonances which have been attributed to reactions 58 and 59. Assuming the C_4F_9 radical appearing in reaction 60 to be of the normal variety, that is, the one for which

$$C_4F_{10} + e \xrightarrow{60} F^- + C_4F_9$$

thermochemical data is available,[127] the minimum enthalpy requirement for the reaction is estimated to be 1·9eV. The appearance potential at 2·0 ± 0·1eV may therefore correspond to this reaction involving little or no excess energy. This presents an interesting situation as the least energetically demanding reaction is that involving formation of the iso-C_4F_9 radical. The occurrence of this situation in C_3F_8 also (reaction 21) suggests one of the following; (i) the secondary C-F bonds in these perfluorocarbons are in fact ~5·3eV and the thermochemical data is in error, (ii) that the iso-radicals are produced in reactions 21 and 60 with ~0·6eV of excess energy distributed between the fragments, or (iii) that reactions 21 and 60 involve formation of the normal perfluoroalkyl radicals involving little or no excess energy and consequently that the published thermochemical data is not seriously in error.

Although it would be rather difficult to justify the preferential formation of the normal-perfluoroalkyl radicals the C-F bond dissociation energies calculated from reactions 21 and 60, $D(C_3F_7\text{-}F) \leq 5{\cdot}25 \pm 0{\cdot}1$eV and $D(C_4F_9\text{-}F) \leq 5{\cdot}45 \pm 0{\cdot}1$eV, are in good agreement with the following primary C-F bond dissociation energies reported in the literature, $D(CF_3\text{-}F) = 5{\cdot}3$eV[130] and $D(C_2F_5\text{-}F) \leq 5{\cdot}25 \pm 0{\cdot}1$eV.[17] It is therefore suggested that either (ii) or (iii) reflects the real situation.

Reactions 61 and 62, which both have minimum enthalpy requirements of 3·5eV, are tentatively proposed

$$C_4F_{10} + e \xrightarrow{61} F^- + F + C_4F_8\text{-}2$$
$$\xrightarrow{62} F^- + C_2F_5 + C_2F_4$$

to account for F^- ion formation by reaction 59.

From Fig. 7.6(a) it can be seen that the CF_3^- ionisation efficiency curve is broad and may correspond to several overlapping resonances. The deconvoluted curve reveals the lower cross-section resonance which is apparent in the onset edge of the experimental data and also a smaller peak at ~5·7eV. This higher energy shoulder was not reproducible and is therefore attributed to ineffectual unfolding of the broad tail of the resonance. Spurious peaks sometimes occur after the deconvolution of peaks which are several times broader than the electron energy distribution.

If the initial onset at 2·3 ± 0·1eV corresponds to the following reaction,

$$C_4F_{10} + e \xrightarrow{63} CF_3^- + C_3F_7$$

then, using the established value for $E(CF_3) = 2{\cdot}0 \pm 0{\cdot}1eV$[4,17,119,122], the $CF_3\text{-}C_3F_7$ bond dissociation energy is estimated to be $\leq 4{\cdot}3 \pm 0{\cdot}2eV$. This is in good agreement with the C-C bond dissociation energies deduced above; $D(CF_3\text{-}C_2F_3) \simeq 4{\cdot}4$ and $D(CF_3\text{-}C_2F_5) \leq 4{\cdot}55 \pm 0{\cdot}2eV$. Reactions 64 and 65, which have estimated minimum enthalpy requirements of 3·5 and 4·0eV respectively, may both contribute to

$$C_4F_{10} + e \xrightarrow{64} CF_3^- + C_2F_4 + CF_3$$
$$\xrightarrow{65} CF_3^- + CF_2 + C_2F_5$$

ion formation at 3·8 ± 0·2eV.

Assuming the C_2F_5-C_2F_5 bond dissociation energy is not too different from the CF_3-C_3F_7 bond strength deduced above then, if the $C_2F_5^-$ appearance potential at 2·1 ± 0·1eV corresponds to ion formation by reaction 66,

$$C_4F_{10} + e \xrightarrow{66} C_2F_5^- + C_2F_5$$

the electron affinity of the C_2F_5 radical is estimated to be ~2·2 ± 0·3eV. This may be compared to the value of 2·1 ± 0·2eV estimated from reaction 27 and values of 2·3[122] and 2·4eV[17] reported in the literature. This agreement lends support to the C-C bond dissociation energies deduced above which are 0·5 to 0·7eV higher than the corresponding hydrocarbon bonds.[133]

$$C_4F_{10} + e \xrightarrow{67} C_2F_5^- + CF_2 + CF_3$$

Reaction 67, with a minimum enthalpy requirement of 3·8eV, is proposed as the dissociation channel following reaction 59 at 3·8 ± 0·2eV.

The $C_3F_7^-$ ion exhibits a single sharp resonance peak onsetting at 2·1 ± 0·1eV. Providing reactions 63 and 68 do not involve excess energy,

$$C_4F_{10} + e \xrightarrow{68} C_3F_7^- + CF_3$$

the expression $A(CF_3^-) + E(CF_3) = A(C_3F_7^-) + E(C_3F_7)$ may be used to estimate a value of 22 ± 0·2eV for the electron affinity of the C_3F_7 radical. This may be compared with the value of 2·35 ± 0·2eV deduced from reactions 21 and 28 above and values of 2·0[4] and ~2·4eV[122] reported in the literature.

The $C_4F_9^-$ ion was formed with a very low cross-section at 2·2 ± 0·2eV in agreement with the result as reported by Greenhaus.[132] If $C_4F_9^-$ is formed by reaction 69 (the complementary process to reaction 60)

$$C_4F_{10} + e \xrightarrow{69} C_4F_9^- + F$$

the electron affinity of the C_4F_9 radical is estimated to be 3·25 ± 0·3eV. There is no other reported value with which this may be compared except that deduced for the C_4F_7 radical from reaction 57, ~3·5eV.

C_4F_{10} was found to have a low attachment cross-section, $\sigma_a \sim 10^{-18}$ cm.^{2}; measurement of this required

$$C_4F_{10} + e \xrightarrow{70} C_4F_{10}^-$$

the use of abnormally high electron trap currents for the measurement of the ionisation efficiency curve shown in Fig. 7.6. For this reason the curve appears broader than that measured for $C_4F_8^-$ shown in Fig. 7.4.

(f) Perfluorocyclobutene, c-C_4F_6.

Perfluorocyclobutene was found to exhibit a low cross-section for ion formation; only the ions F^-, $C_3F_3^-$, $C_4F_5^-$ and $C_4F_6^-$ with relative abundances in the ratio 1000:160:16:20 at their respective capture maxima being formed with intensities amenable to investigation. A CF_3^- ion current was also detected at low electron energies but its low intensity precluded measurement of the ionisation efficiency curve.

Experimental and deconvoluted ionisation data are

shown in Figs. 7.7(a) and (b) respectively and the corresponding appearance potential data is given in Table 7.10. The energy scale in Fig. 7.7 is calibrated against the appearance potential of the O^- ion formed from SO_2 at 4·2 and 6·6eV.

The observation of the CF_3^- ion in the 70eV mass spectrum of c-C_4F_6 has been discussed in section (a) and its formation attributed to reaction 1 involving ring cleavage and fluorine atom transfer. In this scheme the $C_3F_3^-$ ion was considered to be the complementary ion. Both of these rearrangement ions were observed at low electron energies and from Fig. 7.7(a) it can be seen that at least two resonance processes are involved in $C_3F_3^-$ ion formation in the 0 - 15eV energy range. It is further apparent from Figs. 7.7(a) and (b) that all ions exhibit narrow coincident

Table 7.10. Appearance potential data for c-C_4F_6

Ion	Appearance Potential(eV)	Peak Maximum(eV)	Peak Width at ½-height(eV)
F^-	1·9 ± 0·1	4·1 ± 0·1	1·5 ± 0·1
	~4·9	shoulder	-
	~5·9	6·4 ± 0·2	
	~7·6	7·9 ± 0·2	
	9·7 ± 0·2	11·2 ± 0·2	1·8 ± 0·2
$C_3F_3^-$	2·7 ± 0·1	3·95 ± 0·1	1·1 ± 0·1
	~4·7	shoulder	-
	5·9 ± 0·2	6·6 ± 0·1	1·1 ± 0·1
	7·4 ± 0·2	7·8 ± 0·2	-
$C_4F_5^-$	3·65 ± 0·1	4·4 ± 0·1	0·8 ± 0·1
	5·65 ± 0·1	6·55 ± 0·1	0·9 ± 0·1
$C_4F_6^-$	0·0 ± 0·1	0·45 ± 0·1	0·5 ± 0·1

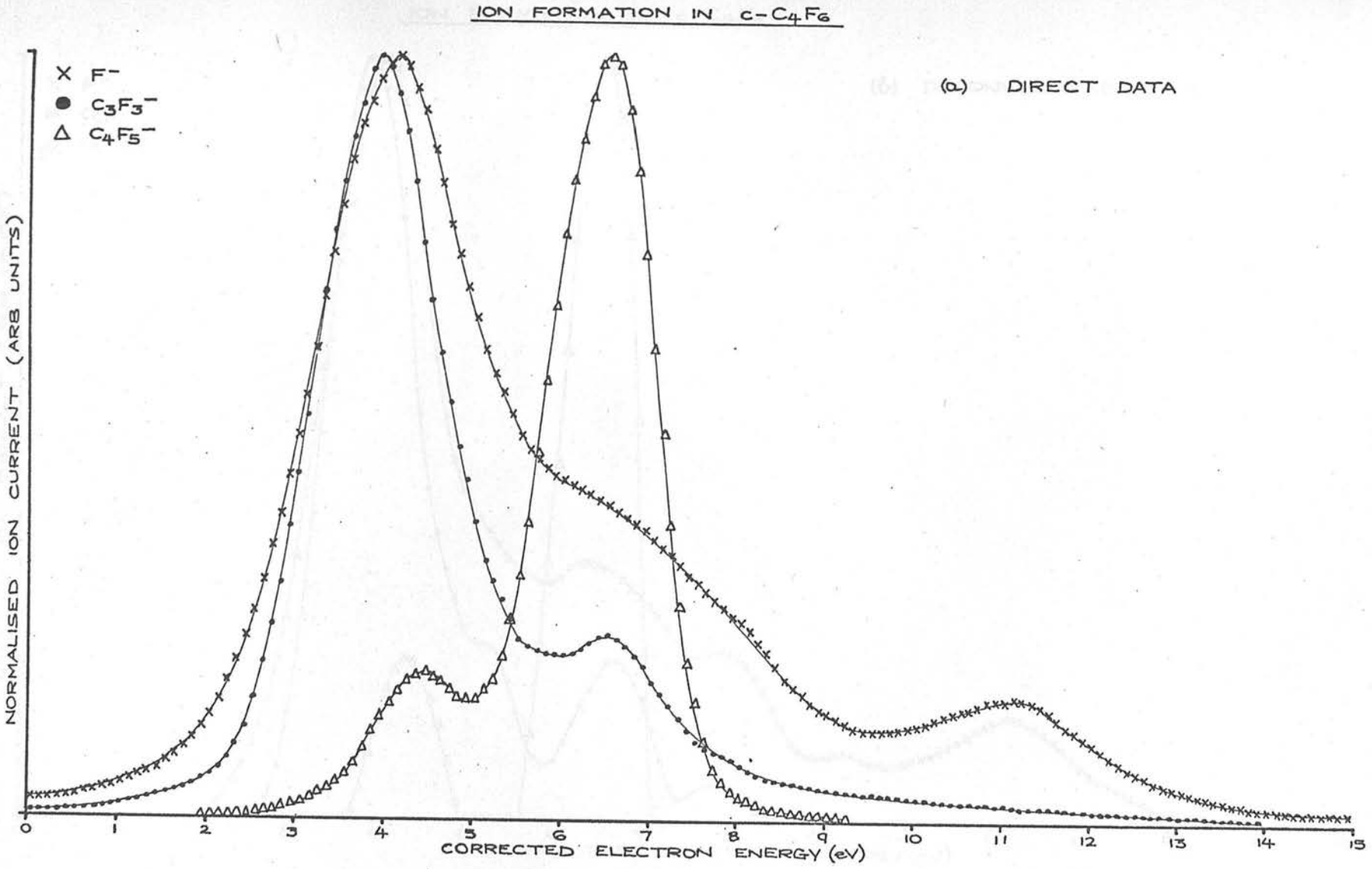
ION FORMATION IN c-C4F6
(a) DIRECT DATA
X F⁻
● C3F3⁻
△ C4F5⁻
NORMALISED ION CURRENT (ARB UNITS)
0
1
2
3
4
5
6
7
8
9
10
11
12
13
14
15
CORRECTED ELECTRON ENERGY (eV)

Fig 7.7

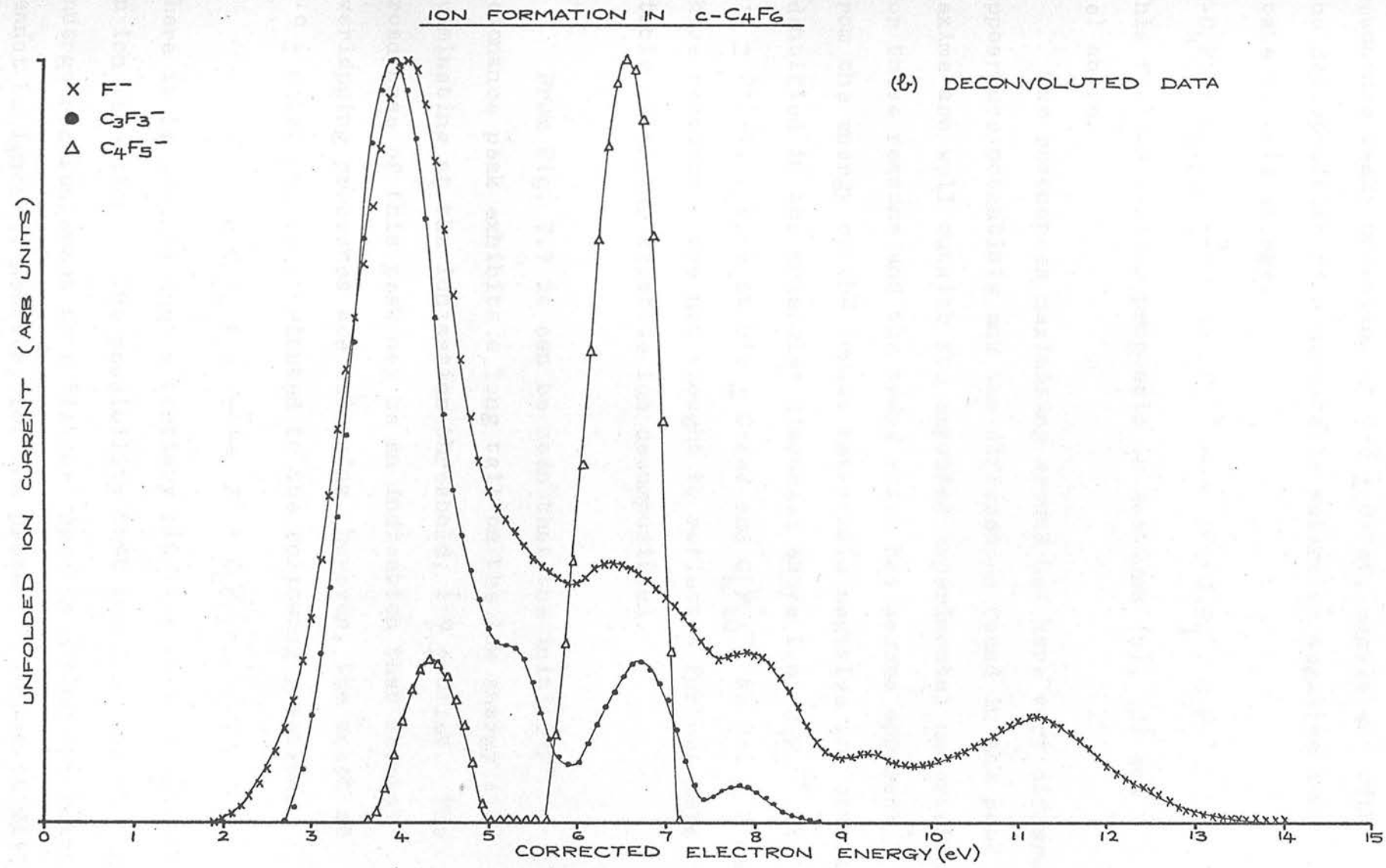
ION FORMATION IN c-C4F6
(b) DECONVOLUTED DATA
X F⁻
● C3F3⁻
△ C4F5⁻
UNFOLDED ION CURRENT (ARB UNITS)
0
1
2
3
4
5
6
7
8
9
10
11
12
13
14
15
CORRECTED ELECTRON ENERGY (eV)

Fig 7.7

resonance peaks onsetting at 5·8 ± 0·2eV, consistent with the decomposition of a metastable molecular negative ion state at this energy,

$$c\text{-}C_4F_6 + e_{5\cdot8eV} \xrightarrow{71} c\text{-}C_4F_6^{-*} \longrightarrow F^-, C_3F_3^-, C_4F_5^-, \ldots\ldots$$

This follows similar proposals in sections (b), (d) and (e) above.

The resonances maximising around 4eV have very different appearance potentials and the differences found in the peak maxima are well outwith the expected experimental uncertainty. For these reasons and the trend which has become apparent from the energy of the lowest metastable negative ion states identified in the molecules discussed above i.e. $C_3F_6^{-*}$ at 6·2 ± 0·2eV, C_4F_8-2 at 4·0 ± 0·2eV and $C_4F_{10}^{-*}$ at 2·1 ± 0·2eV, these resonances are not thought to reflect a further metastable molecular negative ion decomposition.

From Fig. 7.7 it can be seen that the initial F^- resonance peak exhibits a long tail on the low energy side culminating at the ionisation threshold, 1·9 ± 0·1eV. The broad base of this peak may be an indication that several overlapping processes are occurring, however, the onset at 1·9 ± 0·1eV may be attributed to the following reaction,

$$c\text{-}C_4F_6 + e \xrightarrow{72} F^- + C_4F_5$$

where it is assumed that a tertiary fluorine atom is involved in ion formation. The possibility that the C_4F_5 radical may undergo rearrangement to a 'linear' species during the reaction cannot be ignored, however, for the present argument it will

be assumed that C_4F_5 represents the cyclic isomer. Then, from the following expression, $D(C_4F_5\text{-}F) \leq A(F^-) + E(F)$ where $E(F) = 3{\cdot}45eV$,[36] the C-F bond dissociation energy is estimated to be $\leq 5{\cdot}35 \pm 0{\cdot}1eV$. If the measured onset at $1{\cdot}9 \pm 0{\cdot}1eV$ is assumed to be the minimum energy requirement of reaction 72 then, using known thermochemical data,[129,134] the heat of formation of the C_4F_5 radical is calculated to be $\leq -5{\cdot}6 \pm 0{\cdot}2eV$. There is no other value with which this can be compared.

The F^- ion is formed extensively over the energy range up to 13eV and many processes may be suggested to account for ion formation. The following examples, for which the minimum enthalpy requirements are shown, are proposed as contributory sources of ion formation in the 3 to 11eV region,

		ΔH_{min}(eV)
$c\text{-}C_4F_6 + e \xrightarrow{73}$	$F^- + C_2F + C_2F_4$	3·8
$\xrightarrow{74}$	$F^- + CF_2 + C_3F_3$	~4·9
$\xrightarrow{75}$	$F^- + CFCF + CFCF_2$	5·5
$\xrightarrow{76}$	$F^- + C_2F + 2CF_2$	6·8
$\xrightarrow{77}$	$F^- + CF + CF_2 + CFCF$	8·2
$\xrightarrow{78}$	$F^- + C + CF + C_2F_4$	10·8

Of these reactions, 73 is tentatively attributed to the initial resonance peak maximising at $4{\cdot}1 \pm 0{\cdot}1eV$, 74, 75, 76 and 77 to the resonances onsetting at ~4·9, ~5·9, ~7·6 and $9{\cdot}7 \pm 0{\cdot}2eV$ respectively and 78 as a possible contributor to the broad low cross-section resonance peak in the 9 - 13eV region. Reaction 75 therefore corresponds to the F^- dissociation channel from reaction 71.

If the complementary process to reaction 72 is responsible for the initial $C_4F_5^-$ ion resonance onsetting at 3·65 ± 0·1,

$$c\text{-}C_4F_6 + e \xrightarrow{79} C_4F_5^- + F$$

then, in the absence of excess energy in reactions 72 and 79, the electron affinity of the C_4F_5 radical is estimated to be 1·7 ± 0·2eV. This value is considerably lower than those calculated above for linear perfluoro-radicals of similar size i.e. $E(C_3F_5)$ = 2·7 ± 0·2 and ≥ 2·4 ± 0·3, $E(C_3F_7)$ = 2·35 ± 0·2 and 2·2 ± 0·2, $E(C_4F_7)$ ~3·5 and $E(C_4F_9)$ = 3·25 ± 0·3eV, which may indicate that the C_4F_5 species produced in reactions 72 and 79 is the cyclic species and not the rearranged linear isomer for which the electron affinity may be higher.

The second $C_4F_5^-$ resonance onsetting at 5·65 ± 0·1eV has been attributed to reaction 71 and must involve ≥ 2·0 ± 0·2eV of excess energy distributed between the fragments,

$$c\text{-}C_4F_6 + e \xrightarrow{80} C_4F_5^{-*} + F^*$$

$C_3F_3^-$ ion formation has been attributed to reaction 1 (Section (a)),

$$c\text{-}C_4F_6 + e \xrightarrow{1} C_3F_3^- + CF_3$$

If there is no excess energy involvement in this reaction at 2·7 ± 0·1eV then, the heat of formation of the $C_3F_3^-$ ion is estimated to be ≤ -2·5 ± 0·3eV. The electron affinity of the C_3F_3 radical was predicted in section (a) to be greater than that of the trifluoromethyl radical, the complementary species in reaction 1, on the grounds of their relative abundances at 70eV and at their respective capture maxima, i.e. $E(C_3F_3)$ > 2·0 ± 0·1eV where $E(CF_3)$ = 2·0 ± 0·1eV[4,17,119]. An upper limit of -0·5 ± 0·4eV may therefore

be deduced for $\Delta H_f(C_3F_3)$. There is no other value with which this can be compared.

The next least energetically demanding $C_3F_3^-$ ion forming processes,

$$c\text{-}C_4F_6 + e \xrightarrow{81} C_3F_3^- + CF_2 + F$$
$$c\text{-}C_4F_6 + e \xrightarrow{82} C_3F_3^- + CF + F_2$$

require $6{\cdot}6 \pm 0{\cdot}5$ and $10{\cdot}1 \pm 0{\cdot}5$eV respectively. Reaction 81 is therefore attributed to the observed onset at $5{\cdot}9 \pm 0{\cdot}2$eV, which corresponds to the $C_3F_3^-$ dissociative capture channel from reaction 71. Accordingly the shoulders at ~$4{\cdot}7$ and $7{\cdot}4 \pm 0{\cdot}2$eV can only result from reactions 1 and 81 respectively in which ~2eV of excess energy is involved in each case.

The $C_4F_6^-$ ion was examined simultaneously with the SF_6^- ion from SF_6 and found to have an identical peak profile and energy scale parameters. The autodetachment lifetime and attachment cross-section have already been presented and discussed in Chapter 4.

(g) Perfluorocyclobutane, $c\text{-}C_4F_8$.

The average dissociative electron capture cross-section in $c\text{-}C_4F_8$ was found to be approximately a magnitude higher than observed for $c\text{-}C_4F_6$. Typical experimental and deconvoluted ionisation data are shown in Figs. 7.8(a) and (b) respectively where the energy scale is calibrated against the appearance potential of the O^- ion formed from SO_2 at

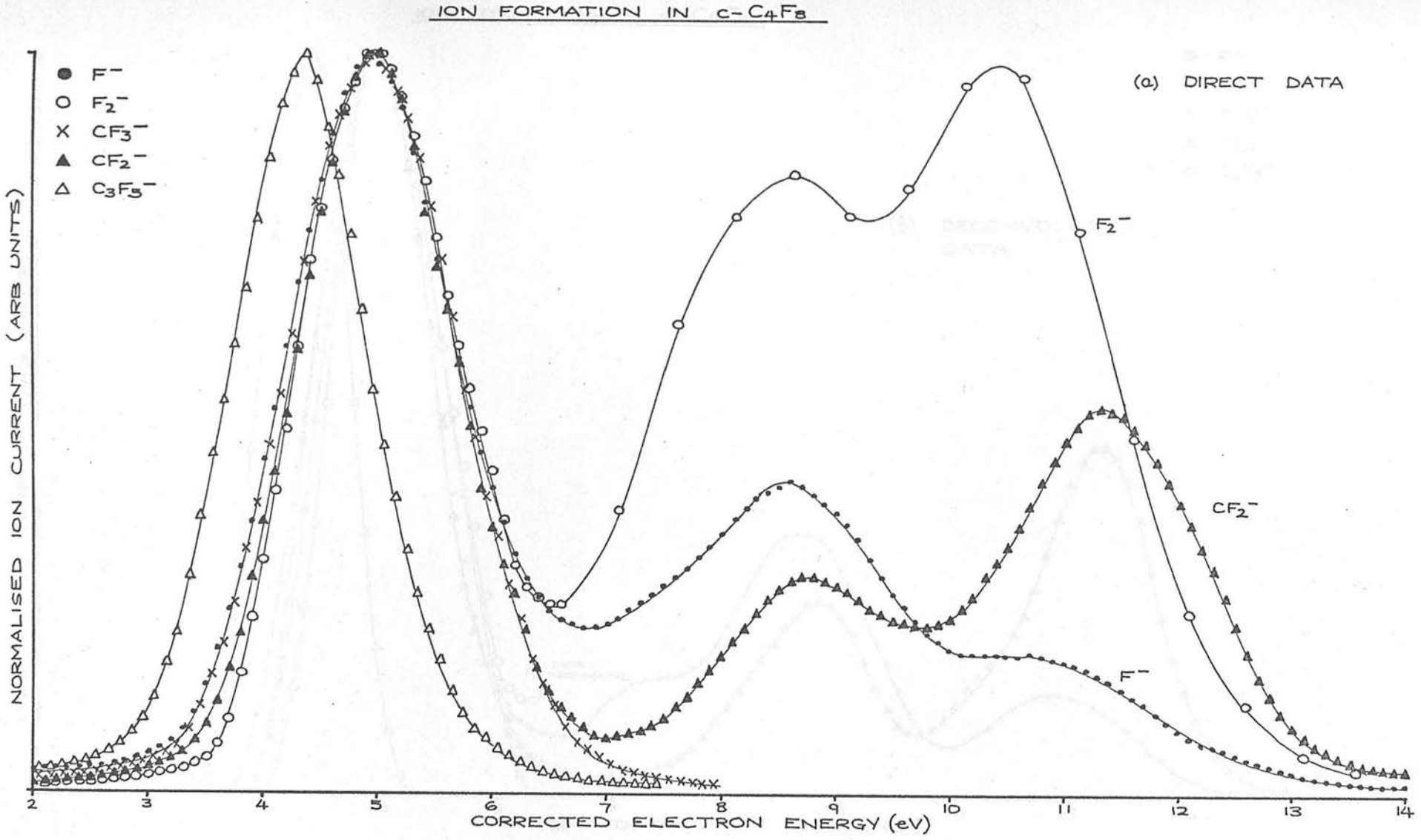
ION FORMATION IN c-C4F8
(a) DIRECT DATA
F⁻
F2⁻
CF3⁻
CF2⁻
C3F5⁻
F2⁻
CF2⁻
F⁻
NORMALISED ION CURRENT (ARB UNITS)
CORRECTED ELECTRON ENERGY (eV)
2
3
4
5
6
7
8
9
10
11
12
13
14

Fig 7.8

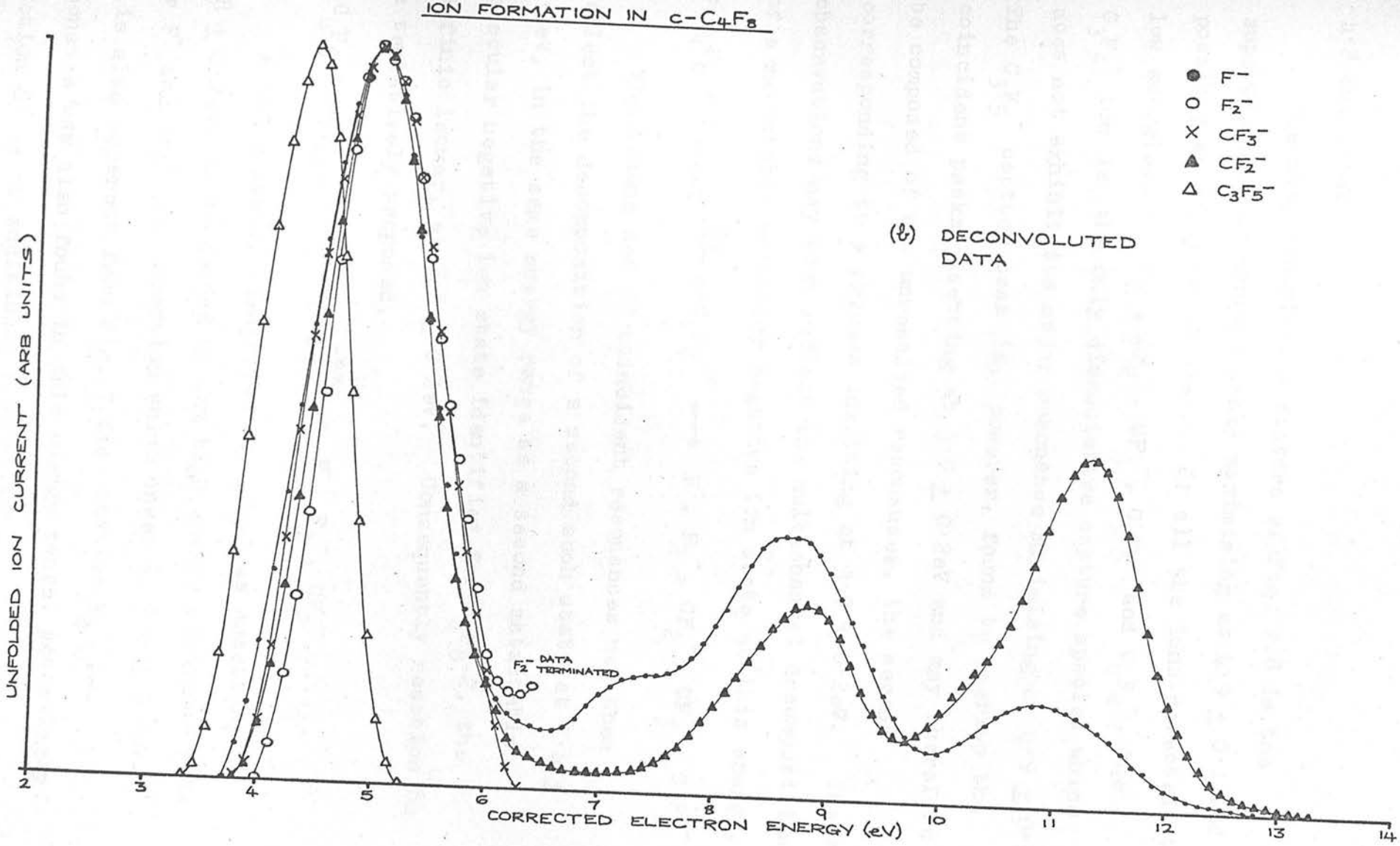
ION FORMATION IN c-C4F8
F⁻
F2⁻
CF3⁻
CF2⁻
C3F5⁻
(b) DECONVOLUTED DATA
F2⁻ DATA TERMINATED
UNFOLDED ION CURRENT (ARB UNITS)
CORRECTED ELECTRON ENERGY (eV)
2
3
4
5
6
7
8
9
10
11
12
13
14

Fig 7.8

4·2 and 6·6eV.

The most conspicuous feature of Fig. 7.8 is the superposition of capture peaks maximising at 4·9 ± 0·1 and possibly at 8·5 ± 0·2eV also. Of all the ions detected at low energies, F^-, F_2^-, CF_2^-, CF_3^-, $C_3F_5^-$ and $C_4F_8^-$, the $C_3F_5^-$ ion is the only dissociative capture species which does not exhibit its major resonance maximising at 4·9 ± 0·1eV. The $C_3F_5^-$ capture peak is, however, found to overlap the coincident peaks onsetting at 3·9 ± 0·2eV and may therefore be composed of two unresolved resonances, the second corresponding to a process onsetting at 3·9 ± 0·2eV. These observations may then reflect the multichannel decomposition of a metastable molecular negative ion state at this energy,

$$c\text{-}C_4F_8 + e_{3\cdot9eV} \xrightarrow{83} c\text{-}C_4F_8^{-*} \longrightarrow F^-, F_2^-, CF_2^-, CF_3^-, C_3F_5^-, \ldots$$

The second set of coincident resonances may then reflect the decomposition of a second such state at 7·4 ± 0·3eV, in the same energy range as a second metastable molecular negative ion state identified for C_4F_8-2, the olefinic isomer, at 7·8 ± 0·2eV. Consequently reaction 84 is tentatively proposed,

$$c\text{-}C_4F_8 + e_{7\cdot4eV} \xrightarrow{84} c\text{-}C_4F_8^{-**} \longrightarrow F^-, F_2^-, CF_2^-, \ldots\ldots$$

A third state, identified in C_4F_8-2 as onsetting at 9·8 ± 0·2eV, is suggested by the high energy resonance peaks for F^- and CF_2^- ion formation which onset at 9·8 ± 0·2eV. It is also apparent from Fig. 7.8(a) that an F_2^- ion resonance was also found in this energy range, accordingly reaction 85 is an additional possibility,

$$c\text{-}C_4F_8 + e_{9.8eV} \xrightarrow{85} c\text{-}C_4F_8^{-***} \longrightarrow F^-, F_2^-, CF_2^-, \ldots\ldots$$

Negative ion formation in $c\text{-}C_4F_8$ has been previously investigated by Bibby and Carter.[124,125] The F^- and CF_3^- ionisation efficiency curves were reported and shown to exhibit coincident maxima at 5·0 ± 0·2eV and to onset at 3·7 (with a tail extending to 1·8 ± 0·1eV) and 3·9 ± 0·1eV respectively. These values are in agreement with those measured in this study and which are shown in Table 7.11.

Table 7.11. Appearance potential data for $c\text{-}C_4F_8$.

Ion	Appearance Potential(eV)	Peak Maximum(eV)	Peak Width at ½-height(eV)
F^-	3·7 ± 0·1	4·95 ± 0·1	1·2 ± 0·1
	6·6 ± 0·2	7·4 ± 0·2	-
	7·5 ± 0·2	8·6 ± 0·2	1·2 ± 0·2
	10·0 ± 0·2	10·8 ± 0·2	1·5 ± 0·2
F_2^-	4·0 ± 0·1	4·95 ± 0·1	1·2 ± 0·1
	6·3 ± 0·3	8·5 ± 0·3	)
	9·3 ± 0·3	10·4 ± 0·3	) doublet
CF_2^-	3·85 ± 0·1	4·95 ± 0·1	1·1 ± 0·1
	7·2 ± 0·3	8·8 ± 0·1	1·3 ± 0·2
	9·7 ± 0·2	11·2 ± 0·2	1·3 ± 0·2
CF_3^-	3·85 ± 0·1	4·95 ± 0·1	1·3 ± 0·1
$C_3F_5^-$	3·35 ± 0·1	4·35 ± 0·1	0·9 ± 0·1
$C_4F_8^-$	0·0 ± 0·1	0·45 ± 0·1	0·5 ± 0·1

The CF_3^- and $C_3F_5^-$ ions are formed with single sharp resonance peaks onsetting at 3·85 ± 0·1 and 3·35 ± 0·1eV respectively. The observation of a CF_3 ion both in the positive[124,125] and negative ion mass spectra of c-C_4F_8 and a linear dependence of the CF_3^- ion current on source pressure at the capture peak maximum clearly indicates formation by a process involving an intramolecular rearrangement in which the ring is broken and a fluorine atom transferred to form a terminal CF_3 group (not necessarily in that order). The electron is simultaneously captured by either the CF_3 or C_3F_5 fragment in one of the following complementary reactions,

$$c\text{-}C_4F_8 + e \xrightarrow{2} CF_3^- + C_3F_5$$
$$\xrightarrow{86} C_3F_5^- + CF_3$$

In the absence of excess energy, the electron affinity of the C_3F_5 radical may then be estimated from the following expression; $A(CF_3^-) + E(CF_3) = A(C_3F_5^-) + E(C_3F_5)$, where $E(CF_3)$ is taken to be 2·0 ± 0·1eV,[4,17,119,122] to be 2·5 ± 0·3eV. This value may be compared to others of 2·7 ± 0·2 and ≥ 2·4 ± 0·3eV deduced for the same species formed from C_3F_6 and C_4F_8-2 respectively. Reactions 2 and 86 are therefore attributed to ion formation at 3·85 ± 0·1 and 3·35 ± 0·1eV respectively. Reversing this argument and setting 3·85 ± 0·1eV equal to the minimum enthalpy requirement of reaction 2, the heat of formation of the C_3F_5 radical is estimated to be ≤ -4·95 ± 0·3eV. This does not compare favourably with the values deduced for the same species,

C_3F_5, formed from C_3F_6 and C_4F_8-2 i.e. $\leq$ -6·8 $\pm$ 0·2 and $\leq$ -7·3 $\pm$ 0·6eV respectively.

The agreement found between the electron affinities appeared to indicate that a single C_3F_5 structure was probably involved in each case although this is difficult to reconcile with the heat of formation deduced for C_3F_5 in this present section. The structure suggested from ion formation in C_3F_6 was CF_3CCF_2, which is probably resonant with the structure suggested from ion formation in C_4F_8-2, CF_3CFCF and indeed equivalent values for both $E(C_3F_5)$ and $\Delta H_f(C_3F_5)$ are calculated for each case. The discrepancy in the present case must therefore result from one of the following possibilities; (i) errors in the thermochemical data used in the calculations is responsible for the discrepancy found or (ii) the structure of the C_3F_5 radical involved in reactions 2 and 86 is different and non-resonant with the species involved in reactions 5 and 53. A possible alternative structure might be CF_2CFCF_2 which would involve a minimum degree of rearrangement and in which the extra electron might be delocalised between the three carbon atoms thereby contributing greatly to stabilisation.

The F^- ion is shown in Fig. 7.8 to exhibit four principal appearance potentials, the first onsetting at 3·7 $\pm$ 0·1eV. Bibby and Carter[124,125] reported the F^- onset to be 1·8 $\pm$ 0·1eV which, from their ionisation efficiency curve, appears to result from a low cross-section tail on

the onset edge of the major peak. A low intensity F^- ion current was also detected in this study on the low energy side of the major peak, Fig. 7.8(a), but it was not observed to fall to zero and was still detected at zero electron energy. As a definite resonance could not be identified, the C_4F_7-F bond dissociation energy will be assumed to be not too different from those already measured in this study and therefore taken to be $5{\cdot}3 \pm 0{\cdot}2$eV i.e. equivalent to an appearance potential of $1{\cdot}9 \pm 0{\cdot}2$eV in accord with that reported by Bibby and Carter.[124,125] Using this value for $D(C_4F_7\text{-}F)$, the heat of formation of the C_4F_7 radical is estimated to be $\leq -11{\cdot}2 \pm 0{\cdot}4$eV from the reaction

$$c\text{-}C_4F_8 + e \xrightarrow{87} F^- + C_4F_7$$

There is no other value with which this can be compared.

Reactions 88 to 92 which have the estimated minimum enthalpy requirements shown are tentatively assigned to ion formation onsetting at $3{\cdot}7 \pm 0{\cdot}1$, $6{\cdot}6 \pm 0{\cdot}2$, $7{\cdot}5 \pm 0{\cdot}2$ and $10{\cdot}0 \pm 0{\cdot}2$eV respectively.

		ΔH_{min}(eV)
$c\text{-}C_4F_8 + e \xrightarrow{88}$	$F^- + CF + C_3F_6$	4·3
$\xrightarrow{89}$	$F^- + CF_2CF + C_2F_4$	4·5
$\xrightarrow{90}$	$F^- + CF_2 + C_3F_5$	6·3
$\xrightarrow{91}$	$F^- + CF_2CF + 2CF_2$	7·5
$\xrightarrow{92}$	$F^- + CF + 3CF_2$	10·2

The minimum enthalpy requirement of reaction 90 was calculated using the value of $\leq -4{\cdot}95 \pm 0{\cdot}3$eV estimated for $\Delta H_f(C_3F_5)$ above. Reactions 88, 91 and 92 are therefore suggested as

corresponding to the F^- ion dissociative capture channels of reactions 83, 84 and 85 respectively.

F_2^- ion formation occurs by three major resonances the first of which, onsetting at $4{\cdot}0 \pm 0{\cdot}1$eV, can be attributed to reaction 93 which involves formation of c-C_4F_6,

$$c\text{-}C_4F_8 + e \xrightarrow{93} F_2^- + c\text{-}C_4F_6$$

Using estimated thermochemical data[134] and taking $E(F_2) = 2{\cdot}9 \pm 0{\cdot}2$eV,[65] the minimum enthalpy requirement of reaction 92 is calculated to be $2{\cdot}7 \pm 0{\cdot}4$eV from which it is concluded that approximately 1eV of excess energy (depending on the uncertainties associated with the thermochemical data) is associated with reaction 93. Reactions 94 and 95 and/or 96, which have minimum enthalpy requirements of 6·3, 8·8 and 9·2eV respectively, are considered to be responsible for the measured appearance potentials at $6{\cdot}3 \pm 0{\cdot}3$ and $9{\cdot}3 \pm 0{\cdot}3$eV respectively.

$$\begin{aligned} c\text{-}C_4F_8 + e &\xrightarrow{94} F_2^- + C_2F_2 + C_2F_4 \\ &\xrightarrow{95} F_2^- + 2CF_2CF \\ &\xrightarrow{96} F_2^- + C_2F_2 + 2CF_2 \end{aligned}$$

The CF_2^- ion, which had not been observed previously (other than at 70eV) during this study, was formed extensively over the energy range investigated. Reactions 97 and 98, with respective minimum enthalpy requirements of $2{\cdot}7 - E(CF_2)$ and $5{\cdot}5 - E(CF_2)$eV, are the only energetically favourable reactions for initial CF_2^- ion formation at $3{\cdot}85 \pm 0{\cdot}1$eV.

$$c\text{-}C_4F_8 + e \xrightarrow{97} CF_2^- + C_3F_6$$
$$\xrightarrow{98} CF_2^- + CF_2 + C_2F_4$$

The following diverse values have been reported for the electron affinity of the CF_2 radical in the literature; $\geq 0{\cdot}2$,[119] $\geq 0{\cdot}6 \pm 1{\cdot}0$[113] and 2·65eV.[4] The exceptionally high value reported by Page and Goode[4] from a magnetron study of tetrafluoroethylene would infer that reactions 97 and 98 involve 3·8 and 1·0eV of excess energy respectively, reaction 97 thereby being very unlikely. The large difference between the electron impact values[113,119] and that reported by the magnetron technique[4] may be explained by incorrect identification of the ion species in the surface ionisation experiment, which did not facilitate mass identification. Assuming then that the electron impact values are more correct, reaction 97 is still shown to involve considerable excess energy, ~1·5 and ~2·0eV respectively for $E(CF_2) \geq 0{\cdot}2$ and $\geq 0{\cdot}6 \pm 1{\cdot}0$eV. In the event of no excess energy involvement in CF_2^- ion formation it will be assumed that reaction 98 is that responsible for CF_2^- ion formation at $3{\cdot}85 \pm 0{\cdot}1$eV, from which the electron affinity of the CF_2 radical is calculated to be $\leq 1{\cdot}6 \pm 0{\cdot}5$eV. Within the uncertainties quoted this value is in agreement with the electron impact values and it will be used to evaluate the energetics of reactions 99 and 100, the next least energetically demanding processes.

$$c\text{-}C_4F_8 + e \xrightarrow{99} CF_2^- + 3CF_2$$
$$\xrightarrow{100} CF_2^- + C_2F_4 + CF + F$$

Minimum enthalpy requirements of 6·9 ± 0·7 and 9·0 ± 0·8eV respectively are estimated, in good accord with the observed onsets at 7·2 ± 0·3 and 9·7 ± 0·2eV. Reactions 98, 99 and 100 are therefore assigned to account for CF_2^- ion formation at 3·85 ± 0·1, 7·2 ± 0·3 and 9·7 ± 0·3eV respectively and the electron affinity of the CF_2 radical is thereby suggested to be ≤ 1·6 ± 0·5eV.

The c-$C_4F_8^-$ ionisation efficiency curve was found to be a facsimile of the SF_6^- curve measured simultaneously and the attachment cross-section and autodetachment lifetime, which were both measured, have been presented and discussed in Chapter 4.

(h) Perfluoro-ortho-dimethylcyclobutane, $C_4F_6(CF_3)_2$.

Perfluorodimethylcyclobutane, C_6F_{12}, was found to exhibit a high dissociative capture cross-section, particularly in the energy range up to 5eV where the following negative ions were detected and measured; F^-, CF_3^-, $C_2F_5^-$, $C_4F_7^-$, $C_5F_9^-$, $C_6F_{11}^-$ and $C_6F_{12}^-$, the last of these is formed by associative electron capture and is shown in Fig. 7.9 with the SF_6^- curve measured simultaneously. The remaining ions are shown in Fig. 7.10 where the energy scale is calibrated against the appearance potential of the O^- ion formed from SO_2 at 4·2 and 6·6eV.

Lifshitz et al.[135] examined the negative ion breakdown curves resulting from thermal electron capture by $C_4F_6(CF_3)_2$ and reported the following ions in the 0 to 1eV energy range,

ION FORMATION IN $C_4F_6(CF_3)_2$

ASSOCIATNE CAPTURE

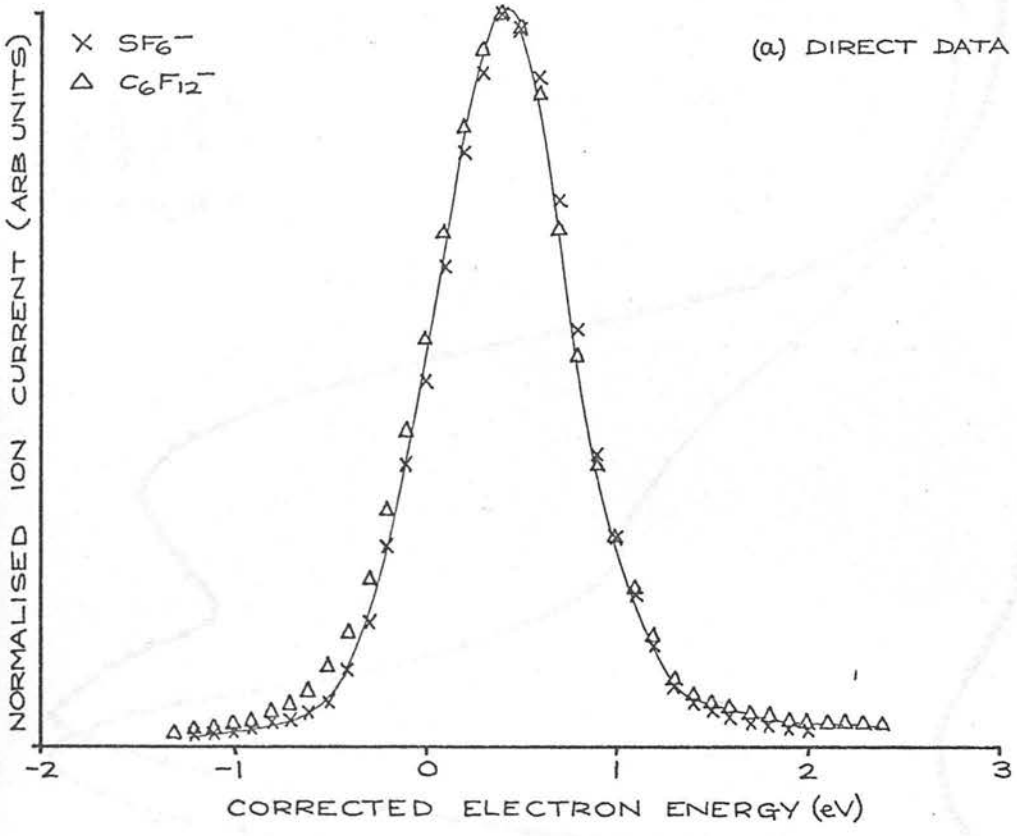

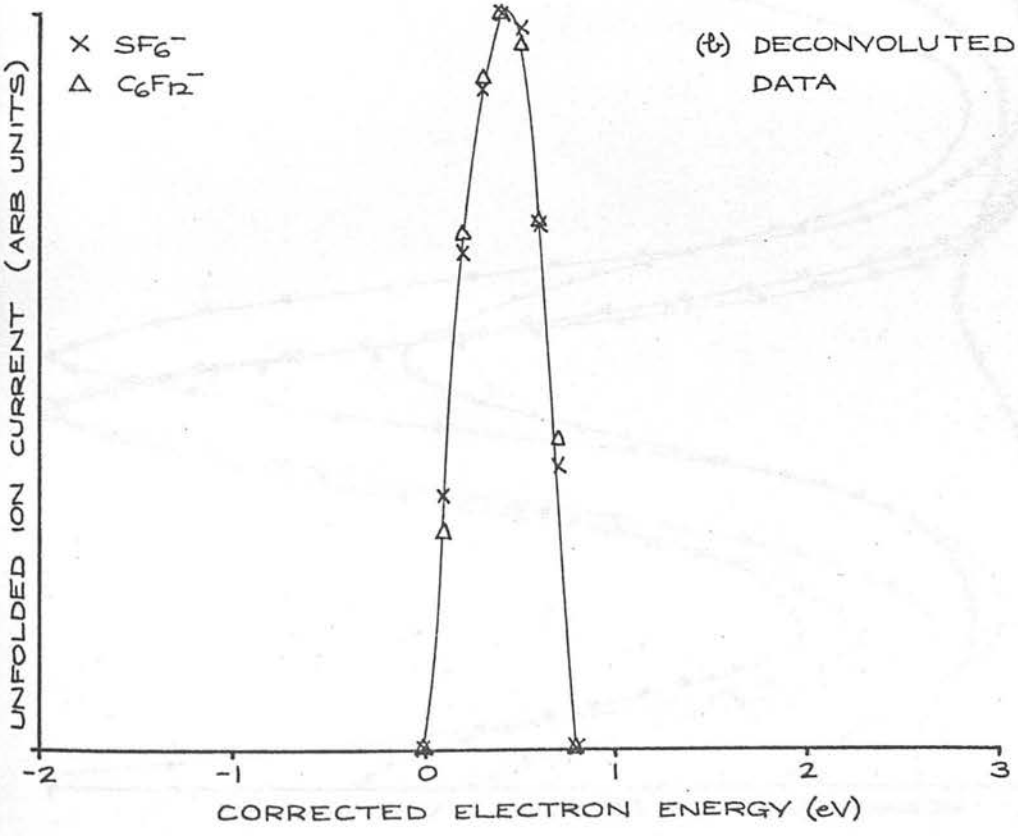

Fig 7.9

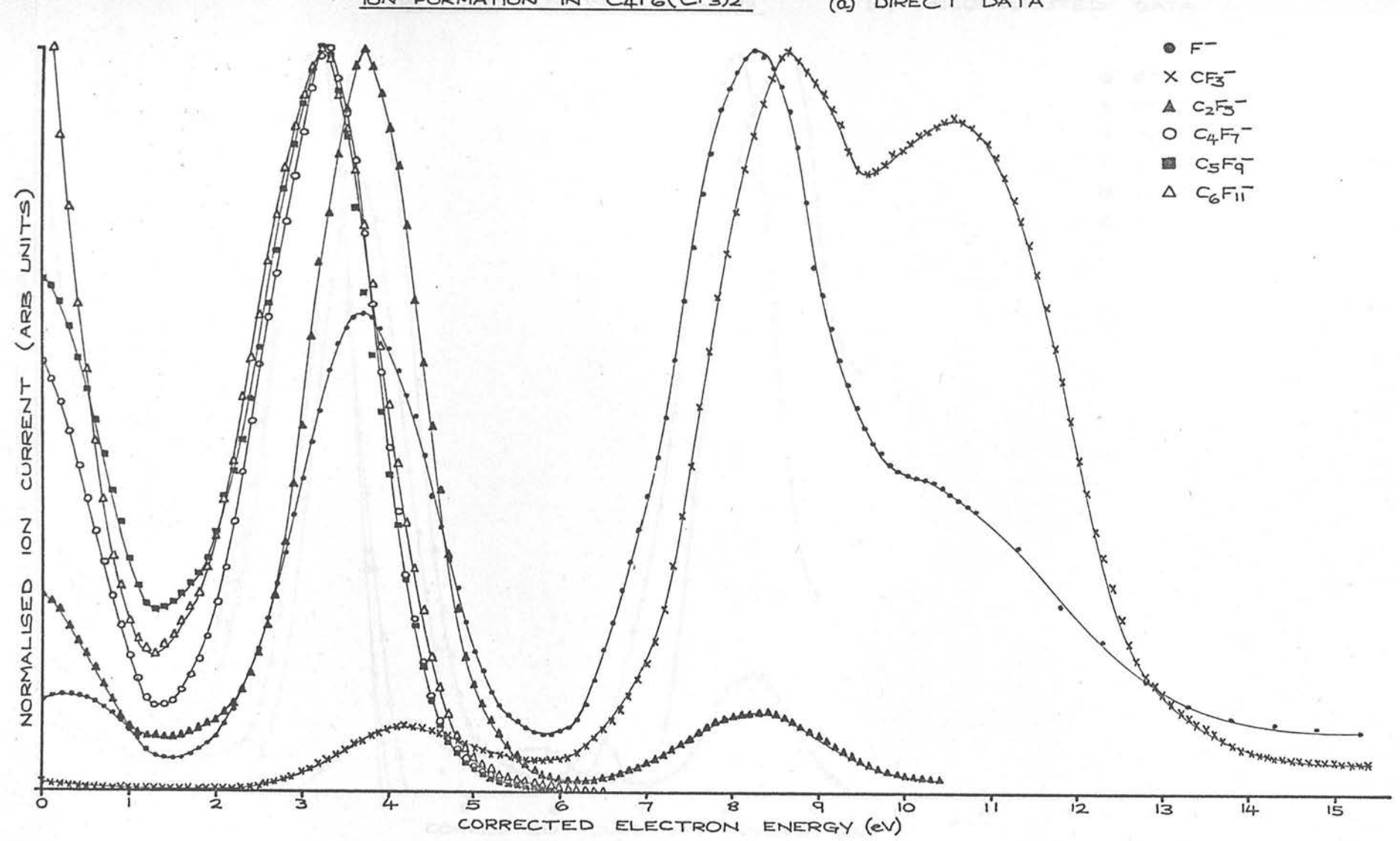
ION FORMATION IN $C_4F_6(CF_3)_2$
(a) DIRECT DATA
F^-
CF_3^-
$C_2F_5^-$
$C_4F_7^-$
$C_5F_9^-$
$C_6F_{11}^-$
NORMALISED ION CURRENT (ARB UNITS)
CORRECTED ELECTRON ENERGY (eV)
0
1
2
3
4
5
6
7
8
9
10
11
12
13
14
15

Fig 7.10

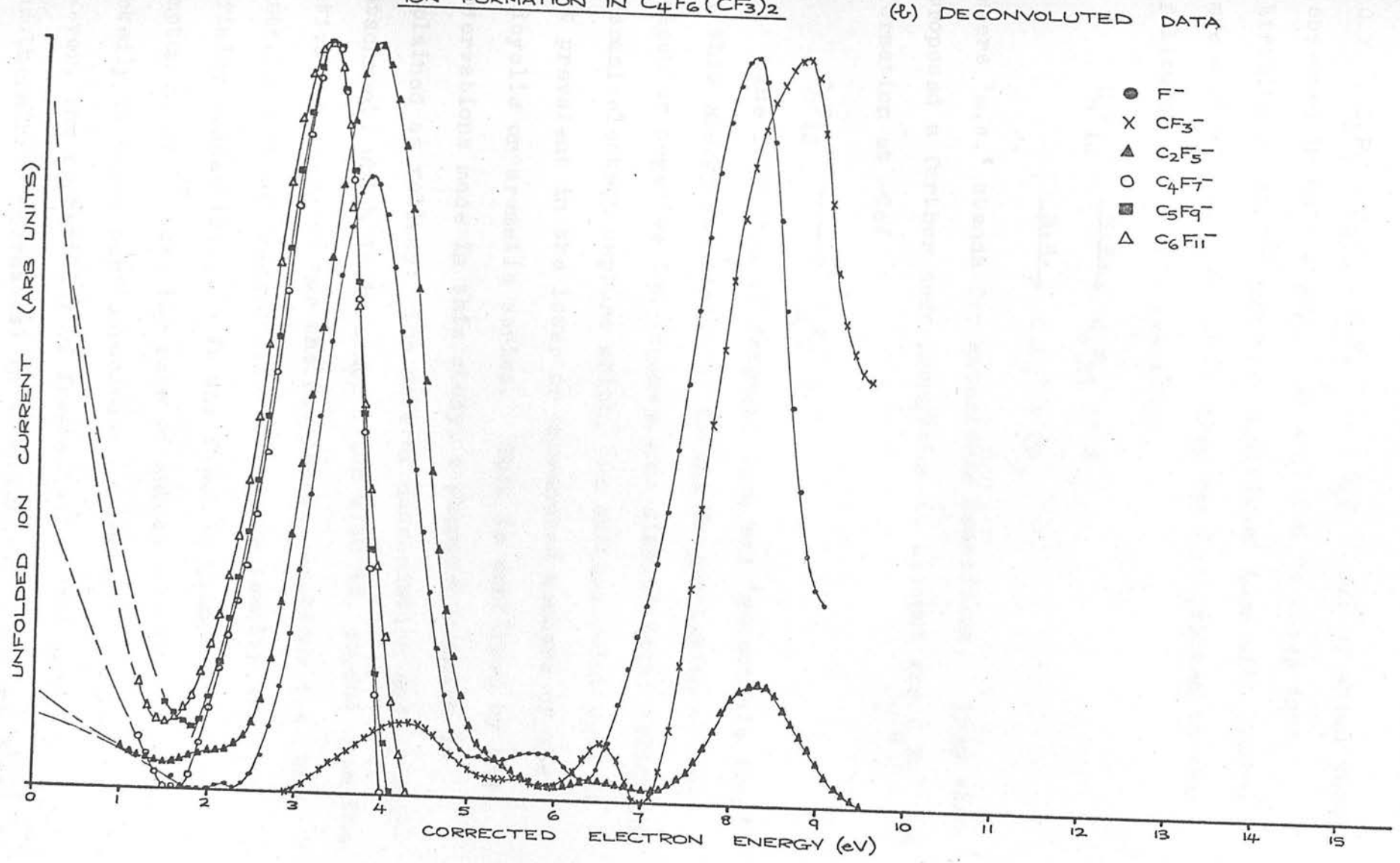
ION FORMATION IN $C_4F_6(CF_3)_2$
(b) DECONVOLUTED DATA
F^-
CF_3^-
$C_2F_5^-$
$C_4F_7^-$
$C_5F_9^-$
$C_6F_{11}^-$
UNFOLDED ION CURRENT (ARB UNITS)
0
1
2
3
4
5
6
7
8
9
10
11
12
13
14
15
CORRECTED ELECTRON ENERGY (eV)

Fig 7.10

$C_2F_5^-$, $C_4F_7^-$, $C_5F_9^-$, $C_6F_{11}^-$ and $C_6F_{12}^-$ all of which were observed in this study. In addition to these ions Lifshitz et al.[135] reported additional ions with apparent m/e = 263·2 and 177·9 which they have attributed to the following metastable reactions,

$$C_6F_{12}^- \xrightarrow{m.s.} C_6F_{11}^- + F$$

$$\xrightarrow{m.s.} C_5F_9^- + CF_3$$

where 'm.s.' stands for metastable transition. They also proposed a further such transition to account for $C_4F_7^-$ ion formation at ~0eV

$$C_6F_{12}^- \longrightarrow C_4F_7^- + ?$$

The formation of fragment ions and 'metastable ions' at this energy is attributed to the fragmentation of the molecular negative ion (spontaneous dissociation) following thermal electron capture which, the authors point out, is not prevalent in the lower or unbranched members of the alicyclic or aromatic series. This is confirmed by the observations made in this study, a phenomenon which is explained as follows: the rate of dissociation and of autodetachment, which is in competition with it, depend upon the activation energies for the respective reactions i.e. the exothermicity of fragmentation and the molecular electron affinity respectively. It was found in Chapter 4 and by Compton et al.[37] that the rate of autodetachment decreases markedly as these perfluorocarbon series are ascended, however, the probability of fragmentation increases (endothermicity decreases) in ascending these series until

fragmentation becomes evident, as for $C_4F_6(CF_3)_2$, despite the fact that the competing autodetachment process has a lower activation energy. Lifshitz et al.[135] estimated that the endothermicity of $C_6F_{11}^-$ ion formation from $C_4F_6(CF_3)_2$ for thermal electron capture is $0{\cdot}8 \pm 0{\cdot}2$eV.

This suggestion[135] is consistent with the observations in sections (b), (d), (e) and (f) that the lowest dissociating metastable molecular negative ion state appears at lower energies as the perfluorocarbon series are ascended: $C_3F_6^{-*}$ at $6{\cdot}2 \pm 0{\cdot}2$, c-$C_4F_6^{-*}$ at $5{\cdot}8 \pm 0{\cdot}2$, C_4F_8-2^{-*} at $4{\cdot}0 \pm 0{\cdot}2$, c-$C_4F_8^{-*}$ at $3{\cdot}9 \pm 0{\cdot}2$ and $C_4F_{10}^{-*}$ at $2{\cdot}1 \pm 0{\cdot}2$eV and now $C_6F_{12}^{-*}$ at ~0eV. Following the identification of such states in other perfluorocarbons reaction 101 is suggested for the observations made with $C_4F_6(CF_3)_2$.

$$C_6F_{12} + e_{\sim 0eV} \xrightarrow{101} C_6F_{12}^{-*} \longrightarrow F^-, CF_3^-, C_2F_5^-, C_4F_7^-, C_5F_9^-, C_6F_{11}^-, \ldots\ldots$$

It is further suggested (see Fig. 7.10(a)) that a second multichannel fragmentation is occurring from one or more metastable molecular negative ion states at ~$1{\cdot}5$eV where all ions appear in a band of overlapping resonances,

$$C_6F_{12} + e_{\sim 1{\cdot}5eV} \xrightarrow{102} C_6F_{12}^{-**} \longrightarrow F^-, CF_3^-, \ldots\ldots$$

Considering first the state at ~0eV; the relative ion intensities reflect the probability of the various dissociation channels a nd the following relative abundances were found; $C_6F_{11}^-$(100), $C_5F_9^-$(60), $C_4F_7^-$(50), F^-(28), $C_2F_5^-$(25) and CF_3^-(1), where $C_6F_{12}^-$(1000). The high

relative abundance of the $C_6F_{11}^-$ ion may be compared to the endothermicity of 0·8 ± 0·2eV estimated for this reaction by Lifshitz et al.[135] From this comparison it is apparent that the endothermicity for CF_3^- ion formation must be substantially higher than this, i.e. $D(C\text{-}CF_3) - E(CF_3)$, assuming $D(C\text{-}CF_3)$ ~4·0eV the endothermicity of this particular dissociation channel is expected to be ~2eV and the endothermicity of the remaining channels must therefore lie between 0·8 and 2·0eV.

The appearance potential data for the processes occurring above 1eV are given in Table 7.12. Because of the high background ion current in the energy region between the major resonance peaks at ~0eV and ~3eV, in some cases, namely F^- and $C_2F_5^-$, the possibility of spurious peaks appearing in the deconvoluted curve gave rise to some uncertainty in the identification of possible minor resonances in this region. The existence of such resonances, which would correspond to dissociation channels of reaction 101, will therefore be ignored and only the appearance potentials of the major peaks will be discussed.

If the F^- ion and $C_6F_{11}^-$ ion resonances, onsetting at 2·3 ± 0·1 and 1·5 ± 0·1eV respectively, correspond to the complementary reactions,

$$C_6F_{12} + e \xrightarrow{103} F^- + C_6F_{11}$$
$$\xrightarrow{104} C_6F_{11}^- + F$$

then, assuming that approximately the same amount of excess energy is involved in each case (endothermicity of reaction

Table 7.12. Appearance potential data for $C_4F_6(CF_3)_2$

Ion	Appearance Potential(eV)	Peak Maximum(eV)	Peak Width at ½-height(eV)
F^-	2·3 ± 0·1	3·75 ± 0·1	1·0 ± 0·1
	6·4 ±0·2	8·1 ± 0·2	1·2 ± 0·1
	~9·4	10·4 ± 0·3	-
CF_3^-	2·9 ± 0·1	4·3 ± 0·2	1·3 ± 0·2
	7·0 ± 0·1	8·6 ± 0·3	)
	9·5 ± 0·2	10·5 ± 0·2	)doublet
$C_2F_5^-$	2·1 ± 0·2	3·75 ± 0·1	1·3 ± 0·1
	7·1 ± 0·2	8·3 ± 0·2	1·1 ± 0·1
$C_4F_7^-$	1·7 ± 0·1	3·25 ± 0·1	1·0 ± 0·1
$C_5F_9^-$	1·8 ± 0·1	3·25 ± 0·1	1·0 ± 0·1
$C_6F_{11}^-$	1·5 ± 0·1	3·25 ± 0·1	1·2 ± 0·1
$C_6F_{12}^-$	0·0 ± 0·1	0·4 ± 0·1	0·5 ± 0·1

104 is ~0·8eV) the electron affinity of the C_6F_{11} radical is estimated to be 4·2 ± 0·2eV. This is in reasonable accord with the value of ~3·5eV estimated by Lifshitz et al.[135] The discrepancy between these two values may result from either the assumptions made by Lifshitz et al.[135] such as D(C-F) = 99 Kcals.mole^{-1}, or unequal excess energy in the above reactions.

Because of the number and complexity of the possible fragmentation reactions involving F^- ion formation in the 2 - 15eV energy range and the large uncertainties associated with the thermochemical data, when available, no attempt at further process identification will be made.

It was suggested in section (a) and later confirmed by Lifshitz et al.[135] that CF_3^- and $C_5F_9^-$ are formed by the complementary reactions,

$$C_6F_{12} + e \xrightarrow{105} CF_3^- + C_5F_9$$
$$\xrightarrow{106} C_5F_9^- + CF_3$$

From the expression, $A(CF_3^-) + E(CF_3) = A(C_5F_9^-) + E(C_5F_9)$ where $E(CF_3) = 2{\cdot}0 \pm 0{\cdot}1$eV,[4,17,119,122] $A(CF_3^-) = 2{\cdot}9 \pm 0{\cdot}1$ and $A(C_5F_9^-) = 1{\cdot}8 \pm 0{\cdot}1$eV, the electron affinity of the C_5F_9 radical is deduced to be $3{\cdot}1 \pm 0{\cdot}3$eV, in exact agreement with the value of 3·1 estimated by Lifshitz et al.[135]

Lifshitz et al.[135] also showed that the $C_2F_5^-$ and $C_4F_7^-$ ions originate from the reactions predicted in section (a),

$$C_6F_{12} + e \xrightarrow{3} C_2F_5^- + C_4F_7$$
$$\xrightarrow{107} C_4F_7^- + C_2F_5$$

Substituting the values $E(C_2F_5)$ average (measured above) = $2{\cdot}2 \pm 0{\cdot}2$, $A(C_2F_5^-) = 2{\cdot}1 \pm 0{\cdot}2$ and $A(C_4F_7^-) = 1{\cdot}7 \pm 0{\cdot}1$eV into the appropriate expression the electron affinity of the C_4F_7 radical is estimated to be $2{\cdot}6 \pm 0{\cdot}5$eV. This value is in reasonable agreement with that of ~3·5eV deduced for the same species formed from C_4F_8-2 by reaction 57.

The attachment cross-section and autodetachment lifetime of the $C_6F_{12}^-$ molecular negative ion shown in Fig. 7.9 have been presented and discussed in Chapter 4.

(i) Perfluorocyclopentene, c-C_5F_8.

c-C_5F_8 was examined briefly in order to provide a comparison between four and five-membered ring systems towards electron capture. c-C_5F_8 was found to exhibit a low cross-section for negative ion formation and the only ions detected at low electron energies; F^-, $C_3F_3^-$, $C_5F_7^-$ and $C_5F_8^-$, were formed in the ratio 1000:25:8:90 at their respective capture maxima. The CF_3^- ion, and the anticipated complementary species $C_4F_5^-$, were both detected at 70eV but with abundances of less than 0·1% of the $C_5F_8^-$ ion current. This observation is in complete contrast to the high abundance rearrangement ions detected in all three four-membered ring systems studied and suggests that the five-membered ring is sufficiency stable (strain free) to undergo dissociative electron capture in the absence of a simultaneous intramolecular rearrangement involving ring cleavage.

The $C_3F_3^-$ ion, which was formed abundantly at low electron energies, may result from a rearrangement process although the most probable complementary ion accompanying such a reaction, $C_2F_5^-$, was not detected at high or low energies. The experimental ionisation efficiency curves are shown in Fig. 7.11 where the energy scale is calibrated against the appearance potentials of the O^- ion formed from SO_2 at 4·2 and 6·6eV and the SF_6^- ion formed from SF_6 at 0·0eV.

In a previous investigation of c-C_5F_8 Bibby and Carter[124] identified the F^-, $C_5F_6^-$, $C_5F_7^-$ and $C_5F_8^-$ ions at low electron

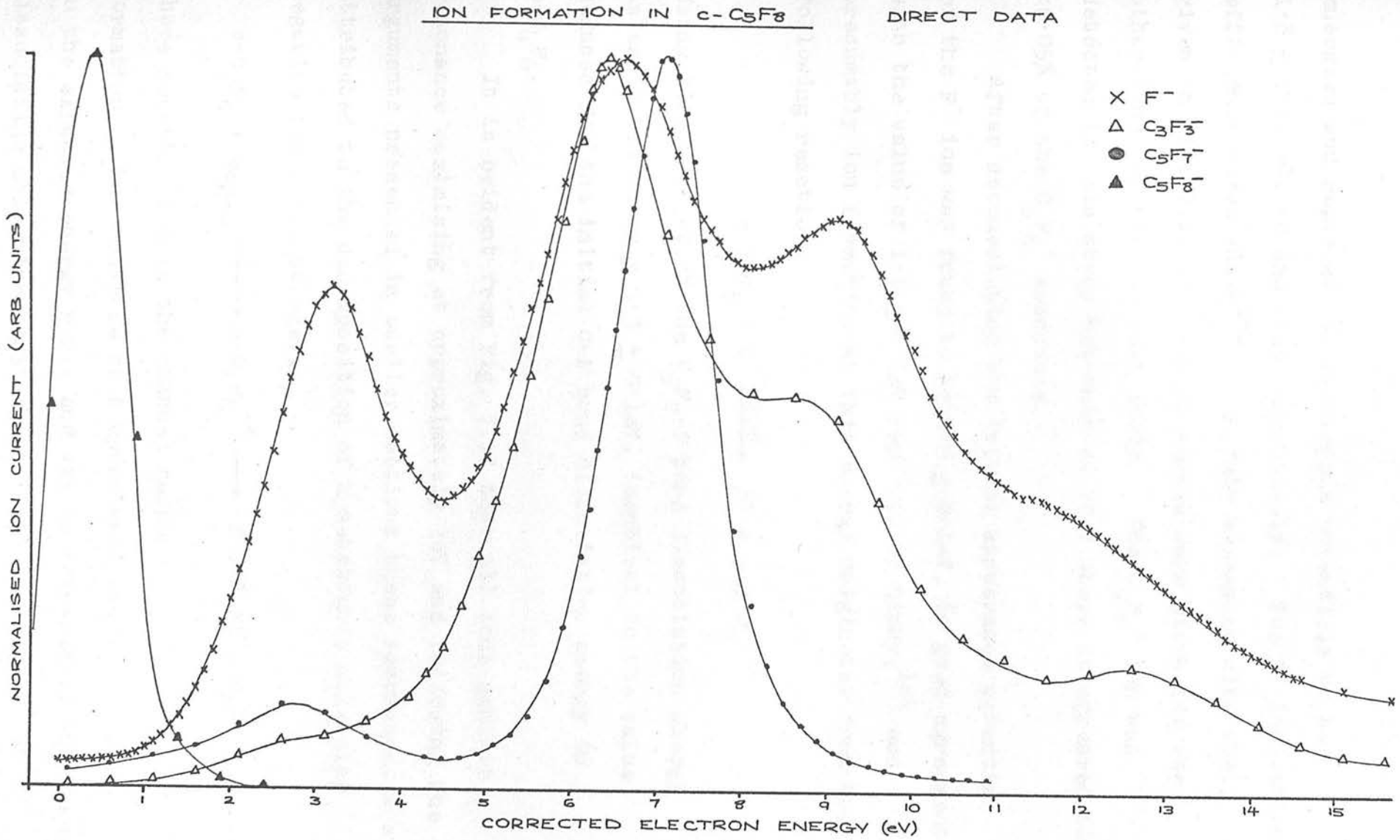
ION FORMATION IN c-C5F8
DIRECT DATA
F⁻
C3F3⁻
C5F7⁻
C5F8⁻
NORMALISED ION CURRENT (ARB UNITS)
0
1
2
3
4
5
6
7
8
9
10
11
12
13
14
15
CORRECTED ELECTRON ENERGY (eV)

Fig 7.11

energies and reported the appearance potentials to be $1{\cdot}8 \pm 0{\cdot}1$, ~0, ~0 and ~0eV respectively. The F^- ionisation efficiency curve shown[124] is in fair agreement with that given in Fig. 7.11 although no curves were given for the other ions reported in that study. The $C_5F_6^-$ ion was detected in this study but only at 70eV where it appeared to <0·05% of the $C_5F_8^-$ abundance.

After deconvolution the initial appearance potential of the F^- ion was found to be $1{\cdot}9 \pm 0{\cdot}1$eV, in good agreement with the value of $1{\cdot}8 \pm 0{\cdot}1$eV reported by Bibby,[124] and presumably ion formation at this energy originates from the following reaction,

$$c\text{-}C_5F_8 + e \xrightarrow{108} F^- + c\text{-}C_5F_7$$

Using E(F) = 3·4eV,[36] the C_5F_7-F bond dissociation energy is estimated to be $\leq 5{\cdot}3 \pm 0{\cdot}1$eV, identical to the value deduced for the initial C-F bond dissociation energy in $c\text{-}C_4F_6$.

It is evident from Fig. 7.11 that all ions exhibit a resonance maximising at approximately 3eV and following the arguments presented in earlier sections these resonances are attributed to the decomposition of a metastable molecular negative ion state at ~2eV,

$$c\text{-}C_5F_8 + e_{\sim 2{\cdot}0} \xrightarrow{109} c\text{-}C_5F_8^{-*} \longrightarrow F^-, C_3F_3^-, C_5F_7^-, \ldots\ldots$$

where reaction 108 is the channel responsible for F^- ion formation. The presence of a metastable state at ~2eV is in the expected energy range and may be compared to the lowest dissociating molecular negative ion states, $c\text{-}C_4F_6^{-*}$ at

$5{\cdot}8 \pm 0{\cdot}2$ and $c\text{-}C_4F_6(CF_3)_2^{-*}$ at ~0eV. The appearance of a second $C_5F_7^-$ resonance onsetting at $6{\cdot}2 \pm 0{\cdot}3$eV suggests the presence of a second metastable state at this energy where reaction 111 is one of the dissociative capture channels,

$$c\text{-}C_5F_8 + e_{\sim 6{\cdot}2} \xrightarrow{110} c\text{-}C_5F_8^{-**} \xrightarrow{111} C_5F_7^{-*} + F^*$$

involving ~4eV of excess energy distributed as internal excitation and/or kinetic energy between the fragments.

Further coincident $C_3F_3^-$ and F^- resonances at ~9 and ~12·5eV may reflect other dissociating states of $C_5F_8^-$ but in the absence of a more detailed investigation these suggestions remain speculative.

The $C_5F_8^-$ molecular negative ion was examined in detail and the results have been fully discussed in Chapter 4.

(j) Perfluoronormalhexane, C_6F_{14}.

$n\text{-}C_6F_{14}$ was investigated as part of a final year B.Sc. project by Miss J.A. Logan and the general findings are in accord with the behaviour anticipated from the above sections. Because of instrumental malfunctions prevalent during the course of that study the appearance potential data is subject to uncertainties considerably exceeding those normally obtained, consequently this data will not be presented for detailed discussion. However, it was found that most ions exhibited single resonances onsetting in the energy range between 1 and ~1·5eV leading to the suggestion of a metastable molecular negative ion state in this energy range, in accord with the trend already established above,

$$n\text{-}C_6F_{14} + e_{1\text{-}1\cdot5eV} \xrightarrow{112} n\text{-}C_6F_{14}^{-*} \longrightarrow F^-,\ CF_3^-,\ldots\ldots$$

The fragmentation pattern follows that established above for $n\text{-}C_3F_8$ and $n\text{-}C_4F_{10}$ where negative ion formation occurs by the successive rupture of C-C bonds and the following ions were detected at low electron energies; F^-, CF_3^-, $C_2F_5^-$, $C_3F_7^-$, $C_4F_9^-$, $C_5F_{11}^-$, $C_6F_{13}^-$ and $C_6F_{14}^-$.

(k) Summary

It has become increasingly apparent during the course of the work described in this chapter that as the perfluorocarbon series are ascended the following points are realized; (i) the average dissociative electron capture cross-section increases, (ii) there is an increase in the variety of negative ion species formed and the complexity of the reaction mechanisms involved, (iii) negative ion formation as a result of the multichannel decomposition of a metastable state of the molecular negative ion takes place at progressively lower energies and (iv) parent ion intensity and autodetachment lifetimes increase.

Although the amount of information which may be obtained from electron impact experiments in the higher perfluorocarbons increases enormously as the series are ascended the lack of accurate thermochemical data (when available at all) renders reaction identification and therefore the deduction of unknown radical parameters virtually impossible, e.g. for $C_4F_6(CF_3)_2$ only the initial ionisation processes may be confidently identified.

The dissociative capture processes which have been established in the course of this chapter and identified with the lowest dissociating state of their molecular negative ion are listed below in order of decreasing energy:

section (b);

$$C_3F_6 + e_{6\cdot2eV} \xrightarrow{4} C_3F_6^{-*} \xrightarrow{5} F^{-*} + C_3F_5^{*}$$

$$\xrightarrow{9} F^- + CF_3CF + CF$$

$$\xrightarrow{16} C_3F_5^{-*} + F^*$$

$$\xrightarrow{18} CF_3^- + CF + CF_2$$

$$\xrightarrow{19} CF_3^- + F + CCF_2$$

section (f);

$$c\text{-}C_4F_6 + e_{5\cdot8eV} \xrightarrow{71} c\text{-}C_4F_6^{-*} \xrightarrow{75} F^- + C_2F_2 + CFCF_2$$

$$\xrightarrow{80} C_4F_5^{-*} + F^*$$

$$\xrightarrow{81} C_3F_3^- + CF_2 + F$$

section (d);

$$C_4F_8\text{-}2 + e_{4\cdot0eV} \xrightarrow{31} C_4F_8\text{-}2^{-*} \xrightarrow{34} F^{-*} + C_4F_7^{*}$$

$$\xrightarrow{42} F_2^{-*} + C_4F_6\text{-}2^{*}$$

$$\xrightarrow{47} CF_3^{-*} + C_3F_5^{*}$$

$$\longrightarrow C_3F_3^- + ?$$

$$\xrightarrow{53} C_3F_5^{-*} + CF_3^{*}$$

section (g);

$$c\text{-}C_4F_8 + e_{3\cdot9eV} \xrightarrow{83} c\text{-}C_4F_8^{-*} \xrightarrow{2} CF_3^- + C_3F_5$$

$$\xrightarrow{86} C_3F_5^{-*} + CF_3^{*}$$

$$\xrightarrow{88} F^- + CF + C_3F_6$$

$$\xrightarrow{93} F_2^{-*} + c\text{-}C_4F_6^{*}$$

$$\xrightarrow{98} CF_2^- + CF_2 + C_2F_4$$

section (e);

$$C_4F_{10} + e_{2\cdot1eV} \xrightarrow{58} C_4F_{10}^{-*} \xrightarrow{60} F^- + C_4F_9$$
$$\xrightarrow{63} CF_3^- + C_3F_7$$
$$\xrightarrow{66} C_2F_5^- + C_2F_5$$
$$\xrightarrow{68} C_3F_7^- + CF_3$$
$$\xrightarrow{69} C_4F_9^- + F$$

section (i);

$$c\text{-}C_5F_8 + e_{\sim2eV} \xrightarrow{109} c\text{-}C_5F_8^{-*} \longrightarrow F^-, C_3F_3^-, C_5F_7^-, \ldots\ldots$$

section (j);

$$C_6F_{14} + e_{1\text{-}1\cdot5eV} \xrightarrow{112} C_6F_{14}^{-*} \longrightarrow F^-, CF_3^-, C_2F_5^-, C_3F_7^-,$$
$$C_4F_9^-, C_5F_{11}^-, C_6F_{13}^-.$$

section (h);

$$C_4F_6(CF_3)_2 + e_{\sim0eV} \xrightarrow{101} C_4F_6(CF_3)_2^{-*} \longrightarrow C_6F_{11}^- + F$$
$$\longrightarrow C_5F_9^- + CF_3$$
$$\longrightarrow C_4F_7^- + C_2F_5$$
$$\longrightarrow C_2F_5^-, CF_3^-, F^-.$$

No dissociating metastable molecular negative ion state was identified in the study of ion formation in C_3F_8, although the existence of such a state, perhaps with a low cross-section for decomposition, is not excluded. A brief investigation of negative ion formation in hexafluorobutyne-2, C_4F_6-2, showed that all the ions which were formed at low electron energies, F^-, CF_3^-, $C_3F_3^-$ and $C_4F_5^-$ exhibited coincident resonances onsetting in the energy range between 5·0 and 5·5eV. The fdlowing reaction is therefore added to those presented above,

$$C_4F_6\text{-}2 + e_{5\cdot0\text{-}5\cdot5eV} \xrightarrow{113} C_4F_6\text{-}2^{-*} \longrightarrow F^-,\ CF_3^-,\ C_3F_3^-,\ C_4F_5^-,\ldots\ldots$$

Finally a comment on the structures of the metastable molecular negative ion states involved in these processes. In the above reaction schemes the transient intermediate species have been depicted as c-$C_4F_6^{-*}$, $C_4F_6^{-*}$, $C_4F_6(CF_3)_2^{-*}$ etc. inferring retention of the ground state neutral molecular structure. It is recognised that this is clearly not the case and that distortion of the neutral molecular framework in the excited negative ion states is inevitable. However, it has been found in this study that each fluorocarbon isomer exhibits distinct fragmentation behaviour and each isomer has a distinct autodetachment lifetime and attachment cross-section for thermal electron capture. It is therefore evident that 'common-ion states' i.e. from C_4F_6-2 and c-C_4F_6 or from C_4F_8-2 and c-C_4F_8, do not play a significant role as intermediates following the interaction of slow electrons (0 - 15eV) with the perfluorocarbon molecules examined in this study.

CHAPTER 8

THE FLUOROALDEHYDES; CF_3CHO, C_2F_5CHO and C_3F_7CHO, the FLUOROKETONES; CF_3COCH_3 and $(CF_3)_2CO$ and the FLUORONITROXIDE $(CF_3)_2NO$

This chapter has been subdivided into three sections; (a) the fluoroaldehydes, (b) the fluoroketones and (c) the stable free-radical bis-trifluoromethylnitroxide.

(a) The fluoroaldehydes

(i) Trifluoroacetaldehyde, CF_3CHO

A large variety of dissociative capture ions were formed from CF_3CHO at low electron energies and the ions detected with intensities amenable to investigation were O^-, F^-, CF_2^-, CF_3^-, $C_2F_2^-$, $C_2F_3^-$ and CF_2CO^- which were formed in the ratio 45:1000:5:72:20:4:4 at 70eV. At 10eV, this ratio was 63:840:4:900:1000:160:3. The experimental and deconvoluted ionisation efficiency curves are shown in Figs. 8.1 and 8.2 where the energy scale is calibrated against the appearance potential of the O^- ion formed from SO_2 at 4·2 and 6·6eV. The appearance potential data are given below in Table 8.1.

The heat of formation of trifluoroacetaldehyde is not known directly, however, an approximate value may be estimated using the group additivity tables compiled by Benson et al.[136] This method gave a value of -188·6 Kcals/mole or -8·2eV for $\Delta H_f(CF_3CHO)$ with an uncertainty not expected to exceed $\pm$ 0·5eV.

ION FORMATION IN CF_3CHO (LOW ENERGY)

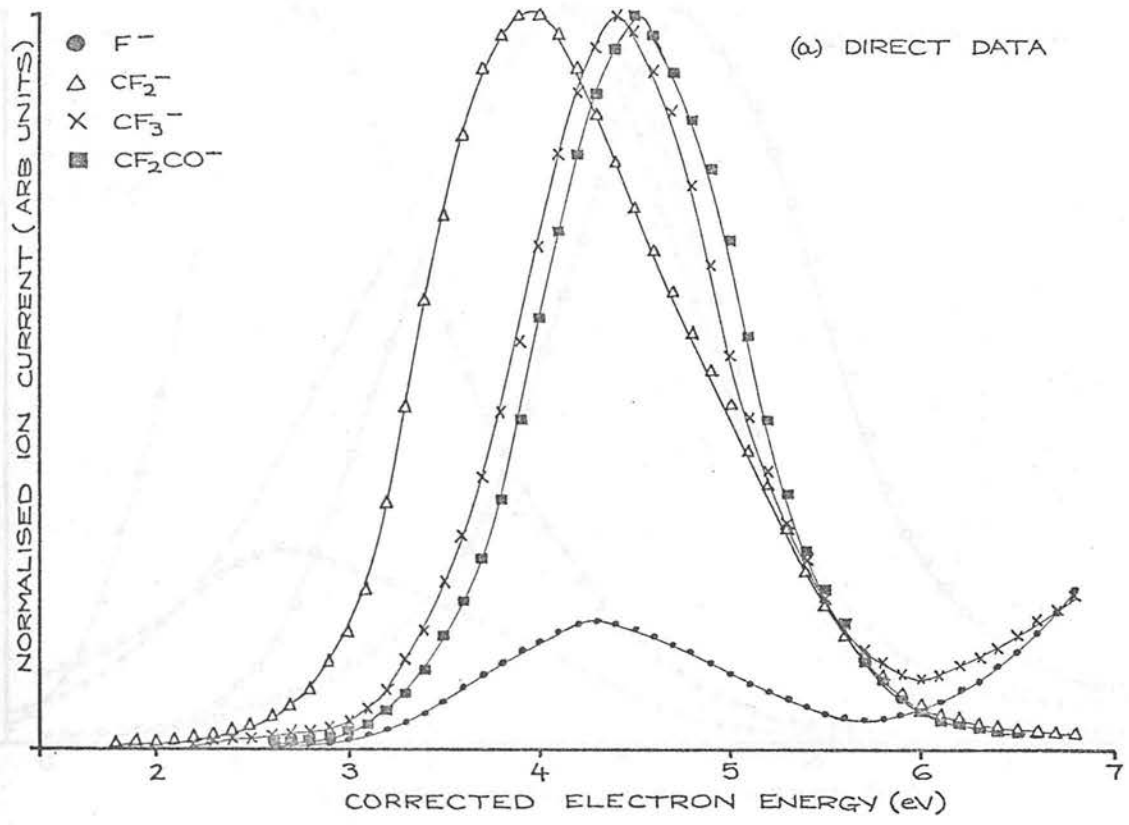

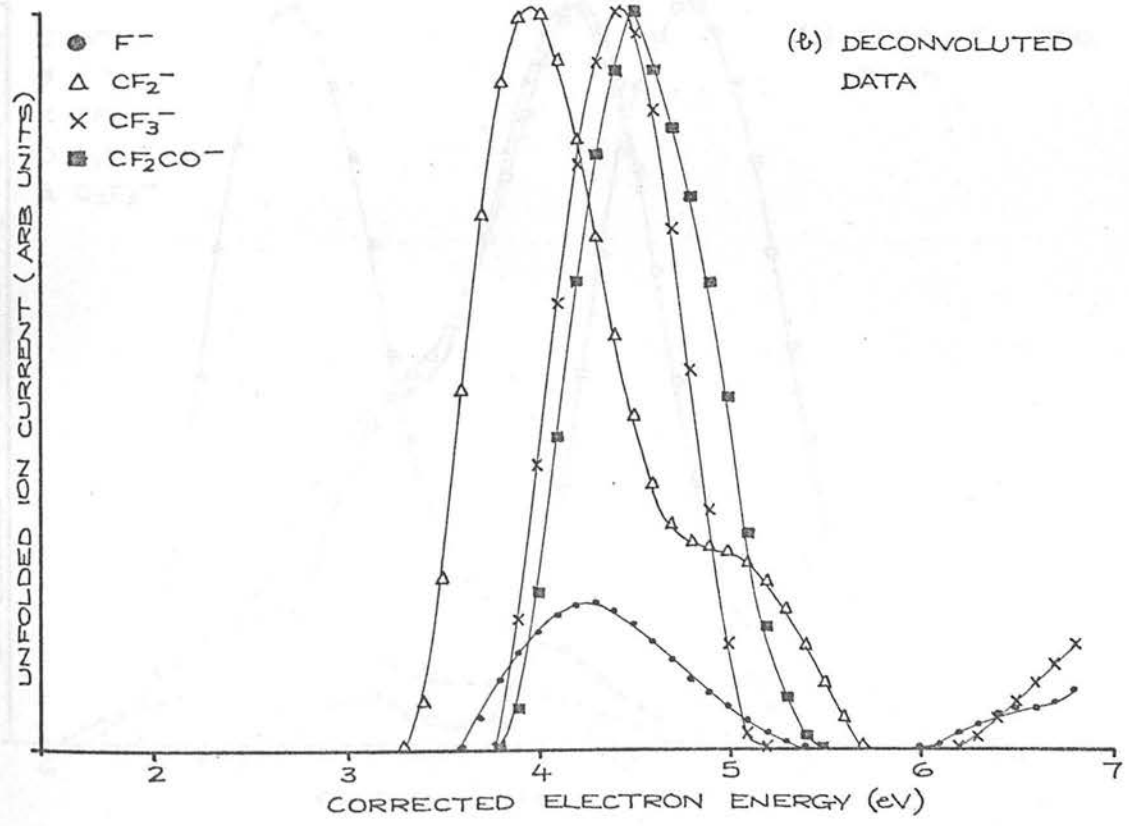

Fig 8.1

ION FORMATION IN CF_3CHO (HIGH ENERGY)

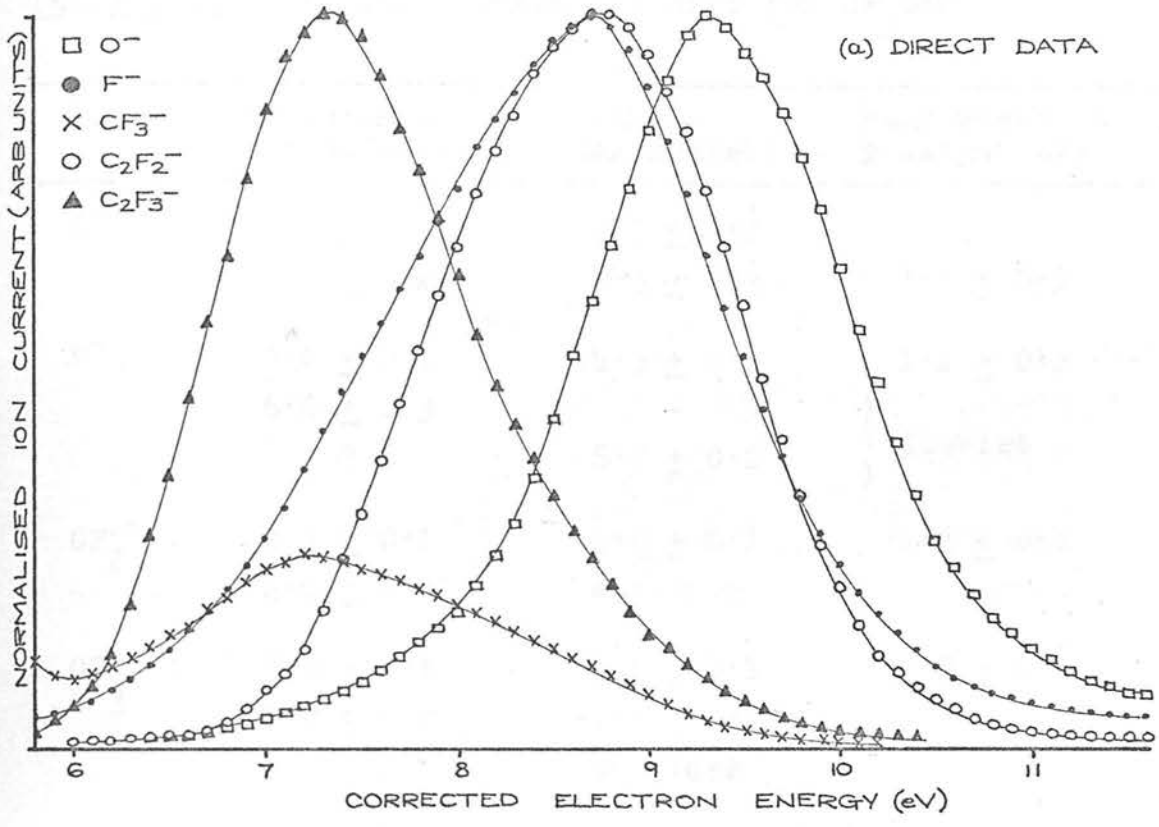

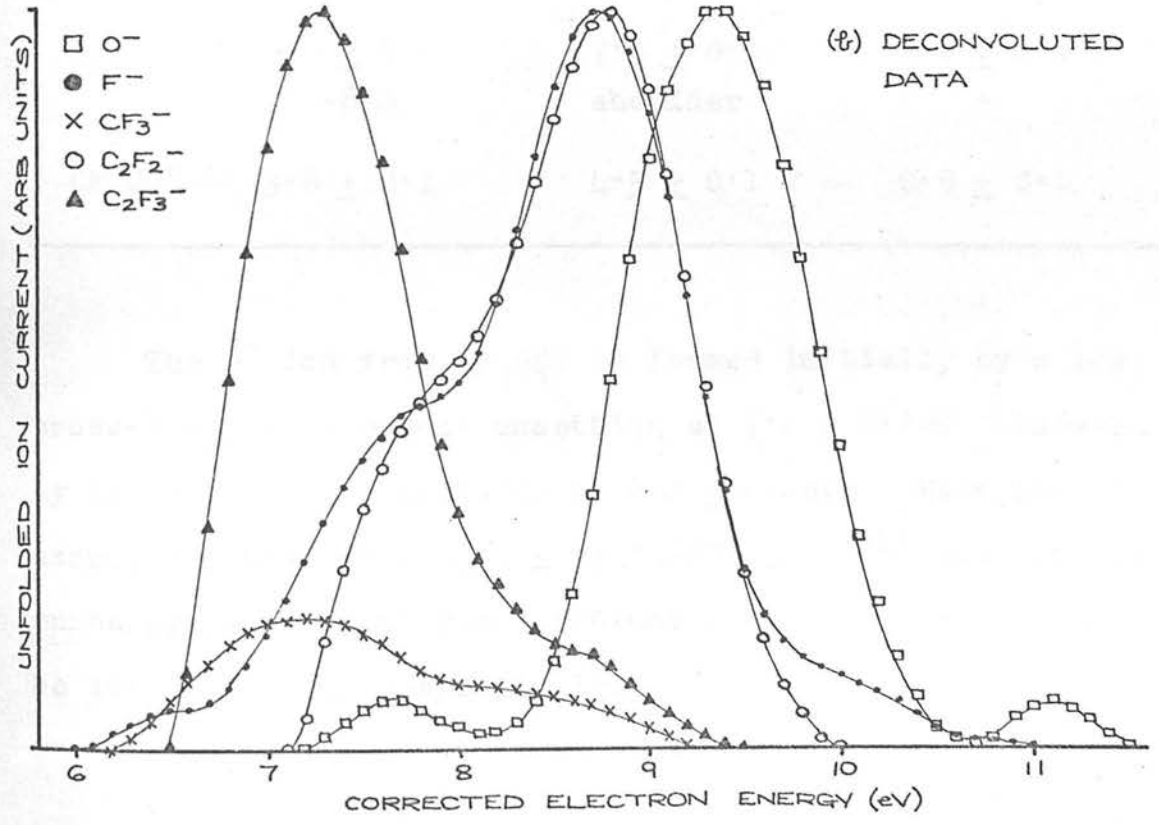

Fig 8.2

Table 8.1. Appearance potential data for CF_3CHO

Ion	Appearance Potential(eV)	Peak Maximum(eV)	Peak Width at ½-height(eV)
O^-	7·2 ± 0·2	7·7 ± 0·2	-
	8·1 ± 0·2	9·3 ± 0·2	1·1 ± 0·2
F^-	3·6 ± 0·1	4·3 ± 0·1	1·1 ± 0·2
	6·6 ± 0·3	-	)
	~7·8	8·7 ± 0·2	) doublet
			)
CF_2^-	3·3 ± 0·1	4·0 ± 0·1	0·8 ± 0·1
	4·6 ± 0·3	shoulder	-
CF_3^-	3·8 ± 0·1	4·4 ± 0·1	0·8 ± 0·1
	6·2 ± 0·2	7·2 ± 0·2	-
	~8·0	shoulder	-
$C_2F_2^-$	7·1 ± 0·1	shoulder	)
	~7·8	8·8 ± 0·2	) doublet
$C_2F_3^-$	6·5 ± 0·1	7·3 ± 0·1	1·0 ± 0·1
	~8·0	shoulder	-
CF_2CO^-	3·8 ± 0·1	4·5 ± 0·1	0·9 ± 0·1

The O^- ion from CF_3CHO is formed initially by a low cross-section resonance onsetting at 7·2 ± 0·2eV followed by the major peak onsetting at 8·2 ± 0·2eV. With the assumption that $\Delta H_f(CF_2C) \simeq \Delta H_f(CFCF) \simeq 0eV$[128] the minimum enthalpy requirement for reactions 2 and 3 are estimated to be 10·7 and 6·6eV respectively.

$$CF_3CHO + e \xrightarrow{1} O^- + CF_3CH$$
$$\xrightarrow{2} O^- + CF_3 + CH$$
$$\xrightarrow{3} O^- + CF_2C + HF$$
$$\xrightarrow{4} O^- CF_3C + H$$

The energetics of reactions 1 and 4 cannot be examined in the absence of thermochemical data for the CF_3CH and CF_3C radicals, however, if reaction 1 is assumed to be that responsible for O^- ion formation at $7{\cdot}2 \pm 0{\cdot}2$eV, a value of $\leq 8{\cdot}6 \pm 0{\cdot}3$eV may be deduced for the $CF_3CH = O$ bond dissociation energy. This value is probably too high (e.g. compare D(OC = O) ~5·7eV) and so it suggests that either reaction 1 is accompanied by several volts of excess energy or more possibly that reaction 3 is that responsible for O^- ion formation at $7{\cdot}2 \pm 0{\cdot}2$eV; the formation of an abundant CF_2C^- ion at low electron energies lends support to this mechanism. Reversing this argument and setting the initial O^- appearance potential equal to the minimum enthalpy requirement of reaction 3 the heat of formation of the CF_2C radical is estimated to be $\lesssim 0{\cdot}6$eV which is in good accord with that of $\leq 1{\cdot}0 \pm 0{\cdot}3$eV deduced for this radical from perfluoropropylene in Chapter 7. Reaction 3 is therefore attributed to the appearance potential at $7{\cdot}2 \pm 0{\cdot}2$eV.

If reaction 4 is now assumed responsible for O^- ion formation at $8{\cdot}2 \pm 0{\cdot}2$eV then, using the argument employed above, the heat of formation of the CF_3C radical is estimated to be $\lesssim -3{\cdot}5$eV. Although there is no other value for $\Delta H_f(CF_3C)$ reported in the literature the following heats of formation suggest the value deduced to be of the correct

magnitude; $\Delta H_f(CF_2CF) = -2{\cdot}0eV$[127] and $\Delta H_f(CF_3CF) = -4{\cdot}8eV$.[129]

It can be seen from Figs. 8.1(a) and 8.2(a) that F^- ion formation occurs as the result of two major resonances, the first maximising at $4{\cdot}3 \pm 0{\cdot}1eV$ and the second at $8{\cdot}7 \pm 0{\cdot}2eV$. After deconvolution, Fig. 8.2(b), the second peak is found to exhibit a shoulder on the leading edge and to be bounded by low cross-section tails at low and high energies. As these tails were not reproducible over five experimental runs it has been concluded that they are spurious diffraction peaks resulting from the ineffective unfolding of the broad peak; the onset of the double resonance is therefore taken to be $6{\cdot}6 \pm 0{\cdot}3eV$.

Reaction 5, which has an estimated minimum enthalpy requirement of $3{\cdot}6eV$, is suggested as that responsible for F^- ion formation at $3{\cdot}6 \pm 0{\cdot}1eV$ although reactions 6 and 7, which have minimum enthalpy requirements of approximately $4{\cdot}1$ and $4{\cdot}9eV$ respectively, may also be contributing processes.

$$CF_3CHO + e \xrightarrow{5} F^- + CF_2 + CHO$$
$$\xrightarrow{6} F^- + CF + CO + HF$$
$$\xrightarrow{7} F^- + CF_2 + CO + H$$

Reactions 8 and 9, which have minimum enthalpy requirements of $\sim 7{\cdot}0$ and $\sim 8{\cdot}7eV$ respectively are further proposed to account for the broad resonance onsetting at $6{\cdot}6 \pm 0{\cdot}3eV$.

$$CF_3CHO + e \xrightarrow{8} F^- + CF_2CH + O$$
$$\xrightarrow{9} F^- + CF + F + CHO$$

Using the electron affinity of the CF_2 radical (estimated in Chapter 7 (section g) to be $\leq 1{\cdot}6 \pm 0{\cdot}5$eV) in conjunction with $\Delta H_f(CF_2) = -1{\cdot}8$eV[128] the heat of formation of the CF_2^- ion is estimated to be $-3{\cdot}4 \pm 0{\cdot}6$eV from which the minimum enthalpy requirements of reactions 10 and 11 are calculated to be approximately 0·8 and 5·4eV respectively.

$$CF_3CHO + e \xrightarrow{10} CF_2^- + CO + HF$$
$$\xrightarrow{11} CF_2^- + F + CHO$$

Reaction 10, involving ~2eV of excess energy, is therefore suggested to account for CF_2^- ion formation at $3{\cdot}3 \pm 0{\cdot}1$eV and reaction 11 is tentatively proposed for ion formation at $4{\cdot}6 \pm 0{\cdot}3$eV.

Following CF_2^- ion formation the reactions responsible for CF_3^- ion formation must also involve considerable amounts of excess energy, 2·7 or 1·4eV, depending on whether reaction 12 or 13, which have minimum enthalpy requirements of 1·1 and 2·4eV respectively, is responsible for the appearance potential at $3{\cdot}8 \pm 0{\cdot}1$eV.

$$CF_3CHO + e \xrightarrow{12} CF_3^- + CHO$$
$$\xrightarrow{13} CF_3^- + CO + H$$
$$\xrightarrow{14} CF_3^- + CH + O$$

The next least energetically demanding process, reaction 14, requires approximately 10eV so, as the CF_3^- ion current falls to zero at ~9eV this reaction does not appear to contribute to the ionisation efficiency curve observed. If reaction 13, where $\Delta H_{min} = 2{\cdot}4$eV, is responsible for ion

formation at 6·2 ± 0·2eV then ~3·8eV of excess energy must be distributed as internal energy (possibly of CO where the first excited state lies ~2·5eV above the ground state) and/or translational energy of the fragments.

If CF_2C^- ion formation onsetting at 7·1 ± 0·1eV corresponds to reaction 15, the complementary reaction to 3, the heat of formation of the CF_2C^- ion may be estimated to be $\lesssim$ -0·9eV.

$$CF_3CHO + e \xrightarrow{15} CF_2C^- + HF + O$$

As the heat of formation of the CF_2C radical has been estimated above to be $\lesssim$ 0·6eV and $\leq$ 1·0 ± 0·3eV (Chapter 7, section b) i.e. $\leq$ 0·8 ± 0·3eV average, the electron affinity of the CF_2C radical is deduced to be $\lesssim$ 1·5 and $\lesssim$ 1·9eV respectively i.e. $\leq$ 1·7eV average. There are no other literature values with which these data can be compared. The unresolved second CF_2C^- resonance onsetting at ~7·8eV is attributed to reaction 15 in which excess energy is involved.

From the energetics of reaction 16, which is proposed to account for CF_3C^- ion formation at 6·5 ± 0·1eV, the heat of formation of the CF_3C^- ion is estimated to be $\lesssim$ -6·6eV.

$$CF_3CHO + e \xrightarrow{16} CF_3C^- + O + H$$

Used in conjunction with the value of $\lesssim$ -3·5 estimated for $\Delta H_f(CF_3C)$ from reaction 4, $\Delta H_f(CF_3C^-) \lesssim$ -6·6eV yields a value of $\lesssim$ 3·1eV for $E(CF_3C)$.

The CF_2CO^- ion exhibits a single sharp resonance peak onsetting at 3·8 ± 0·1eV which must result from reaction 17 or 18.

$$CF_3CHO + e \xrightarrow{17} CF_2CO^- + HF$$
$$\xrightarrow{18} CF_2CO^- + H + F$$

In the absence of thermochemical data process identification is precluded.

(ii) Pentafluoropropionaldehyde, C_2F_5CHO.

The negative ions detected and measured at low electron energies from C_2F_5CHO were F^-, CF_3^-, $C_2F_5^-$ and $C_2F_4CO^-$ which were formed with the relative abundances 200:6:4:1000 at 70eV and 1000:580:190:460 at 10eV. The appearance potential data are given in Table 8.2 and the ionisation efficiency data are shown in Fig. 8.3 where the energy scale is calibrated against the appearance potential of the O^- ion formed from SO_2 at 4·2 and 6·6eV.

In order to prevent confusion the $C_2F_4CO^-$ ionisation efficiency curve has not been included in Fig. 8.3. This ion exhibited a broad peak at zero eV with three smaller resonances onsetting at 3·0 ± 0·3, 5·9 ± 0·3 and 7·7 ± 0·3eV followed by secondary electron capture onsetting at ~10eV; at no point on the energy scale between 0 and 100eV did the $C_2F_4CO^-$ ion current fall to zero which may be partially the result of surface ionisation which occurred to some extent at the lower electron energies.

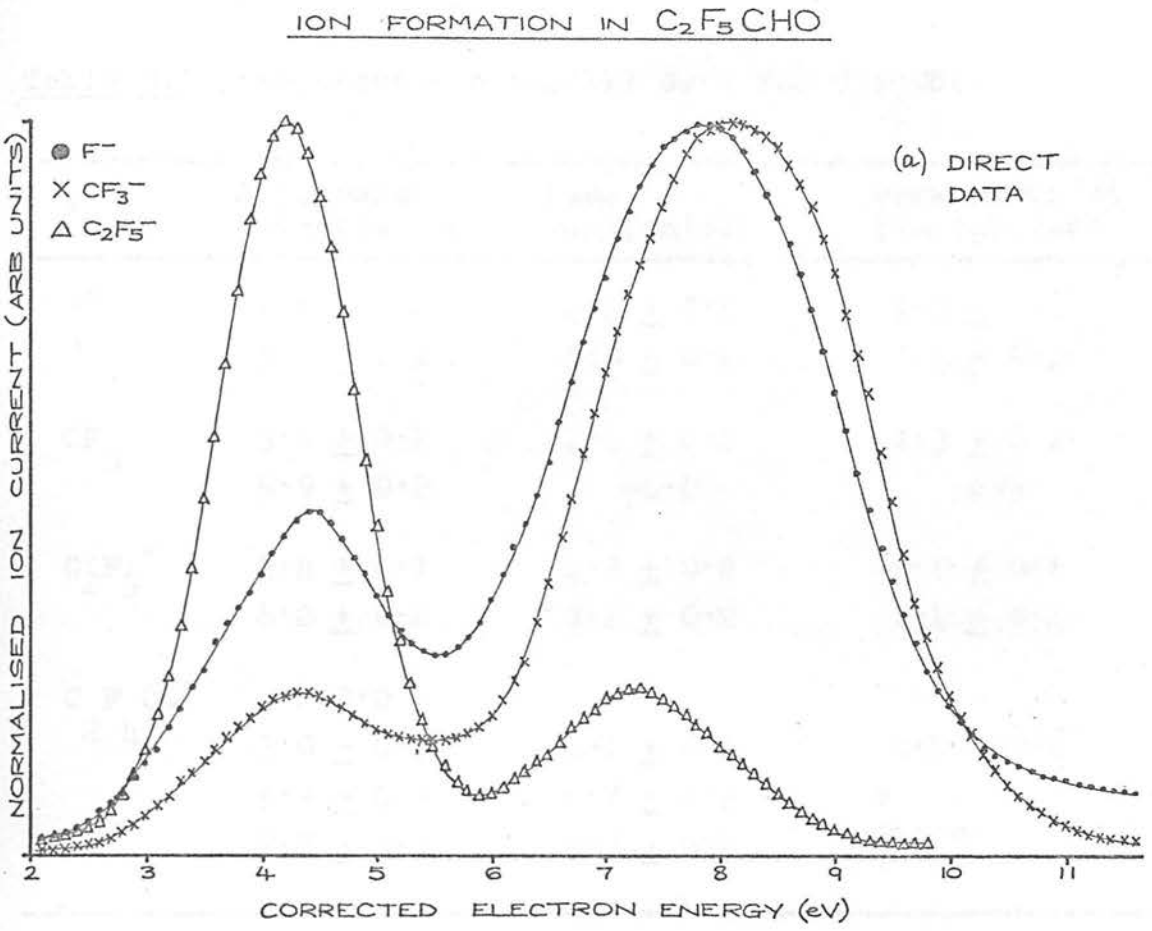
ION FORMATION IN C_2F_5CHO
● F^-
X CF_3^-
Δ $C_2F_5^-$
(a) DIRECT DATA
NORMALISED ION CURRENT (ARB UNITS)
2
3
4
5
6
7
8
9
10
11
CORRECTED ELECTRON ENERGY (eV)

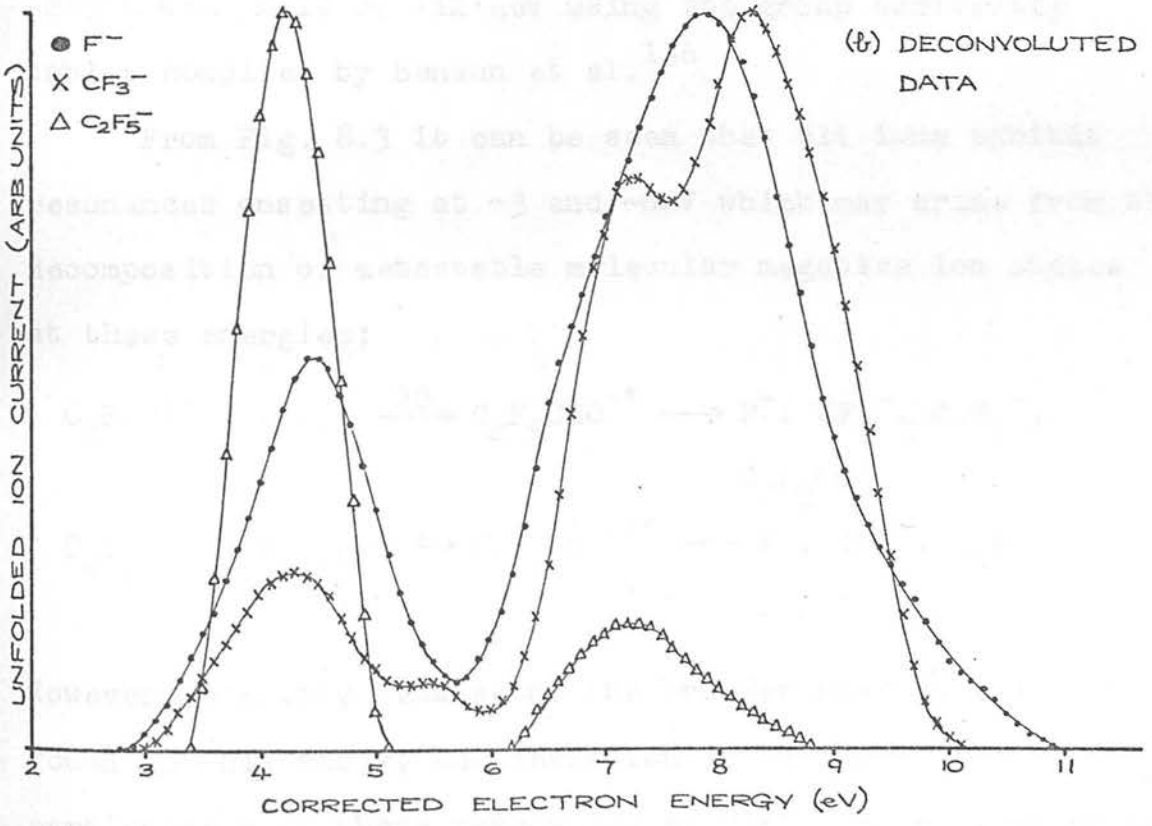
● F^-
X CF_3^-
Δ $C_2F_5^-$
(b) DECONVOLUTED DATA
UNFOLDED ION CURRENT (ARB UNITS)
2
3
4
5
6
7
8
9
10
11
CORRECTED ELECTRON ENERGY (eV)

Fig 8.3

Table 8.2. Appearance potential data for C_2F_5CHO.

Ion	Appearance Potential(eV)	Peak Maximum(eV)	Peak Width at ½-height(eV)
F^-	2·9 ± 0·2	4·4 ± 0·2	1·3 ± 0·1
	5·7 ± 0·2	7·9 ± 0·2	2·4 ± 0·2
CF_3^-	3·0 ± 0·2	4·3 ± 0·2	1·3 ± 0·1
	5·9 ± 0·2	~8·0	~2·5
$C_2F_5^-$	3·4 ± 0·1	4·2 ± 0·2	0·9 ± 0·1
	6·2 ± 0·2	7·2 ± 0·2	1·4 ± 0·2
$C_2F_4CO^-$	~0·0	-	-
	3·0 ± 0·3	4·1 ± 0·2	0·8 ± 0·2
	5·9 ± 0·3	6·7 ± 0·2	)
	7·7 ± 0·3	8·7 ± 0·2	)broad

The heat of formation of C_2F_5CHO was estimated to be -285·6 Kcal/mole or -12·4eV using the group additivity tables compiled by Benson et al.[136]

From Fig. 8.3 it can be seen that all ions exhibit resonances onsetting at ~3 and ~6eV which may arise from the decomposition of metastable molecular negative ion states at these energies;

$$C_2F_5CHO + e_{\sim 3eV} \xrightarrow{20} C_2F_5CHO^{-*} \longrightarrow F^-,\ CF_3^-,\ C_2F_5^-,\ C_2F_4CO^-,\ldots\ldots$$

$$C_2F_5CHO + e_{\sim 6eV} \xrightarrow{21} C_2F_5CHO^{-**} \longrightarrow F^-,\ CF_3^-,\ C_2F_5^-,\ C_2F_4CO^-,\ldots\ldots$$

However, possibly because of the broader resonance curves found in this study, the deviation in superposition, particularly of those resonances at ~3eV, is far greater than

that found for the perfluorocarbon molecular negative ion states in Chapter 7 and therefore reactions 20 and 21 cannot be identified with the same degree of confidence.

Reaction 22, which has an estimated minimum enthalpy requirement of 3·0eV, is suggested to account for F^- ion formation onsetting at 2·9 ± 0·2eV,

$$C_2F_5CHO + e \xrightarrow{22} F^- + C_2F_4 + CHO$$

Reactions 23 and 24, with minimum enthalpy requirements of 4·3 and 4·8eV respectively, may also contribute to the observed ionisation efficiency curve which does not fall to zero between the two major resonance peaks.

$$C_2F_5CHO + e \xrightarrow{23} F^- + C_2F_4 + CO + H$$
$$\xrightarrow{24} F^- + CF_3CF + CHO$$

The second F^- resonance peak which onsets at 5·7 ± 0·2eV is unusually broad, $W_{\frac{1}{2}}$ = 2·4 ± 0·2eV, and may well be composed of several overlapping resonances which have not been resolved by the deconvolution procedure. The following are among the possible reactions which may contribute to ion formation at these energies;

	ΔH_{min}(eV)
$C_2F_5CHO + e \xrightarrow{25} F^- + 2CF_2 + CHO$	6·0
$\xrightarrow{26} F^- + CF_3CF + CO + H$	6·1
$\xrightarrow{27} F^- + CF_2 + CF + CO + HF$	6·6
$\xrightarrow{28} F^- + CF_3 + CF + CHO$	7·6

Using the value $E(CF_3) = 2{\cdot}0 \pm 0{\cdot}1eV$[4,17,119,122] with known thermochemical data[23,127] the minimum enthalpy requirements of reactions 29 and 30, which are proposed to account for CF_3^- ion formation at $3{\cdot}0 \pm 0{\cdot}2$ and $5{\cdot}9 \pm 0{\cdot}2eV$, are estimated to be $3{\cdot}5$ and $4{\cdot}8eV$ respectively

$$C_2F_5CHO + e \xrightarrow{29} CF_3^- + CF_2 + CHO$$
$$\xrightarrow{30} CF_3^- + CF_2 + CO + H$$

In order to reconcile the $C_2F_5^-$ appearance potential data with the minimum enthalpy requirements estimated for reactions 31 and 32 approximately $2{\cdot}6$ and $4{\cdot}7eV$ of excess energy must be attributed to ion formation at $3{\cdot}4 \pm 0{\cdot}1$ and $6{\cdot}2 \pm 0{\cdot}2eV$ respectively.

	ΔH_{min}(eV)
$C_2F_5CHO + e \xrightarrow{31} C_2F_5^- + CHO$	0·8
$\xrightarrow{32} C_2F_5^- + CO + H$	2·1
$\xrightarrow{33} C_2F_5^- + CH + O$	9·8

Similar conclusions were drawn for CF_3^- ion formation from CF_3CHO where reaction 12 i.e. that analogous to reaction 31 above, involved almost the same amount of excess energy i.e. $2{\cdot}7eV$.

If reaction 34 is that responsible for $C_2F_4CO^-$ ion formation at ~0eV the heat of formation of the $C_2F_4CO^-$ ion may be estimated

$$C_2F_5CHO + e \xrightarrow{34} C_2F_4CO^- + HF$$

to be $\lesssim$ -9·6eV. Using this value the energy requirement of reaction 35 is calculated to be ~5·9eV, this reaction is therefore forwarded as that responsible for the appearance

$$C_2F_5CHO + e \xrightarrow{35} C_2F_4CO^- + H + F$$

potential at 5·9 ± 0·3eV. The other resonances at 3·0 ± 0·3 and 7·7 ± 0·3eV must therefore correspond to reactions 34 and/or reaction 35 in which excess energy contributions are involved.

(iii) Heptafluorobutyraldehyde, C_3F_7CHO.

The average cross-section for dissociative electron capture by C_3F_7CHO was found to be approximately an order of magnitude lower than that found for CF_3CHO. F^- and $C_3F_7^-$ were the only two ions formed with sufficient intensity to enable accurate measurements to be undertaken and the experimental and deconvoluted ionisation efficiency curves are shown in Fig. 8.4 where the energy scale is calibrated against the appearance potential of the O^- ion formed from SO_2 at 4·2 and 6·6eV.

The CF_3^-, $C_2F_5^-$ and $C_3F_6CO^-$ ions were also detected at low electron energies and higher electron trap currents were employed (~0·1μAmp) in order to obtain appearance potential data for these ions. The $C_3F_6CO^-$ ion appeared at ~0eV and was, at least in part, formed as the result of surface ionisation at the filament. The ions measured at low electron energies F^-, CF_3^-, $C_2F_5^-$, $C_3F_7^-$ and $C_3F_6CO^-$ were formed with relative abundances in the ratio 350:12:2:6:1000 at 70eV and 1000:7:<1:<1:28 at 10eV. The appearance

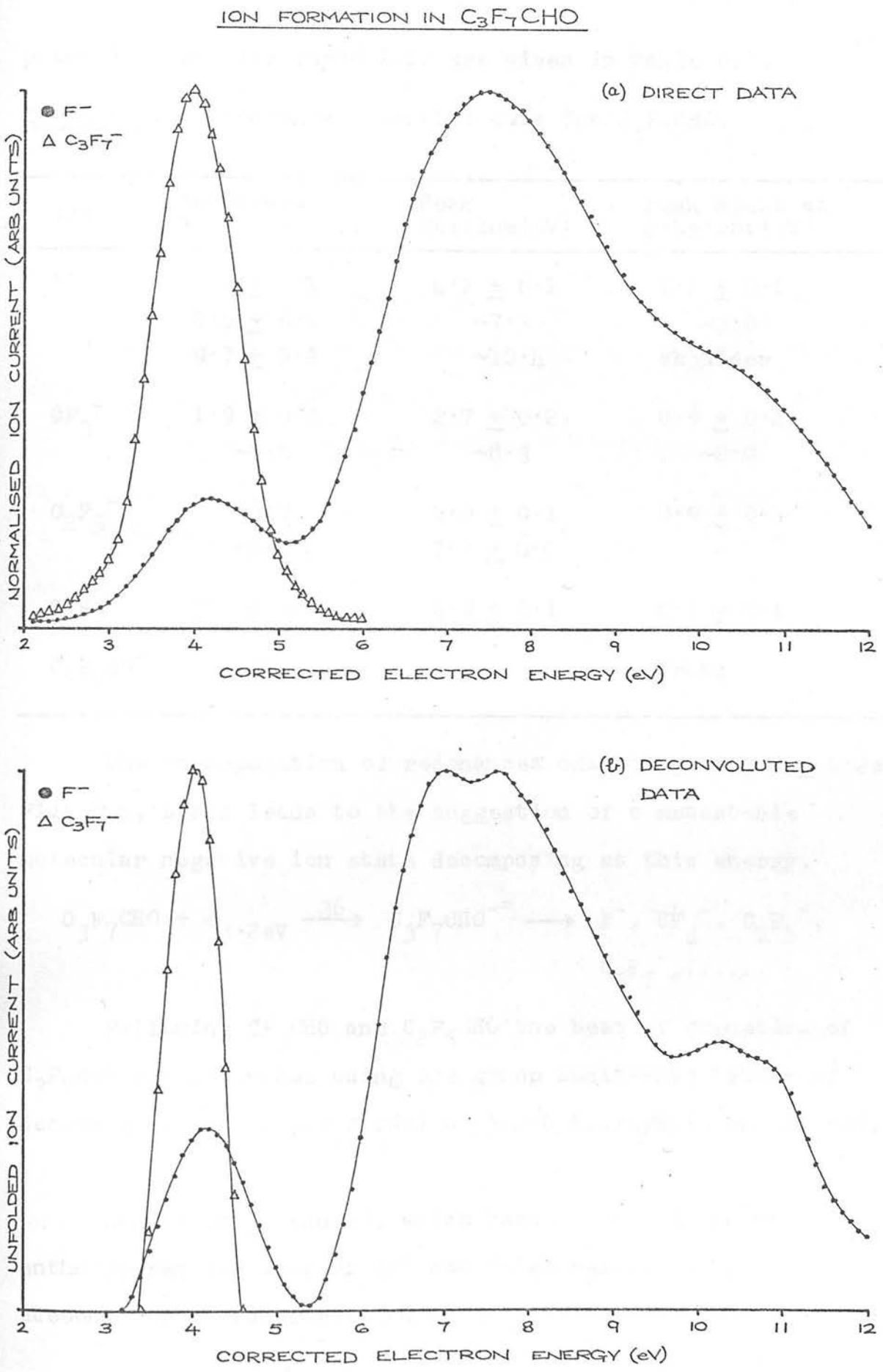
ION FORMATION IN C_3F_7CHO
(a) DIRECT DATA
● F^-
Δ $C_3F_7^-$
NORMALISED ION CURRENT (ARB UNITS)
2 3 4 5 6 7 8 9 10 11 12
CORRECTED ELECTRON ENERGY (eV)
(b) DECONVOLUTED DATA
● F^-
Δ $C_3F_7^-$
UNFOLDED ION CURRENT (ARB. UNITS)
2 3 4 5 6 7 8 9 10 11 12
CORRECTED ELECTRON ENERGY (eV)

Fig 8.4

potential data for these ions are given in Table 8.3.

Table 8.3. Appearance potential data for C_3F_7CHO.

Ion	Appearance Potential(eV)	Peak Maximum(eV)	Peak Width at $\frac{1}{2}$-height(eV)
F^-	3·2 ± 0·1	4·2 ± 0·1	1·1 ± 0·1
	5·4 ± 0·1	~7·5	~3·0
	9·7 ± 0·2	~10·4	shoulder
CF_3^-	1·9 ± 0·2	2·7 ± 0·2	0·9 ± 0·2
	~6·5	~8·3	~2·0
$C_2F_5^-$	~3·0	4·0 ± 0·1	0·9 ± 0·1
	~6·5	7·2 ± 0·2	-
$C_3F_7^-$	3·4 ± 0·1	4·0 ± 0·1	0·7 ± 0·1
$C_3F_6CO^-$	~0·0	-	broad

The superposition of resonances onsetting at 3·2 ± 0·2eV, Fig. 8.4, again leads to the suggestion of a metastable molecular negative ion state decomposing at this energy,

$$C_3F_7CHO + e_{3\cdot2eV} \xrightarrow{36} C_3F_7CHO^{-*} \longrightarrow F^-, CF_3^-, C_2F_5^-, C_3F_7^-, \ldots\ldots$$

Following CF_3CHO and C_2F_5CHO the heat of formation of C_3F_7CHO was estimated using the group additivity tables of Benson et al;[136] $\Delta H_f(C_3F_7CHO)$ = -382·6 Kcals/mole or -16·6eV.

Reactions 37 and 38, which have estimated minimum enthalpy requirements of 2·5 and 3·2eV respectively, may account for F^- ion formation at 3·2 ± 0·1eV.

$$C_3F_7CHO + e \xrightarrow{37} F^- + C_3F_6 + CHO$$
$$\xrightarrow{38} F^- + C_3F_5 + CO + HF$$

$\Delta H_f(C_3F_5) \leq -6{\cdot}8 \pm 0{\cdot}2$eV deduced in Chapter 7, section (b), was used to calculate the energetics of reaction 38. In the absence of a translational energy analysis of the products unequivocal process identification is precluded although reaction 37, which does not involve intramolecular rearrangement, is that preferred.

The second F^- resonance peak, onsetting at $5{\cdot}4 \pm 0{\cdot}1$eV, is shown after deconvolution, Fig. 8.4(b), to be a double peak with further unresolved resonances evident in the trailing edge of the peak. A large number of reactions could be written to fulfil the energy requirements imposed by this broad peak of which the following are some of the more likely possibilities,

	ΔH_{min}(eV)
$C_3F_7CHO + e \xrightarrow{39} F^- + CF_2 + C_2F_4 + CHO$	5·4
$\xrightarrow{40} F^- + CF_2 + C_2F_4 + CO + H$	6·7
$\xrightarrow{41} F^- + CF_3 + CF_2CF + CHO$	6·9
$\xrightarrow{42} F^- + C_2F_5 + CF + CHO$	7·1
$\xrightarrow{43} F^- + CF_3CF + CF_2 + CHO$	7·2

Reaction 39 is tentatively suggested as the initial process onsetting at $5{\cdot}4 \pm 0{\cdot}2$eV and reaction 44, which has a minimum enthalpy requirement of 9·6eV, as that corresponding to the minimum in the ionisation efficiency curve at $9{\cdot}7 \pm 0{\cdot}2$eV.

$$C_3F_7CHO + e \xrightarrow{44} F^- + CF_3 + CF_2 + CF + CHO$$

If the CF_3^- appearance potential at 1·9 ± 0·2eV corresponds to the following reaction,

$$C_3F_7CHO + e \xrightarrow{45} CF_3^- + C_2F_4CHO$$

then, using $E(CF_3) = 2{\cdot}0 \pm 0{\cdot}1eV$[4,17,119] the CF_3-C_2F_4CHO bond dissociation energy is estimated to be $\leq 3{\cdot}9 \pm 0{\cdot}3eV$. This may be compared with the C-C bond dissociation energies in C_3F_8 and C_4F_{10} deduced in the course of Chapter 7; $D(CF_3\text{-}C_2F_5) \leq 4{\cdot}55 \pm 0{\cdot}2eV$ and $D(CF_3\text{-}C_3F_7) \leq 4{\cdot}3 \pm 0{\cdot}2eV$.

Reaction 46 and/or 47, which have minimum enthalpy requirements of 5·9 and 6·4eV respectively, are tentatively suggested to account for the CF_3^- appearance potential at ~6·5eV,

$$C_3F_7CHO + e \xrightarrow{46} CF_3^- + 2CF_2 + CHO$$
$$\xrightarrow{47} CF_3^- + CF_2 + CF + CO + HF$$

Assuming $E(C_2F_5)$ to be approximately 2·2eV (see Table 9.1) the minimum enthalpy requirement of reaction 48 is estimated to be 3·2eV. This reaction is therefore attributed to ion formation at ~3·0eV

$$C_3F_7CHO + e \xrightarrow{48} C_2F_5^- + CF_2 + CHO$$

thereby lending support to the values deduced for $E(C_2F_5)$ in the course of Chapter 7 i.e. 2·1 ± 0·2, section (c) and 2·2 ± 0·3eV, section (e).

$$C_3F_7CHO + e \xrightarrow{49} C_2F_5^- + CF_2 + CO + H$$
$$\xrightarrow{50} C_2F_5^- + CF + CO + H + F$$

Reaction 49 involving ~2eV of excess energy, and reaction 50, which has a minimum enthalpy requirement of approximately

6·8eV may both contribute to the $C_2F_5^-$ appearance potential observed at ~6·5eV.

The $C_3F_7^-$ ion exhibits a single sharp resonance peak onsetting at 3·4 ± 0·1eV. Assuming that $E(C_3F_7)$ ~2·3eV (Chapter 7, sections (c) and (e)) the minimum enthalpy requirements for $C_3F_7^-$ ion formation by reactions 51 and 52 are approximately 0·8 and 2·1eV respectively,

$$C_3F_7CHO + e \xrightarrow{51} C_3F_7^- + CHO$$
$$\xrightarrow{52} C_3F_7^- + CO + H$$

Therefore, depending on whether reaction 51 or 52 is responsible for ion formation at 3·4 ± 0·1eV, 2·6 or 1·3eV of excess energy must accompany ionisation. CF_3^- ion formation from CF_3CHO and $C_2F_5^-$ ion formation from C_2F_5CHO were similarly found to involve large amounts of excess energy, i.e. 2·7 or 1·4eV for CF_3^- ion formation by reactions 12 or 13 respectively and 2·6 or 1·3eV for $C_2F_5^-$ ion formation by reactions 31 or 32 respectively. The comparable releases of excess energy accompanying perfluoroalkyl ion formation in each case suggests that excitation of the CHO radical, if reactions 12, 31 and 51 are those responsible for ion formation, or excitation of the CO molecule, for the occurrence of reactions 13, 32 and 52, may be involved in ion formation. However, the first excited state of carbon monoxide lies 2·5eV above the ground state[23] and as insufficient energy is available from reactions 13, 32 and 52 it is suggested that reactions 12, 31 and 51 involving excitation of the CHO radical to an excited state(s)

lying $\leq$2·6eV above ground are those reactions responsible for perfluoroalkyl ion formation from these fluoroaldehydes.

	APeV	Excess Energy(eV)
$CF_3CHO + e \xrightarrow{12} CF_3^- + CHO^*$	3·8 ± 0·1	2·7
$C_2F_5CHO + e \xrightarrow{31} C_2F_5^- + CHO^*$	3·4 ± 0·1	2·6
$C_3F_7CHO + e \xrightarrow{51} C_3F_7^- + CHO^*$	3·4 ± 0·1	2·6

These suggestions are consistent with the reported electronic spectrum of the formyl radical.[138] The A and B states, which lie 1·5eV above the ground state, precede a broad, diffuse band which includes the amount of excess energy associated with the above reactions.

The $C_3F_6CO^-$ ion was detected at ~0eV and its formation is partially attributed to surface ionisation although reaction 52 may also contribute to the ion current observed.

$$C_3F_7CHO + e \xrightarrow{52} C_3F_6CO^- + HF$$

Assuming this to be the case the heat of formation of the $C_3F_6CO^-$ ion is estimated to be $\lesssim$ -13·8eV which may be compared to the value deduced for the anabgous ion formed from C_2F_5CHO, $\Delta H_f(C_2F_4CO^-) \lesssim$ -9·6eV.

(b) Fluoroketones

(i) Trifluoroacetone, CF_3COCH_3.

Negative ion formation occurred extensively in the fluoroketones, the ions detected and measured in CF_3COCH_3

at low electron energies being O^-, F^-, CF_2^-, CF_3^-, $CFCOCH_3^-$ and $CF_2COCH_3^-$ which were formed with relative abundances in the ratio 110:1000:4:100:5:10 at 70eV. The molecular negative ion, $CF_3COCH_3^-$, was also detected at 70eV but with an abundance of only 0·1% of the F^- ion current. The experimental and deconvoluted ionisation efficiency curves are shown in Figs. 8.5(a) and (b) respectively where the energy scale is referenced to the O^- ion formed from SO_2 at 4·2 and 6·6eV.

From Fig. 8.5 it can be seen that the resonances occur in two distinct bands the first maximising around 5eV and the second between 8 and 10eV; the following processes are consistent with these observations,

$$CF_3COCH_3 + e_{4\cdot3eV} \xrightarrow{53} CF_3COCH_3^{-*} \longrightarrow F^-,\ CF_2^-,\ CF_3^-,\ CF_2COCH_3^-,\ldots\ldots$$

$$CF_3COCH_3 + e_{7\cdot4eV} \xrightarrow{54} CF_3COCH_3^{-**} \longrightarrow O^-,\ F^-,\ CF_3^-,\ CFCOCH_3,\ CF_2COCH_3,\ldots\ldots\ldots$$

The F^- and CF_3^- ionisation curves, which do not exhibit well defined appearance potentials at 7·4 ± 0·3eV, show broad resonances onsetting at 6·8 ± 0·2eV and extending across the relevant energy range. It would therefore appear that several unresolved resonances (possibly including the dissociation channels of reaction 54) contribute to the observed curves. This argument also applies to the CF_2^- ionisation curve which onsets at 3·9 ± 0·1eV i.e. ~0·4eV lower than the appearance potential identified with reaction 53 at 4·3 ± 0·3eV, but which has a peak width of 1·1 ± 0·1eV

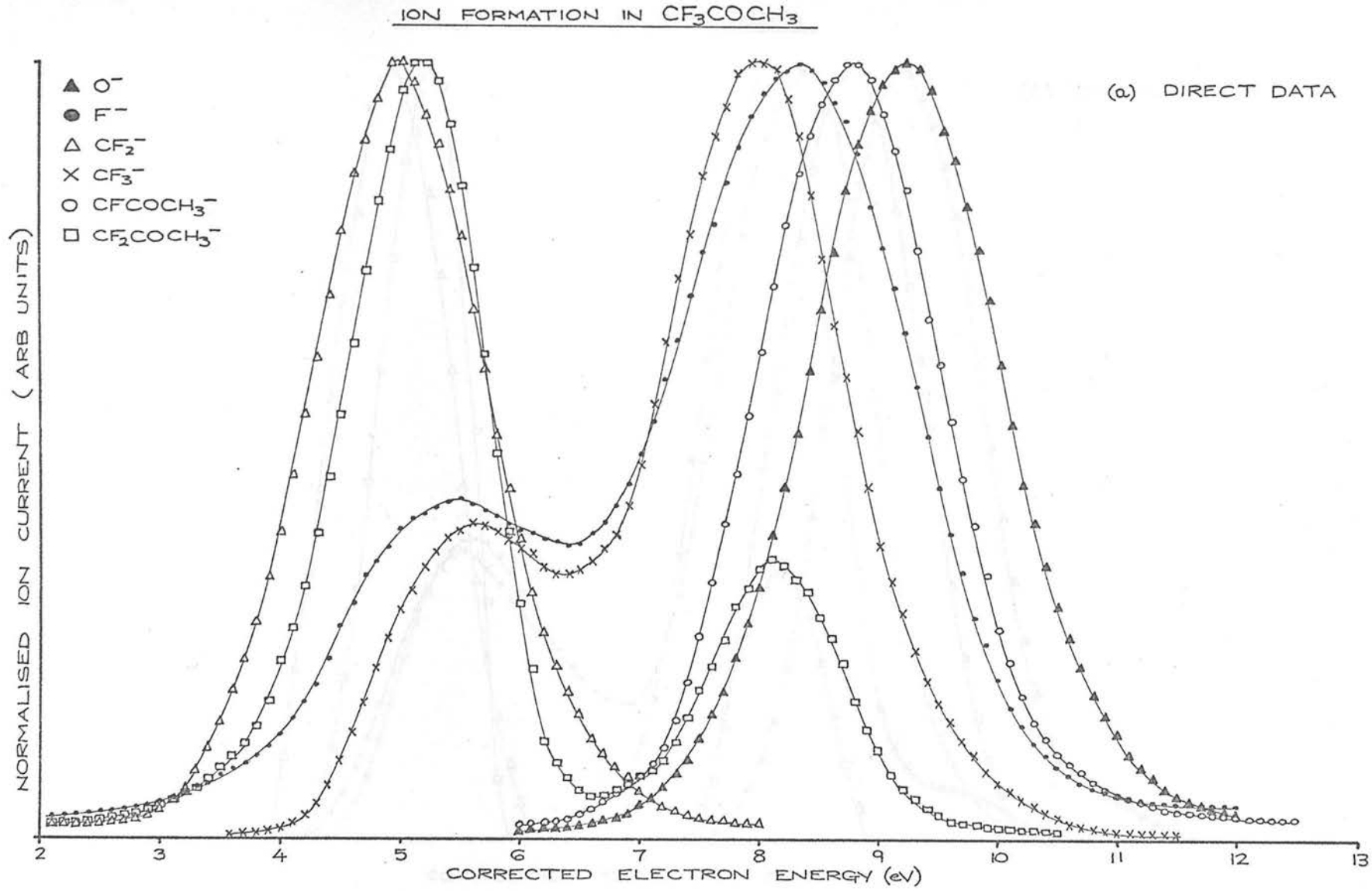
ION FORMATION IN CF_3COCH_3
(a) DIRECT DATA
O^-
F^-
CF_2^-
CF_3^-
$CFCOCH_3^-$
$CF_2COCH_3^-$
NORMALISED ION CURRENT (ARB UNITS)
CORRECTED ELECTRON ENERGY (eV)
2
3
4
5
6
7
8
9
10
11
12
13

Fig 8.5

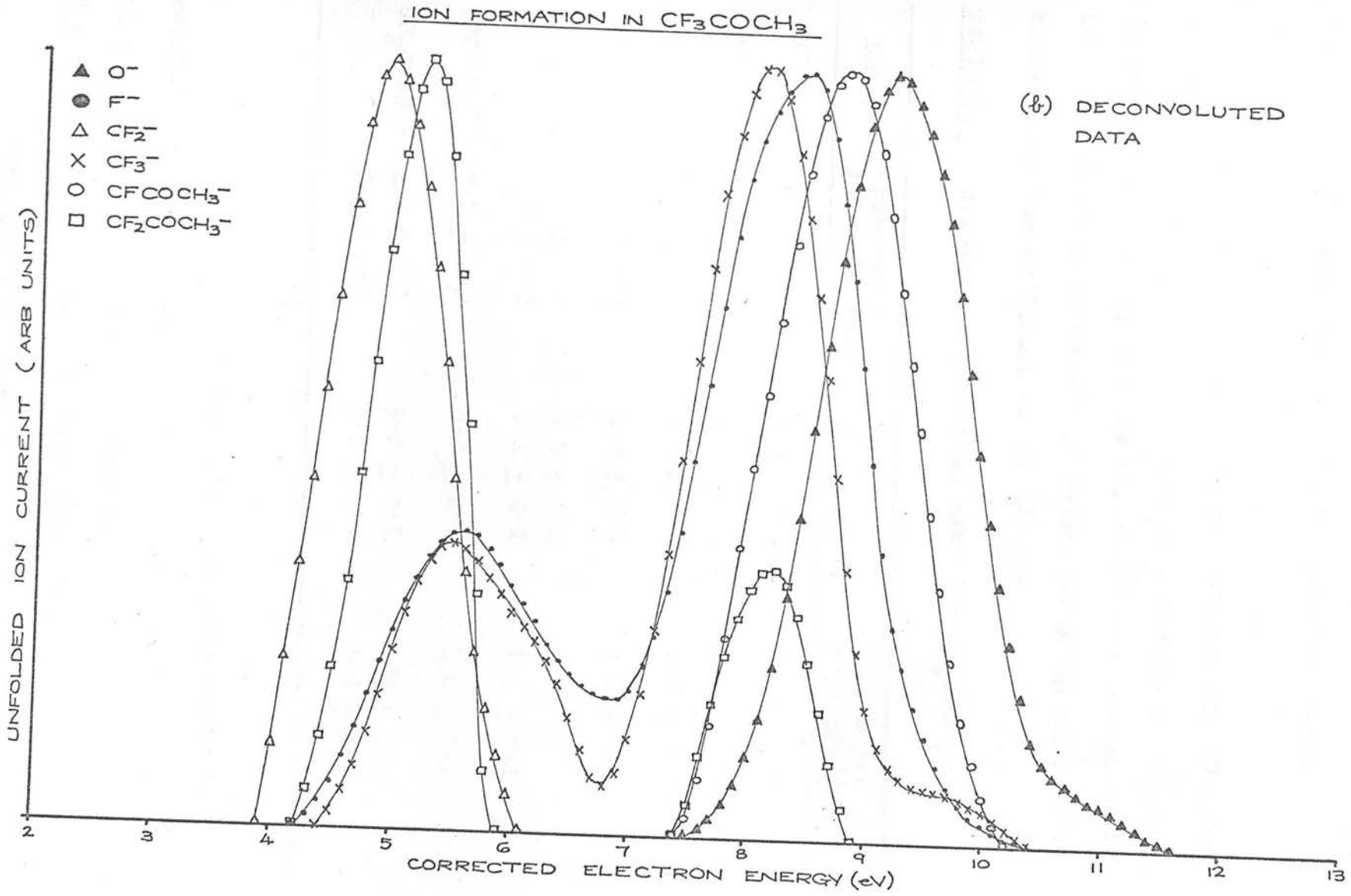
ION FORMATION IN CF_3COCH_3
O^-
F^-
CF_2^-
CF_3^-
$CFCOCH_3^-$
$CF_2COCH_3^-$
(&) DECONVOLUTED DATA
UNFOLDED ION CURRENT (ARB UNITS)
2
3
4
5
6
7
8
9
10
11
12
13
CORRECTED ELECTRON ENERGY (eV)

Fig 8.5

at half-height and does not fall to zero ion current until about 6eV.

The appearance potential data measured for CF_3COCH_3 is given in Table 8.4. The heat of formation of CF_3COCH_3 is not known directly and has therefore been estimated to be -200·0 Kcals/mole or -8·7eV using the group additivity tables compiled by Benson et al.[136]

Table 8.4. Appearance potential data for CF_3COCH_3.

Ion	Appearance Potential(eV)	Peak Maximum(eV)	Peak Width at ½-height(eV)
O^-	7·5 ± 0·2	9·1 ± 0·1	1·4 ± 0·1
F^-	4·2 ± 0·2	5·6 ± 0·2	~1·5
	6·8 ± 0·2	8·3 ± 0·2	1·5 ± 0·2
CF_2^-	3·9 ± 0·1	4·9 ± 0·1	1·1 ± 0·1
CF_3^-	4·4 ± 0·2	5·5 ± 0·2	~1·3
	6·8 ± 0·2	8·1 ± 0·1	1·3 ± 0·1
$CFCOCH_3^-$	7·4 ± 0·2	8·7 ± 0·1	1·4 ± 0·1
$CF_2COCH_3^-$	4·2 ± 0·1	5·2 ± 0·1	0·9 ± 0·1
	7·4 ± 0·2	8·2 ± 0·2	0·9 ± 0·1

The O^- ion exhibited a single, low cross-section, resonance peak onsetting at 7·5 ± 0·2eV. Using E(0) = 1·4 ± 0·1eV[4] ion formation by reaction 55 yields a value of ≤ 8·9 ± 0·3eV for the C-O bond dissociation energy.

$$CF_3COCH_3 + e \xrightarrow{55} O^- + CF_3CCH_3$$

As this value is probably too high by several volts, i.e. $D(OC=O)$ ~5·7eV and $D(CH_2=O)$ ~7·4eV, the appropriate amount of excess energy would have to be attributed to ion formation by this reaction. Reaction 55, however, is analogous to reaction 4 which was proposed to account for O^- ion formation from CF_3CHO and is therefore suggested as a more probable alternative to reaction 54.

$$CF_3COCH_3 + e \xrightarrow{55} O^- + CF_3C + CH_3$$

Assuming this to be the case and reversing the argument by setting the appearance potential equal to the minimum enthalpy requirement of reaction 55, the heat of formation of the CF_3C radical may be estimated to be $\lesssim$ -3·8eV. This is in good agreement with the value of $\lesssim$ -3·5eV deduced from reaction 4 for this species. Reaction 55 is therefore proposed to account for O^- ion formation and using $\Delta H_f(CF_3C) \lesssim$ -3·8eV deduced from this reaction in conjunction with the value $\Delta H_f(CF_3C^-) \lesssim$ -6·6eV deduced from reaction 16 the electron affinity of this species, CF_3C, is estimated to be $\lesssim$ 2·8eV.

Reactions 56 and 57, which have minimum enthalpy requirements of 4·1 and 6·0eV respectively, are suggested to account for F^- ion formation at 4·2 ± 0·2 and 6·8 ± 0·2eV.

$$CF_3COCH_3 + e \xrightarrow{56} F^- + CF_2 + COCH_3$$
$$\xrightarrow{57} F^- + CF_2 + CH_2CO + H$$

Using $E(CF_2) \leq 1{\cdot}6 \pm 0{\cdot}5$eV deduced in Chapter 7, section (g), the minimum enthalpy requirements of reactions 58 and 59, which are the only two energetically favourable reactions below the appearance potential at $3{\cdot}9 \pm 0{\cdot}1$eV, are estimated to be 1·2 and 1·9eV respectively.

$$CF_3COCH_3 + e \xrightarrow{58} CF_2^- + CO + CH_3F$$
$$\xrightarrow{59} CF_2^- + CH_2CO + HF$$

Reaction 59, being analogous to that proposed to account for CF_2^- ion formation from CF_3CHO, is that preferred. CF_2^- ion formation must therefore be accompanied by ~2eV of excess energy.

Reactions 60 and 61, which have calculated minimum enthalpy requirements of approximately 3·5 and 7·0eV respectively, are tentatively suggested as those responsible for CF_3^- ion formation at $4{\cdot}4 \pm 0{\cdot}2$ and $6{\cdot}8 \pm 0{\cdot}2$eV.

$$CF_3COCH_3 + e \xrightarrow{60} CF_3^- + COCH_2 + H$$
$$\xrightarrow{61} CF_3^- + CO + CH_2 + H$$

Ion formation at $4{\cdot}4 \pm 0{\cdot}2$eV would therefore involve ~0·9eV of excess energy.

$CFCOCH_3^-$ ion formation occurs by a single resonance onsetting at $7{\cdot}4 \pm 0{\cdot}2$eV and which may correspond to the following reaction,

$$CF_3COCH_3 + e \xrightarrow{62} CFCOCH_3^- + 2F$$

If the $F\text{-}CF_2COCH_3$ bond dissociation energy is approximately

equal to the average value for the equivalent fluorocarbon bond dissociation energy i.e. 5·2 ± 0·2eV, and assuming that the F-$CFCOCH_3$ bond dissociation energy is not too different from D(F-CF_2), which is calculated to be 3·9 ± 0·1eV from known thermochemical data, the electron affinity of the $CFCOCH_3$ radical is estimated to be ≥ 1·7 ± 0·5eV and the heat of formation of the $CFCOCH_3^-$ ion to be ≲-2·9eV. There are no other values with which these may be compared.

The $CF_2COCH_3^-$ ion exhibits two sharp resonances, the first onsetting at 4·2 ± 0·1 and the second at 7·4 ± 0·2eV. Assuming that D(F-CF_2COCH_3) = 5·2 ± 0·2eV, as above, then from reaction 63 the electron affinity of the CF_2COCH_3 radical may be estimated to be ≥ 1·0 ± 0·3eV and $\Delta H_f(CF_2COCH_3^-)$ to be ≲ -5·3eV.

$$CF_3COCH_3 + e \xrightarrow{63} CF_2COCH_3^- + F$$

The second peak at 7·4 ± 0·2eV corresponds to a dissociation channel of reaction 54 and must involve reaction 63 accompanied by the release of ~3·2eV of excess energy.

$$CF_3COCH_3 + e_{7\cdot4eV} \xrightarrow{54} CF_3COCH_3^{-**} \xrightarrow{63} CF_2COCH_3^{-*} + F^*$$

(ii) Hexafluoroacetone, $(CF_3)_2CO$.

The negative ions detected in hexafluoroacetone at low electron energies were F^-, CF_3^-, CFO^-, CF_3CO^-, $(CF_3)_2C^-$, $CF_3COCF_2^-$ and the molecular ion $(CF_3)_2CO^-$ which was found to have a thermal electron capture cross-section of 2·0 x 10^{-16}cm.^{2} relative to 1·17 x 10^{-14}cm.^{2} for SF_6.[35] These ions were

formed with relative abundances in the ratio 1000:257:18:17: 4:36:67 at 70eV and 751:1000:25:10:8:6:8 at 10eV.

The ionisation efficiency curves of $(CF_3)_2\,CO^-$ and SF_6^- measured simultaneously are shown in Fig. 8.6. A 50/50 mixture of hexafluoroacetone and sulphur hexafluoride was used and so the two sets of ionisation data have been normalised for convenience of presentation; the ordinate for $(CF_3)_2CO^-$ being 58·9 times greater than that for SF_6^-. It is apparent from Fig. 8.6 that both ions exhibit very similar energy dependence, the ionisation curve for the ketone being slightly broader in the wings than is that for the hexafluoride. This probably reflects the experimental difficulties encountered in measuring the very small $(CF_3)_2CO^-$ ion current, particularly as this work was carried out in the earlier stages of this research project using a tungsten filament.

The appearance potential data for all the ions examined from hexafluoroacetone are given in Table 8.5 and the ionisation efficiency data for most of the ions are shown in Fig. 8.7. where the energy scale is calibrated against the appearance potentials of the O^- ion formed from SO_2 at 4·2 and 6·6eV. It is apparent from the figure that several of the ions; F^-, CF_3^-, FCO^-, CF_3CO^- and $CF_3COCF_2^-$, exhibit coincident appearance potentials at 3·1 $\pm$ 0·1 and 5·4 $\pm$ 0·3eV. This suggests a common origin for these ions and following from above it is suggested that this is an electronically excited metastable state of the ketone which subsequently undergoes multichannel decomposition to form the ions mentioned.

ION FORMATION IN CF_3COCF_3

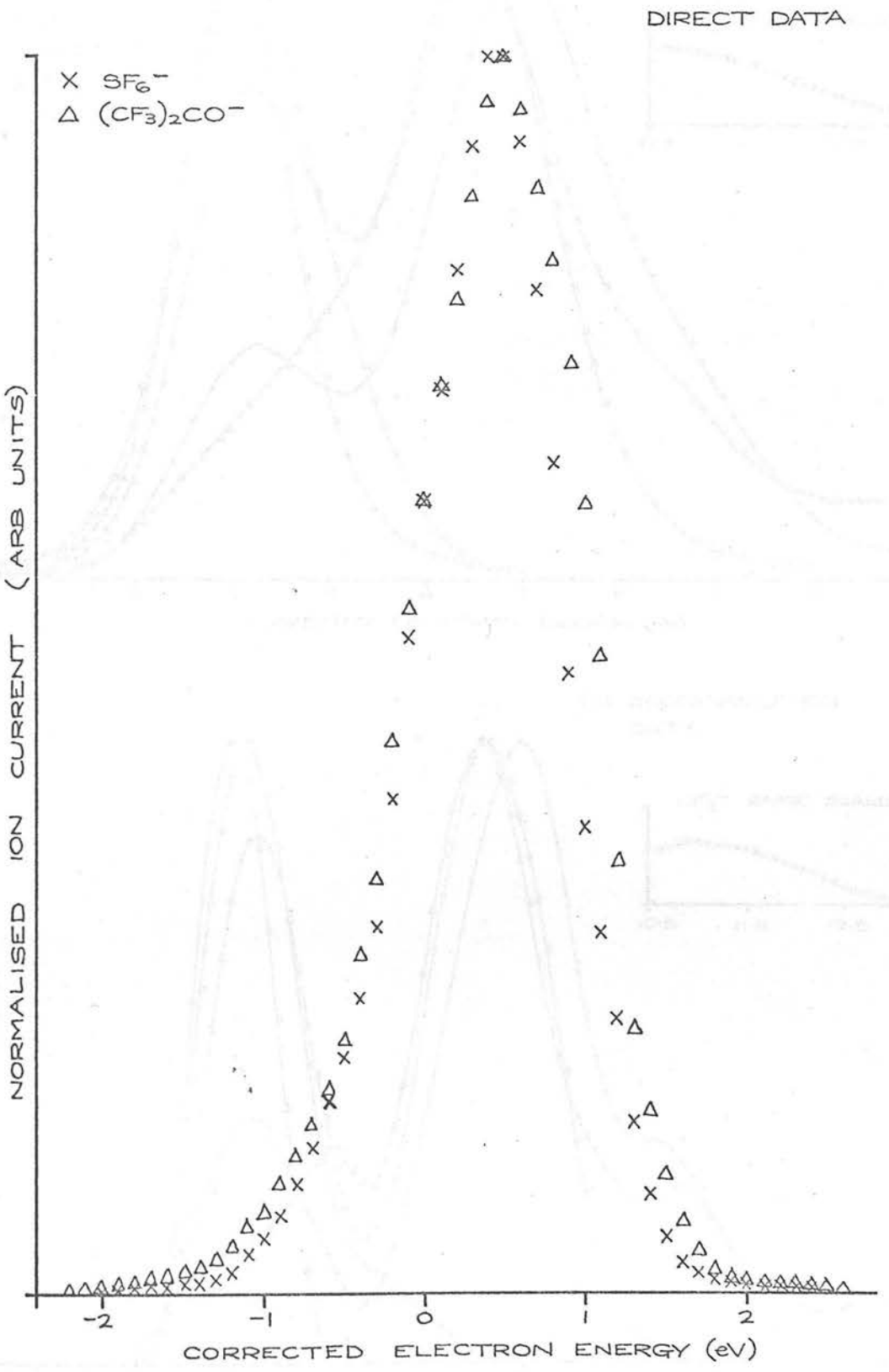

Fig 8.6

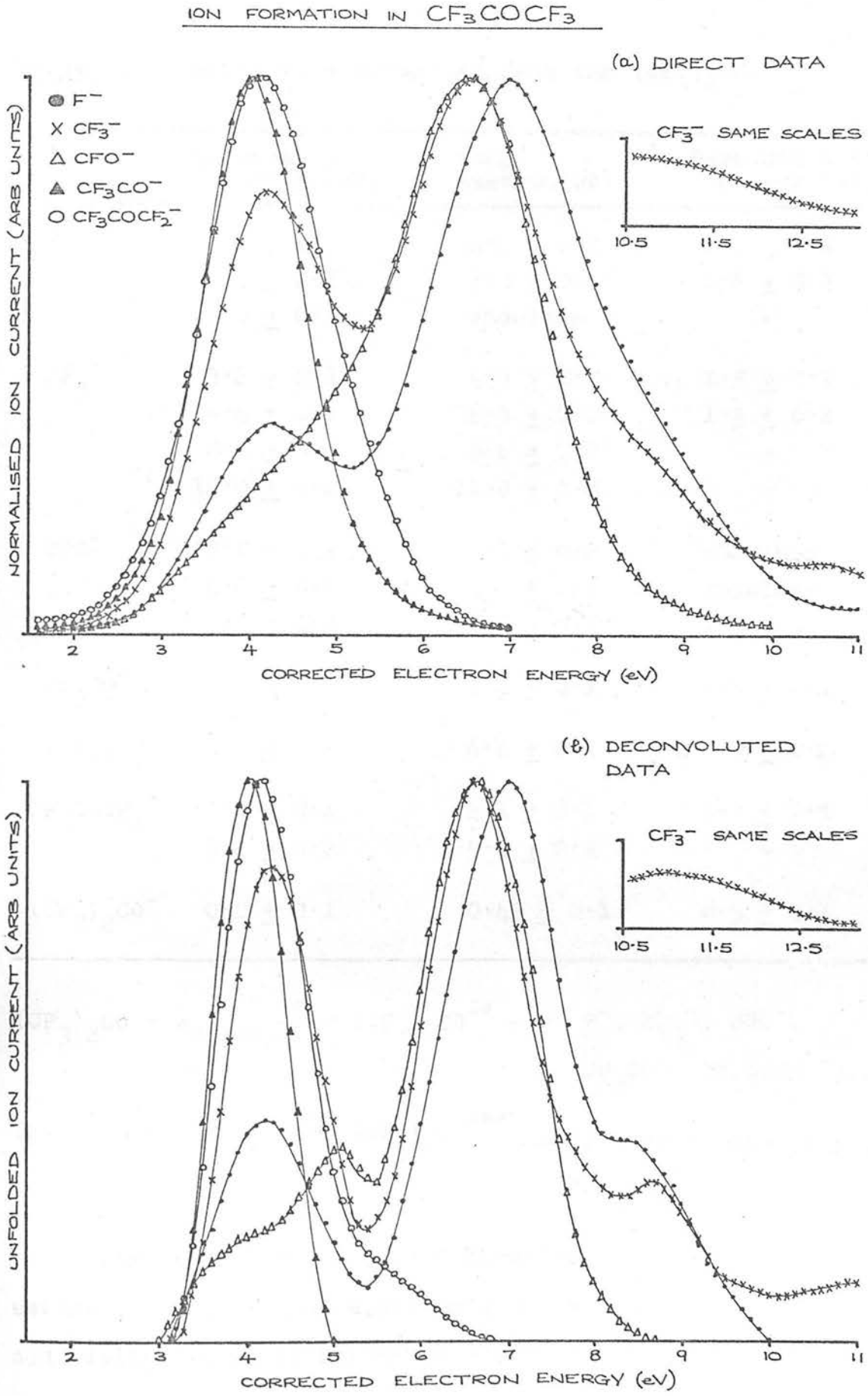
ION FORMATION IN CF_3COCF_3
(a) DIRECT DATA
F^-
CF_3^-
CFO^-
CF_3CO^-
$CF_3COCF_2^-$
CF_3^- SAME SCALES
10·5
11·5
12·5
NORMALISED ION CURRENT (ARB UNITS)
2
3
4
5
6
7
8
9
10
11
CORRECTED ELECTRON ENERGY (eV)
(b) DECONVOLUTED DATA
CF_3^- SAME SCALES
10·5
11·5
12·5
UNFOLDED ION CURRENT (ARB UNITS)
2
3
4
5
6
7
8
9
10
11
CORRECTED ELECTRON ENERGY (eV)

Fig 8.7

Table 8.7. Appearance potential data for $(CF_3)_2CO$.

Ion	Appearance Potential(eV)	Peak Maximum(eV)	Peak Width at ½-height (eV)
F^-	3·1 ± 0·1	4·2 ± 0·1	1·3 ± 0·1
	5·4 ± 0·2	7·0 ± 0·1	1·6 ± 0·1
	8·0 ± 0·3	shoulder	-
CF_3^-	3·2 ± 0·1	4·3 ± 0·1	1·2 ± 0·1
	5·4 ± 0·2	6·6 ± 0·1	1·5 ± 0·1
	8·1 ± 0·3	8·6 ± 0·2	-
	10·0 ± 0·2	11·0 ± 0·2	-
CFO^-	3·0 ± 0·1	4·1 ± 0·2	shoulder
	4·2 ± 0·2	5·1 ± 0·1	shoulder
	5·5 ± 0·2	6·6 ± 0·1	1·5 ± 0·1
CF_3CO^-	3·2 ± 0·1	4·0 ± 0·1	1·0 ± 0·1
$(CF_3)_2C^-$	5·1 ± 0·2	6·2 ± 0·2	1·0 ± 0·2
$CF_3COCF_2^-$	3·2 ± 0·1	4·1 ± 0·1	1·1 ± 0·1
	5·2 ± 0·2	5·8 ± 0·2	-
$(CF_3)_2CO^-$	0·0 ± 0·1	0·45 ± 0·1	0·5 ± 0·1

$$(CF_3)_2CO + e_{3\cdot1eV} \xrightarrow{64} (CF_3)_2CO^{-*} \longrightarrow F^-,\ CF_3^-,\ CFO^-,\ CF_3CO^-,\ CF_3COCF_2^-,\ldots\ldots$$

$$(CF_3)_2CO + e_{5\cdot4eV} \xrightarrow{65} (CF_3)_2CO^{-**} \longrightarrow F^-,\ CF_3^-,\ CFO^-,(CF_3)_2C^-,\ CF_3COCF_2^-,\ldots\ldots\ldots$$

The heat of formation of hexafluoroacetone was estimated to be -348·3 Kcals/mole or -15·1eV using the group additivity tables of Benson et al.[136]

If the $F\text{-}CF_2COCF_3$ bond dissociation energy is not too different from the average value of 5·2 ± 0·2eV found for the fluorocarbons (Chapter 7) then F^- ion formation by reaction 66 at 3·1 ± 0·1eV would involve 1·3eV of excess energy.

$$(CF_3)_2CO + e \xrightarrow{66} F^- + CF_2COCF_3$$
$$\xrightarrow{67} F^- + CF_2 + COCF_3$$
$$\xrightarrow{68} F^- + CF_2 + CF_3 + CO$$

As the estimated minimum enthalpy requirement of reaction 68 is 4·6eV the less energetically demanding reaction, 67, i.e. that which is analogous to the reaction proposed to account for F^- ion formation from CF_3COCH_3 at 4·2eV, may be responsible for the appearance potential at 3·1 ± 0·1eV. Assuming this to be so the heat of formation of the trifluoromethyl acetyl radical, CF_3CO, may be estimated to be $\leq$ -7·6 ± 0·3eV and using this in conjunction with known thermochemical data the $CF_3\text{-}COCF_3$ bond dissociation energy is calculated to be $\geq$ 3·6eV. The corresponding bond dissociation energy in acetone has a strength of 3·8eV[133] but it is likely[137] that the $CF_3\text{-}COCF_3$ bond is 0·1eV weaker i.e. ~3·7eV. The value estimated above is consistent with the difference expected between the bond energies and consequently reaction 67 is proposed to account for F^- ion formation at 3·1 ± 0·1eV.

Reaction 68 involving ~0·9eV of excess energy or reaction 69, which has a minimum enthalpy requirement of approximately 5·2eV, are the most probable sources of F^-

ion formation at 5·4 ± 0·2eV and reaction 70, for which

$$(CF_3)_2CO + e \xrightarrow{69} F^- + CF_2 + CF_2CO + F$$
$$\xrightarrow{70} F^- + 2CF_2 + CO + F$$

$\Delta H_{min} \simeq 8{\cdot}5$eV, is suggested to account for the shoulder at ~8eV in the trailing edge of the major F^- peak, Fig. 8.6(b).

It can be seen from Fig. 8.7 that the CF_3^- ion is formed extensively over the 3 - 13eV energy range. Using $E(CF_3) = 2{\cdot}0 \pm 0{\cdot}1$eV[4,17,119] and known thermochemical data[23,129] including values deduced above i.e. $\Delta H_f(CF_2CO)$ and $\Delta H_f(CF_3C)$, the following reactions have the minimum enthalpy requirements shown,

		ΔH_{min}(eV)
$(CF_3)_2CO + e \xrightarrow{71}$	$CF_3^- + CF_3CO$	0·6
$\xrightarrow{72}$	$CF_3^- + CO + CF_3$	2·1
$\xrightarrow{73}$	$CF_3^- + CF_2CO + F$	2·9
$\xrightarrow{74}$	$CF_3^- + CFO + CF_2$	4·7
$\xrightarrow{75}$	$CF_3^- + CF_2 + CO + F$	6·0
$\xrightarrow{76}$	$CF_3^- + CF_3C + O$	7·0 - 7·3
$\xrightarrow{77}$	$CF_3^- + CO + CF + F_2$	9·5
$\xrightarrow{78}$	$CF_3^- + COF + CF + F$	9·8
$\xrightarrow{79}$	$CF_3^- + CO + CF + 2F$	11·1

Assuming minimum excess energy involvement in ion formation, reactions 73, 74, 76 and 78 are suggested to account for the observed appearance potentials at 3·2 ± 0·1, 5·4 ± 0·2, 8·1 ± 0·3 and 10·0 ± 0·2eV respectively.

CFO^- ion formation showed a linear dependence on ion source pressure over the energy range shown in Fig. 8.7. If reaction 80 is that responsible for ion formation at $3{\cdot}0 \pm 0{\cdot}1$eV,

$$(CF_3)_2CO + e \xrightarrow{80} CFO^- + CF_3 + CF_2$$

the heat of formation of the fluoroformyl negative ion is calculated to be $\lesssim -5{\cdot}4$eV. This value is in reasonable agreement with that of $\leq -4{\cdot}65 \pm 0{\cdot}5$eV deduced for this species from ion formation in carbonyl fluoride.[55,113] Reaction 80, possibly involving excess energy, is therefore attributed to ion formation at $3{\cdot}0 \pm 0{\cdot}1$eV. As the next least energetically demanding process, reaction 81, requires over 6eV the shoulder at $4{\cdot}2 \pm 0{\cdot}2$eV and the major peak, onsetting at $5{\cdot}5 \pm 0{\cdot}2$eV, must correspond to reaction 80 in which excess energy is involved.

$$(CF_3)_2CO + e \xrightarrow{81} CFO^- + 2CF_2 + F$$

The trifluoroacetyl negative ion exhibited a single resonance peak onsetting at $3{\cdot}2 \pm 0{\cdot}1$eV and which probably corresponds to the following reaction,

$$(CF_3)_2CO + e \xrightarrow{82} CF_3CO^- + CF_3$$

From the relationship $D(CF_3\text{-}COCF_3) \leq A(CF_3CO^-) + E(CF_3CO)$, using the value of $\geq 3{\cdot}6$eV deduced above for $D(CF_3\text{-}COCF_3)$, the electron affinity of CF_3CO is estimated to be $\geq 0{\cdot}4$eV.

The $(CF_3)_2C^-$ ion was formed with a low cross-section onsetting at $5{\cdot}0 \pm 0{\cdot}2$eV and formation is attributed to

reaction 83.

$$(CF_3)_2CO + e \xrightarrow{83} (CF_3)_2C^- + O$$

If $D((CF_3)_2C=O) \sim D(CH_2=O)$, which is calculated to be 5·45eV from thermochemical data,[23] the electron affinity of the $(CF_3)_2C$ radical is estimated to be $\gtrsim$ 0·45eV. There is no other reported value with which this can be compared.

The $CF_3COCF_2^-$ ion, formed by reaction 84, exhibits

$$(CF_3)_2CO + e \xrightarrow{84} CF_3COCF_2^- + F$$

a sharp resonance at 3·2 ± 0·1eV and a lower cross-section resonance appearing as a shoulder on the trailing edge of this resonance at 5·2 ± 0·2eV. If $D(F\text{-}CF_2COCF_3)$ is approximately equal to the average C-F bond dissociation energy found for the fluorcarbons i.e. 5·2 ± 0·2eV, then, from the appearance potential of reaction 84 at 3·2 ± 0·1eV, $E(CF_2COCF_3)$ is estimated to be $\geq$ 2·0 ± 0·3eV.

The second appearance potential at 5·2 ± 0·2eV, which may be identified as a dissociation channel of reaction 65, must correspond to reaction 84 in which ~2eV of excess energy is involved.

(c) Bis-trifluoromethylnitroxide, $(CF_3)_2NO$.

$(CF_3)_2NO$ is a yellow solid at liquid nitrogen temperature which melts into a purple liquid before evaporating at -45°C into a blue-purple gas. The chemical reactivity of $(CF_3)_2NO$ has not been reported in the

literature and so the mass spectrum of the pure gas was compared with those of A, CO, SO_2 and SF_6 mixtures (50/50 total P = 1 torr) from which it was concluded that significant chemical reaction with these molecules does not take place at room temperature in the time period required for an ionisation efficiency run (~2 hrs).

This molecule was of particular interest as the molecular negative ion, if formed, would be isoelectronic with CF_3OOCF_3 and $(CF_3)_2NF$ which are both well-known and stable molecules. As electron capture would involve lone pair formation, it might also be expected to exhibit unusual stability for a molecular ion with only 24 vibrational degrees of freedom. These suspicions were realized and the average autodetachment lifetime of the molecular negative ion, which was formed at 0eV with a broad resonance maximising at 1·2 ± 0·1eV, was found to be ~650 μsec. This may be compared to the autodetachment lifetimes of the following molecules which also have 24 vibrational degrees of freedom; C_4F_6-2 (16·3 μsec.), c-C_4F_6 (11·2 μsec.) and $(CF_3)_2CO$ (60 μsec.[66]). Although it is apparent from these examples that the carbonyl group exerts a strong influence on the stability (lifetime) of the negative ion state reconciliation of the nitroxide lifetime can only be found in the stability incurred by lone pair formation.

$(CF_3)_2NO$ proved to be an abundant source of negative ions, the average cross-section for dissociative electron capture being several orders of magnitude higher than that found for hexafluoroacetone i.e. comparable with SF_6

($\sim 10^{-15}$cm.^{2}). The ions F^-, CF_3^-, CF_3O^-, CF_3NO^-, $(CF_3)_2N^-$ and $(CF_3)_2NO^-$ were all shown by pressure dependence measurements to be primary ions and were formed with relative abundances in the ratio 97:131:1000:53:946:32 at their respective capture maxima and in the ratio 1000:551:123:170:240:13 at 70eV. The rearrangement ion CF_3O^- exhibited the highest cross-section at low electron energies, the peak profile being exactly similar to that of the molecular negative ion which is shown, together with the $(CF_3)_2N^-$ ionisation curve, in Fig. 8.8.

It can be seen from Fig. 8.8 that the $(CF_3)_2NO^-$ resonance peak is considerably broader than that exhibited by SF_6^- and from Fig. 8.9(a) and (b) that all the fragmentation ions are also formed at this energy. The magnitude of the low energy peaks (below 1·5eV) was found to be partially dependent upon the electron trap current whilst the relative dimensions of the remaining part of the ionisation curves remained unaffected by source conditions. It is therefore apparent that surface ionisation effects are prevalent at the lower electron energies although this, being inconsistent with the stability found for the other peak parameters i.e. peak onsets and maxima, does not provide the complete explanation. The width of the $(CF_3)_2NO^-$ capture peak compared to that of SF_6^- indicates that a broad band of closely spaced energy states are involved in ion formation and the appearance of all ions in this energy range may then suggest that some of these states are unstable toward the corresponding dissociative capture channels;

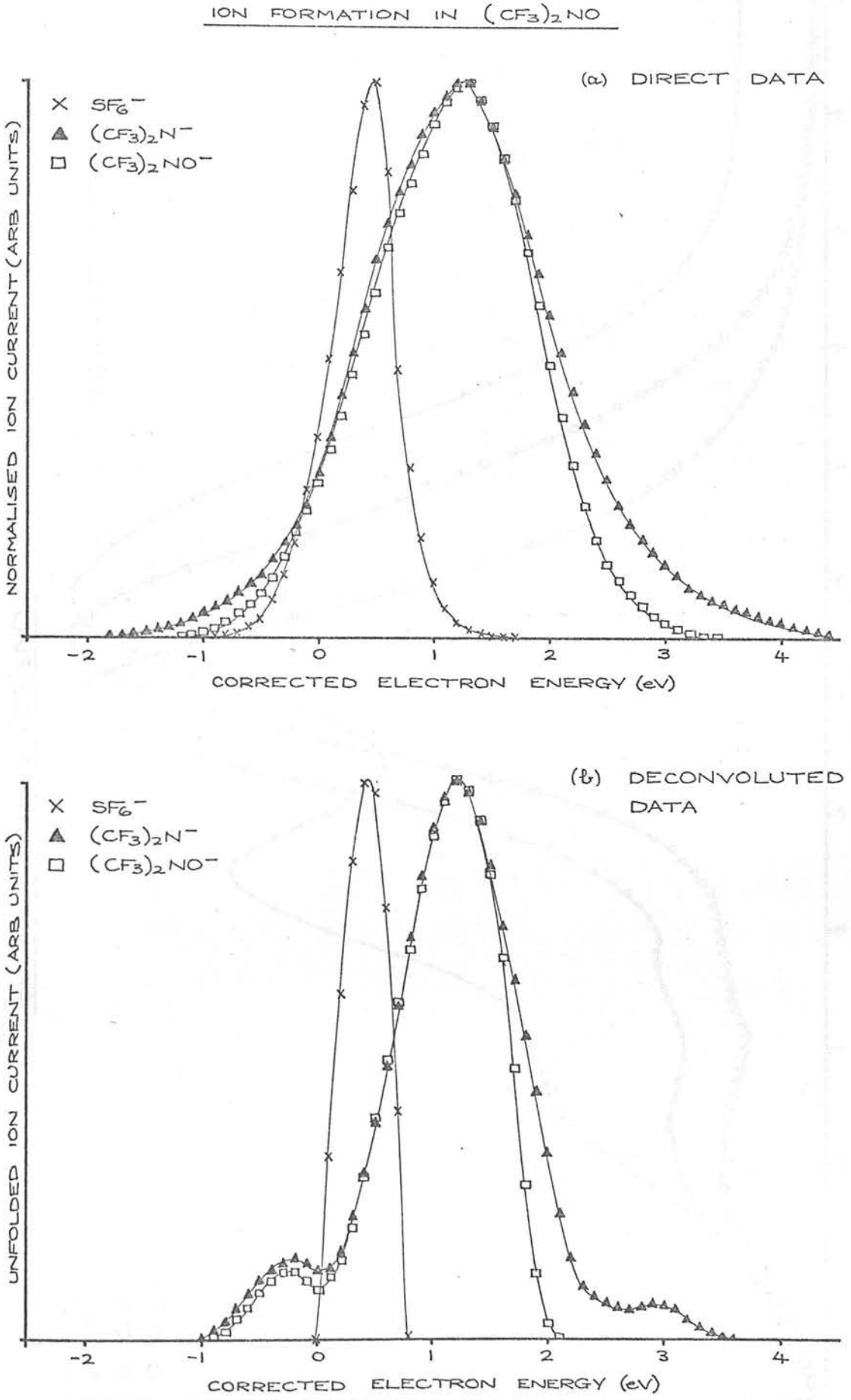
ION FORMATION IN $(CF_3)_2NO$
(a) DIRECT DATA
SF_6^-
$(CF_3)_2N^-$
$(CF_3)_2NO^-$
NORMALISED ION CURRENT (ARB UNITS)
-2
-1
0
1
2
3
4
CORRECTED ELECTRON ENERGY (eV)
(b) DECONVOLUTED DATA
SF_6^-
$(CF_3)_2N^-$
$(CF_3)_2NO^-$
UNFOLDED ION CURRENT (ARB UNITS)
-2
-1
0
1
2
3
4
CORRECTED ELECTRON ENERGY (eV)

Fig 8.8

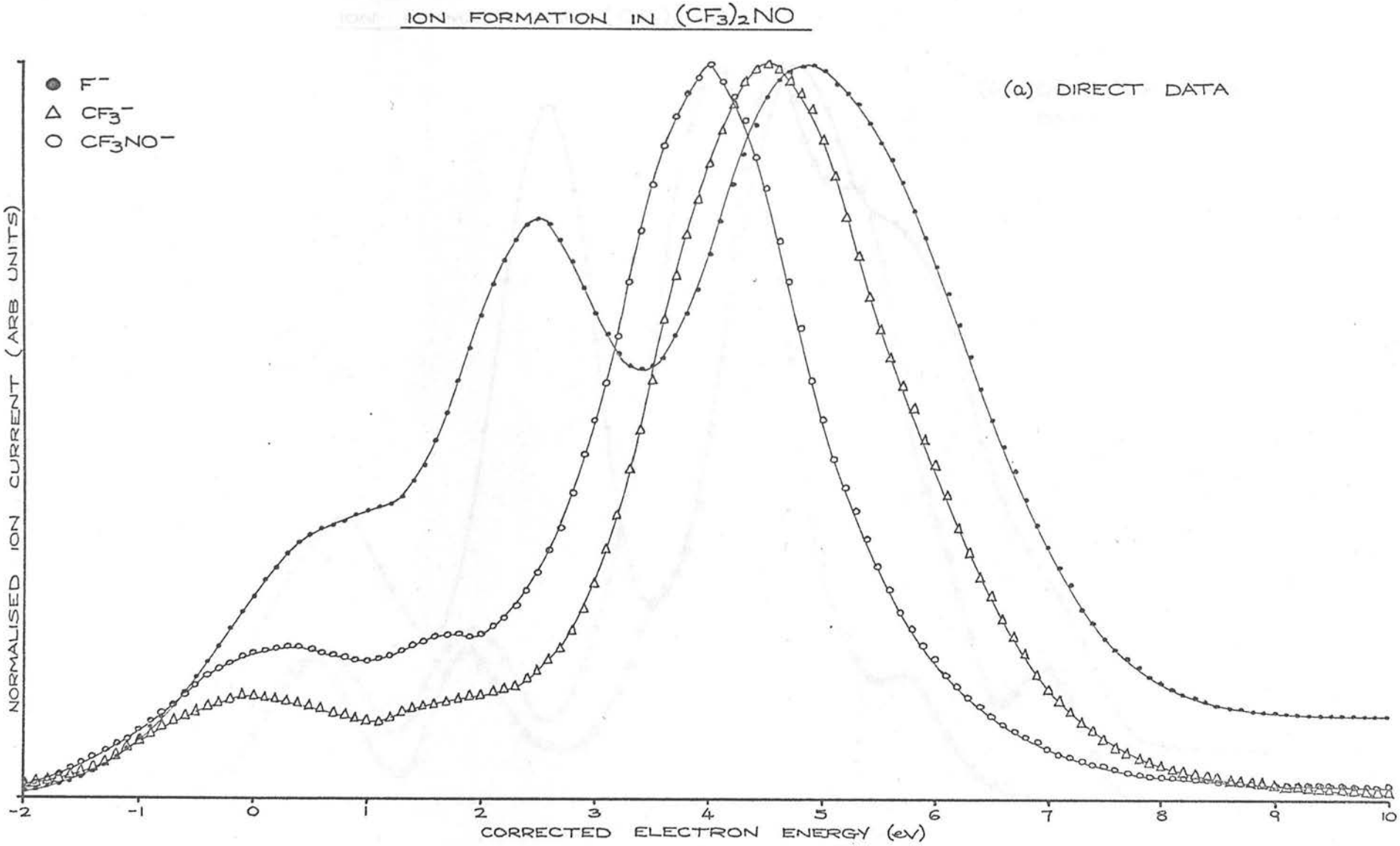
ION FORMATION IN $(CF_3)_2NO$
(a) DIRECT DATA
● F^-
△ CF_3^-
○ CF_3NO^-
NORMALISED ION CURRENT (ARB UNITS)
-2
-1
0
1
2
3
4
5
6
7
8
9
10
CORRECTED ELECTRON ENERGY (eV)

Fig 8.9

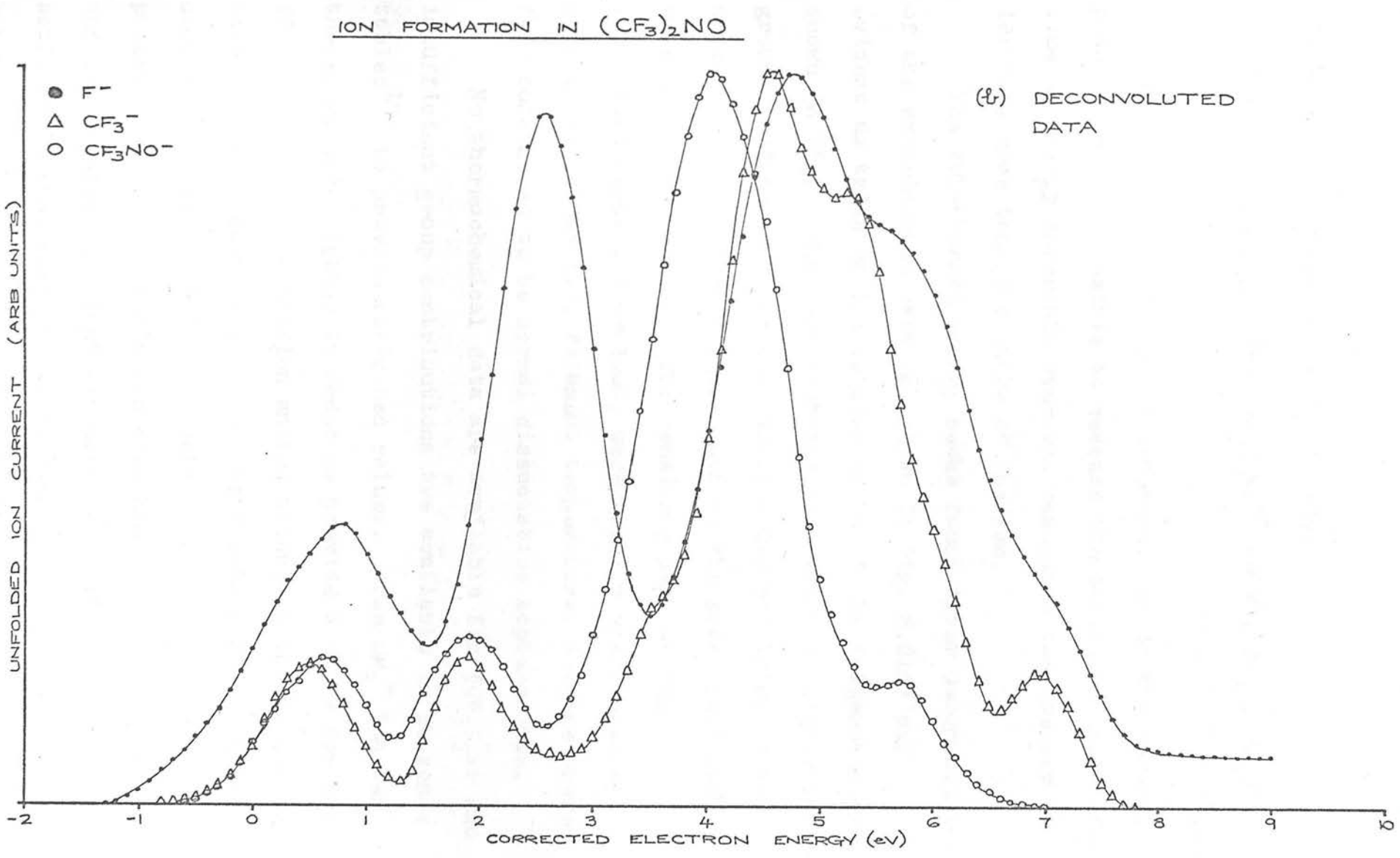
ION FORMATION IN $(CF_3)_2NO$
F^-
CF_3^-
CF_3NO^-
(r) DECONVOLUTED DATA
UNFOLDED ION CURRENT (ARB UNITS)
-2
-1
0
1
2
3
4
5
6
7
8
9
CORRECTED ELECTRON ENERGY (eV)

Fig 8.9

cf. $C_4F_6(CF_3)_2$ Chapter 7 and ref. 135.

$$(CF_3)_2NO + e_{0\rightarrow 1\cdot 5eV} \xrightarrow{85} (CF_3)_2NO^{-*} \longrightarrow F^-,\ CF_3^-,\ CF_3O^-,\ CF_3NO^-,\ (CF_3)_2N^-,\ldots..$$

Because of the relatively low cross-section of the neutral peak it was not possible to measure the autodetachment lifetime at energy intervals over the resonance and thereby to identify more than one state of the ion.

The sub-thermal energy peaks found after deconvolution of the experimental data and shown in Fig. 8.8(b) and evident as tails on the leading edges of the fragment peaks shown in Fig. 8.9(b) are probably the result of either background surface ionisation or ineffective unfolding of the broad tails peculiar to these data as the peak amplitudes were not reproducible. The remaining part of the ionisation curves, 1 $\longrightarrow$ 10eV, were totally unaffected by source conditions i.e. filament temperature, and are therefore considered to be normal dissociative capture data.

No thermochemical data are available for $(CF_3)_2NO$ and insufficient group contributions are available in Benson's tables[136] to provide estimated values. The CF_3^+ ion was therefore investigated in order to provide a value for the CF_3-$NOCF_3$ bond dissociation energy which, in the absence of thermochemical data, may be used as a comparison with values deduced from the negative ion data. The ionisation potential of the molecule was also measured at the same time and the appearance potentials measured relative to an energy scale calibrated against the spectroscopic appearance potential of A^+/Argon at 15·76eV[15] are given in Table 8.6.

Table 8.6. Positive ion data for $(CF_3)_2NO$

Ion	Appearance Potential (eV)
CF_3^+	13·0 ± 0·5
$(CF_3)_2NO^+$	10·5 ± 0·2

Using the appearance potential of the CF_3^+ ion in conjunction with the known ionisation potential of CF_3, 10·1 ± 0·1eV,[23] the CF_3-$NOCF_3$ bond dissociation energy is estimated to be ≤ 2·9 ± 0·6eV.

Excluding the thermal energy peaks the negative ion appearance potential data is given in Table 8.7 where the uncertainties shown are the average of several repeated determinations. The energy scale in Fig. 8.9 is calibrated against the appearance potentials of the O^- ion formed from SO_2 at 4·2 and 6·6eV. Initially all ions were intercalibrated in the pure gas before addition of a small SO_2 sample and all experiments were carried out within 48 hours of breaking the ampoule seal.

It can be seen from Fig. 8.9(b) that the F^- ion exhibits three major resonances the first onsetting at 1·6 ± 0·1eV, the second at 3·5 ± 0·1eV and the third, a shoulder on the trailing edge of the second peak, at ~5·2eV. The initial onset probably corresponds to the following reaction,

$$(CF_3)_2NO + e \xrightarrow{86} F^- + CF_2NOCF_3$$

Table 8.7. Appearance potential data for $(CF_3)_2NO$.

Ion	Appearance Potential(eV)	Peak Maximum(eV)	Peak Width at ½-height(eV)
F^-	1·6 ± 0·1	2·5 ± 0·1	1·1 ± 0·1
	3·5 ± 0·1	4·7 ± 0·1	~2·4
	~5·2	shoulder	
	~6·5	shoulder	-
CF_3^-	1·3 ± 0·1	1·9 ± 0·1	0·8 ± 0·1
	2·7 ± 0·2	4·5 ± 0·2	1·8 ± 0·2
	~5·0	shoulder	
	~6·5	shoulder	-
CF_3O^-	0·0 ± 0·1	1·2 ± 0·1	1·0 ± 0·1
CF_3NO^-	1·2 ± 0·1	1·9 ± 0·1	1·1 ± 0·1
	2·6 ± 0·1	4·0 ± 0·1	1·4 ± 0·1
	~5·4	shoulder	-
$(CF_3)_2N^-$	0·0 ± 0·1	1·2 ± 0·1	1·2 ± 0·1
	2·7 ± 0·2	shoulder	-
$(CF_3)_2NO^-$	0·0 ± 0·1	1·2 ± 0·1	1·0 ± 0·1

from which the $F\text{-}CF_2NOCF_3$ bond dissociation energy is estimated to be $\leq 5{\cdot}05 \pm 0{\cdot}1$eV in accord with values deduced for similar bonds above or reported in the literature, i.e. $D(F\text{-}CF_3) = 5{\cdot}3$eV,[130] $D(F\text{-}C_2F_5) \leq 5{\cdot}25 \pm 0{\cdot}1$eV,[17] $D(F\text{-}C_3F_7) \leq 5{\cdot}25 \pm 0{\cdot}1$eV (Chapter 7).

If the appearance potential at $3{\cdot}5 \pm 0{\cdot}1$eV corresponds to reaction 87 which is analogous to that identified with F^- ion formation from $(CF_3)_2CO$ at $3{\cdot}1 \pm 0{\cdot}1$eV and CF_3COCH_3 at $4{\cdot}2 \pm 0{\cdot}2$eV then,

$$(CF_3)_2NO + e \xrightarrow{87} F^- + CF_2 + CF_3NO$$

$D(CF_2\text{-}NOCF_3)$ is deduced to be $1{\cdot}9 \pm 0{\cdot}2$eV. In the absence of thermochemical data further process identification is precluded

The CF_3^- ionisation curve bears a close resemblance to that of the F^- ion and four processes are apparent. The following reaction is proposed to account for the initial appearance potential at $1{\cdot}3 \pm 0{\cdot}1$eV,

$$(CF_3)_2NO + e \xrightarrow{88} CF_3^- + CF_3NO$$

Using $E(CF_3) = 2{\cdot}0 \pm 0{\cdot}1$eV[4,17,119] the $CF_3\text{-}NOCF_3$ bond dissociation energy is estimated to be $\leq 3{\cdot}3 \pm 0{\cdot}2$eV in good agreement with the value $\leq 2{\cdot}9 \pm 0{\cdot}6$eV deduced from the positive ion data. Reaction 88 is therefore attributed to ion formation at $1{\cdot}3 \pm 0{\cdot}1$eV. Reversing this argument and setting the appearance potential equal to the minimum enthalpy requirement the following may be deduced, $\Delta H_f(CF_3)_2NO - \Delta H_f CF_3NO \leq -8{\cdot}2 \pm 0{\cdot}2$eV. Now, assuming that the onset at $2{\cdot}7 \pm 0{\cdot}2$eV corresponds to the next least energetically demanding reaction:-

$$(CF_3)_2NO + e \xrightarrow{89} CF_3^- + NO + CF_3$$

the heat of formation of $(CF_3)_2NO$ is estimated to be $\leq -13{\cdot}6 \pm 0{\cdot}4$eV. Using this in conjunction with the difference calculated from reaction 88 $\Delta H_f(CF_3NO)$ is estimated to be $\leq -5{\cdot}4 \pm 0{\cdot}6$eV. Support for these values and therefore the reactions suggested is found from their use in a calculation of the minimum enthalpy requirements

of reaction 87 which has been proposed to account for F^- ion formation at $3{\cdot}5 \pm 0{\cdot}1$eV; $\Delta H_{min} = 3{\cdot}8 \pm 1{\cdot}1$eV.

Using the values deduced above the minimum enthalpy requirement of reaction 90 is estimated to be 6·6eV and is therefore suggested to account for the observed appearance potential at ~6·5eV.

$$(CF_3)_2NO + e \xrightarrow{90} CF_3^- + NO + CF_2 + F$$
$$\xrightarrow{91} CF_3^- + CF_2NO + F$$

The reaction responsible for the shoulder at ~5·0eV cannot be unequivocally identified but may correspond to reaction 91.

Using the value $\leq 3{\cdot}3 \pm 0{\cdot}2$eV deduced for $D(CF_3\text{-}NOCF_3)$ from reaction 88 in conjunction with the appearance potential of the CF_3NO^- ion formed by reaction 92 at $1{\cdot}2 \pm 0{\cdot}1$eV,

$$(CF_3)_2NO + e \xrightarrow{92} CF_3NO^- + CF_3$$

the electron affinity of the trifluoromethylnitroxide radical is estimated to be $\geq 2{\cdot}1 \pm 0{\cdot}3$eV. Reversing the argument $\Delta H_f(CF_3NO^-)$ is calculated to be $\leq -7{\cdot}5 \pm 0{\cdot}5$eV. Reaction 93, the next least energetically demanding reaction, is then estimated to have a minimum enthalpy requirement of $5{\cdot}1 \pm 1{\cdot}1$eV and may therefore correspond to the process relevant to the low cross-section shoulder at ~5·4eV.

$$(CF_3)_2NO + e \xrightarrow{93} CF_3NO^- + CF_2 + F$$

The major peak onsetting at $2{\cdot}6 \pm 0{\cdot}1$eV must therefore correspond to reaction 92 with an excess energy involvement of ~1·4eV.

The $(CF_3)_2N^-$ ion was found to exhibit a similar cross-section profile to that of the molecular negative ion except for the presence of a second, low cross-section, resonance in the tail of the peak. If the onset at 0·0 ± 0·1eV corresponds to reaction 94 then that

$$(CF_3)_2NO + e \xrightarrow{94} (CF_3)_2N^- + O$$

at 2·7 ± 0·2eV must also result from reaction 94 involving ~2·7eV of excess energy. From reaction 94 it may be deduced that $E((CF_3)_2N) \geq D((CF_3)_2N=O)$.

The CF_3O^- ion was formed with a very high cross-section at 0eV and its formation has been partially attributed to effects at the surface of the filament. However, the stability of the cross-section profile under different ion source conditions indicates that contributions to the ion current must originate from a rearrangement reaction of the type shown,

$$(CF_3)_2NO + e \xrightarrow{95} CF_3O^- + CF_3N$$
$$\xrightarrow{96} CF_3O^- + CF_3 + N$$

Using known thermochemical data[4,23,113] in conjunction with $\Delta H_f(CF_3)_2NO$ deduced above the minimum enthalpy requirement of reaction 96 is calculated to be approximately 5·6eV. Reaction 96 does not therefore contribute to ion formation and reaction 95 is proposed to account for the ionisation curve observed. Using $E(CF_3O) \geq 1·9 \pm 0·2eV$[113] and the appearance potential at 0·0 ± 0·1eV, the heat of formation of the CF_3N radical is estimated from reaction 95 to be $\leq -5·1 \pm 0·7eV$.

The electron affinities, bond dissociation energies and heats of formation measured and deduced in the course of this chapter are tabulated and discussed in Chapter 9.

CHAPTER 9

SUMMARY OF RESULTS

In this chapter, values obtained for electron affinities, ionisation potentials, bond dissociation energies and heats of formation are collated, discussed and compared to the results reported, if any, by other workers.

Table 9.1. Electron Affinities.

Species	Electron Affinity (eV)	Source Molecule	Other Literature Values (eV)
FCN	$\geq 2{\cdot}8 \pm 1{\cdot}7$	PF_2CN	
FCl	$1{\cdot}5 \pm 0{\cdot}4$	SF_5Cl	$\geq 1{\cdot}04$ (stability)
NCO	$\geq 2{\cdot}6 \pm 0{\cdot}4$	PF_2NCO	
PF_2	$\geq 1{\cdot}6 \pm 0{\cdot}5$	PF_2NCS	
SF_3	$2{\cdot}95 \pm 0{\cdot}1$	SF_4	2·71[4]
SF_4	1·24 (calculated)	SF_4	
	~1·2	SF_6	
SF_6	1·44 (calculated)		1·43[4]
WF_4	$\gtrsim 2{\cdot}5$	WF_6	
WF_5	$\geq 0{\cdot}85 \pm 0{\cdot}2$	WF_6	
CF_2	$\leq 1{\cdot}6 \pm 0{\cdot}5$	$c\text{-}C_4F_8$	$\geq 0{\cdot}2$,[119] $\geq 0{\cdot}6 \pm 1{\cdot}0$,[113] 2·65[4]
CF_2C	$\lesssim 1{\cdot}9$	CF_3CHO	
	$\lesssim 1{\cdot}5$	CF_3CHO	

[Contd.

Table 9.1 (contd.)

Species	Electron Affinity (eV)	Source Molecule	Other Literature Values (eV)
CF_3C	$\lesssim 3{\cdot}1$	CF_3CHO	
	$\lesssim 2{\cdot}8$	CF_3COCH_3	
C_2F_5	$2{\cdot}1 \pm 0{\cdot}2$	n-C_3F_8	$1{\cdot}8 \pm 0{\cdot}2$,[124] $1{\cdot}95 \pm 0{\cdot}2$,[124]
	$2{\cdot}2 \pm 0{\cdot}3$	n-C_4F_{10}	$\sim 2{\cdot}3$,[122] $\sim 2{\cdot}4$[17]
C_3F_5	$2{\cdot}7 \pm 0{\cdot}2$	C_3F_6	
	$\geq 2{\cdot}4 \pm 0{\cdot}3$	C_4F_8-2	
	$2{\cdot}5 \pm 0{\cdot}3$	c-C_4F_8	
$(CF_3)_2C$	$\gtrsim 0{\cdot}45$	$(CF_3)_2CO$	
C_3F_7	$2{\cdot}35 \pm 0{\cdot}2$	n-C_3F_8	$2{\cdot}0$,[4] $\sim 2{\cdot}4$[122]
	$2{\cdot}2 \pm 0{\cdot}2$	n-C_4F_{10}	
C_4F_5	$1{\cdot}7 \pm 0{\cdot}2$	c-C_4F_6	
C_4F_7	$\sim 3{\cdot}5$	C_4F_8-2	
	$2{\cdot}6 \pm 0{\cdot}5$	$C_4F_6(CF_3)_2$	
C_4F_9	$3{\cdot}25 \pm 0{\cdot}3$	n-C_4F_{10}	
C_5F_9	$3{\cdot}1 \pm 0{\cdot}3$	$C_4F_6(CF_3)_2$	$\sim 3{\cdot}1$[135]
C_6F_{11}	$4{\cdot}2 \pm 0{\cdot}2$	$C_4F_6(CF_3)_2$	$\sim 3{\cdot}5$[135]
CF_3CO	$\gtrsim 0{\cdot}4$	$(CF_3)_2CO$	
CF_3NO	$\geq 2{\cdot}1 \pm 0{\cdot}3$	$(CF_3)_2NO$	
$CFCOCH_3$	$\geq 1{\cdot}7 \pm 0{\cdot}5$	CF_3COCH_3	
CF_2COCH_3	$\geq 1{\cdot}0 \pm 0{\cdot}3$	CF_3COCH_3	
CF_2COCF_3	$\geq 2{\cdot}0 \pm 0{\cdot}3$	$(CF_3)_2CO$	

It can be seen from Table 9.1 that only in a few cases have electron affinities been reported previously but in these cases the agreement is generally good. The value of E(FCl) = 1·5 ± 0·4eV, although estimated from a single reaction, is in good accord with the lower limit (1·04eV) calculated for this species from the stability of the ion against decomposition to Cl^- plus F. $E(SF_3)$, reported from a magnetron study of sulphur tetrafluoride to be 2·71eV[4] and deduced in this work to be 2·95 ± 0·1eV, also from ion formation in sulphur tetrafluoride, are in complete agreement within their respective experimental uncertainties. The value of 1·44eV calculated for $E(SF_6)$ from the statistical theory of electron attachment[35] is in excellent agreement with the value reported from a magnetron investigation of sulphur hexafluoride by Page and Goode[4] (1·43eV), therefore lending support to the treatment of small molecules by this approach.

The electron affinity of the CF_2 radical determined from a single reaction to be ≤ 1·6 ± 0·5eV may be compared with the previously reported electron impact values of ≥ 0·2[119] and ≥ 0·6 ± 1·0eV.[113] As the use of this value, ≤ 1·6 ± 0·5eV, in the calculation of the energy requirements for further CF_2^- ion forming reactions by c-C_4F_8 resulted in values which matched the measured appearance potential data this value is preferred.

The electron affinity of the trifluoromethyl radical has been determined by several groups of workers[4,17,119,122] and the average value of 2·0eV is accepted and has been used in the main text. It is also found, from the electron

affinity data reported in the literature, that the electron affinities of fluorinated radicals increases as the homologous series are ascended. The values deduced in this work for $E(C_2F_5)$ i.e., 2·1 ± 0·2 and 2·2 ± 0·3eV, are in accord with these observations and in agreement with the previously reported values of ~2·3[122] and ~2·4eV.

Of the two determinations for $E(C_3F_7)$ the higher value, 2·35 ± 0·2eV, which was calculated from ion formation in C_3F_8 by a reaction which does not involve C-C bond cleavage, is preferred. This is in agreement with the value of ~2·4eV estimated by Lifshitz and Grajower[122] also from ion formation in C_3F_8.

The values deduced for $E(C_5F_9)$ and $E(C_6F_{11})$ from ion formation in $C_4F_6(CF_3)_2$ are in reasonable accord with the values estimated by Lifshitz et al.[135]

The electron affinity deduced for FCN, ≥ 2·8 ± 1·7eV, may be compared with the electron affinities of other dihalogen negative ions i.e. $E(F_2)$ = 2·9 ± 0·2,[65] $E(Cl_2)$ = 2·52 ± 0·17[65] and E(FCl) = 1·5 ± 0·4eV (above).

Values for the electron affinities of the CN and NCS radicals have been reported by Page and Goode[4] to be 3·1 ± 0·3 and 2·2eV respectively and a survey of the literature shows that those radicals containing an oxygen atom in place of a sulphur atom exhibit lower electron affinities. E(NCO), deduced above to be ≥ 2·6 ± 0·4eV, may therefore be slightly high thereby indicating excess energy in the relevant reaction.

There are no previous values reported for $E(PF_2)$ but this work puts it as $\gtrsim 2{\cdot}9$ and $\geq 1{\cdot}6 \pm 0{\cdot}5$eV respectively.

$E(SF_4)$ was calculated (Chapter 4) from the statistical theory for electron attachment[35] to be $1{\cdot}24$eV. Using this value, reconciliation of the SF_4^- appearance potential data from SF_6 and SF_5Cl with the energetically favourable reactions was achieved, thereby lending support to the value calculated.

The electron affinities of WF_4 and WF_5 are estimated to be $\gtrsim 2{\cdot}5$ and $\geq 0{\cdot}85 \pm 0{\cdot}2$eV respectively. The value for $E(WF_4)$, which was estimated from a reaction identified on the assumption that a trend exists for the dissociative capture behaviour of the inorganic fluorides, is not expected to be as reliable as the value deduced for $E(WF_5)$.

The respective values obtained for $E(CF_2C)$ and $E(CF_3C)$ from reactions involving different source molecules are in good accord but because of the possibility of excess energy in the relevant reactions these results may be expected to be upper limits.

Although the molecular structure of the C_3F_5 radicals formed from the source molecules examined may or may not be identical the electron affinity of the C_3F_5 radical from the three systems show excellent agreement and an average value of $2{\cdot}6 \pm 0{\cdot}4$eV is suggested.

$E((CF_3)_2C)$, $E(C_4F_5)$, $E(C_4F_7)$ and $E(C_4F_9)$ have not been reported previously but the values measured in this study appear to be consistent with the general trend of increasing

electron affinity with ascent of the homologous series.

There are no other reported values with which the remaining electron affinities shown in Table 9.1 can be compared.

Table 9.2. Ionisation Potentials.

Species	Ionisation Potential(eV)	Source Molecule	Other Literature Values (eV)
CN	< 16·5	PF_2CN	14·2[22] (CH_3CN), ≤ 15·8[57] (CH_3CN)
NCO	< 14·1	PF_2NCO	
NCS	< 12·9	PF_2NCS	≤ 10·4[22] (CH_3NCS)
GeF	≤ 6·5	GeF_4	
GeF_2	≤ 9·8	GeF_4	
GeF_3	≤ 10·3	GeF_4	
PF	≥ 10·7 ± 2·2	PF_3	
PF_2	≥ 9·8 ± 1·4	PF_3	
PF_3	11·3 ± 0·2	PF_3	9·71[22,23], 11·5 ± 0·1[56]
PFCN	≳ 10·1	PF_2CN	
PF_2CN	11·6 ± 0·2	PF_2CN	
PFNCO	≳ 9·7	PF_2NCO	
PF_2NCO	10·5 ± 0·2	PF_2NCO	
PFNCS	≳ 9·2	PF_2NCS	
PF_2NCS	9·8 ± 0·2	PF_2NCS	
SF_4Cl	≤ 12·5 ± 0·2	SF_5Cl	
$(CF_3)_2NO$	10·5 ± 0·2	$(CF_3)_2NO$	

It is apparent from Table 9.2 that there are few ionisation potential data available from the literature with which comparisons can be made.

Because of possible excess energy involvement in the relevant reactions the values deduced for I(CN), I(NCO) and I(NCS) are expected to be upper limits. However, the value I(CN) < 16·5eV is in reasonable agreement with the upper limit of 15·8eV proposed by McDowell and Warren[57] and, as discussed in the text (Chapter 6) I(NCS) < 12·9eV is viewed with more confidence than is the earlier value of $\leq$ 10·4eV.[22]

$I(PF_3)$ = 11·3 $\pm$ 0·2eV is in agreement with the higher of the reported values i.e. 11·5 $\pm$ 0·1eV,[56] which was measured from a photo-electron spectroscopic study of PF_3.

The values for I(PF) and $I(PF_2)$ estimated in this work from a study of positive ion formation in PF_3 are associated with large uncertainties as a consequence of the thermochemical data used in the calculations. These uncertainties are not believed to be realistic (see text) and I(PF) $\geq$ 10·7eV and $I(PF_2)$ $\geq$ 9·8eV are suggested to be acceptable values.

Table 9.3. Bond Dissociation Energies.

Bond	Dissociation Energy (eV)	Source Molecule	Other Literature Values (eV)
F-Ge (average)	~5·4 (positive ion data)	GeF_4	
F-P	~4·4	PF_2CN	4·5 $\pm$ 1·0[18]
	~4·5	PF_2CN	
	~4·4	PF_2NCO	

[Contd.

Table 9.3 (contd.)

Bond	Dissociation Energy (eV)	Source Molecule	Other Literature Values (eV)
F-PF	~4·6	PF_2CN	4·8 ± 0·7
	~4·9	PF_2CN	(thermochemistry/PF_3)
	≤ 5·0 ± 0·5	PF_2NCO	
	4·5 ± 0·2	PF_2OPF_2	
F-S	2·55 ± 0·2	SF_6	2·8 ± 0·2[18]
F-SF	5·3 ± 0·7	SF_6	
$F-SF_2$	2·7 ± 0·4	SF_6	
$F-SF_3$	≤ 3·65 ± 0·05	SF_4	3·4[114]
	3·5 ± 0·3	SF_6	
$F-SF_4$	≤ 2·65	SF_6	
$F-SF_5$	≤ 3·45	SF_6	~3·4(average) (thermochemistry)
$F-WF_4$	5·8 ± 0·3	WF_6	
$F-WF_5$	≤ 5·25 ± 0·1	WF_6	5·4 ± 0·3(average) (thermochemistry)
$F-CF_2NOCF_3$	≤ 5·05 ± 0·1	$(CF_3)_2NO$	
$F-C_3F_5$	≤ 5·35 ± 0·1	C_3F_6	
$F-C_3F_7$	≤ 5·25 ± 0·1	C_3F_8	
$F-C_4F_5$	≤ 5·35 ± 0·1	$c-C_4F_6$	
$F-C_4F_9$	≤ 5·45 ± 0·1	$n-C_4F_{10}$	
$F-C_5F_7$	≤ 5·35 ± 0·1	$c-C_5F_8$	
$Cl-SF_5$	≤ 2·05	SF_5Cl	
$F_2C-NOCF_3$	1·9 ± 0·2	$(CF_3)_2NO$	

[Contd.

Table 9.3 (contd.)

Bond	Dissociation Energy (eV)	Source Molecule	Other Literature Values (eV)
F_3C-$NOCF_3$	$\leq 3{\cdot}3 \pm 0{\cdot}2$ (negative ion data) $\leq 2{\cdot}9 \pm 0{\cdot}6$ (positive ion data)	$(CF_3)_2NO$	
F_3C-$COCF_3$	$\geq 3{\cdot}6$	$(CF_3)_2CO$	$\sim 3{\cdot}7$[137]
F_3C-C_2F_5	$\leq 4{\cdot}55 \pm 0{\cdot}2$	n-C_3F_8	
F_3C-C_3F_7	$\leq 4{\cdot}3 \pm 0{\cdot}2$	n-C_4F_{10}	
F_3C-C_2F_4CHO	$\leq 3{\cdot}9 \pm 0{\cdot}3$	C_3F_7CHO	
NC-PF_2	$\leq 3{\cdot}1 \pm 0{\cdot}3$ (negative ion data) $\leq 3{\cdot}6 \pm 1{\cdot}6$ (positive ion data)	PF_2CN	
OCN-PF_2	$\leq 3{\cdot}0 \pm 0{\cdot}3$ (negative ion data) $\leq 3{\cdot}5 \pm 1{\cdot}6$ (positive ion data)	PF_2NCO	
SCN-PF_2	$\leq 2{\cdot}2 \pm 0{\cdot}1$ (negative ion data) $\leq 2{\cdot}7 \pm 1{\cdot}6$ (positive ion data)	PF_2NCS	
S=CNPF_2	$\leq 5{\cdot}1 \pm 0{\cdot}5$ $\leq 4{\cdot}1 \pm 0{\cdot}2$	PF_2NCS PF_2NCS	

From Table 9.3 it can be seen that agreement between the available literature values and those deduced in this study is found to be quite reasonable in every case.

$D(F\text{-}SF_5)$, $D(F\text{-}SF_4)$ and $D(F\text{-}SF_3)$ were calculated from appearance potential data which were confidently identified with reaction processes for which calculations could be readily performed. Although the F-S, F-SF and $F\text{-}SF_2$ bond dissociation energies were determined on the assumption that excess energy was not involved in the respective reactions proposed to account for F^- ion formation from SF_6, the value deduced for D(S-F) i.e. $2{\cdot}55 \pm 0{\cdot}2$eV, is in good agreement with the value of $2{\cdot}8 \pm 0{\cdot}2$eV reported by Gaydon.[18]

The (F-C) bond dissociation energies deduced lie in the range $\leq 5{\cdot}05 \pm 0{\cdot}1$ for $D(F\text{-}CF_2NOCF_3)$ to $\leq 5{\cdot}45 \pm 0{\cdot}1$eV for $D(F\text{-}C_4F_9)$; this is in agreement with the magnitudes reported for similar bonds in the literature i.e. $D(F\text{-}CF_3) = 5{\cdot}3$,[130] $D(F\text{-}C_2F_5) \leq 5{\cdot}2$,[17] $D(F\text{-}C_2F_3) \leq 5{\cdot}25 \pm 0{\cdot}1$[119] and $D(F\text{-}CFO) \leq 5{\cdot}5 \pm 0{\cdot}1$eV.[55]

Although the discrepancies between the carbon-carbon bonds deduced for C_3F_8 and C_4F_{10} in this study i.e. $\leq 4{\cdot}55 \pm 0{\cdot}2$ and $\leq 4{\cdot}3 \pm 0{\cdot}2$eV respectively, and the hydrocarbon bonds $D(H_3C\text{-}C_2H_5) = 3{\cdot}7$ and $D(H_5C_2\text{-}C_2H_5) = 3{\cdot}8$eV reported by Kerr[133] are difficult to reconcile the electron affinities of C_2F_5 and C_3F_7 which were calculated using these values are in good agreement with independent values deduced from other reactions and those in the literature. It is concluded from these observations that either (i) the C-C bond energies

obtained in this study are correct within their respective uncertainties or (ii) that comparable amounts of excess energy are released in the complementary reactions involving rupture of the bonds in question.

The PF_2-X (where X = CN, NCO or NCS) bond dissociation energies estimated from the positive and negative ion data are in agreement within their respective uncertainties. Use of accurately measured appearance potentials and available electron affinities[4] results in a preference for the negative ion values.

Table 9.4. Heats of Formation.

Species	Heat of Formation (eV)	Source Molecule
GeF_4	> -15·1 (positive ion data)	GeF_4
	≤ -17·5 ± 0·4 (negative ion data)	
SF_3	≤ -5·15 ± 0·15	SF_4
WF_5	≤ -13·9 ± 0·2	WF_6
CCF_2	≤ 1·0 ± 0·3	C_3F_6
	≲ 0·6	CF_3CHO
CCF_3	≲ -3·5	CF_3CHO
	≲ -3·8	CF_3COCH_3
C_3F_3	≤ -0·5 ± 0·3	c-C_4F_6
$C_3F_3^-$ ($CF_3C_2^-$)	≤ -4·1 ± 0·4	C_4F_6-2
(CF_2CCF^-?)	≤ -2·5 ± 0·3	c-C_4F_6

[Contd.

Table 9.4 (contd.)

Species	Heat of Formation (eV)	Source Molecule
C_3F_5 (CF_3CCF_2)	$\leq -6{\cdot}8 \pm 0{\cdot}2$	C_3F_6
(CF_3CFCF)	$\leq -7{\cdot}3 \pm 0{\cdot}6$	C_4F_8-2
$(CF_2CFCF_2?)$	$\leq -4{\cdot}95 \pm 0{\cdot}3$	c-C_4F_8
$C_3F_5^-$	$\leq -9{\cdot}5 \pm 0{\cdot}4$	C_3F_6
	$\leq -9{\cdot}7 \pm 0{\cdot}3$	C_4F_8-2
C_4F_5	$\leq -5{\cdot}6 \pm 0{\cdot}2$	c-C_4F_6
$C_4F_7\cdot$	$\leq -11{\cdot}2 \pm 0{\cdot}4$	c-C_4F_8
CF_3N	$\leq -5{\cdot}1 \pm 0{\cdot}7$	$(CF_3)_2NO$
CF_3NO	$\leq -5{\cdot}4 \pm 0{\cdot}6$	$(CF_3)_2NO$
CF_3CO	$\leq -7{\cdot}6 \pm 0{\cdot}3$	$(CF_3)_2CO$
$(CF_3)_2NO$	$\leq -13{\cdot}6 \pm 0{\cdot}4$	$(CF_3)_2NO$
CFO^-	$\lesssim -5{\cdot}4$	$(CF_3)_2CO$
$C_2F_4CO^-$	$\lesssim -9{\cdot}6$	C_2F_5CHO
$C_3F_6CO^-$	$\lesssim -13{\cdot}8$	C_3F_7CHO
$CFCOCH_3^-$	$\lesssim -2{\cdot}9$	CF_3COCH_3
$CF_2COCH_3^-$	$\lesssim -5{\cdot}3$	CF_3COCH_3

CFO is the only species listed in Table 9.4 for which previous data have been reported. From ion formation in CF_2O, MacNeil and Thynne[55,113] have reported a value of $2{\cdot}75 \pm 0{\cdot}2$eV for the electron affinity of the fluoroformyl radical and $-1{\cdot}8 \pm 0{\cdot}3$eV for the heat of formation.

$\Delta H_f(CFO^-)$ is therefore given to be $-4{\cdot}55 \pm 0{\cdot}5$eV, in reasonable accord with the upper limit of $-5{\cdot}4$eV deduced in this study.

For $\Delta H_f(GeF_4)$, the upper limit of $-17{\cdot}5 \pm 0{\cdot}4$eV deduced from the negative ion study is preferred.

Differences in the heats of formation of the $C_3F_3^-$ ion may indicate that different isomeric species are involved. $C_3F_3^-$ ion formation from C_4F_6-2 is identified as having the stable acetylenic structure $CF_3C{\equiv}C^-$ in which the captured electron forms a lone pair with the odd electron on the terminal carbon atom thereby acting as a substituent group. The $C_3F_3^-$ ion formed from c-C_4F_6 by a reaction involving intramolecular rearrangement is unlikely to share the same structure as this would involve the simultaneous transfer of two fluorine atoms in the rearrangement. Single fluorine atom transfer across the ring results in the stable diene structure $CF_2 = C = CF^-$ again in which a lone pair is created on a terminal carbon atom. An investigation of negative ion formation in CF_2CCF_2 may serve to substantiate this argument.

The same reasoning can be applied to the values deduced for $\Delta H_f(C_3F_5)$. Those estimated from ion formation in C_3F_6 and C_4F_8-2 are in good agreement, as are the electron affinities, and the values for $\Delta H_f(C_3F_5^-)$ suggest that the same isomeric species is involved in both cases. However, from energetic considerations and assuming the absence of rearrangement the following structures have been proposed for the C_3F_5 radical; $CF_3\dot{C} = CF_2$ from C_3F_6 and $CF_3CF = \dot{C}F$ from C_4F_8-2. These structures may then be resonant isomers

or alternatively the structure of the C_3F_5 radical formed from C_3F_6, identified on the assumption that the tertiary fluorine atom is lost in the reaction, may be $CF_3CF=\dot{C}F$ in which case a secondary fluorine atom is involved in ion formation. Following the argument advanced for $C_3F_3^-$ ion formation from c-C_4F_6 above and assuming that fluorine atom transfer across the ring occurs in c-C_4F_8 the structure of the C_3F_5 radical is anticipated to be $CF_2=CF-\dot{C}F_2$ in which the odd electron resonates between the three carbon atoms in the chain. If this is so then, it is difficult to reconcile the argument suggested above for the resonating structures without also including the $CF_2=CF-\dot{C}F_2$ isomer. The formation of C_3F_5 from C_3F_6 by the loss of a secondary fluorine atom is therefore preferred and the ethylenic structure, $CF_3CF=\dot{C}F$ proposed for the C_3F_5 radical formed from C_3F_6 and C_4F_8-2.

The remaining values shown in Table 9.4 were calculated from single reactions and in the absence of literature values cannot be compared with other determinations.

REFERENCES

1. Thomson, J.J., Proc. Roy. Soc. (London), 89 1 (1913).
2. Edelson,D., Griffiths, J.E. and McAfee, Jr., K.B., J. Chem. Phys., 37 917 (1962).
3. Calcote, H.F., Kurzius, S.C. and Miller, W.J., 10th International Symposium on Combustion, 10 605 (1965).
4. Page, F.M. and Goode, G.C., 'Negative Ions and the Magnetron', John Wiley and Sons, Inc., New York, (1969).
5. MacNeil, K.A.G. and Thynne, J.C.J., Trans. Faraday Soc., 64 2112 (1968).
6. Ferguson, E.E., Can. J. Chem., 47 1815 (1969).
7. Ahearn, A.J. and Hannay, N.B., J. Chem. Phys., 21 119 (1953).
8. Marriott, J., Ph.D. Thesis, University of Liverpool, (1954).
9. Hickam, W.H. and Fox, R.E., J. Chem. Phys., 25 642 (1956).
10. Curran, R.K., J. Chem. Phys., 34 1069 (1961)
11. Fox, R.E. and Curran, R.K., J. Chem. Phys., 34 1595 (1961).
12. Brion, C.E., Int. J. Mass. Spectrom. Ion Phys., 3 197 (1969).
13. Fehsenfeld, F.C., J. Chem. Phys., 53 2000 (1970).
14. Henis, J.M.S. and Mabie, C.A., J. Chem. Phys., 53 2999 (1970).
15. Bacher, R.F. and Goudsmit, S., 'Atomic Energy States', McGraw-Hill Book Co., New York, (1932).
16. Roberts, H.L. and Ray, N.H., J. Chem. Soc., 665 (1960).
17. MacNeil, K.A.G. and Thynne, J.C.J., Int. J. Mass Spectrom. Ion Phys., 2 1 (1969).
18. Gaydon, A.G., 'Dissociation Energies and Spectra of Diatomic Molecules', Chapman and Hall, London, (1968).
19. Hickam, W.H. and Berg, D., Advan. Mass Spectry., (1958).
20. Clark, H.C. and Dixon, K.R., Chem. Commun., 717 (1967).

21. MacNeil, K.A.G. and Thynne, J.C.J., Int. J. Mass Spectrom. Ion Phys., 3 455 (1970).

22. Kiser, R.W., 'Introduction to Mass Spectrometry and Its Applications', Prentice-Hall, Inc., (1965).

23. Franklin, J.L., Dilland, J.G., Rosenstock, H.M., Herron, J.T., Draxl, K. and Field, F.H., 'Ionisation Potentials, Appearance Potentials and Heats of Formation of Gaseous Positive Ions., NSRDS-NBS 26, (1969).

24. Chantry, P.J., Phys. Rev., 172 125 (1968).

25. Margrave, J.L., private communication, (1970).

26. Domalski, E.S. and Armstrong, G.T., J. Res. Natl. Bur. Standards., 71A 105 (1967).

27. 'JANAF Thermochemical Tables', Dow Chemical Co., Midland, Mich., (1961).

28. Kay, J. and Page, F.M., Trans. Faraday Soc., 60 1042 (1964).

29. National Bureau of Standards Technical Note 270-3, Jan. (1968).

30. Thynne, J.C.J., J. Phys. Chem., 73 1586 (1969).

31. Stephens, W.E., Bull. Am. Phys. Soc., 21 22 (1946).

32. Wiley, W.C. and McLaren, I.H., Rev. Sci. Instr., 26 1151 (1955).

33. Wiley, W.C., Science, 124 817 (1956).

34. Stamatovic, A. and Schulz, G.J., Rev. Sci. Instr., 39 1752 (1968).

35. Christophorou, L.G., McCorkle, D.L. and Carter, J.D., J. Chem. Phys., 54 253 (1971).

36. Berry, R.S. and Riemann, C.W., J. Chem. Phys., 38, 1540 (1963).

37. Compton, R.N., Christophorou, L.G., Hurst, G.S. and Reinhardt, P.W., J. Chem. Phys., 45 4634 (1966).

38. Nottingham, W.B., Phys. Rev., 55 203 (1939).

39. Sugden, T.M. and Price, W.C., Trans. Faraday Soc., 44 108 (1948).

40. Clarke, E.M., Can. J. Phys., 32 764 (1954).

41. Hutchison, D.A., Advan. Mass Spectry., 2 527 (1963).

42. Marmet, P. and Kerwin, L., J. Appl. Phys., 31 2071 (1960).

43. Marmet, P. and Morrison, J.D., J. Chem. Phys., 36 1238 (1962).

44. Brion, C.E., Frost, D.C. and McDowell, C.A., J. Chem. Phys., 44 1034 (1966).

45. Fox, R.E., Hickam, W.H., Grove, D.J. and Kjeldaas, T., Rev. Sci. Instr., 26 1101 (1955).

46. Cloutier, G.G. and Schiff, H.I., J. Chem. Phys., 31 793 (1959).

47. Stockdale, J.A.D., Compton, R.N. and Reinhardt, P.W., Phys. Rev., 184 81 (1969).

48. Marmet, P., Can. J. Phys., 42 2102 (1964).

49. Frost, D.C. and McDowell, C.A., Proc. Roy. Soc. (London), A232 227 (1955).

50. Frost, D.C. and McDowell, C.A., J. Chem. Phys., 29 964 (1958).

51. Simpson, J.A., Rev. Sci. Instr., 32 1283 (1961).

52. Gordon, S.M., Haarhoff, P.C. and Krige, G.J., Int. J. Mass Spectrom. Ion Phys., 3 13 (1969).

53. Morrison, J.D., J. Chem. Phys., 39 200 (1963).

54. Ioup, G.E. and Thomas, B.S., J. Chem. Phys., 46 3959 (1967).

55. MacNeil, K.A.G. and Thynne, J.C.J., Int. J. Mass Spectrom. Ion Phys., 3 35 (1969).

56. Cradock, S., private communication, (1971).

57. McDowell, C.A. and Warren, J.W., Trans. Faraday Soc., 48 1084 (1952).

58. Pritchard, H.O., Chem. Reviews, 52 529 (1953).

59. Lineberger, W.C., 'Negative Ions' Conference, Liverpool, March, (1971).

60. MacNeil, K.A.G. and Thynne, J.C.J., J. Phys. Chem., 73 2960 (1969).

61. Schulz, G.J., J. Appl. Phys., 31 1134 (1960).

62. Christophorou, L.G., Compton, R.N., Hurst, G.S. and Reinhardt, P.W., J. Chem. Phys., 43 4273 (1965).

63. Kraus, K., Z. Naturforsch., 16a 1378 (1961).

64. O'Hare, P.A.G., private communication, (1971).

65. DeCorpo, J.J. and Franklin, J.L., J. Chem. Phys., 54 1885 (1971).

66. Collins, P.M., Ph.D. Thesis, Graduate School of the University of Tennessee, (1970).

67. Holstein, T., Phys. Rev., 84 1073 (1951).

68. Rapp, D., Sharp, T.E. and Briglia, D.D., Phys. Rev. Letters, 14 533 (1965).

69. Schulz, G.J., Phys. Rev., 113 816 (1959).

70. Schulz, G.J., Phys. Rev., 128 178 (1962).

71. Schulz, G.J. and Asundi, R.K., Phys. Rev., 158 25 (1967).

72. Bloch, F. and Bradbury, N.E., Phys. Rev., 48 689 (1935).

73. Bradbury, N.E., Phys. Rev., 44 883 (1933).

74. Massey, H.S.W., 'Negative Ions', Cambridge University Press, (1950).

75. Stanton, R.E., J. Chem. Phys., 32 1348 (1960).

76. Chen, J.C.Y., Phys. Rev., 129 202 (1963).

77. Bardsley, J.N., Herzenberg, A. and Mandl, F., 'Atomic Collision Processes', edited by McDowell, M.R.C., North Holland Publishing Co., Amsterdam, p. 415 (1964).

78. Chen, J.C.Y., Phys. Rev., 148 66 (1966).

79. Chen, J.C.Y. and Peacher, J.L., Phys. Rev., 163 103 (1967).

80. O'Malley, T.F., Phys. Rev., 150 14 (1966).

81. O'Malley, T.F., Phys. Rev., 155 59 (1967).

82. Bardsley, J.N. and Mandl, F., Reports on Progress in Physics, Vol. XXXI, Part II, p. 471 (1968).

83. Taylor, H.S., Nazaroff, G.V. and Golebiewski, A., J. Chem. Phys., 45 2872 (1966).

84. Asundi, R.K. and Craggs, J.D., Phys. Soc. (London), 83 611 (1964).

85. Naff, W.T., Cooper, C.D. and Compton, R.N., J. Chem. Phys., 49 2784 (1968).

86. Schiff, L.I., 'Quantum Mechanics', McGraw-Hill Book Co. Inc., New York, p. 200 (1955).

87. Rabinovitch, B.S. and Diesen, R.W., J. Chem. Phys., 30 735 (1959).

88. Whitten, G.Z. and Rabinovitch, B.S., J. Chem. Phys., 38 2466 (1963).

89. Klots, C.E., J. Chem. Phys., 46 1197 (1967).

90. Feshbach, H., Ann. Phys., 5 357 (1958).

91. Feshbach, H., Ann. Phys., 19 287 (1962).

92. Sharp, T.E. and Dowell, J.T., J. Chem. Phys., 46 1530 (1967).

93. Christophorou, L.G., Compton, R.N. and Dickson, H.W., J. Chem. Phys., 48 1949 (1968).

94. Compton, R.N. and Christophorou, L.G., Phys. Rev., 154 110 (1967).

95. Christophorou, L.G. and Stockdale, J.A.D., 48 1956 (1968).

96. Fite, W.L. and Brackmann, R.T., Proceedings of the Sixth International Conference on the Ionisation Phenomena in Gases, Paris, Vol. I, p. 21, (1963).

97. Kieffer, L.J. and Dunn, G.H., Reviews of Modern Physics, 38 1 (1966).

98. Jones, T.J., Phys. Rev., 29 822 (1927).

99. Smith, P.T., Phys. Rev., 36 1293 (1930).

100. Tate, J.T. and Smith, P.T., Phys. Rev., 39 270 (1932).

101. Mahan, B.H. and Young, C.E., J. Chem. Phys., 44 2192 (1966).

102. van Cittert, P.H., Z. Phys., 69 298 (1931).

103. MacNeil, K.A.G. and Thynne, J.C.J., J. Phys. Chem., 74 2257 (1970).

104. Rajbenbach, L.A., J. Am. Chem. Soc., 88(18) 4275 (1966).

105. Noller, C.R., 'Chemistry of Organic Compounds', 3rd edition, W.B. Sanders Company, (1965).

106. Naff, W.T., Compton, R.N. and Cooper, C.D., J. Chem. Phys., 54 212 (1971).

107. Compton, R.N. and Bouby, L., Compt. Rend., 264 1153 (1967).

108. Pitzer, K.S., J. Chem. Phys., 8 711 (1940).

109. Pace, E.L., Plaush, A.C. and Samuelson, H.V., Spectrochimica Acta, 22 993 (1966).

110. Steele, D. and Whiffen, D.H., Trans. Faraday Soc., 55 369 (1959).

111. Dodd, R.E., Woodward, L.A. and Roberts, H.L., Trans. Faraday Soc., 52 1052 (1956).

112. Nagakura, S. and Tanaka, J., J. Chem. Phys., 22 236 (1954).

113. MacNeil, K.A.G., Ph.D. Thesis, University of Edinburgh, (1970).

114. Bott, J.F., Am. Chem. Soc. Meeting, Feb., (1970). Abstracts of Division of Physical Chemistry, No. 144.

115. Stevenson, D.P., Disc. Faraday Soc., 10 35 (1951).

116. Dibeler, V.H. and Mohler, F.L., J. Res. Nat. Bur. Stand., 40 25 (1948).

117. Lossing, F.P., Tickner, A.W. and Bryce, W.A., J. Chem. Phys., 19 1254 (1951).

118. Dorman, F.H., J. Chem. Phys., 44 3856 (1966).

119. MacNeil, K.A.G. and Thynne, J.C.J., Int. J. Mass Spectrom. Ion Phys., 5 329 (1970).

120. Honig, R.E., J. Chem. Phys., 22 126 (1954).

121. v. Trepka, L. and Neuert, H., Z. Naturforsch., 18a 1295 (1963).

122. Lifshitz, C. and Grajower, R., Int. J. Mass Spectrom. Ion Phys., 3 211 (1969).

123. Benson, S.W., 'Thermochemical Kinetics', John Wiley and Sons, Inc., New York, (1969).

124. Bibby, M.M., Ph.D. Thesis, University of Liverpool, (1965).

125. Bibby, M.M. and Carter, G., Trans. Faraday Soc., 62 2637 (1966).

126. Reese, R.M., Dibeler, V.H. and Mohler, F.L., J. Res. Nat. Bur. Stand., 57 367 (1956).

127. Bryant, W.M.D., J. Polymer Sci., 56 277 (1962).

128. Farber, M., Frisch, M.A. and Ko, H.C., Trans. Faraday Soc., 65 3202 (1969).

129. Heicklen, J., Advan. Photochem., 7 57 (1969).

130. Patrick, C.R., Advan. Fluorine Chem., 2 18 (1961).

131. Vedeneyev, V.I., Gurvich, L.V., Kondrat'yev, V.N., Medvedev, V.A. and Frankevich, Ye.L., 'Bond Energies, Ionisation Potentials and Electron Affinities', Edward Arnold, London, (1966).

132. Greenhaus, H.L., Ph.D. Thesis, Rensselaer Polytechnic Institute, Troy, New York, (1965). — University Microfilms Ltd., High Wycombe.

133. Kerr, J.A., Chem. Reviews, 66 465 (1966).

134. Benson, S.W. and O'Neal, H.E., NSRDS-NBS 21, Feb., (1970).

135. Lifshitz, C., Peers, M.A. Grajower, R. and Weiss, M., J. Chem. Phys., 53 4605 (1970).

136. Benson, S.W., Cruickshank, F.R., Golden, D.M., Haugen, G.R., O'Neal, H.E., Rodgers, A.S., Shaw, R. and Walsh, R., Chem. Reviews, (1969).

137. Benson, S.W., private communication, (1969).

138. Herzberg, G., 'Molecular Spectra and Molecular Structure. III, Electronic Spectra and Electronic Structure of Polyatomic Molecules'. Van Nostrand, Princeton, (1967).

139. Kemmitt, R.D.W. and Sharp, D.W.A., Advances in Fluorine Chemistry, 4 142 (1965).

APPENDIX 1

THERMOCHEMICAL DATA

The thermochemical data used in the text are tabulated in this appendix together with their literature references. For ease of presentation the data relevant to each chapter have been grouped together in order of increasing molecular weight and values used in more than one chapter repeated in each case. Heats of formation calculated using the additivity rules[136] and values deduced in the text and then used for further calculations have been marked as such and all values have been given in electron-volts where 1eV = 23·06 Kcals/mole.

Species	Heat of Formation at 298°K (eV)	Literature Source
CHAPTER 5		
F	0·82	129
S	2·8 ± 0·6	27
Cl	1·26	23
F_2	0·0	27
FCl	-0·6	27
SF_4	-8·0	29
GeF_2	-5·9 ± 0·1	25
SF_6	-12·7	29
SF_5Cl	-10·9	29
W	8·75 ± 0·1	27
WF_6	-18·2 ± 0·2	27

[Contd.

Species	Heat of Formation at 298°K (eV)	Literature Source
CHAPTER 6		
C	7·4	23
N	4·9	23
O	2·3	23
F	0·82	129
CN	4·3	23
P	3·5	27
S	2·8 ± 0·6	27
F_2	0·0	27
PF	-0·74	27
PF_2	-4·7 ± 0·6	27
PF_3	-9·6 ± 0·4	27
CHAPTER 7		
C	7·4	23
F	0·82	129
C_2	8·5 ± 0·2	27
CF	2·52	128
F_2	0·0	27
C_2F	2·9 ± 0·4	131
CF_2	-1·81	128
CFCF	~0·0	128
CF_3	-4·9	127
CF_2CF	-2·0	127
CF_4	-9·4	127
CF_3CF	-4·8	129
$C_2F_4(CF_2CF_2)$	-6·6	127
C_2F_5	-9·2	127
C_2F_6	-13·7	127
c-C_4F_6	-10·1	134
C_4F_6-2	-9·7	134
n-C_3F_7	-13·3	127
i-C_3F_7	-13·9	127

[Contd.

Species	Heat of Formation at 298°K (eV)	Literature Source
C_3F_8	-17·8	127
c-C_4F_8	-15·7	134
C_4F_8-2	-16·6	134
n-C_4F_9	-17·4	127
n-C_4F_{10}	-21·9	127
CHAPTER 8		
H	2·26	23
C	7·4	23
CH	6·2	23
CH_2	4·06	23
N	4·9	23
CH_3	1·4	23
O	2·6	23
OH	4·0	23
F	0·82	129
HF	-2·81	23
CO	-1·15	23
CHO	-0·2	23
NO	0·9	23
CF	2·52	128
CH_3F	-2·9	23
OF	1·8	23
F_2	0·0	27
CH_2CO	-0·63	23
CH_3CO	-0·2	23
CFO	-1·8 $\pm$ 0·3	55
CF_2	-1·81	128
CCF_2	$\leq$1·0 $\pm$ 0·3	Ch.7, section (b).
CF_2CH	-1·2 $\pm$ 0·4	113
CF_3	-4·9	127
CCF_3	$\lesssim$-3·5, $\lesssim$-3·8	Ch.8, sections (a) and (b).

[Contd.

Species	Heat of Formation at 298°K (eV)	Literature Source
CF_2CF	-2·0	127
CF_3O	-6·6	139
CF_3CHO	-8·2	Additivity rules[136]
CF_3CF	-4·8	129
$C_2F_4(CF_2CF_2)$	-6·6	127
CF_3COCH_3	-8·7	Additivity rules[136]
C_2F_5	-9·2	127
C_3F_5	$\leq$-6·8 $\pm$ 0·2	Ch. 7, section (b).
C_2F_5CHO	-12·4	136
$(CF_3)_2CO$	-15·1	Additivity rules[136]
n-C_3F_7	-13·3	127
C_3F_7CHO	-16·6	Additivity rules[136]

APPENDIX 2

PUBLICATIONS.

1. Studies of Negative Ion Formation at Low Electron Energies.
   P.W. Harland, K.A.G. MacNeil and J.C.J. Thynne.
   Dynamic Mass Spectrometry, Editors: D. Price and J.E. Williams, Volume 1 (1969).

2. Ionisation and Dissociation of Pentafluorosulphur Chloride by Electron Impact.
   P. Harland and J.C.J. Thynne.
   J. Phys. Chem., 73 4031 (1969).

3. Positive and Negative Ion Formation in Hexafluoroacetone by Electron Impact.
   P. Harland and J.C.J. Thynne.
   J. Phys. Chem., 74 52 (1970).

4. Ionisation by Electron Impact of GeF_4 and some other Inorganic Fluorides.
   P.W. Harland and J.C.J. Thynne.
   Proceedings of the Triennial International Conference on Mass Spectrometry, Brussels, September (1970).

5. Autoionisation Lifetimes, Attachment Cross-sections and Negative Ion Formation in SF_4 and SF_6.
   P.W. Harland, R. McDonald and J.C.J. Thynne.
   Dynamic Mass Spectrometry, Editors: D. Price and J.E. Williams, Volume 2 (1970).

[Reprinted from the Journal of Physical Chemistry, 73, 4031 (1969).]

Ionization and Dissociation of Pentafluorosulfur Chloride by Electron Impact

by P. Harland and J. C. J. Thynne

Chemistry Department, Edinburgh University, Edinburgh, Scotland *(Received July 31, 1969)*

Positive and negative ion formation as a result of the electron bombardment of pentafluorosulfur chloride has been studied. Various ionization processes have been suggested to account for the formation of the ions, and for several negative ions the dependence of their formation upon electron energy has been studied.

As part of a continuing study of positive and negative ion formation by molecules as a result of electron impact,[1,2] we have examined pentafluorosulfur chloride, SF_5Cl. This molecule is of particular interest from a negative ion standpoint since the closely related molecule sulfur hexafluoride readily forms the ion SF_6^- at low energies,[3,4] and it is of interest to observe if the SF_5Cl^- ion is formed similarly.

In electron impact studies, when the electron source is a heated filament, uncertainties arise in the evaluation of experimental ionization data because of the energy spread of the thermionically emitted electron beam; this is largely due to the ionization thresholds becoming smeared-out as a result of the high energy tail of the electron energy distribution. Analytical methods have been developed to reduce this problem for positive[5] and negative[2] ions, and we have applied this technique to the negative ions formed by SF_5Cl at low electron energies.

Experimental Section

The data were obtained using a Bendix time-of-flight mass spectrometer, Model 3015. The pressure in the ion source was usually maintained below 5×10^{-6} mm in order to reduce the possibility of ion formation due to ion–molecule reactions. The energy of the ionizing electrons was read on a Solatron digital voltmeter, Model LM 1619, and the spectra recorded on two 1-mV Kent potentiometric recorders.

In both the positive and negative ion studies, the electron current was maintained constant by automatic regulation over the whole energy range investigated. Ionization curves were usually measured three to five times, the appearance potentials for negative ions being reproducible to ±0.1 eV. The appearance potential of the O^- ion from SO_2 was used as the reference for energy scale calibration,[3] both the onset at 4.2 eV and the maximum of the resonance peak at 5.0 eV being taken as the calibration points.[6-8] For the positive ion studies argon was used to calibrate the energy scale, the method used for determining the appearance potentials being the semilogarithmic plot technique.

The electron energy distribution, which was required to be known for the deconvolution procedure,[2] was measured using the SF_6^- ion formed by sulfur hexafluoride.[3,4] It was found that performing 15 smoothing and 20 unfolding iterations on the basic experimental data enabled satisfactory evaluation of appearance po-

(1) K. A. G. MacNeil and J. C. J. Thynne, *Int. J. Mass Spec.*, **2**, 1 (1969).
(2) K. A. G. MacNeil and J. C. J. Thynne, *ibid.*, **2**, 35 (1969).
(3) W. M. Hickman and R. E. Fox, *J. Chem. Phys.*, **25**, 642 (1956).
(4) G. J. Schulz, *J. Appl. Phys.*, **31**, 1134 (1960).
(5) J. D. Morrison, *J. Chem. Phys.*, **39**, 200 (1963).
(6) K. Kraus, *Z. Naturforsch.*, **16a**, 1378 (1961).
(7) J. G. Dillard and J. L. Franklin, *J. Chem. Phys.*, **48**, 2349 (1968).
(8) F. H. Dorman, *ibid.*, **44**, 3856 (1966).

tentials, resonance peak maxima, and peak widths (at half-height) to be made.

Results and Discussion

(1) *Positive Ion Formation by Pentafluorosulfur Chloride.* In Table I we show the positive ion mass spectra for SF_5Cl and SF_6 measured at 70 eV. For both molecules, doubly charged fragments containing sulfur and fluorine are common, but it is noteworthy that for SF_5Cl few ions containing sulfur, fluorine, and chlorine are formed and these are generally of low abundance.

Table I: Positive Ion Mass Spectrum of SF_5Cl and SF_6 for 70-V Electrons

	SF_5Cl		SF_6	
m/e	Ion	Rel. intensity	Ion	Rel. intensity
16	S^{2+}	0.14	S^{2+}	0.06
19	F^+	0.44	F^+	0.35
32	S^+	3.10	S^+	1.44
35	Cl^+	2.02		
	SF_2^{2+}	1.53	SF_2^{2+}	0.68
37	Cl^+	0.67		
44.5	SF_3^{2+}	0.04	SF_3^{2+}	0.01
51	SF^+	6.13	SF^+	4.65
54	SF_4^{2+}	0.44	SF_4^{2+}	0.39
63.5	SF_5^{2+}	<0.01		
67	SCl^+	1.57		
70	SF_2^+	6.77	SF_2^+	4.72
86	$SFCl^+$	0.63		
89	SF_3^+	36.8	SF_3^+	18.0
105	SF_2Cl^+	0.20		
108	SF_4^+	5.25	SF_4^+	3.17
124	SF_3Cl^+	<0.1		
127	SF_5^+	100	SF_5^+	100
143	SF_4Cl^+	11.0		
162	SF_5Cl^+	<0.1		

A low intensity parent ion is formed in the case of SF_5Cl although the most probable ionization process involves the loss of a chlorine atom from the molecule. Positive ion appearance potential data for SF_6 have been reported by Dibeler and Mohler.[9] Results of mass spectra of SF_5Cl and SF_6 as shown in Table I.

Energetics of Decomposition. For dissociation into atoms SF_6 and SF_6Cl require 20.3 and 18.9 eV, respectively.

$$SF_6 \longrightarrow S + 6F \quad (1)$$

$$SF_5Cl \longrightarrow S + 5F + Cl \quad (2)$$

If the S–F bonds have a constant bond energy, then $D(SF_5\text{–}F) - D(SF_6\text{–}Cl) = 1.4$ eV and, using the value of $\leqslant 3.4$ eV deduced for $D(SF_5\text{–}F)$ by Curran,[10] then $D(SF_5\text{–}Cl) \leqslant 2.0$ eV. This relatively low bond strength is compatible with the observation[11] that pentafluorosulfur chloride thermally decomposes at about 200°.

(a) SF_5^+. We have measured a value of 13.2 ± 0.2 eV for the appearance potential of the SF_5^+ ion.

$$SF_5Cl + e \longrightarrow SF_5^+ + Cl + 2e \quad (3)$$

Dibeler and Mohler[9] have reported that, for SF_6, $A(SF_5^+) = 15.9 \pm 0.2$ eV. These results suggest that, neglecting possible excess energy contributions, $D(SF_5\text{–}F) - D(SF_5\text{–}Cl) = 2.5 \pm 0.4$ eV, a result which is in reasonable accord with the difference deduced above.

(b) Cl^+. Our data yield a value of 20.8 ± 0.3 eV for the appearance potential for the Cl^+ ion (Table II);

Table II: Appearance Potentials of Various Ions in the Mass Spectrum of SF_5Cl

m/e	Ion	*A*, eV
19	F^+	33.8 ± 0.3
32	S^+	33.2 ± 0.5
35	Cl^+	20.8 ± 0.3
127	SF_5^+	13.2 ± 0.2
143	SF_4Cl^+	15.9 ± 0.1

possible ionization processes to explain the formation of the ion include

$$SF_5Cl + e \longrightarrow SF_5 + Cl^+ + 2e \quad (4)$$

$$\longrightarrow SF_4 + F + Cl^+ + 2e \quad (5)$$

$$\longrightarrow S + 5F + Cl^+ + 2e \quad (6)$$

If $D(SF_5\text{–}Cl) \simeq 2.0$ eV, then the enthalpy requirements of reaction 4 are about 16.2 eV. Reactions 5 and 6 require minimum energies of 19.1 and 33.1 eV, respectively; it is therefore probable that reaction 5 is responsible for Cl^+ ion formation.

(c) F^+. An appearance potential of 33.8 ± 0.3 eV was obtained for this ion; in addition breaks in the F^- and Cl^- ionization efficiency curves were noted at 32.8 and 33.5 eV, respectively.

$$SF_5Cl + e \longrightarrow S + 4F + Cl + F^+ + 2e \quad (7)$$

$$\longrightarrow S + 3F + Cl + F^+ + F^- + 2e \quad (8)$$

$$\longrightarrow S + 4F + Cl^- + F^+ + 2e \quad (9)$$

Reactions 7, 8, and 9 have minimum enthalpy requirements of 37.1, 33.7, and 33.5, respectively. Our data for $A(F^+)$, together with the observed breaks in the F^- and Cl^- curves, suggest that both reactions 8 and 9 are contributing to F^+ ion formation.

(d) S^+.

$$SF_5Cl + e \longrightarrow S^+ + 5F + Cl + 2e \quad (10)$$

(9) V. H. Dibeler and F. L. Mohler, *J. Res. Nat. Bur. Stand.*, 40, 25 (1948).

(10) R. K. Curran, *J. Chem. Phys.*, 34, 1069 (1961).

(11) H. L. Roberts and N. H. Ray, *J. Chem. Soc.*, 665 (1960).

Table III: Appearance Potentials (A), Resonance Peak Maxima (M), and Half-Widths (PW) for Negative Ions Formed by SF_6[a]

Ion	A	M	PW	Process
SF_6^-	0	0.4 ± 0.1	0.6 ± 0.1	$SF_6 + e \rightarrow SF_6^-$
SF_5^-	0.1	0.5 ± 0.1	0.8 ± 0.1	$\rightarrow SF_5^- + F$
SF_4^-	5.0 ± 0.1	6.0 ± 0.1	1.7 ± 0.1	$\rightarrow SF_4^- + 2F$
F^-	4.3 ± 0.1	5.7 ± 0.1	1.4 ± 0.1	$\rightarrow SF_4 + F + F^-$
	7.8 ± 0.1	9.3 ± 0.1	~2	$\rightarrow SF_3 + 2F + F^-$
	10.5 ± 0.1	11.8 ± 0.1	1.6 ± 0.1	$\rightarrow SF_2 + 3F + F^-$

[a] All values in eV.

The enthalpy change for reaction 10 is 32.2 eV; this is in reasonable accord with the value of 33.2 ± 0.5 eV we have measured for the appearance potential of the S^+ ion. Any ion-pair process would have energy requirements at least 3.4 eV lower than this for (10) since it would involve F^- or Cl^- formation; we therefore attribute S^+ ion production to reaction 10.

(*e*) *SF_4Cl^+.*

$$SF_5Cl + e \longrightarrow SF_4Cl^+ + F + 2e \qquad (11)$$

$A(SF_4Cl^+) = 15.9 \pm 0.1$ eV; if we assume that $D(F\text{–}SF_4Cl)$ is the same as the S–F bond strength in SF_6, *i.e.*, ~3.4 eV, then a maximum value of 12.5 eV may be deduced for the ionization potential of SF_4Cl.

(*2*) *Negative Ion Formation.* (*a*) *O^- Ion Formation by Sulfur Dioxide.* The formation of negative ions by sulfur dioxide has been investigated by several workers, and the appearance potential of the O^- ion is sufficiently well established[6-8] at 4.2 eV to be used to calibrate the energy scale.

Our results for this ion are shown in Figure 1; the two resonance peaks observed have clear maxima but uncertain appearance potentials. Deconvolution of these data, using an electron energy distribution measured using SF_6^-/SF_6, give the results shown by the open circles. The threshold for the first peak is sharp and is separated from the peak maximum by 0.80 eV; this is in exact agreement with the difference obtained by Kraus[6] (using a retarding-potential-difference technique) and by Dillard and Franklin.[7]

The onset of the second resonance peak is not quite resolved; Kraus[6] also was unable to completely separate the two peaks. The onset of the first peak and the minimum between the resonance peaks are separated by 2.4 eV in both our work and that of Kraus.

(*b*) *Negative Ion Formation by Sulfur Hexafluoride.* The negative ions observed at 70 eV are F^-, S^-, F_2^-, SF^-, SF_2^-, SF_3^-, SF_4^-, SF_5^-, and SF_6^-, with F^- and SF_6^- being the most abundant. The formation of most of these ions is well known, in particular the SF_6^- ion which has been used to determine the electron energy distribution.[3,4] The data are presented in Table III.

(*i*) *SF_5^-.* The SF_5^- ion is formed abundantly, presumably by the dissociative capture reaction

$$SF_6 + e \longrightarrow SF_5^- + F$$

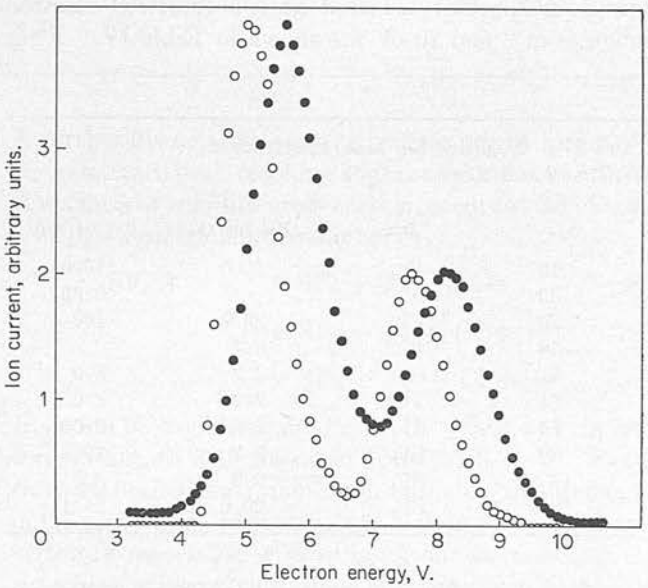

Figure 1. Ionization efficiency curve for O^- ion formation by sulfur dioxide. Full circles, original experimental results; open circles, deconvoluted results obtained using 15 smoothing and 20 unfolding iterations.

and we have measured an appearance potential of 0.1 eV for this ion, a result in good accord with those of other workers.[12,13]

(*ii*) *SF_4^-.*

$$SF_6 + e \longrightarrow SF_4^- + 2F \qquad (12)$$

Our experimental data indicate that $A(SF_4^-) = 5.0 \pm 0.1$ eV; if reaction 12 is responsible for ion formation, then a value of 1.7 eV may be estimated for the electron affinity of sulfur tetrafluoride, $E(SF_4)$.

(*iii*) *F^-.* Ion formation was observed initially at electron energies near to zero, indicating that $D(SF_5\text{–}F) \simeq E(F)$. Three other ionization processes were noted at 4.3, 7.8, and 10.5 eV, the process at 4.3 having considerably the largest cross section.

$$SF_6 + e \longrightarrow SF_4 + F + F^- \qquad (13)$$

$$\longrightarrow SF_3 + 2F + F^- \qquad (14)$$

$$\longrightarrow SF_2 + 3F + F^- \qquad (15)$$

(12) W. M. Hickman and D. Berg, *Advan. Mass Spectrometry*, 458 (1958).

(13) A. J. Ahearn and N. B. Hannay, *J. Chem. Phys.*, 21, 19 (1953).

The minimum enthalpy requirements for reaction 13 are 3.3 eV, so we suggest that this reaction is responsible for the increase in ion current at 4.3 eV. Reactions 14 and 15 have higher energy requirements than 13 in both cases S–F bonds being broken which probably require ~3 eV. The energy difference observed between the ionization processes are 3.5 and 2.7 eV; this is close to the likely S–F bond energies and we tentatively suggest that reactions 14 and 15 also participate in ion formation.

(c) *Negative Ion Formation by SF_5Cl.* The negative ion mass spectra measured at (uncorrected) electron energies of 2 and 70 eV are shown in Table IV. F^- is

Table IV: Negative Ion Mass Spectrum of SF_5Cl at 2 and 70 eV

m/e	Ion	Rel. int. (2)	Rel. int. (70)
19	F^-	1000	1000
32	S^-	...	0.65
35	Cl^-	26.7	100
38	F_2^-	6.7	...
51	SF^-	2.2	8.0
54	FCl^-	2.2	2.0
70	SF_2^-	2.0	0.65
89	SF_3^-	2.2	16.2
108	SF_4^-	2.3	3.3
127	SF_5^-	20.0	24.1

the most abundant ion but, unlike SF_6, no parent negative ion is observed either at low electron energies (where it could be formed by primary electron capture) nor at higher energies where secondary electrons might be involved in the capture process. No ions which contain S, F, and Cl or S and Cl are formed. Some Cl^- and F^- ion formation occurs at ~0 eV as a consequence of thermal decomposition of the pentafluorosulfur chloride on the hot filament.

(i) *SF_5^-.* This ion is observed at 0.2 ± 0.1 eV, the resonance peak attaining a maximum value a 0.7 eV. Ionization is attributed to the reaction

$$SF_5Cl + e \longrightarrow SF_5^- + Cl \qquad (16)$$

(ii) *SF_4^-.* Our appearance potential data for this ion are given in Table V.

$$SF_5Cl + e \longrightarrow SF_4^- + F + Cl \qquad (17)$$

If reaction 17 is responsible for ion formation, then we can estimate a value of 1.0 eV for $E(SF_4)$; this may be compared with the value of 1.7 eV deduced for $E(SF_4)$ in the experiments using SF_6.

(iii) *SF_3^-.* The dissociation energy into atoms of SF_4 is 14.0 eV; if we assume that the four S–F bonds have equal strengths, then $D(SF_3\text{–}F) \simeq 3.5$ eV and we may estimate that the heat of formation of SF_3, $\Delta H_f(SF_3) = -5.3$ eV.

$$SF_5Cl + e \longrightarrow SF_3^- + 2F + Cl \qquad (18)$$

$A(SF_3^-) = 7.9$ eV so that, from reaction 18, we may estimate the electron affinity of SF_3 to be 0.5 eV. The similarity of the appearance potentials of SF_3^- and FCl^- initially suggest the occurrence of the reaction

$$SF_5Cl + e \longrightarrow SF_3^- + F + FCl$$

but the energetic requirements for this reaction are such as to indicate $E(SF_3) < 0$, and so the reaction is neglected.

(iv) *FCl^-.* This ion must be formed either by an ion–molecule reaction involving F^- or Cl^-, *e.g.*

$$F^- + SF_5Cl \longrightarrow FCl^- + SF_5 \qquad (19)$$

or by rearrangement reactions such as

$$SF_5Cl + e \longrightarrow SF_4 + FCl^- \qquad (20)$$

$$\longrightarrow SF_3 + F + FCl^- \qquad (21)$$

$$\longrightarrow SF_2 + 2F + FCl^- \qquad (22)$$

A study of the pressure dependence of FCl^- ion formation at 7.6 eV showed it to be a primary ion, and we may therefore rule out secondary reactions such as (19).

Reactions 20 and 21 may also be neglected as sources of the FCl^- ion on energetic grounds. To estimate the energetics of (22) we require to know $\Delta H_f(SF_2)$. If we assume $D(SF_2\text{–}F) \simeq 3.3$ eV, then $\Delta H_f(SF_2) \simeq -2.8$ eV. Using this estimate we can calculate that $E(FCl) \simeq 1.5$ eV. We know of no value with which this may be compared but values of 2.8 and $\leqslant 1.7$ eV have been reported for $E(F_2)$[2] and $E(Cl_2)$,[14] respectively.

(v) *Cl^-.* Our data for this ion showed it to have an appearance potential at 4.0 eV, the broad resonance peak rising slowly with a much more intense resonance process having an appearance potential at 7.6 ± 0.2 eV, the peak maximum being attained at 9.1 eV. Some ion formation also occurred at electron energies ~0 eV, this may be due to thermal decomposition of SF_5Cl or to the occurrence of reaction 23 since $D(SF_5\text{–}Cl) < E(Cl)$.

$$SF_5Cl + e \longrightarrow SF_5 + Cl^- \qquad (23)$$

$$\longrightarrow SF_4 + F + Cl^- \qquad (24)$$

$$\longrightarrow SF_3 + 2F + Cl^- \qquad (25)$$

$$\longrightarrow SF_3 + F_2 + Cl^- \qquad (26)$$

$$\longrightarrow SF_2 + 3F + Cl^- \qquad (27)$$

The broad peak which has its onset at 4.0 eV may be attributable to reaction 26 for which the enthalpy requirements are ~3.2 eV. Reactions 25 and 27 would correspond to appearance potentials for Cl^- of 4.8 and 8.1 eV; we are therefore unable to identify the second

(14) N. S. Buchel'nikova, *Usp. Fiz. Nauk*, 65, 351 (1958).

Table V: Appearance Potentials (A), Resonance Peak Maxima (M) and Half-Widths (PW) for Negative Ions Formed by Pentafluorosulfur Chloride[a]

Ion	A	M	PW	Process
SF_5^-	0.2 ± 0.1	0.7 ± 0.1	0.8 ± 0.1	$SF_5Cl \rightarrow SF_5^- + Cl$
SF_4^-	4.1 ± 0.1	4.65 ± 0.1	1.0 ± 0.1	$\rightarrow SF_4^- + F + Cl$
SF_3^-	7.9 ± 0.2	8.9 ± 0.1	1.4 ± 0.2	$\rightarrow SF_3^- + 2F + Cl$
FCl^-	7.6 ± 0.1	9.1 ± 0.1	1.7 ± 0.1	$\rightarrow SF_2 + 2F + FCl^-$
Cl^-	4.0 ± 0.1	Uncertain	...	$\rightarrow SF_3 + F_2 + Cl^-$
	7.6 ± 0.2	9.1 ± 0.1	1.6 ± 0.1	$\rightarrow SF_2 + 3F + Cl^-$(?)
F^-	3.2 ± 0.1	5.1 ± 0.1	1.3 ± 0.1	$\rightarrow SF_3 + FCl + F^-$
	6.3 ± 0.2	6.5 ± 0.1	...	$\rightarrow SF_2 + F_2 + Cl + F^-$
	8.0 ± 0.1	9.4 ± 0.1	~1.5	$\rightarrow SF_2 + 2F + Cl + F^-$

[a] All values in eV.

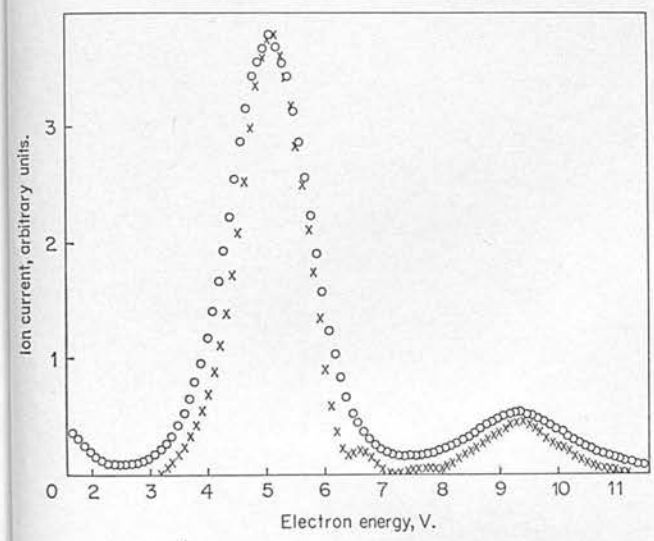

Figure 2. Ionization efficiency curve for F^- ion formation by SF_5Cl. Open circles, original experimental data; crosses, deconvoluted results.

ionization process more than tentatively and suggest that (27) is responsible.

(*vi*) F^-. A typical ionization efficiency curve for this ion before and after performing 15 smoothing and 20 unfolding iterations is shown in Figure 2. Ion formation of low intensity occurs at energies near to zero, presumably due to the reaction

$$SF_5Cl + e \longrightarrow SF_4 + Cl + F^- \quad (28)$$

A further dissociative capture process occurs at 3.3 eV, the resonance peak reaching a maximum value at 5.1 eV. A reaction of very low cross section, occurs at 6.3 eV and a further ionization process at 8.0 eV.

$$SF_5Cl + e \longrightarrow SF_3 + FCl + F^- \quad (28)$$

$$\longrightarrow SF_2 + F_2 + Cl + F^- \quad (29)$$

$$\longrightarrow SF_2 + 2F + Cl + F^- \quad (30)$$

Reaction 28 would require that $A(F^-) \simeq 2.4$ eV, in reasonable accord with the onset noted at 3.2 eV. Reactions 29 and 30 have minimum enthalpy requirements of 6.7 and 8.3 eV, respectively, which in view of the uncertainty associated with some of our thermochemical estimates, suggest that they may be assigned to the resonance processes occurring at 6.3 and 8.0 eV.

(*d*) *Thermochemical Data.* We have used the following values for heats of formation (at 298°K) in our calculations (in eV); SF_6, −12.7;[15] SF_5Cl, −10.9;[16] SF_4, −8.0;[16] FCl, −0.6;[17] Cl, 1.2;[17] S, 2.8;[17] F, 0.8.[17]

Acknowledgments. We thank the Science Research Council for a grant in aid of this work and Dr. H. L. Roberts of I. C. I. (Mond Division) for a gift of the pentafluorosulfur chloride.

(15) P. A. G. O'Hare, J. L. Settle, and W. N. Hubbard, *Trans. Faraday Soc.*, 62, 558 (1966).

(16) National Bureau of Standards, Technical Note 270-3, Jan 1968.

(17) JANAF Thermochemical Tables, Dow Chemical Co., Midland, Mich., 1961.

[Reprinted from the Journal of Physical Chemistry, 74, 52 (1970).]

Positive and Negative Ion Formation In Hexafluoroacetone by Electron Impact

by P. Harland and J. C. J. Thynne

Chemistry Department, Edinburgh University, Edinburgh, Scotland *(Received June 25, 1969)*

Positive and negative ion formation as a result of the electron bombardment of hexafluoroacetone has been studied and, from the positive ion data, a value of ≤ 4.16 eV calculated for the bond dissociation energy $D(CF_3-COCF_3)$. Hexafluoroacetone is an abundant source of negative ions, the principal ions being $CF_3COCF_3^-$, $CF_3COCF_2^-$, $(CF_3)_2C^-$, CF_3CO^-, CF_3^-, CF_2^-, CFO^- and F^-. The dependence of their formation upon electron energy has been studied and a deconvolution method used to analyze the results; ionization processes have been suggested to account for the formation of most of these ions at low electron energies and electron affinities calculated for several species. $CF_3COCF_3^-$ is formed as a result of both primary and secondary electron capture and a value of 0.61×10^{-16} cm^2 has been calculated for the electron attachment cross section for the ketone.

Introduction

Electron bombardment of a molecule may result in the formation of positive and negative ions.[1] The latter may be produced by (i) resonance attachment $AB + e \rightarrow AB^-$; (ii) dissociative resonance capture, $AB + e \rightarrow A^- + B$; or (iii) ion-pair formation; $AB + e \rightarrow A^- + B^+ + e$.

These mechanisms usually operate at different electron energies, the resonance processes usually occurring in the 0–10 eV energy region and the ion-pair processes at energies above this.

We have examined positive and negative ion formation in hexafluoroacetone over the energy range 0–70 eV. This compound was chosen because appearance potential studies of positive ions should yield information regarding the carbon–carbon bond strength and enable comparison to be made with the analogous bond strength in acetone; in addition, preliminary studies showed several negative ions to be formed and we have examined some of these ions and their electron energy dependence.

In electron impact studies, when the source of the electrons is a heated filament, uncertainties arise in the interpretation of the experimental ionization data because of the energy spread of the thermionically-emitted electron beam. This is because the ionization thresholds become smeared-out as a result of the high-energy tail of the electron energy distribution. Morrison[2]

(1) H. S. W. Massey, "Negative Ions," Cambridge University Press, London, 1950.

(2) J. D. Morrison, *J. Chem. Phys.*, **39**, 200 (1963).

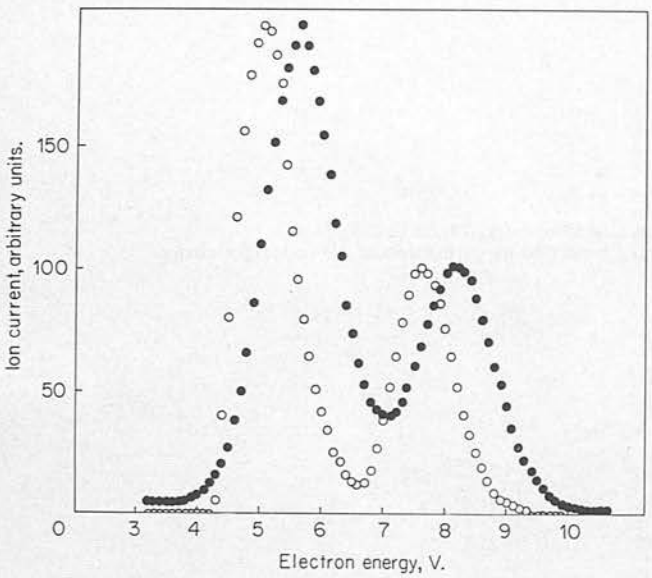

Figure 1. Ionization efficiency curve for O^- ion formation by SO_2. Full circles, original experimental data; open circles, deconvoluted results obtained using 15 smoothing and 20 unfolding iterations.

has used analytical methods to remove the energy spread and has applied the technique to the problem of positive ions. We have applied such methods to study negative ion formation at low electron energies[3] and have extended their use in this work to include hexafluoroacetone.

Experimental Section

The data were obtained using a Bendix time-of-flight mass spectrometer, Model 3015. The pressure in the ion source was usually maintained below 5×10^{-6} mm in order to reduce the possibility of ion formation due to ion–molecule reactions. The energy of the ionizing electrons was read on a Solartron digital voltmeter, Model LM 1619, and the spectra recorded on a 1-mV Kent potentiometric recorder.

In both the positive and negative ion studies, the electron current was maintained constant by automatic regulation over the whole energy range investigated. Ionization curves were usually measured three to five times, the appearance potentials for negative ions being reproducible to ± 0.1 eV.

The appearance potential of the O^- ion from SO_2 was used as the reference for electron energy scale calibration.[3-5] In a previous paper[6] we used the S^- ion from CS_2 for scale calibration purposes; this is a satisfactory calibrant but we now find the O^- ion formed by SO_2 to be superior. Our principal reasons are that the O^- ion is a more intense ion and also (as can be seen in Figure 1) two resonance peaks are observed for the O^- ion. As a consequence, although the appearance potential of the ion at 4.2 eV is chosen for calibration purposes, the second appearance potential (6.6 eV), the positions of the peak maxima (4.9 and 7.5 eV) and the energy differences between these peak parameters serve as checks on the reliability of the calibration. For positive ion studies, argon was used to calibrate the energy scale, the method used for determining the appearance potentials being the semilogarithmic plot technique.

The electron energy distribution, which was required to be known for the deconvolution procedure, was measured using the SF_6^- ion formed by sulfur hexafluoride.[7,8] It was found that performing 15 smoothing and 20 unfolding iterations on the basic experimental data enabled satisfactory evaluation of appearance potentials, resonance peak maxima and peak widths (at half-height) to be made.

Materials. Hexafluoroacetone was obtained by dehydration of the sesquihydrate. The impurities were fluoroform, hexafluoroethane, and carbon dioxide and these were removed by prolonged pumping on a vacuum line at −130°.

Results and Discussion

(*a*) *Positive Ion Formation.* We have measured the appearance potentials of the CF_3^+ and CF_3CO^+ ions formed from hexafluoroacetone and obtained $A(CF_3^+) = 14.26 \pm 0.10$ eV, and $A(CF_3CO^+) = 12.04 \pm 0.12$ eV.

If the ionization processes leading the formation of these ions correspond to

$$CF_3COCF_3 + e \longrightarrow CF_3^+ + COCF_3 + 2e \quad (1)$$

$$\longrightarrow CF_3CO^+ + CF_3 + 2e \quad (2)$$

then we may use these results to evaluate the strength of the CF_3–$COCF_3$ bond by means of such relations as $D(CF_3\text{–}COCF_3) \leqslant A(CF_3^+) - I(CF_3)$,
where $I(CF_3)$ refers to the ionization potential of the trifluoromethyl radical.

$I(CF_3)$ has been measured directly by electron impact by two groups of workers[9,10] and a value of 10.1 eV obtained. It has been suggested,[11] on the basis of reasonable values for the carbon–halogen bond strength in the trifluoromethyl halides, that this measured ionization potential is too high by about 0.8 eV.

Recently, Lifschitz and Chupka[12] have measured the

(3) K. A. G. MacNeil and J. C. J. Thynne, *Int. J. Mass Spectrom.*, **3**, 35 (1969).
(4) K. Kraus, *Z. Naturforsch.*, **16a**, 1378 (1961).
(5) J. G. Dillard and J. L. Franklin, *J. Chem. Phys.*, **48**, 2349 (1968).
(6) J. C. J. Thynne, *J. Phys. Chem.*, **73**, 1586 (1969).
(7) W. M. Hickam and R. E. Fox, *J. Chem. Phys.*, **25**, 642 (1956).
(8) G. J. Schulz, *J. Appl. Phys.*, **31**, 1134 (1960).
(9) J. B. Farmer, I. H. S. Henderson, and F. P. Lossing, *J. Chem. Phys.*, **23**, 403 (1955).
(10) R. I. Reed and W. Snedden, *Trans. Faraday Soc.*, **54**, 301 (1958).
(11) V. H. Dibeler, R. M. Reese, and F. L. Mohler, *J. Res. Natl. Bur. Stand.*, **57**, (1956).
(12) C. Lifschitz and W. A. Chupka, *J. Chem. Phys.*, **47**, 3439 (1967).

ionization potential for the trifluoromethyl radical by a photoionization technique and have reported that $I(CF_3)$ is 9.25 ± 0.04 eV. It appears that the difference between this value and the directly measured value is largely due to the fact that the adiabatic ionization potential of the radical is much lower than the vertical ionization potential, the configuration of the CF_3^+ ion being very different from that of the radical.

If we use the direct electron impact[9,10] value for $I(CF_3)$ in conjunction with our data for $A(CF_3^+)$ we find that $D(CF_3\text{–}COCF_3) \leqslant 4.16$ eV.

There are no other values reported for the CF_3–$COCF_3$ bond dissociation energy in hexafluoroacetone; because of the displacement reaction observed[13] when methyl radicals and hexafluoroacetone are present in the same system, it is likely[14] that the CF_3–$COCF_3$ bond is about 0.1 eV weaker than the corresponding bond in acetone (which has a strength of 3.8 eV), so that $D(CF_3\text{–}COCF_3) \sim 3.7$ eV.

Electron impact methods for measuring bond dissociation energies usually yield upper limit values because of the necessary neglect and uncertainty of the kinetic and excitation energies involved in the ionization and fragmentation processes. It may be therefore that our experimental value of $\leqslant 4.16$ eV compared with the estimated value of 3.7 eV reflects this uncertainty. However, the trifluoroacetyl radical has been shown to be unstable,[15] decomposing readily by reaction 3.

$$CF_3CO \longrightarrow CF_3 + CO \qquad (3)$$

Some or all of this energy difference of <0.46 eV may be used in decomposing the trifluoroacetyl radical formed in the initial ionization process; if this is so, then we may estimate a maximum value of 0.46 eV for the activation energy for reaction 3. Whittle,[16] using a kinetic method, has deduced an upper limit of 0.43 eV for this reaction.

Our data for $A(CF_3CO^+)$ should, in principle, provide an unequivocal value for $D(CF_3CO\text{–}CF_3)$, however no value is available for the ionization potential of the trifluoroacetyl radical. We may estimate $I(CF_3CO)$ if we assume that $D(CF_3CO\text{–}CF_3) = 3.7$ eV; our results indicate that $I(CF_3CO) < 8.3$ eV. This value may be compared with the value of 8.05 ± 0.17 eV reported[17] for $I(CH_3CO)$.

(*b*) *Negative Ion Formation. O^- Ion Formation by Sulfur Dioxide.* The formation of negative ions by sulfur dioxide has been investigated by several workers and the appearance potential of the O^- ion is sufficiently well established[4,5] at 4.2 eV to be used to calibrate the energy scale.

Our experimental data for this ion are shown in Figure 1; two resonance peaks are observed which have clear maxima but uncertain appearance potentials. Deconvolution of these data, using an electron energy distribution measured using SF_6^-/SF_6, give the results shown by the open circles. The threshold for the first peak is sharp and is separated from the peak maximum by 0.70 eV; this is in good agreement with the difference obtained by Kraus[4] (using a retarding-potential-difference technique) and by Dillard and Franklin.[5]

The onset of the second resonance peak is not quite resolved; Kraus[4] also was unable to completely separate the two peaks. The onset of the first peak and the minimum between the resonance peaks are separated by 2.4 eV in both our work and that of Kraus.

Hexafluoroacetone (HFA). In Table I we show the negative ion mass spectrum of HFA measured at nominal electron energies of 10 and 70 eV. The absence of ions such as C^-, O^-, and C_2^- from the lower energy spectrum suggests that they are formed principally by ion-pair processes. We have studied the energy dependence of formation of the ions; $CF_3COCF_3^-$, $CF_3COCF_2^-$, $(CF_3)_2C^-$, CF_3CO^-, CF_3^-, CF_2^-, CFO^-, and F^-.

Table I: Negative Ion Mass Spectrum of Hexafluoroacetone at Electron Energies (Uncorrected) of 10 and 70 eV

m/e	Ion	Rel. int., 10 eV	Rel. int., 70 eV
12	C^-	0	3.0
16	O^-	0	21.5
19	F^-	751	1000
24	C_2^-	0	4.0
31	CF^-	15.2	3.6
38	F_2^-	0	3.0
43	C_2F^-	0	2.0
47	CFO^-	25.4	18.3
50	CF_2^-	12.7	4.0
69	CF_3^-	1000	257
97	CF_3CO^-	10.1	17.0
147	$CF_3COCF_2^-$	5.7	36.0
150	$(CF_3)_2C^-$	7.6	4.0
166	$CF_3COCF_3^-$	7.6	67

It is apparent from our data (discussed below) that several of the ions ($CF_3COCF_2^-$, CF_3CO^-, CF_3^-, CFO^-, and F^-) have almost identical appearance potentials (~3.1 ± 0.1 eV) and their respective resonance peaks attain a maximum value at ~4.2 ± 0.1 eV. This suggests a common origin for these ions and we suggest that this is an electronically excited unstable state of the ketone which subsequently decomposes to form the ions mentioned

(13) R. M. Smith and J. G. Calvert, *J. Amer. Chem. Soc.*, **78**, 2345 (1956).

(14) S. W. Benson, private communication, 1969.

(15) P. B. Ayscough and E. W. R. Steacie, *Proc. Roy. Soc.*, **A234**, 476 (1956).

(16) J. C. Amphlett and E. Whittle, *Trans. Faraday Soc.*, **63**, 80 (1967).

(17) R. I. Reed and J. C. D. Brand, *ibid.*, **54**, 478 (1958).

$$CF_3COCF_3 + e \longrightarrow CF_3COCF_3^{-*} \longrightarrow CF_3COCF_2^- + F \quad (4)$$

$$\longrightarrow CF_3CO^- + CF_3 \quad (5)$$

$$\longrightarrow CF_3^- + COCF_3(+CO + CF_3?) \quad (6)$$

$$\longrightarrow CFO^- + CF_2 + CF_3 \quad (7)$$

$$\longrightarrow F^- + CF_2COCF_3 \quad (8)$$

(*i*) *Charge-Transfer Reactions Involving the O⁻ Ion.* The ionization curves for several of the ions (*e.g.*, $CF_3COCF_2^-$, CF_3^-, F^-) show inflections at energies ~5 eV; this corresponds to the resonance peak maximum observed for the O^- ion formed by SO_2 (which was used to calibrate the electron energy scale). These inflections were not observed when SO_2 was not present in the ionization chamber; accordingly we attribute their occurrence to the charge-transfer reaction (9). This produces an unstable state of the parent ion which decomposes to yield the appropriate ions.

$$O^- + CF_3COCF_3 \longrightarrow O + CF_3COCF_3^- \longrightarrow CF_3COCF_2^- \text{ etc.} \quad (9)$$

It is noteworthy that, even at the low ion source pressures maintained in this work, negative ion–molecule reactions may occur to a sufficient extent to contribute noticeably to the ionization efficiency curves.

(*ii*) *$CF_3COCF_3^-$.* The observation of a stable molecule–ion is relatively unusual; few other such ions have been observed. Its formation must involve the electron capture process

$$CF_3COCF_3 + e \longrightarrow CF_3COCF_3^- \quad (10)$$

Our data for this ion indicate two main regions of ion formation, one ~0 eV and the second[18] commencing at about 10 eV. In earlier work,[18] only the higher energy process was detected, the ion being formed as a result of secondary electron capture, the secondary electrons being produced by such positive ionization processes as $CF_2COCF_3 + e \rightarrow CF_3COCF_3^+ + 2e$.

At that time, we were unable to observe ion formation at very low electron energies; however, an improved experimental technique and introduction of a 3V dry cell into the electron energy circuit so that 'negative' voltages could be obtained has enabled us to examine the primary electron capture reaction.

When hexafluoroacetone was studied at electron energies ~0 eV, a parent ion was observed; admission of a small quantity of sulfur hexafluoride to the ionization chamber resulted in a considerable diminution of the $CF_3COCF_3^-$ ion intensity. This suggested that the electron attachment cross section for reaction 10 was much less than that for SF_6^- ion formation by

$$SF_6 + e \longrightarrow SF_6^- \quad (11)$$

In Figure 2, we show the data obtained for SF_6^- and

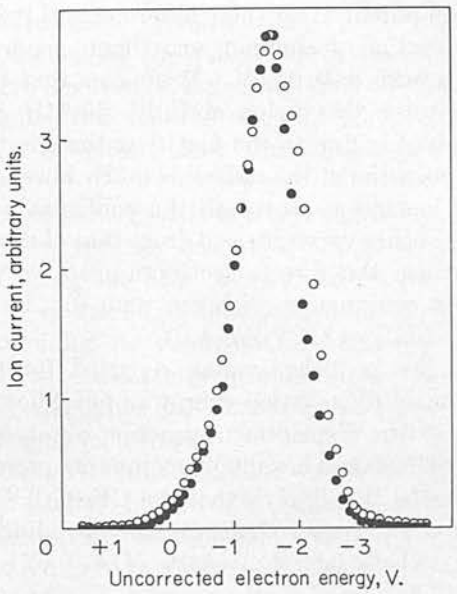

Figure 2. Ion current *vs.* electron accelerating energy. Full circles, SF_6^-; open circles, $CF_3COCF_3^-$. Ion current scale for hexafluoroacetone 58.9 times greater than that for SF_6.

$CF_3COCF_3^-$ ion formation as a function of the electron energy. A 50/50 mixture of hexafluoroacetone and sulphur hexafluoride was used; the two sets of ionization data have been normalized for convenience in presentation, the ordinate for $CF_3COCF_3^-$ being 58.9 times greater than that for SF_6^-.

Formation of the SF_6^- ion in this energy region has been used to mirror the electron energy distribution and calibrate the electron energy scale.[7,8] It is apparent from Figure 2 that the $CF_3COCF_3^-$ and SF_6^- ions have a very similar energy dependence, both ions attaining a maximum value at the same electron energy. The ionization curve for the ketone is slightly broader in the wings than is that for the hexafluoride, this may reflect either a slightly different energy dependence for electron attachment or the experimental uncertainties in measuring the very small ion currents for the $CF_3COCF_3^-$.

Because of their similar energy dependence we consider that the relative heights of the two ion peaks may be used to indicate the relative attachment cross-sections of reactions 10 and 11. If it is assumed that both ions have the same collection efficiency, then

$$\frac{\sigma_{SF_6}}{\sigma_{HFA}} = 58.9$$

where σ_x refers to the electron attachment cross-section of X. A value of 3.6×10^{-15} cm² has been reported[19] for σ_{SF_6}, so that $\sigma_{HFA} = 0.61 \times 10^{-16}$cm².

It has been observed that both sulfur hexafluoride[20]

(18) J. C. J. Thynne, *Chem. Commun.*, 1075 (1968).

(19) R. N. Compton, L. G. Christophorou, G. S. Hurst, and P. W. Reinhardt, *J. Chem. Phys.*, **45**, 4634 (1966).

(20) A. J. Ahearn and N. B. Hannay, *ibid.*, **21**, 119 (1953).

and hexafluoroacetone[18] form parent molecule-ions at higher electron energies as a result of secondary electron capture. We considered that competition between sulfur hexafluoride and hexafluoroacetone for secondary electrons might enable us to measure $\sigma_{SF_6}/\sigma_{HFA}$. Accordingly, using a 39.2:1 mixture of CF_3COCF_3:SF_6, we measured the intensities of the $CF_3COCF_3^-$ and SF_6^- ions, I_{HFA}^- and $I_{SF_6}^-$, at ten electron energy intervals over the range 15–60 eV. Our experimental data indicated that the ion current ratio, $I_{SF_6}^-/I_{HFA}^-$ was effectively constant over the entire energy range having a value of 1.44 ± 0.06; this result yields a value for $\sigma_{SF_6}/\sigma_{HFA}$ of 56 ± 2, which is in good accord with our directly-measured value at low electron energies.

An alternative explanation for the decrease in the $CF_3COCF_3^-$ ion current is the possibility of occurrence of the charge exchange reaction

$$CF_3COCF_3^- + SF_6 \longrightarrow CF_3COCF_3 + SF_6^- \quad (11a)$$

Our data for SF_6^- formation cannot definitely distinguish between this reaction and reaction 11; however, at our ion source pressure ($\sim 5 \times 10^{-6}$ mm) although some collisions between $CF_3COCF_3^-$ and SF_6 will occur, we consider the probability of interactions occurring to a sufficient extent to account for the considerable decrease in $CF_3COCF_3^-$ ion current noted experimentally at very low SF_6 pressures ($\sim 10^{-7}$ mm) to be negligible unless the cross-section for reaction 11a is very large. The data obtained for secondary electron capture in the high energy study also suggest that reactions such as 11a may reasonably be neglected since, at these energies, other negative ion species (*e.g.*, CF_3^-, CF_3CO^-) will be present which might undergo charge transfer reactions.

$$X^- + SF_6 \longrightarrow SF_6^- + X$$

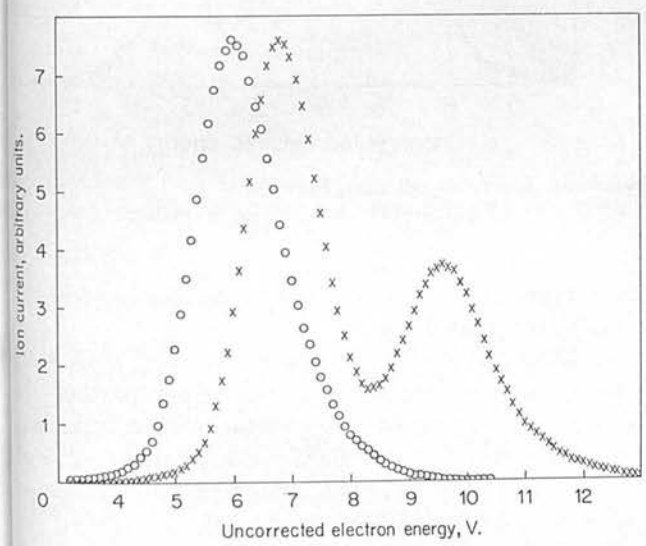

Figure 3. Ionization efficiency curve for $CF_3COCF_2^-/CF_3COCF_3$ (○) and O^-/SO_2 (×) ion formation.

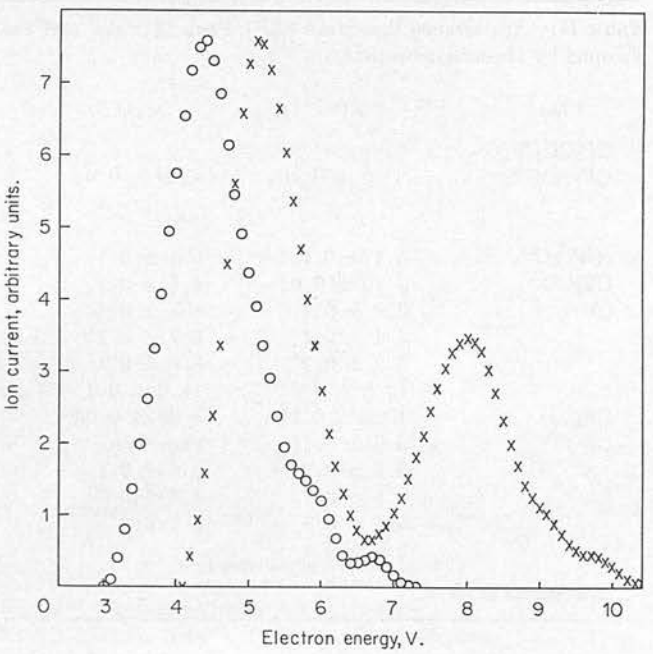

Figure 4. Deconvoluted results. $CF_3COCF_2^-/CF_3COCF_3$, ○; O^-/SO_2, ×.

If such reactions occurred significantly then it would result in the ratio $\sigma_{SF_6}/\sigma_{HFA}$ being greater at higher energies than at ~0 eV, whereas our experimental data show the two values to be in good agreement.

(*iii*) *$CF_3COCF_2^-$*. Typical experimental data and the smoothed, deconvoluted results are shown in Figures 3 and 4 together with the corresponding O^-/SO_2 ionization curves.

Examination of the pressure dependence of the $CF_3COCF_2^-$ ion current at low electron energies showed it to be a primary ion, we may therefore neglect the possibility of the ion being formed by secondary ionic reactions.

A sharp onset at 3.10 ± 0.10 eV is observed, the resonance peak reaching a maximum at 4.20 ± 0.05 eV; the peak width at half-height is 1.35 ± 0.05 eV. The common origin of the ions formed at this energy has been discussed above and we attribute $CF_3COCF_2^-$ ion formation to reaction 4.

If a value of ~5.2 eV is assumed for the bond dissociation energy $D(CF_3COCF_2\text{–}F)$, (values of 5.3, 5.2, and 5.0 eV having been reported for the C–F bond strengths in CF_4,[21] C_2F_6[22], and C_6H_5F[23], respectively), then using the relation: $D(CF_3COCF_2\text{–}F) \leqslant A(CF_3COCF_2^-) + E(CF_3COCF_2)$, a value of ~2.1 eV may be estimated for the electron affinity of the perfluoroacetonyl radical.

Figure 4 shows clearly the inflection in the ionization

(21) C. R. Patrick, *Advan. Fluorine Chem.*, **2**, 18 (1961).

(22) K. A. G. MacNeil and J. C. J. Thynne, *Int. J. Mass Spectrom.*, **2**, 1 (1969).

(23) P. Smith, *J. Chem. Phys.*, **29**, 681 (1958).

Table II: Appearance Potentials (AP), Peak Maxima, and Peak Widths at Half Height (PW) of Negative Ions Formed by Hexafluoroacetone

Ion	AP[a]	Max[a]	PW[a]	Process
$CF_3COCF_3^-$	0			$CF_3COCF_3 + e \rightarrow CF_3COCF_3^-$
$CF_3COCF_2^-$	3.10 ± 0.10	4.20 ± 0.05	1.35 ± 0.05	$CF_3COCF_3 + e \rightarrow CF_3COCF_3^- * \downarrow CF_3COCF_2^- + F$
$(CF_3)_2C^-$	5.1 ± 0.1	6.4 ± 0.1	0.6 ± 0.1	$CF_3COCF_3 + e \rightarrow (CF_3)_2C^- + O$
CF_3CO^-	3.10 ± 0.05	4.1 ± 0.1	1.0 ± 0.2	$CF_3COCF_3^- * \rightarrow CF_3CO^- + CF_3$
CF_3^-	3.0 ± 0.1	4.3 ± 0.1	1.5 ± 0.2	$CF_3COCF_3^- * \rightarrow CF_3^- + CF_3CO$
	5.4 ± 0.1	6.7 ± 0.1	1.7 ± 0.1	$CF_3COCF_3 + e \rightarrow CF_3^- + CO + CF_2 + F$
	8.2 ± 0.2	8.6 ± 0.1	...	?
	10.5 ± 0.2	11.0 ± 0.2	...	?
CF_2^-	4.25 ± 0.10	5.25 ± 0.05	0.7 ± 0.1	$CF_3COCF_3 + e \rightarrow CF_2^- + F + CO + CF_3$?
CFO^-	3.0 ± 0.1	uncertain	2	$CF_3COCF_3^- * \rightarrow CFO^- + CF_2 + CF_3$
	5.3 ± 0.2	6.6 ± 0.1	2.0 ± 0.1	$CF_3COCF_3 + e \rightarrow CFO^- + 2F + C_2F_3$
F^-	3.1 ± 0.1	4.3 ± 0.2	1.3 ± 0.3	$CF_3COCF_3^- * \rightarrow F^- + CF_2COCF_3$
	5.7 ± 0.1	7.2 ± 0.2	1.8 ± 0.3	$CF_3COCF_3 + e \rightarrow F^- + CF_2 + CO + CF_3$
	9.0 ± 0.1	...	...	$\rightarrow F^- + F + CO + 2CF_2$

[a] All values in eV.

curve which we have considered above to be the result of the charge-transfer reaction 9.

(*iv*) $(CF_3)_3C^-$. Our experimental data for this ion when smoothed and deconvoluted yield the values shown in Table II. Ion formation is attributed to the reaction

$$CF_3COCF_3 + e \longrightarrow (CF_3)_2C^- + O \qquad (12)$$

It is noteworthy that the resonance peak is very narrow, the width at half-height being only 0.6 eV. A value of ~0.6 eV may be estimated for the electron affinity of $(CF_3)_2C$ if the bond strength $D(O - C(CF_3)_2)$ is assumed to be similar to that in carbon dioxide, *i.e.*, ~5.7 eV.

(*v*) CF_3CO^-. At low electron energies, this ion is formed quite abundantly but not at 70 eV; this suggests that the ion-pair process $CF_3COCF_3 + e \rightarrow CF_3CO^- + CF_3^+ + 2e$ does not occur extensively. Our results for this ion are shown in Table II, and we consider reaction 5 to account for ion formation. If a value of 3.7 eV is assumed for $D(CF_3CO\text{–}CF_3)$, then our data yield a value of $\leqslant$ 0.6 eV for the electron affinity of the trifluoroacetyl radical.

(*vi*) CF_3^-. Ion formation in this case is rather complex; several appearance potentials are noted for this ion.

Initially ion formation occurred at 3.0 ± 0.1 eV and is attributed to decomposition of the electronically excited ketone by reaction 6. Because the trifluoroacetyl radical has been shown to have limited stability in the gas phase, the decomposition reaction 6 may involve the formation of CO and CF_3 as fragmentation products.

It is apparent from Figures 5 and 6 that the CF_3^- ionization curve has inflections at ~5 eV and ~7.6 eV, *i.e.*, where the O^-/SO_2 ion reaches a maximum intensity;

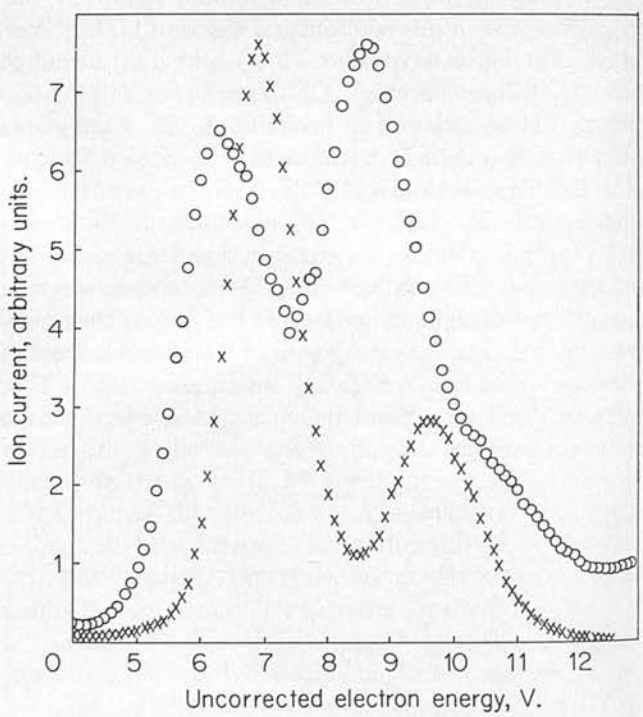

Figure 5. Ionization efficiency curve for CF_3^-/CF_3COCF_3, ○, and O^-/SO_2, ×, ion formation.

these inflections are attributed to the change transfer reaction mentioned above.

A second resonance process is observed at 5.4 eV (based upon extrapolation of the upper part of the curve). If reaction 13 is responsible for ion formation at this energy, then our data yield a value of 2.5 eV for $E(CF_3)$; this may be compared with values of $\leqslant$2.6 eV[22] and 1.8 eV[24] reported for this quantity.

(24) F. M. Page, private communication, 1968.

$$CF_3COCF_3 + e \longrightarrow CF_3^- + CO + CF_2 + F \quad (13)$$

Further resonance processes of very low cross section are noted at 8.2 and 10.5 eV; we cannot account for these ionization processes.

(*vii*) CF_2^-. Our data for this ion are shown in Table II; a narrow resonance peak having an onset at 4.25 ± 0.10 eV is obtained. If ion formation was due to the reaction

$$CF_3COCF_3 + e \longrightarrow CF_2^- + F + CO + CF_3 \quad (14)$$

then a value of $E(CF_2) \leqslant 3.75$ eV would be obtained; this seems improbably large. The narrow resonance peak would suggest that little excess energy was involved in the ionization process. A rearrangement reaction such as

$$CF_3COCF_3 + e \longrightarrow CF_2^- + CF_4 + CO \quad (15)$$

would yield a negative value for $E(CF_2)$; we are therefore unable to assign the ionization process responsible for CF_2^- formation.

(*viii*) CFO^-. This ion must be formed as the result of rearrangement; ion formation is observed initially at 3.0 ± 0.1 eV and is attributed to reaction 7. Although a sharp onset is obtained at this energy, the resonance peak is broad (~2 eV) and does not attain a clear maximum before a second resonance process occurs at 5.3 eV. This resonance peak is also broad and this perhaps suggests the involvement of considerable excess energy in the rearrangement.

$$CF_3COCF_3 + e \longrightarrow CFO^- + 2F + C_2F_3 \quad (16)$$

The second ionization process may correspond to reaction 16, *i.e.*, the C–O bond is broken and the oxygen transferred to a CF group in the rearrangement. This probably would have higher energy requirements than reaction 7 where simple fluorine transfer to CO may be involved but such assignments are tentative.

The heat of formation of the fluoroformyl radical, $\Delta H_f(CFO)$, has been estimated[3] to be −1.7 eV, so that our data for reaction 7 indicate $E(CFO)$ ~3.3 eV. A study[3] of CFO^- ion formation by carbonyl fluoride showed $E(CFO) = 2.7$ eV; the resonance peak in that

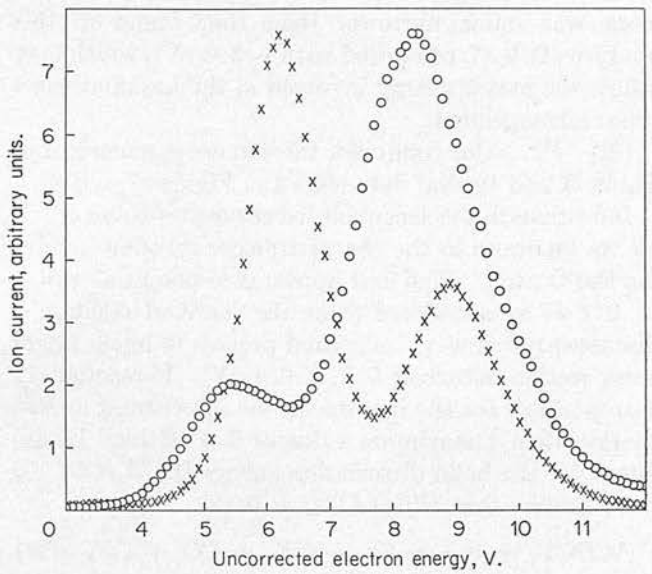

Figure 7. Ionization efficiency curve for F^-/CF_3COCF_3, ○ and O^-/SO_2, ×, ion formation.

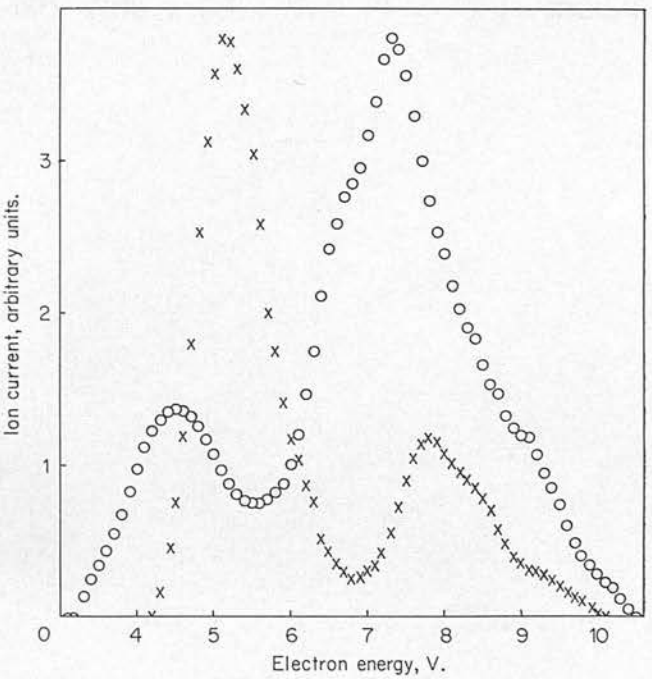

Figure 8. Deconvoluted results. F^-/CF_3COCF_3, ○; O^-/SO_2, ×.

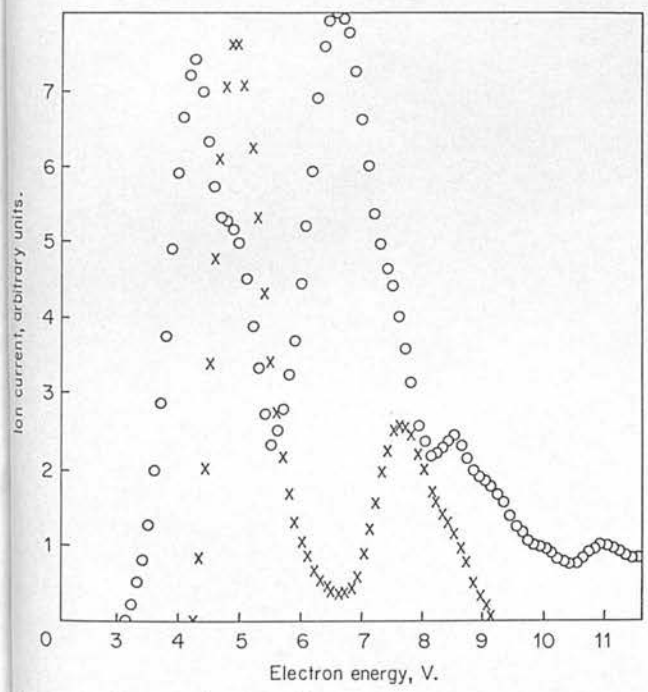

Figure 6. Deconvoluted results. CF_3^-/CF_3COCF_3, ○; O^-/SO_2, ×.

work was much narrower than that found in this study (~0.5 eV compared with ~2.0 eV), which may reflect the excess energy involved in the hexafluoroacetone rearrangement.

(*ix*) F^-. Our results for this ion are summarized in Table II and typical data shown in Figures 7 and 8.

Inflections in the deconvoluted curve at ~5 and ~7.5 eV we attribute to the charge-transfer reaction involving the O^- ion. The first appearance potential at 3.1 ± 0.1 eV is considered to be the result of reaction 8 discussed previously; a second process of much larger cross section occurs at 5.7 ± 0.1 eV. If reaction 17 is responsible for the increase in the ion current at this energy, then a maximum value of 2.6 eV may be deduced for the bond dissociation energy $D(CF_2\text{–}COCF_3)$ if we assume that $D(CO\text{–}CF_3) = 0$ eV.

$$CF_3COCF_3 + e \longrightarrow F^- + CF_2 + CO + CF_3 \quad (17)$$

A further ionization process of very low cross-section may be seen on the tail of the second resonance peak, the onset energy being 9.0 eV.

$$CF_3COCF_3 + e \longrightarrow F^- + F + CO + 2CF_2 \quad (18)$$

The minimum enthalpy requirement for reaction 18 is 9.0 eV and we therefore attribute ionization to this reaction.

(*c*) *Thermochemical Data.* The following values for the heats of formation have been used in this work (in eV) CF_3COCF_3 −15.1; CF_3 −5.2;[25] CF_2 −1.6;[26] CF, 3.2;[27] F, 0.8;[27] CO, −1.1;[27] and CF_3^+, 3.7.[28]

The heat of formation of hexafluoroacetone has been estimated using the additivity rules[29] based upon the C–C and C–F bond contributions to the enthalpies of various fluorine-containing molecules.[21,29]

Acknowledgment. We thank Dr. S.W. Benson of the Stanford Research Institute for comments regarding the bond dissociation energy of hexafluoroacetone.

(25) B. S. Rabinovitch and J. F. Reed, *J. Chem. Phys.*, **22**, 2092 (1954).

(26) J. R. Majer and C. R. Patrick, *Nature*, **201**, 1022 (1964).

(27) "JANAF Thermochemical Tables," Dow Chemical Co., Midland, Mich., (1961).

(28) C. Lifschitz and F. A. Long, *J. Phys. Chem.*, **69**, 3731 (1965).

(29) S. W. Benson and J. H. Buss, *J. Chem. Phys.*, **29**, 546 (1958).